REGIONE AUTONOMA DELLA SARDEGNA

Ph.D. in Electronic and Computer Engineering
Dept. of Electrical and Electronic Engineering
University of Cagliari

State Estimation in Electrical Distribution Systems

Marco Pau

Advisor: Prof. Carlo Muscas
Curriculum: ING-INF/07 Electrical and Electronic Measurements

XXVII Cycle
2013-2014

Marco Pau gratefully acknowledges Sardinia Regional Government for the financial support of his PhD scholarship (P.O.R. Sardegna F.S.E. Operational Programme of the Autonomous Region of Sardinia, European Social Fund 2007-2013 - Axis IV Human Resources, Objective l.3, Line of Activity l.3.1.)

Dedicated to Antonella

Contents

Introduction

In last years, several changes have affected the way in which the electrical systems must be operated and conceived. As an example, due to the deregulation of the energy market, the power generation dispatch is now established through economical criteria and not only according to technical considerations, leading in this way to new issues in the management of the system. Recently, the increasing attention towards a sustainable and environmentally friendly future has pushed many countries to provide incentives for the installation of generation plants supplied by renewable energy sources, such as wind power or photovoltaic plants. Consequently, a large number of small-size units has been installed and connected to the distribution level of the system, creating the so-called Distributed Generation (DG). This overturns the traditional view of the electrical systems to be composed of large-scale generation plants connected to the transmission grid, and with the distribution network responsible only for the final delivery of the energy to the customers.

In the upcoming future, the investments in the sphere of electric mobility are expected to bring a massive increase of Electrical Vehicles (EVs) connected to the distribution system, and energy storage devices are expected to be deployed throughout the network. All these elements, together with the DG, go under the more general name of Distributed Energy Resources (DERs). The availability of DERs has the potentiality to provide significant benefits for a flexible and efficient operation of the network. However, their presence also increases the complexity of the system. As a result, a new management and control philosophy is required to deal with this evolving scenario and to satisfy the always stricter requirements on system reliability and efficiency.

The renowned concept of Smart Grid was born in this context, as an answer to the need of smarter solutions for the management of the modern electrical systems. Many definitions, with different nuances, can be found to describe the concept of Smart Grid, depending on the features that are to be highlighted. In general, the Smart Grid can be seen as a modernized power network in which advanced automated functions are implemented, exploiting a suitable communication infrastructure, to efficiently perform the management, control and protection of the network.

In the Smart Grid paradigm, a key role is played by the measurement system

deployed to monitor the network. In fact, all the possible control and management applications have to rely either on the picture of the operating conditions or on the knowledge of specific quantities of the network. Such information is provided by the measurement system, which, therefore, represents the core for the operation of the Smart Grid. It is worth underlining that, in this context, the measurement system has to be intended with an extended meaning, including both the measurement infrastructure (i.e. the measurement devices installed on the field) and the algorithms provided for processing the raw measurement data (i.e. the applications envisaged for collection, coordination and elaboration of the measurement data).

State Estimation (SE) algorithms are an essential part of the measurement system of an electrical grid. SE is a mathematical technique that uses the measurements gathered from the instruments deployed on the field to identify the current operating state of the network. Therefore, it represents the link between the measurement infrastructure and the management system in the control centers. Once the state of the network is known, all the electrical quantities can be computed and any control or management function can be run. For the successful operation of such functions, the accuracy of the estimated electrical quantities is a fundamental feature. SE plays a crucial role also from this standpoint, because it allows filtering out the errors intrinsically present in the measurements due to their limited accuracy. The relevance of SE within the measurement system is thus evident, since it can be considered as the final ring of the measurement chain, and since it is essential for enhancing the accuracy of the quantities provided to the upper level functions.

SE has been used, since several decades, in the control centers of the transmission systems. In the Smart Grid scenario, distribution systems, which currently are usually unmonitored, will also be equipped with computational centers having appropriate management systems. As a consequence, SE is expected to play a key role also at the distribution level. However, SE has to be suitably revised for fitting the distribution systems, and this is not an easy task due to several reasons. First of all, distribution networks differ significantly from transmission grids, hence a simple adjustment of existing algorithms developed for the transmission level is not sufficient. As a result, ad hoc state estimators, tailored to the features of the distribution systems, have to be conceived. Moreover, since distribution grids have been so far poorly monitored, the penetration of measurement instruments in these networks is minimal, often limited to the High Voltage to Medium Voltage (HV/MV) substations. To tackle this problem, and make the SE possible, all the types of available information must be exploited. Statistical or historical data are then used to create the so-called pseudo-measurements. Pseudo-measurements allow SE to be performed but, since such information is based on forecast data, the accuracy of the SE results can be drastically affected. Another major issue in the context of distribution systems is given by the huge dimension of such networks. This aspect

emphasizes the problem of the computational efficiency of the estimation algorithms. To this purpose, proper solutions have to be found to allow real-time running of SE with the reporting rates required by the downstream control and management functions.

For all these reasons, Distribution System State Estimation (DSSE) is an important research topic nowadays, and it still represents a challenging task. This thesis aims at addressing some of the issues related to SE in distribution systems. In particular, the main goals are:

- to propose a state estimation algorithm tailored for distribution networks, able to fit the main features of these grids and to combine the requirements of accuracy and computational efficiency needed for the practical purposes;

- to present approaches able to further enhance the computational efficiency of the estimation algorithm without reducing its accuracy performance;

- to assess the impact of the measurements, in terms of both typology and placement, on the final accuracy of the estimated quantities and to highlight the importance of a proper modeling of the measurement uncertainties for the achievement of the best possible accuracy in the output results;

- to advance proposals for the effective deployment of both SE and the measurement infrastructure, taking into account the requirements of accuracy, efficiency, robustness and low costs predictable in real distribution systems.

The thesis is organized according to the following outline. In Chapter 1, after an overview on the basics and on the methods commonly used to perform SE, the challenges related to the realization of SE in distribution systems are described. Then, a new state estimation algorithm, using the branch currents as state variables, and tailored for the distribution networks, is proposed. The novel algorithm overcomes the issues present in previous branch-current estimators and allows for easy integration of all the kinds of measurements, including the new generation Phasor Measurement Units (PMUs).

In Chapter 2, formulations traditionally used for the inclusion of the equality constraints into the estimation algorithms are presented. Then, a new approach well-suited to the proposed branch-current estimator is shown and compared to existing methods. Such approach allows reducing the execution times of the estimator and to improve its convergence properties.

Chapter 3 reports a comprehensive analysis of the performance of the proposed branch-current state estimator, in terms of estimation accuracy, numerical properties and computational efficiency. In particular, these features are compared to those of other estimators existing in the literature, based on different state variables, in

order to highlight both strengths and weaknesses of the proposed solution. Such analysis aims at providing a benchmark for the choice of the state estimator most suitable for networks with different topologies and for different configurations of the available measurement infrastructure.

In Chapter 4, an analysis of the impact of different measurement types, and of their placement, on the final accuracy of the SE results is presented. Such analysis provides useful information for the selection of the measurement infrastructure to be deployed in future distribution grids, and points out some important considerations for a smart choice of the meter placement.

Chapter 5 focuses on the impact of the measurements and in particular of their modeling on the final accuracy of the estimation results. The importance of duly considering all the measurement aspects into the estimator model is pointed out. In particular, proper consideration of the correlations existing among measurements is shown to be crucial to achieve significant improvements in the accuracy of the estimation outcome.

In Chapter 6, a multi-area architecture, based on a distributed measurement configuration, is proposed as overall measurement system for the distribution grids. The multi-area scheme is almost a compulsory solution at the distribution level, due to the large size of these networks. In this framework, the state estimator has to be adapted for integrating the information provided by different areas. The proposed solution allows for the estimation of the operating conditions on the whole area with reduced execution times, minimum communication costs, and robustness to possible communication failures. High accuracy performance are also obtained, thanks to the proper modeling of the correlations arising among the data provided by different areas into the multi-area estimator.

Summary comments on the obtained results and final considerations conclude this thesis.

Chapter 1

Branch Current Distribution System State Estimation

1.1 State Estimation overview

The idea to apply State Estimation (SE) methods to the electrical power systems dates back to the 1970s, when Fred Schweppe proposed the use of SE techniques for achieving an accurate knowledge of the operating conditions of transmission networks [1–3]. In [1], Schweppe describes SE as the result of the combination of two big fields, load flow and statistical estimation theory. Basically, SE can be defined as a mathematical technique that, through the processing of raw measurements and network data (such as, for example, topology of the network, impedances of the lines, etc.), allows the estimation of the most probable operating state of a network. According to Schweppe's definitions, the state of an electrical system is given by the set of the voltage magnitudes and angles at all the network buses. The estimation of the voltages, together with the knowledge of the network data, allows also the computation of all the other quantities representative of the electrical system, thus providing an overall picture of the operating conditions of the network.

SE was identified by Schweppe as the necessary link between the raw measurement data provided by the instruments deployed on the field and the management programs installed in the control centers. In fact, measurements are always affected by errors due to the limited accuracy of the measurement devices. Moreover, bad data, instrument failures, communication errors and telemetry loss can also occur. As a result, meter readings are not always fully reliable and available for direct use in control applications. For this reason, a suitable processing of the telemetered measurements is needed in order to remove clearly erroneous data, to handle possible measurement unavailability and to filter out the random errors intrinsically present in the measurements.

Since the '70s, SE has been object of large research efforts. Currently, it represents the heart of the control centers of transmission systems, where it enables proper operation of the control programs and serves as monitoring tool for human operators. Comprehensive reviews of the state of the art in power system SE can be found in [4, 5].

In general, SE tools commonly implemented in control centers include the following functionalities [4]:

- *Topology processor*: it allows building the current topology of the network, according to the acquired states of switches and breakers.

- *Observability analysis*: it is a pre-processing stage where all the gathered measurements are analyzed to verify the observability of the whole network; if the redundancy of the available measurements is not sufficient to achieve the full observability of the system, the observable islands have to be detected in order to allow SE to be run at least on them.

- *SE algorithm*: it is the core of the state estimator, that is the algorithm designed to process the collected real-time measurements and to provide the estimated state of the network.

- *Bad data detection and identification*: depending on the estimation approach, this step can be directly included in the estimation algorithm or can be a post-processing step. It allows detecting, identifying and then discarding possible bad data occurring due to instrument malfunctioning, communication errors or other reasons. A preventive bad data check can be also performed before running the SE algorithm in order to immediately reject senseless measurements (such as, for example, negative voltage or current magnitudes).

- *Topology error identification*: similarly to the bad data identification, it is a step where the estimation results are analyzed to identify possible errors in the assumed topology of the network (due to an erroneous or missed communication of the state of a switch).

Fig. 1.1 shows the flowchart for the typical operation of a state estimator. It is possible to observe that, if bad data or topology errors are detected, then SE must be repeated, after the corrective actions, since such errors drastically affect the estimation results. Each one of the stages included in Fig. 1.1 represents an important research topic within the wider field of SE. In this thesis, as recalled in the following, the focus is mainly on the SE algorithms, but it is worth underlining that each one of the mentioned steps is essential for the effective realization and deployment of a SE function into a power system control center.

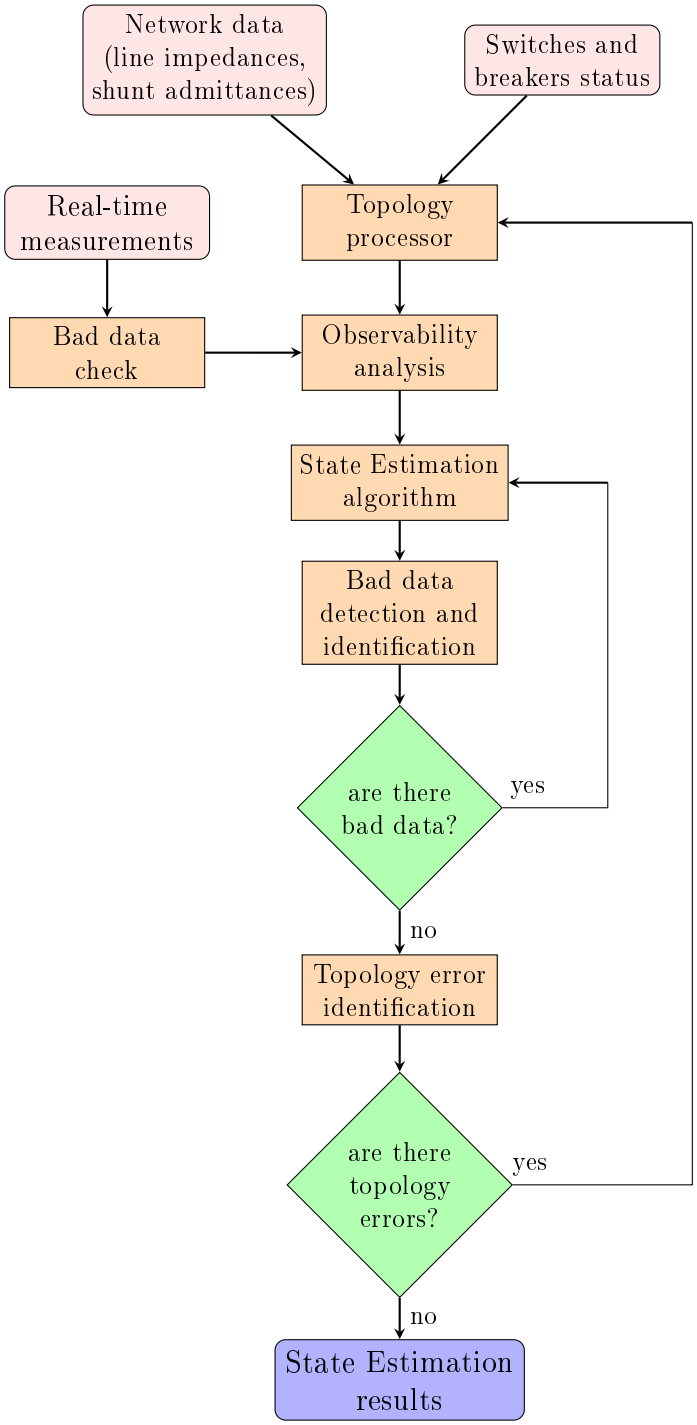

Figure 1.1: Operation flowchart of a state estimator

1.2 State Estimation in distribution systems

1.2.1 Evolution of distribution systems

SE is today an essential part of the Energy Management Systems (EMSs) implemented in the control centers of transmission grids. In distribution systems, instead, the detailed monitoring of the network has not been necessary so far, since the passive operation of these grids allowed an easy management without advanced control tools. As a consequence, until now, SE has not been generally employed at the distribution level.

Currently, however, significant changes are affecting the operation of distribution systems [6]. First of all, because of the massive increase of Distributed Generation (DG), the assumption of passive behaviour is no longer valid; bi-directional power flows are now possible and this calls for a more complex and active management of the network [7]. Moreover, new players are entering (or are going to enter in the upcoming future) in the scenario of distribution systems. Among these, it is worth mentioning the Electric Vehicles (EVs), whose foreseeable spread in next years is expected to have a significant impact on the distribution system operation [8]. If EVs are not properly managed, major issues could arise because of the large power demand occurring in case of contemporary request of charge by many vehicles. On the contrary, a suitable management of the charging strategy can be beneficial for the grid operation, contributing to voltage control and power loss minimization [9, 10]. Besides the EVs, storage devices and demand-side management are also forecast to support the operation of future distribution grids [11, 12]. All these options are included under the more general name of Distributed Energy Resources (DERs); they are an important solution for achieving higher openness to renewable energy sources, postponement of grid refurbishment, and improvement of efficiency and reliability of distribution networks. Again, to coordinate the operation of all these assets, smart Distribution Management Systems (DMSs), equipped with advanced control functions, must be developed.

In this context, SE will be playing a crucial role. In fact, for the proper functioning of the control tools, an accurate awareness of the operating conditions is essential. A poorly accurate knowledge would be detrimental, leading to possible wrong decisions by the DMS with consequent technical issues or unwanted costs [13]. Thus, like in transmission systems, SE is necessary to process measurement data, enhance their accuracy and provide a reliable picture of the operating conditions to the upper level functions within the DMS.

1.2.2 Features of distribution systems

Despite the similar role of SE in both transmission and distribution grids, the realization of the state estimators in the two systems has necessarily to be quite different. In fact, distribution grids differ significantly from the transmission ones under several aspects. Typical features of distribution networks affecting the Distribution System State Estimation (DSSE) are [14]:

- *Imbalance*: distribution grids, like the transmission ones, are three-phase networks. However, transmission grids are generally balanced systems and can be, for this reason, modeled through an equivalent single-phase scheme representing the positive sequence of the system. Distribution grids, instead, can have significant unbalances of the three-phase quantities due to the presence of many non-symmetrical loads and of single-phase portions of the network. The imbalance of the grid is further exacerbated today by the massive growth of small-size generation plants, mainly fed by renewable energy sources, characterized by single-phase connection to the network. As a consequence, distribution systems have necessarily to rely on a three-phase model of the network and to duly consider the mutual coupling among the different phases. Comprehensive references for the three-phase modeling of lines and other components of the distribution systems can be found in [15, 16].

- *Topology*: differently from the transmission systems, which, for reliability reasons, are generally highly meshed networks, most of the distribution systems are radial or weakly meshed. This allows for the development of different formulations of the SE algorithm, tailored to such topology of the system. The idea to consider branch-currents as state variables in the estimator, instead of the traditionally used node voltages, relies on the possibility to achieve simpler and faster estimators exploiting the radial or weakly meshed configuration.

- *Line parameters*: distribution and transmission lines obviously differ because of the associated voltage levels and their physical characteristics. In transmission, the series impedance in the equivalent pi-model of the line is mainly composed of the inductance term, while the resistance term is significantly lower. Having very low R/X ratios allows neglecting the resistance for practical purposes and decoupling the SE algorithms, separating the estimation of voltage magnitudes and angles. In distribution systems, instead, the same considerations do not hold. In fact, it is not unusual to find R/X ratios equal, or even higher, to 1. As a result, decoupling versions of the DSSE algorithms cannot be easily obtained. Another important difference in the modeling of the line concerns the shunt admittances. In distribution systems the capacitive terms are usually very low (above all in case of overhead lines, [15]) and this

allows approximating the line model by considering only its series impedance. As a result, modeling and functions to be included in the DSSE algorithm can be significantly simplified.

- *Number of nodes*: this represents a critical aspect for distribution systems. In fact, the number of nodes in Medium Voltage (MV) networks can be really high, even some orders of magnitude larger than the number of nodes in transmission systems. This situation is further aggravated if the monitoring of the distribution grid is extended to the Low Voltage (LV) lines. As a consequence, it is clear that computational issues arise, together with demanding requirements for data acquisition and storage in the computational centers; thus, suitable solutions have to be found. First of all, the design of fast and efficient DSSE algorithms, able to reduce execution times and to make real-time operation possible, is essential. From this point of view, it is worth recalling that DSSE algorithms cannot be decoupled in the same way of the estimators for transmission systems, and that a three-phase modeling must be used. These factors imply additional computational burden for the estimator and make the goal of efficiency even more challenging. An alternative solution to deal with the large size of distribution networks (presented in Chapter 6) is the design of suitable Multi-Area State Estimation (MASE) architectures. As an example, DSSE could be decomposed according to the different voltage levels of the network or according to geographical criteria. Even if the MASE approach can bring large improvements in terms of execution times, due attention must be paid to the proper design of both the architecture and the MASE algorithm. In fact, a decomposition in too many areas or the use of inaccurate MASE techniques can lead to a significant loss of accuracy in the estimation results or to additional issues concerning communication.

- *Number of measurement devices*: as already mentioned, distribution networks have been so far poorly monitored networks. As a consequence, measurement instruments installed on the grid are very few, often limited only to the High Voltage to Medium Voltage (HV/MV) substation. Because of the huge number of nodes, the redundancy of available measurement devices is not expected to significantly increase in the near future. To deal with this issue, all the possible information has to be exploited to create the so-called pseudo-measurements. Pseudo-measurements can be defined as non-real-time measurements derived from statistical, historical or forecast data owned by the Distribution System Operator (DSO). In particular, typical profiles of loads and generators can be used to create pseudo-measurements for the power injections at the nodes. The use of such pseudo-measurements allows obtaining the observability of the network and thus to solve the DSSE problem. However, since these data are

not based on real measurements, their modeling into the DSSE algorithm must be done using large uncertainties, and this drastically affects the accuracy of the estimation results. To this purpose, many research efforts are currently ongoing for the development of techniques and methods aimed at providing pseudo-measurements with enhanced accuracy and detailed modeling of their uncertainty (see, for example, [17–19]). As additional issue, since the redundancy of the measurements (even when including pseudo-measurements) is not high, other auxiliary functions of the state estimator could work not properly. As an example, in some cases, the bad data detection and identification function can be unable to detect an erroneous measurement or, even if the detection is successful, it could be unable to properly identify the wrong data (problem of bad data on critical measurements, see [4] for details).

- *Uncertainty of network model*: in the SE framework, the data of the network are usually assumed to be known and they serve as input for the SE algorithm. In distribution systems, however, the knowledge on the line parameters can be highly uncertain, due to the network aging and the lack of recent accurate measurement campaigns. As a result, such uncertainty can more or less heavily affect the accuracy of the estimation results. The impact of this uncertainty on the DSSE model has, therefore, to be duly taken into account and evaluated, in order to guarantee the proper operation of the estimator and the reliability of the achieved results.

1.3 Weighted Least Square estimators

Focusing on the SE algorithms, different approaches can be used to perform SE. All the methods usually refer to the same measurement model, which is used as starting point for defining the objective function implemented in the algorithm.

1.3.1 Measurement model

The measurement model commonly used for SE is:

$$\mathbf{y} = \mathbf{h}(\mathbf{x}) + \mathbf{e} \tag{1.1}$$

where:

- $\mathbf{y}$ is the vector of the available measurements that will be used as input in the SE algorithm; measurements can be voltages on the nodes and currents or active and reactive powers either on the branches or on the node injections.

- $\mathbf{x}$ is the vector of the chosen state variables; according to the traditional design of power system state estimators, it is usually composed by the voltage magnitudes and angles at all the network buses; more in general, however, the state of the system can be defined as a set of variables that, once known, allows the computation of all the electrical quantities of the network. Thus, different options for the choice of the state vector are possible.

- $\mathbf{h}(\mathbf{x})$ is the vector of measurement functions (in general nonlinear) linking measurements $\mathbf{y}$ to the state variables $\mathbf{x}$; basically, each function expresses the associated measured quantity in terms of the adopted state variables.

- $\mathbf{e}$ is the vector of the measurement errors; traditionally, they are considered as zero mean ($E(e_i) = 0$), decorrelated ($E(e_i e_j) = 0$, for $i \neq j$) errors, thus with a resulting diagonal covariance matrix ($\Sigma_y = E(\mathbf{e}\mathbf{e}^T) = \text{diag}(\sigma_i^2)$, where σ_i is the standard deviation associated to the i-th measurement y_i).

1.3.2 WLS method

Despite the large number of alternatives proposed in the literature (see, for example, [20–25]), most of the estimators implemented in transmission system control centers refer to a same approach, the Weighted Least Squares (WLS) method.

As for DSSE, different alternative approaches are also possible. In [26], some of the techniques most used in transmission systems have been compared to test their performance when adapted to work in a distribution system context. The analysis shows that the WLS method has the best performance in terms of bias, consistency and quality of the estimation results, and thus it can be considered a proper choice for use also in DSSE.

In the WLS approach, the estimation algorithm is designed to achieve the minimization of the following objective function:

$$J(x) = \sum_{i=1}^{M} w_i \left[y_i - h_i(x)\right]^2 \tag{1.2}$$

where w_i is the weight assigned to the i-th measurement, and M is the total number of measurements available as input for the estimator. The term $y - h(x)$, that is the difference between measured value and corresponding quantity obtained as a function of the state vector, is commonly indicated in the literature as measurement residual.

Equation (1.2) can be generalized in matrix form as:

$$J(x) = \left[\mathbf{y} - \mathbf{h}(\mathbf{x})\right]^T \mathbf{W} \left[\mathbf{y} - \mathbf{h}(\mathbf{x})\right] \tag{1.3}$$

where $\mathbf{W}$ is a resulting $M \times M$ weighting matrix, having the weights w_i on the diagonal elements. The weighting matrix plays a critical role in the WLS approach. In fact, it allows considering the different reliability of measurements, giving more importance to those with higher accuracy. For a proper modeling of the WLS method, it should be chosen as the inverse of the covariance matrix Σ_y of the measurement errors.

The minimization of the objective function $J(x)$ is usually obtained using an iterative Gauss-Newton method. Its application (see [4] for details) leads, at each iteration k, to the following equation system (often referred to as *normal equations* in the literature) to be solved:

$$\mathbf{G}(\mathbf{x}_k)\Delta\mathbf{x}_k = \mathbf{H}_k^T\mathbf{W}\left[\mathbf{y} - \mathbf{h}(\mathbf{x}_k)\right] \tag{1.4}$$

where $\mathbf{H}_k = \mathbf{H}(\mathbf{x}_k)$ is the Jacobian of the measurement functions $\mathbf{h}(\mathbf{x})$, $\mathbf{G}(\mathbf{x_k}) = \mathbf{H}_k^T\mathbf{W}\mathbf{H}_k$ is the so-called Gain matrix, and $\Delta\mathbf{x}_k$ is the updating state vector used to compute the new state according to the following:

$$\mathbf{x}_{k+1} = \mathbf{x}_k + \Delta\mathbf{x}_k \tag{1.5}$$

The iterative process continues until a specified convergence criterion is achieved. Usually, the largest absolute element in the updating state vector $\Delta\mathbf{x}$ is compared to a defined tolerance threshold ϵ, and the algorithm stops when $max(|\Delta\mathbf{x}|) < \epsilon$. The state vector obtained at the last iteration is the estimation outcome provided by the WLS algorithm.

1.4 Branch Current based estimators

First works proposing state estimators specifically conceived for distribution systems date back to the 1990's. A first attempt to address the DSSE issue, relying on a minimum number of available measurement devices, was performed in [27]. In [28, 29], instead, the need to use three-phase models for the modeling of distribution networks was highlighted. To this purpose, the traditional WLS method was adapted to include the three-phase framework and to consider the mutual coupling among the different phases. In [30, 31], different alternatives for the state variables to be used into the DSSE algorithm were proposed. In [30], the WLS algorithm was modified to use the node voltages in rectangular coordinates in place of the traditionally used voltage magnitudes and angles. Some approximations were also made to achieve a decoupled version of this estimator. In [31], instead, Baran and Kelley proposed for the first time the use of a WLS estimator based on branch currents (in rectangular coordinates) as state variables. Such a solution allows exploiting the radial or weakly meshed topology of the distribution grids and to develop simpler and faster estimators.

In the following years, several works have contributed to the development of enhanced Branch Current Distribution System State Estimation (BC-DSSE) algorithms. In [32], the first version of the BC-DSSE was modified in order to achieve a per-phase decoupled version of the estimator. However, both the algorithms proposed in [31, 32] initially allowed processing only power and current measurements. For this reason, developments of these original versions have been presented afterwards in [33, 34], where possible formulations to include the voltage magnitude measurements in the estimator model are presented.

1.4.1 Framework of BC-DSSE

The BC-DSSE approach is based on an iterative WLS algorithm composed, at each iteration, of the following three main steps:

1) definition/update of input measurements;
2) solution of the normal equations (1.4) of the WLS problem;
3) forward sweep calculation to compute the bus voltages of the network.

In the first step, the definition or update of the measurements is required to convert power measurements in equivalent current measurements. This process has been introduced to allow an easier treatment of possible power flow measurements and, above all, of the pseudo-measurements of node power injections. In fact, given a pair of active and reactive power, the following equivalent current measurements can be calculated at each iteration k:

$$i_k^r + j i_k^x = \left(\frac{P + jQ}{v_k} \right)^* \tag{1.6}$$

where i^r and i^x are the real and imaginary components of the current, P and Q are the active and reactive measured powers to be converted, and v_k is the complex voltage available at iteration k either in the node of the power injection or in the sending node of the measured branch power (depending on the type of power measurement). The operator * is instead the complex conjugate operator.

As it can be observed, such transformation converts the power measurements in the same quantities used as state variables in the WLS algorithm, thus allowing an easy and linear inclusion in the estimator. This operation can be really convenient in terms of efficiency of the algorithm, above all considering that the pseudo-measurements of power injection represent, of course, the majority of the input measurements to be processed.

In the second step of the algorithm, relying on the collected input measurements and assuming the knowledge of topology and data of the network, the WLS problem described in Section 1.3.2 has to be solved. The main novelty of the BC-DSSE approach is in the choice of the state variables; in this case, according to the proposals

presented in [31–34], and considering the three-phase formulation of the estimator, the state vector $\mathbf{x}$ is:

$$\mathbf{x} = [\mathbf{x}_A, \mathbf{x}_B, \mathbf{x}_C] \tag{1.7}$$

where the generic state vector $\mathbf{x}_\phi$ associated to phase ϕ (with $\phi = A, B, C$) is:

$$\mathbf{x}_\phi = [i^r_{1\phi}, ..., i^r_{N_{br}\phi}, i^x_{1\phi}, ..., i^x_{N_{br}\phi}] \tag{1.8}$$

with the generic variable $i_{i\phi}$ indicating the current on the i-th branch of phase ϕ and with N_{br} equal to the total number of branches for the considered phase.

Consistently with the used state vector, measurement functions $h(x)$ and Jacobian matrix $H(x)$ have to be calculated, and then the normal equations (1.4) can be solved.

Finally, once the state of the branch currents at iteration k is obtained, the voltages at all the network buses are computed by means of a forward sweep calculation. In the forward sweep, starting from the voltage at the HV/MV substation node, all the remaining voltages are achieved, descending the network and exploiting the temporarily estimated branch currents, through a simple calculation of the voltage drops along the lines. Since the knowledge of the voltage at the HV/MV substation is needed to compute all the remaining ones, in [31] it is proposed, to this purpose, to use the voltage measurement in substation (which is usually available) or, if this is not possible, to set such voltage to 1 per unit (or the rated voltage of the system).

It is worth to recall that, since DSSE has to consider the three-phase nature of the network, the calculation of the voltage drops has to duly consider the mutual coupling among the phases. Thus, given a generic three-phase line, like the one depicted in Fig. 1.2, the voltage on the ending node is given by:

$$\begin{bmatrix} v_{2A} \\ v_{2B} \\ v_{2C} \end{bmatrix} = \begin{bmatrix} v_{1A} \\ v_{1B} \\ v_{1C} \end{bmatrix} - \begin{bmatrix} z_{AA} & z_{AB} & z_{AC} \\ z_{BA} & z_{BB} & z_{BC} \\ z_{CA} & z_{CB} & z_{CC} \end{bmatrix} \begin{bmatrix} i_A \\ i_B \\ i_C \end{bmatrix} \tag{1.9}$$

where z_{ii} (with $i = A, B, C$) is the self impedance of phase i and z_{ij} (with $j = A, B, C$ but $\neq i$) is the mutual impedance between phases i and j.

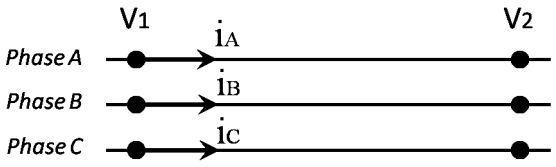

Figure 1.2: Three-phase line.

It is important to underline that the forward sweep is an essential step, not only to obtain the voltage profile of the network and to make it available as output of the estimator, but, above all, to update the estimated voltages and to allow, in this way, the refinement of the equivalent current measurements at each iteration.

As in generic WLS estimators, the BC-DSSE algorithm stops when the largest absolute element of the updating state vector $\Delta\mathbf{x}$ is smaller than a chosen threshold ϵ.

1.4.2 Measurement functions h(x)

Traditional measurements that can be included in the BC-DSSE are: active and reactive power (either on a branch or on a node injection), current magnitude on a branch and voltage magnitude on a node. To solve the WLS problem, all the corresponding measurement functions, which express the measured quantity in terms of the state variables, have to be defined.

- **Active and reactive power flow**

  As described in the previous subsection, in BC-DSSE active and reactive powers are converted in equivalent current measurements. Thus, indicating with $h^{eq}_{i^r_{l\phi}}$ and $h^{eq}_{i^x_{l\phi}}$ the measurement functions associated to the real and the imaginary part of the equivalent current obtained for a power flow measurement on branch l of phase ϕ, it is:

  $$h^{eq}_{i^r_{l\phi}} + jh^{eq}_{i^x_{l\phi}} = \alpha(i^r_{l\phi} + ji^x_{l\phi}) \tag{1.10}$$

  where $\alpha = 1$ if the measured power is in the same direction of the corresponding branch current used in the state vector and $\alpha = -1$ if the power is in the opposite verse. As it can be observed, obviously, the transformation of the powers in equivalent currents leads to a linear relationship for this measurement function. Moreover, these functions are only related to state variables ($i^r_{l\phi}$ and $i^x_{l\phi}$) belonging to the same phase of the measurement, thus, there is no coupling among the different phases.

- **Active and reactive power injection**

  Similarly to the previous case, the power injections are converted in equivalent current injections. The associated measurement functions, for the equivalent current injection on phase ϕ of node i, are:

  $$h^{eq}_{i^r_{inj,i\phi}} + jh^{eq}_{i^x_{inj,i\phi}} = \alpha\left[\sum_{k\in\Omega}(i^r_{k\phi} + ji^x_{k\phi}) - \sum_{m\in\Lambda}(i^r_{m\phi} + ji^x_{m\phi})\right] \tag{1.11}$$

where Ω is the set of branches incoming on node i and Λ is the set of branches outgoing from node i. The variable α in this case, instead, is equal to 1 if the considered power injection is drawn from the network (like for a load), while it is equal to -1 in the opposite case (like for a generator). Even in this case, it is possible to observe that the obtained measurement functions are linearly related to the state variables and that no coupling exists among the different phases.

- **Current magnitude**

  The function associated to a current magnitude measurement $I_{l\phi}$ on phase ϕ of a generic line l is:

  $$h_{I_{l\phi}} = \sqrt{{i^r_{l\phi}}^2 + {i^x_{l\phi}}^2} \tag{1.12}$$

  It is possible to notice that current magnitude measurements introduce non-linearities in the estimator model and lead to the coupling between real and imaginary state variables. However, they are still related to state variables belonging only to the same phase ϕ of the measurement, thus, no coupling among the different phases is introduced.

- **Voltage magnitude**

  The voltage phasor $v_{i\phi}$ on the phase ϕ of a generic node i, can be expressed as:

  $$v_{i\phi} = v_{1\phi} - \sum_{k\in\Gamma} \mathbf{Z}_{k,\phi}\mathbf{i}_k \tag{1.13}$$

  where $v_{1\phi}$ is the voltage phasor on phase ϕ of the starting node of the network (that is usually chosen to be the HV/MV substation bus), $\mathbf{Z}_{k,\phi}$ and $\mathbf{i}_k$ are, respectively, the row related to phase ϕ of the three-phase impedance matrix and the column vector of the three-phase currents associated to branch k, and Γ is the set of branches in the path between the starting node and the considered bus i.

  The related voltage magnitude measurement $V_{i\phi}$ can, instead, be expressed as:

  $$V_{i\phi} = \left[v_{1\phi} - \sum_{k\in\Gamma} \mathbf{Z}_{k,\phi}\mathbf{i}_k \right] e^{-j\delta_{i\phi}} \tag{1.14}$$

  where $\delta_{i\phi}$ is the angle of the considered voltage on the phase ϕ of node i. With further modifications, it is possible to write:

  $$V_{i\phi} = Re\left[V_{1\phi} e^{j(\delta_{1\phi} - \delta_{i\phi})} - \sum_{k\in\Gamma} \mathbf{Z}_{k,\phi}\mathbf{i}_k e^{-j\delta_{i\phi}} \right] \tag{1.15}$$

and the final function of the voltage magnitude measurement is:

$$h_{V_{i\phi}} = V_{1\phi}\cos(\delta_{1\phi}-\delta_{i\phi}) - \sum_{k\in\Gamma}(\mathbf{R}_{k,\phi}\mathbf{i}_k^r - \mathbf{X}_{k,\phi}\mathbf{i}_k^x)\cos(\delta_{i\phi}) - \sum_{k\in\Gamma}(\mathbf{X}_{k,\phi}\mathbf{i}_k^r + \mathbf{R}_{k,\phi}\mathbf{i}_k^x)\sin(\delta_{i\phi}) \tag{1.16}$$

where $\mathbf{R}_{k,\phi}$ and $\mathbf{X}_{k,\phi}$ are the real and imaginary part, respectively, of the considered row vector of the three-phase impedance matrix $\mathbf{Z}_{k,\phi}$ of the branch k. As it can be observed, found relationship for the voltage magnitude measurement is nonlinear and introduces in the estimator model coupling both between real and imaginary components of the currents, and among the different phases of the system.

To solve the WLS problem, besides the definition of the measurement functions, the computation of their derivatives with respect to each state variable has to be developed in order to achieve the Jacobian matrix. Details on the Jacobian terms resulting for each measurement function are provided in Appendix A.1.

1.5 New formulation of BC-DSSE

Branch-current based estimators proposed in [31–34] can be potentially well suited to the problem of DSSE. In fact, they are able to easily include the pseudo-measurements about power injections on the nodes, which are the majority of the measurements available in distribution systems; moreover, they can also include current magnitude measurements without too much complex functions, as it is the case, instead, of the traditional voltage-based estimators. However, the formulations provided in [31–34] show some issues in specific cases. In particular:

- The voltage profile of the network is obtained through the forward sweep step starting from the voltage measurement in the HV/MV substation; thus, the accuracy of the voltage profile is drastically affected by the uncertainty of such voltage measurement; moreover, further issues can arise in case of unavailability or bad data for this measurement.

- Despite the efforts made in [33,34] to include the voltage measurements in the BC-DSSE model, both the papers show that this kind of measurement does not have a clear impact on the accuracy of the BC-DSSE results.

- Reference papers on BC-DSSE date back to the 1990's. As a result, they only consider the possibility to have traditional measurements as input to the estimator. However, recently, new generation measurement devices, such as Phasor Measurement Units (PMUs), are becoming widespread on the market. Therefore, the estimator model has to be adapted in order to include the measurements provided also by these new measurement instruments.

In [35,36], a new formulation of the BC-DSSE model has been proposed to solve the aforementioned issues and to consider phasor measurements. The following subsections present the proposed model and the overall structure of the designed BC-DSSE algorithm. Next section shows the benefits coming from the proposed new formulation. The following section, instead, deals with the inclusion of phasor measurements provided by PMUs in the estimator model.

1.5.1 Extension of the state vector

The voltage profile of a grid is one of the most important information needed in the control center of a network. For this reason, the problems inherent to the proposed versions of the BC-DSSE are a significant limit to its applicability in a real context. To deal with this issue, and to allow an accurate estimation even for the voltage profile, in [35, 36] the BC-DSSE model has been modified to include the slack bus voltage as state variable into the state vector. As a consequence, the proposed new state vector to be used in the estimator model is:

$$\mathbf{x} = [\mathbf{x}_A, \mathbf{x}_B, \mathbf{x}_C] \tag{1.17}$$

with the total state vector composed of the single vectors associated to each phase of the system, and with the generic single-phase state vector $\mathbf{x}_\phi$ equal to:

$$\mathbf{x}_\phi = [V_{s\phi}, i^r_{1\phi}, ..., i^r_{N_{br}\phi}, i^x_{1\phi}, ..., i^x_{N_{br}\phi}] \tag{1.18}$$

where $V_{s\phi}$ is the voltage magnitude of the chosen slack bus of the network on the phase ϕ.

It is worth recalling that, in general, the slack bus voltage is usually used in power networks as a reference for the angles of all the electrical quantities of the system. Thus, the slack bus voltage angle of the first phase is usually set equal to zero and all the other angles are defined as angle differences with respect to this reference. As a consequence, the estimation of the voltage magnitude is sufficient to obtain a complete information on the voltage state of the slack node, and this allows computing all the remaining voltages at the other nodes of the network exploiting the result of such estimation.

It is also important to highlight that the proposed solution meets the proper definition of *state* of a network. In fact, as mentioned in the previous sections, the state of a network can be defined as a set of variables that allow the complete knowledge of the system and, thus, the computation of all the other quantities representative of the network. With the only current state variables this was not possible due to the lack of information for the voltages. Instead, with the inclusion of the slack bus voltage, the definition is now fully respected, and all the other electrical quantities of the grid can be obtained starting from the estimated values.

With respect to the previous formulation, the new one is expected to provide the following advantages:

- to obtain a larger impact on the estimation results by using voltage measurements;
- to achieve an improved knowledge of the slack bus voltage state and a more accurate estimation of the overall voltage profile of the network.

1.5.2 The proposed estimator

The branch-current based estimator here proposed basically keeps many of the features of the original version of BC-DSSE proposed by Baran and Kelley. The main differences are the addition of the slack bus voltage in the state vector and some other details that are described in the following subsections. The overall structure of the estimation algorithm is composed of the following steps:

1) initialization of the state vector $\mathbf{x}$;
2) building of the weighting matrix $\mathbf{W}$;
3) building of the constant Jacobian sub-matrices;
4) start of the iterative procedure;
5) computation of the equivalent current measurements and update of the measurement vector $\mathbf{y}$;
6) building of the non-constant Jacobian sub-matrices;
7) computation of the measurement functions $\mathbf{h}(\mathbf{x})$;
8) calculation of the measurement residuals $\mathbf{r} = \mathbf{y} - \mathbf{h}(\mathbf{x})$;
9) calculation of the Gain matrix $\mathbf{G} = \mathbf{H}^T\mathbf{W}\mathbf{H}$;
10) solving of the normal equations $\mathbf{G}\Delta\mathbf{x}_k = \mathbf{H}^T\mathbf{W}\mathbf{r}$;
11) update of the state vector $\mathbf{x}_{k+1} = \mathbf{x}_k + \Delta\mathbf{x}_k$;
12) execution of the forward sweep step to compute the voltage at the different buses;
13) check of the convergence criterion: if $max(|\Delta\mathbf{x}|) < \epsilon$ then quit the iterative procedure, otherwise go back to step 5.

1.5.3 State initialization

The initialization of the state vector is a procedure that, if properly designed, can lead to a faster convergence of the estimation algorithm. The simplest approach, but also the least efficient, is to initialize the state vector with the so-called flat start. According to this approach all the voltage magnitudes should be set equal to 1 p.u., while the current magnitudes should be set equal to 0. As for the angles, both voltage and current angles should be set equal to 0 for the first phase and $\pm 120°$ for the other phases. Such initialization, since the initial conditions are far from the real ones, leads to a significant number of iterations for the algorithm to converge. Moreover, in [31], where this approach is implemented, the need to discard the current magnitude measurements in the first step of the algorithm is pointed out, since the starting angles of the currents would lead to a wrong calculation of the related Jacobian terms.

In [32], to improve the convergence properties of the algorithm, the current angles are proposed to be set with the opposite angle with respect to the one of the power measurement in substation (that is usually an available measurement). In fact, since it is $S = vi^*$ (where S is the complex power in substation) and under the assumption $v = 1\angle 0$ p.u., it is possible to find that the angles of S and i are equal but opposite in sign. Thus, according to [32], for a feeder with a good power factor it is a good choice to initially set all the currents with such angle value (for the first phase, while angles of the other phases are obtained in the same way but then shifted of $\pm 120°$). In this way, differently from the flat start, it is possible to use the current magnitude measurements also in the first step. However, this procedure works properly only in case of radial networks.

In the proposed BC-DSSE algorithm, a different approach has been conceived to enhance the state initialization. The proposed technique is based on the knowledge of the node power injections (nodes can be load or generation buses where at least the pseudo-measurements should be available, or a priori known zero injection nodes). The power injection on a generic node i can be written as:

$$S_i = v_i \left[\sum_{k \in \Omega} i_k - \sum_{m \in \Lambda} i_m \right] \tag{1.19}$$

where Ω is the set of branches incoming in node i and Λ is the set of branches outgoing from i (with the assumption that powers drawn by loads are positive and powers provided by generators are negative).

Eq. (1.19) can be written in matrix form as:

$$S_i = v_i \mathbf{A}_i \mathbf{i} \tag{1.20}$$

where $\mathbf{i}$ is the column vector of the branch currents of the network and $\mathbf{A}_i$ is a row

vector having terms equal to ± 1 in the positions associated to the currents involved in the considered power injection.

Starting from eq. (1.20), for each phase ϕ, the initialization can be performed using: the value of the voltage measurement $v_{s\phi}$ in substation for all the power injections (the voltage magnitude measurement is usually available and the angle can be set equal to 0 or $\pm 120°$ depending on the considered phase); the row vectors $\mathbf{A_{i\phi}}$ (which depend only on the topology of the network); the known values of the power injections $\mathbf{S}_{i\phi}$. Writing the equation in matrix form, it is:

$$\mathbf{S}_\phi = v_{s\phi}\mathbf{A}_\phi\mathbf{i}_\phi = \mathbf{U}_\phi\mathbf{i}_\phi \tag{1.21}$$

where $\mathbf{S}_\phi$ is the column vector of the power injections, $\mathbf{A}_\phi$ is a matrix composed of the vectors $\mathbf{A_{i\phi}}$ on the rows, and $\mathbf{U}_\phi$ is the matrix obtained from the multiplication $v_{s\phi}\mathbf{A}_\phi$.

It is worth noting that in case of radial networks, both the branch currents and the pseudo-measurements are $n-1$ (where n is the total number of nodes of the grid), since the slack bus (substation) is commonly not considered in the set of the pseudo-measurements. Thus, matrix $\mathbf{U}_\phi$ is a square matrix that can be inverted to find:

$$\mathbf{i}_\phi = {\mathbf{U}_\phi}^{-1}\mathbf{S}_\phi \tag{1.22}$$

The obtained vector is the initialization for the current state of phase ϕ. The initialization for the voltages can be then achieved through a forward sweep, considering the voltage drops starting from the slack bus voltage in substation.

The approach proposed until now works properly only in case of radial networks. If some meshes are present, the number of branches increases while the number of pseudo-measurements does not change: thus, the equation system (1.21) is not solvable, since the number of unknowns is larger than the number of equations. To handle this issue, the following constraint on the Kirchhoff's voltage law on the meshes can be added to the equation system:

$$\sum_{j\in\Psi} \alpha_j \mathbf{Z}_j \mathbf{i}_j = 0 \tag{1.23}$$

where Ψ is the set of branches involved in the considered mesh, $\mathbf{Z}_j$ and $\mathbf{i}_j$ are the three-phase impedance matrix and the three-phase current vector associated to branch j, respectively, and α_j is ± 1 depending on the reference mesh direction with respect to the direction of branch j.

It is worth noting that the presence of meshes causes the coupling among the different phases of the network. Therefore, a three-phase equation system is needed. Building the three-phase version of the equation system in (1.21) and adding the mesh constraints, the following holds:

$$\begin{bmatrix} \mathbf{S}_A \\ \mathbf{S}_B \\ \mathbf{S}_C \\ 0 \end{bmatrix} = \begin{bmatrix} \mathbf{U}_A & 0 & 0 \\ 0 & \mathbf{U}_B & 0 \\ 0 & 0 & \mathbf{U}_C \\ \mathbf{U}_{mesh} \end{bmatrix} \begin{bmatrix} \mathbf{i}_A \\ \mathbf{i}_B \\ \mathbf{i}_C \end{bmatrix} \tag{1.24}$$

where $\mathbf{U}_{mesh}$ is a matrix containing in each row the impedance terms (in the position corresponding to the branch currents to be multiplied) determining the mesh constraint. Writing (1.24) in compact form, it is:

$$\mathbf{S}_{tot} = \mathbf{U}_{tot}\mathbf{i} \tag{1.25}$$

It is worth noting that each additional branch with respect to the radial tree of the network leads to a mesh constraint, thus in the extended equation system the number of unknown branch currents is equal to the number of available equations and $\mathbf{U}_{tot}$ is a square matrix that can be inverted to provide:

$$\mathbf{i} = \mathbf{U}_{tot}^{-1}\mathbf{S}_{tot} \tag{1.26}$$

As in the case of radial systems, the resulting vector provides the initialization for the current state, while the voltage initialization can be then achieved by means of a forward sweep step.

Finally, it is important to underline that the state initialization approach presented here is proposed to improve the convergence properties of the algorithm when any other information is missing. However, in a real environment, the state estimator can rely on the knowledge of the quantities estimated in the previous time step. Thus, in such a scenario, the best choice should be to use the previously estimated quantities as initial state. In particular, in case of high reporting rate for the SE tool and with quasi-stationary operating conditions, such choice can provide an initialization really close to the real conditions, thus allowing a significant reduction of the number of iterations required from the algorithm to converge, and consequently decreasing the total execution times.

1.5.4 Equivalent current measurements

In Section 1.4, the conversion of the power measurements (or pseudo-measurements) in equivalent currents has been introduced. The following relationship is used:

$$i^r + ji^x = \left(\frac{P + jQ}{v}\right)^* \tag{1.27}$$

For a proper modeling, due attention must be paid to the resulting uncertainties of the currents, which have to be calculated for obtaining the weights to be included in the weighting matrix of the SE algorithm.

Manipulating eq. (1.27), the following can be obtained:

$$i^r + ji^x = \frac{(P - jQ)(v^r + jv^x)}{V^2} \tag{1.28}$$

Considering the voltage magnitude approximately equal to 1 p.u., it is:

$$i^r = P\cos\delta + Q\sin\delta \tag{1.29}$$

$$i^x = P\sin\delta - Q\cos\delta \tag{1.30}$$

where δ is the angle of the voltage that, in first approximation, can be considered as 0 for the first phase and $\pm 120°$ for the other phases.

Taking into account the power uncertainties and the law of propagation of the uncertainty, the following holds:

$$\left[\mathbf{\Sigma}_{i^{rx}}\right] = \left[\frac{\partial \mathbf{f}_i rx}{\partial \mathbf{x}_{pq}}\right] \left[\mathbf{\Sigma}_{pq}\right] \left[\frac{\partial \mathbf{f}_i rx}{\partial \mathbf{x}_{pq}}\right]^T \tag{1.31}$$

where $\mathbf{\Sigma}_{pq}$ and $\mathbf{\Sigma}_{i^{rx}}$ are the covariance matrix of the measurement errors in P and Q and the unknown covariance matrix of the resulting measurement errors in i^r and i^x, respectively, while the derivative matrix is a matrix including the derivatives of the functions associated to i^r and i^x (see equations (1.29) and (1.30)) with respect to the variables P and Q.

Expanding the matrices in (1.31), it is possible to obtain:

$$\begin{bmatrix} \sigma^2_{i^r} & \sigma_{i^r i^x} \\ \sigma_{i^r i^x} & \sigma^2_{i^x} \end{bmatrix} = \begin{bmatrix} \cos\delta & \sin\delta \\ \sin\delta & -\cos\delta \end{bmatrix} \begin{bmatrix} \sigma^2_P & \sigma_{PQ} \\ \sigma_{PQ} & \sigma^2_Q \end{bmatrix} \begin{bmatrix} \cos\delta & \sin\delta \\ \sin\delta & -\cos\delta \end{bmatrix} \tag{1.32}$$

where σ^2_P and σ^2_Q are the variances of P and Q, σ_{PQ} is the possible covariance existing between P and Q, and $\sigma^2_{i^r}$, $\sigma^2_{i^x}$ and $\sigma_{i^r i^x}$ are the similar variance and covariance terms referred to the currents i^r and i^x.

Assuming the covariance σ_{PQ} as null, the following results can be found:

$$\sigma^2_{i^r} = \sigma^2_P \cos^2\delta + \sigma^2_Q \sin^2\delta \tag{1.33}$$

$$\sigma^2_{i^x} = \sigma^2_P \sin^2\delta + \sigma^2_Q \cos^2\delta \tag{1.34}$$

$$\sigma_{i^r i^x} = \cos\delta \sin\delta (\sigma^2_P - \sigma^2_Q) \tag{1.35}$$

From the obtained relationships, it is possible to observe that in case of $\delta = 0$, the covariance term is null and the variances of i^r and i^x are equivalent to the ones of P and Q. Instead, when $\delta = \pm 120°$, both the variances and the covariances are nonzero terms and have to be taken into account. As a result, the weights to be considered in the weighting matrix of the BC-DSSE algorithm can be obtained through the inversion of the 2×2 covariance matrix $\mathbf{\Sigma}_{i^{rx}}$ and have to include also the resulting covariance terms.

1.5.5 Building of Jacobian and measurement functions

The measurement functions used in the new formulation of the BC-DSSE algorithm are the same described in Section 1.4.2. Some changes arise instead for the Jacobian matrix, due to the inclusion of the voltage slack bus into the state vector. In fact, the Jacobian terms are the derivatives of the measurement functions with respect to the state variables used in the state vector. Thus, because of the additional voltage into the state vector, also the derivatives with respect to the slack bus voltage state variable have to be calculated. Appendix A.1 reports the Jacobian terms for the derivatives with respect to the real and imaginary current variables. Appendix A.2 reports, instead, the additional terms of the Jacobian associated to the derivatives with respect to the slack bus voltage.

From an implementation standpoint, it is important to observe that some of the measurement functions used in BC-DSSE are linear. This means that the associated Jacobian sub-matrix is constant. Therefore, the computation of these sub-matrices can be made outside the iterative procedure required to solve the WLS problem, in order to reduce the execution times. Moreover, once built the constant Jacobian sub-matrix $\mathbf{H}_y$, the related measurement functions $\mathbf{h}_y(\mathbf{x})$ can be simply computed as a matrix multiplication $\mathbf{H}_y\mathbf{x}$ between Jacobian and temporary state vector. Since the pseudo-measurements, which are the majority of the available input measurements for the estimator, are characterized by linear functions, such implementation scheme allows obtaining important benefits in terms of execution times.

As for the nonlinear measurement functions, instead, the resulting Jacobian sub-matrices depend on the variables included in the state vector, thus they should be updated at each iteration of the WLS procedure. In some papers, it is proposed to stop in any case the update of the Jacobian after a given number of iterations, because if the algorithm is close to converge the changes in the Jacobian terms are minimal. However, the number of iterations needed to converge is strictly dependent on the type of network and on its operating conditions. For this reason, here, the Jacobian sub-matrices related to nonlinear functions are always updated at each iteration of the WLS procedure.

1.5.6 Forward sweep step

As described in Section 1.4, the forward sweep calculation is an essential step in the BC-DSSE model since it allows the computation of all the bus voltages that are needed to refine the equivalent current measurements. Differently from the original proposal of Baran and Kelley in [31], in the BC-DSSE formulation here proposed this calculation is performed starting from the estimated slack bus voltage (instead of the measured substation voltage) and then computing the voltage drops along the lines resulting due to the estimated currents. Thus, the quantities involved in

this calculation are: the estimated state variables (both the slack bus voltage and the currents) and the impedances of the branches in the path between the slack bus and each considered node.

The execution of this step can be performed by building a predefined matrix $\mathbf{Z}_{nod}$, which depends on the particular topology of the network, containing the impedance terms needed to compute the voltage drops involved in the calculation of each bus voltage. Therefore, it can be written:

$$\mathbf{v} = \mathbf{v_{slack}} - \mathbf{Z}_{nod}\mathbf{i} \tag{1.36}$$

where $\mathbf{v}$ is the column vector of the complex voltages of each node of the network; $\mathbf{v_{slack}}$ is a column vector (with the same size of $\mathbf{v}$) composed of the estimated slack bus voltage; $\mathbf{i}$ is the column vector of the complex branch currents.

Expanding eq. (1.36) to highlight all the three-phase components, it is:

$$\begin{bmatrix} \mathbf{v}_A \\ \mathbf{v}_B \\ \mathbf{v}_C \end{bmatrix} = \begin{bmatrix} \mathbf{v}_{slackA} \\ \mathbf{v}_{slackB} \\ \mathbf{v}_{slackC} \end{bmatrix} - \begin{bmatrix} \mathbf{Z}_{nod}^{AA} & \mathbf{Z}_{nod}^{AB} & \mathbf{Z}_{nod}^{AC} \\ \mathbf{Z}_{nod}^{BA} & \mathbf{Z}_{nod}^{BB} & \mathbf{Z}_{nod}^{BC} \\ \mathbf{Z}_{nod}^{CA} & \mathbf{Z}_{nod}^{CB} & \mathbf{Z}_{nod}^{CC} \end{bmatrix} \begin{bmatrix} \mathbf{i}_A \\ \mathbf{i}_B \\ \mathbf{i}_C \end{bmatrix} \tag{1.37}$$

where the subscripts A, B and C indicate the phase to which the vectors are referred. As for the matrix $\mathbf{Z}_{nod}$, the sub-matrices included in the diagonal blocks contain the self-impedance terms of the branches involved in each voltage drop calculation, while the sub-matrices outside the diagonal blocks include the related mutual impedance terms.

1.5.7 Treatment of meshes

Differently from the voltage based estimators, which can handle the meshes without particular modifications of the algorithm, the BC-DSSE model has to be duly adapted to consider possible meshes and the consequent presence of additional current state variables associated to the reclosing branches. To deal with this issue, both [31] and [32] propose the inclusion in the estimator model of the constraint given by the Kirchhoff's voltage law along the mesh. Possible methods to include the equality constraints in the BC-DSSE model are described with more details in Chapter 2. Here, a simple way to tackle this issue is presented, that is the inclusion of the mesh constraint as a virtual measurement.

According to the virtual measurement approach, the constraint has to be considered as any other measurement. Thus, both the measurement function and the related Jacobian sub-matrix have to be computed.

The Kirchhoff's voltage law constraint can be expressed in the following way:

$$\sum_{h \in \Psi} \alpha_h \mathbf{Z}_h \mathbf{i}_h = 0 \tag{1.38}$$

where Ψ is the set of branches involved in the considered mesh, $\mathbf{Z}_h$ is the three-phase impedance matrix of branch h, $\mathbf{i}_h$ is the three-phase vector of the complex currents associated to branch h, and α_h is $+1$ or -1 depending on the mesh direction with respect to the conventional direction assumed for the current of branch h.

Equation (1.38) can be also written in the following form:

$$\sum_{h\in\Psi} \alpha_h \left[(\mathbf{R}_h \mathbf{i}_h^r - \mathbf{X}_h \mathbf{i}_h^x) + j(\mathbf{X}_h \mathbf{i}_h^r + \mathbf{R}_h \mathbf{i}_h^x)\right] = 0 \tag{1.39}$$

where $\mathbf{R}_h$ and $\mathbf{X}_h$ are the real and the imaginary parts of the three-phase impedance matrix $\mathbf{Z}_h$, respectively.

As it can be observed, each mesh includes two constraints, one for the real part of the equation and the other one for the imaginary part. As a result, the following two measurement functions can be obtained:

$$h_{mesh}^r = \sum_{h\in\Psi} \alpha_h (\mathbf{R}_h \mathbf{i}_h^r - \mathbf{X}_h \mathbf{i}_h^x) \tag{1.40}$$

$$h_{mesh}^x = \sum_{h\in\Psi} \alpha_h (\mathbf{X}_h \mathbf{i}_h^r + \mathbf{R}_h \mathbf{i}_h^x) \tag{1.41}$$

The found relationships show that the mesh constraints can be expressed through linear measurement functions. Consequently, the related Jacobian sub-matrix is constant and can be built outside the iterative WLS procedure. Details on the Jacobian terms associated to the mesh constraints, when considered as virtual measurements, can be found in Appendix A.3.

It is worth noting that, if the mesh involves all the three phases of the system, then there are two constraints for each phase, that is overall six constraints to be included in the BC-DSSE model. The virtual measurements associated to the meshes must be set equal to zero and, since these are actually constraints, a large weight must be assigned to each one of them to emphasize their high confidence.

1.6 Advantages of the new formulation

This section presents the benefits brought by the new BC-DSSE model on the accuracy of the estimation results. To this purpose, some tests have been performed on the simple 18-bus network depicted in Fig. 1.3. Details about the line parameters and the rated load consumption can be found in [37]. Generation of 0.35 MW and 0.75 MW has been considered in nodes 7 and 14, respectively.

Tests have been performed by means of a Monte Carlo approach through 25000 trials. True reference operating conditions have been calculated by considering the nominal load consumption and by performing a power flow computation. Then, for

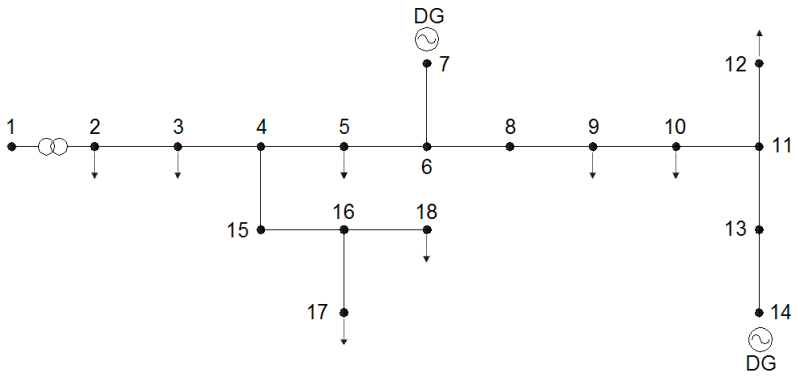

Figure 1.3: 18-bus test network.

each Monte Carlo iteration, measurements are extracted taking into account the assumed measurement uncertainties. In particular: pseudo-measurements on both load and generation nodes have been considered with a maximum deviation of 50% with respect to the nominal values of active and reactive power and with Gaussian distributions; voltage magnitude measurements have been assumed to be available in substation (node 1) and on nodes 4 and 11, with normal distribution and maximum value equal to 1%; measurement of active and reactive power has been supposed on the starting branch of the network, with normal distribution and maximum value equal to 3%.

First of all, the capability of the new BC-DSSE formulation to filter out the errors present in the substation voltage measurement (that is, on the node assumed as slack bus, whose voltage is included in the state vector) has been evaluated. Fig. 1.4 shows the detail of the measured value of voltage and the resulting estimation for

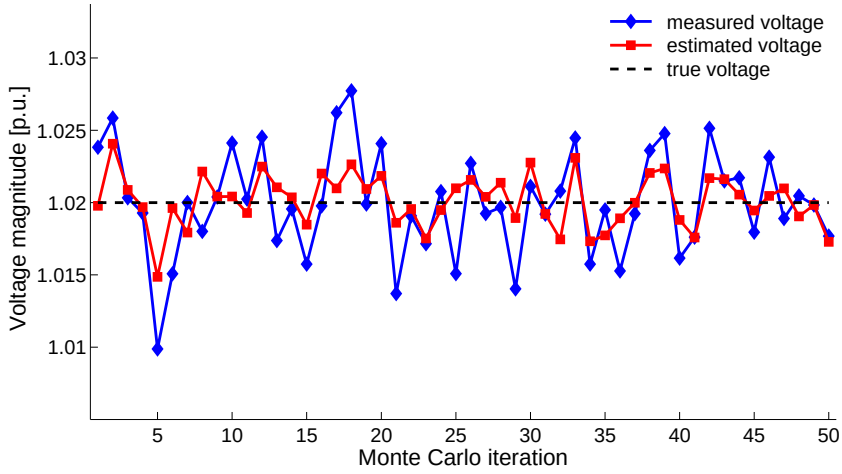

Figure 1.4: Slack bus voltage: measured versus estimated values.

50 Monte Carlo iterations. It is possible to observe that, thanks to the presence of the other voltage measurements on nodes 4 and 11, the measurement in substation can be clearly refined leading to an estimation closer to the true voltage value (that is 1.02 p.u.).

Table 1.1 shows, instead, the overall results for the estimated voltage profile in terms of both magnitudes and angles. In particular, the minimum and the maximum expanded uncertainties (with a coverage factor equal to 3) among all the nodes of the grid are reported.

Table 1.1: Voltage estimation results for original and new BC-DSSE model.

Model Type	Voltage Magnitude		Voltage Angle	
	Min Unc. (%)	Max Unc. (%)	Min Unc. (crad)	Max Unc. (crad)
Original BC-DSSE	0.99	1.04	0.08	0.10
Proposed BC-DSSE	0.56	0.59	0.07	0.09

Results highlight the inability of the original BC-DSSE model to accurately estimate the voltage profile of the network. In fact, all the estimations are strongly affected by the uncertainty of the measurement in substation. This is clear looking at the minimum and the maximum uncertainties for the voltage magnitude: both of them are around 1%, that is the uncertainty of the voltage measurement in substation. In the proposed model, instead, the whole profile can rely on the enhanced estimation of the slack bus voltage and, thus, uncertainties lower than 0.6% can be achieved for all the nodes of the network. Results also show that drawbacks of the original BC-DSSE model are mainly focused on the voltage magnitude estimation. However, a slight degradation of the estimation accuracy also exists for the other quantities, as it can be seen for the voltage angle estimations.

As further confirmation of the obtained results, tests with an increasing number of voltage measurements have been carried out. At the beginning, only the voltage measurement in substation (plus the additional power measurement on the starting branch) has been taken into account. Then, in each following test, an additional voltage measurement is considered on a randomly chosen node. All the voltage measurements have been assumed to have an uncertainty equal to 1%. Fig. 1.5 shows the results for the maximum voltage magnitude expanded uncertainty among the nodes. It is possible to observe that the original BC-DSSE does not allow an enhancement of the voltage magnitude estimation, in spite of the increasing number of voltage measurements placed in the network. With the new state vector, instead, each additional voltage measurement brings an improvement in the resulting estimation, confirming the proper operation of the proposed formulation.

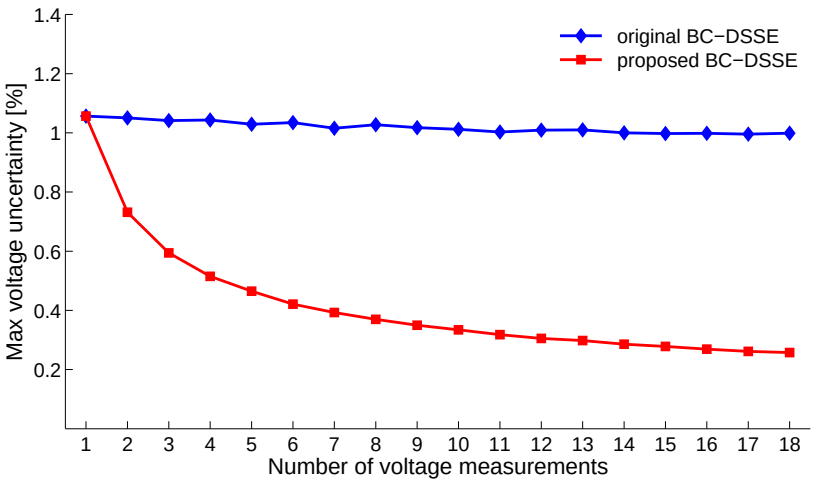

Figure 1.5: Voltage magnitude estimation with an increasing number of voltage measurements.

1.7 Inclusion of PMU measurements

1.7.1 Phasor Measurement Units

The Phasor Measurement Units (PMUs) are new generation measurement devices able to provide accurate measurements of voltage and current phasors synchronized to an absolute time reference [38]. Time synchronization is possible thanks to the Global Positioning System (GPS), which provides a reference time signal synchronized to the Coordinated Universal Time (UTC) with a time uncertainty lower than 1 μs. The use of a common time reference allows for the synchronization of real-time measurements performed in remote points of the network, providing in this way a snapshot of the electrical quantities affecting the grid in a given instant of time. Moreover, using a universal reference allows direct measurement of phase-angles, which was so far technically infeasible.

Besides the time synchronization, PMUs also have other advanced features. First of all, they are digital instruments based on microprocessors, and this allows for the implementation of complex signal processing techniques in order to achieve the highest possible accuracy. In last years, large research efforts have been focused on the design of algorithms able to compute the so-called synchrophasors with the maximum accuracy, even under dynamic conditions [39–42]. In addition, the availability of increasingly powerful and performing processors allows for the attainment of high reporting rates, with the consequent possibility to perform many measurements per second.

For all these reasons, PMUs represent an interesting option for the monitoring and control of modern power networks [43]. In transmission systems, the deployment of PMUs is ongoing since several years. In many countries their operation is still in a testing stage, but in the near future measurement systems based on PMUs are expected to provide support to the Supervisory Control and Data Acquisition (SCADA) systems and to enable new advanced functions into the control centers [44, 45].

State estimation is of course one of the main applications that can take advantage from the deployment of PMUs on the network. Many works deal with the issue of including phasor measurements in state estimators for transmission systems. In [46], the possibility to have linear state estimators based on phasor measurements is shown. However, such possibility is constrained to the presence of PMUs in each node of the network and, thus, it is not applicable in current practical cases. In [47], instead, a two-step state estimator is proposed to minimize the modifications to existing SE algorithms. In this proposal, the first step is performed relying on conventional measurements and using one of the traditional SE formulations; then, an additional step is performed, by introducing the phasor measurements, in order to refine the estimation results. Hybrid formulations of SE, simultaneously incorporating both conventional and phasor measurements, have been also proposed [48]. Furthermore, alternative methods to include the phasor measurements have been also presented. In [49], for example, different solutions for including the current phasor measurements in traditional voltage based estimators are tested and analyzed.

In distribution systems, the need of PMUs for the monitoring and control is still a debated topic. On one hand, the time synchronization, the high accuracy and reporting rate can be important features also at the distribution level. On the other side, the high costs of the commercial PMUs currently available in the market represent an obstacle to their effective deployment. As a result, a trade-off has to be found considering both the costs involved in the installation of the different measurement instruments (and the associated communication infrastructure) and the technical requirements needed for the different applications envisioned in the control center [50].

Whatever the chosen solution for the measurement system, the state estimators conceived for distribution systems should be able to handle the possible presence of PMU measurements. Since in distribution grids SE will be based on newly designed algorithms, an hybrid solution, simultaneously implementing both conventional and synchronized measurements, is the most suitable choice. Next subsections show the arrangement of the BC-DSSE algorithm in case of PMU measurements, the mathematical functions to be considered for handling voltage and current phasors and some implementation details useful to speed up the algorithm.

1.7.2 BC-DSSE formulation with PMU measurements

As aforementioned, PMUs have the capability to provide both magnitude and angle measurements of voltage and currents. In particular, angle measurements are provided with reference to a cosine wave, at the nominal frequency of the system, synchronized to the occurrence of the UTC second [51]. To exploit such angle measurements and to have an information consistent with the other angle quantities, the choice of the slack bus angle as a reference is not possible anymore. In [52], the possibility to use the UTC time as reference for the angles of all the electrical quantities involved in the SE problem, when PMU measurements are available, is presented. Following this solution, the slack bus angle is not a known quantity anymore and it also has to be estimated.

As a consequence, when PMU measurements are available, the BC-DSSE formulation here proposed has to be modified in order to allow the estimation of the slack bus angle. To make this possible, the state vector presented in equations (1.17) and (1.18) has to be extended to include also the slack bus angle information. In particular, with reference to the generic single-phase state vector $\mathbf{x}_\phi$ (associated to phase ϕ), and considering the slack bus voltage in rectangular coordinates, the state vector becomes:

$$\mathbf{x}_\phi = [v^r_{s\phi}, v^x_{s\phi}, i^r_{1\phi}, ..., i^r_{N_{br}\phi}, i^x_{1\phi}, ..., i^x_{N_{br}\phi}] \tag{1.42}$$

where $v^r_{s\phi}$ and $v^x_{s\phi}$ are the real and imaginary part of the slack bus voltage, respectively.

It is worth underlining that the inclusion of the slack bus angle information in the state vector can be obtained using both rectangular and polar coordinates. However, in the proposed BC-DSSE algorithm, the use of rectangular coordinates has been preferred since it allows a simpler implementation of measurement functions and Jacobian in the algorithm. It is also important to recall that, since the state vector is changed, the resulting modifications for the Jacobian terms (that is, the derivatives with respect to both real and imaginary part of the slack bus voltage) have to be duly taken into account (see Appendix A.4).

1.7.3 PMU measurement functions

In the same way of the traditional measurements, even for the phasor measurements it is necessary to find the measurement functions to be considered in the SE algorithm. PMUs usually provide the phasor measurement in terms of magnitude and angle. However, for the inclusion into the BC-DSSE algorithm, their transformation in rectangular coordinates is more convenient since it allows a simpler implementation.

- **Current phasors**

  In this case, the benefits resulting from the transformation of a current phasor in rectangular coordinates are evident, since this choice allows achieving linear functions. Similarly to the case of branch power measurements, the measurement function for a current phasor measured on the phase ϕ of a generic branch l is:

$$h_{i^r_{l\phi}} + jh_{i^x_{l\phi}} = \alpha(i^r_{l\phi} + ji^x_{l\phi}) \tag{1.43}$$

  where α is ± 1 depending on the direction of the measured current with respect to verse assumed as positive for the currents included in the state vector. It is possible to observe that current phasor measurements do not imply coupling among the different phases of the system.

- **Voltage phasors**

  As seen in equation (1.13), the voltage phasor $v_{i\phi}$ on the phase ϕ of a generic node i, can be expressed as:

$$v_{i\phi} = v_{1\phi} - \sum_{k\in\Gamma} \mathbf{Z}_{k,\phi}\mathbf{i}_k \tag{1.44}$$

  where Γ is the set of the branches involved in the path between slack bus and measured node. Starting from this expression, it is possible to find:

$$h_{v^r_{i\phi}} + jh_{v^x_{i\phi}} = Re\left[v_{1\phi} - \sum_{k\in\Gamma} \mathbf{Z}_{k,\phi}\mathbf{i}_k\right] + j\ Im\left[v_{1\phi} - \sum_{k\in\Gamma} \mathbf{Z}_{k,\phi}\mathbf{i}_k\right] \tag{1.45}$$

$$h_{v^r_{i\phi}} = v^r_{1\phi} - \sum_{k\in\Gamma}(\mathbf{R}_{k,\phi}\mathbf{i}^r_k - \mathbf{X}_{k,\phi}\mathbf{i}^x_k) \tag{1.46}$$

$$h_{v^x_{i\phi}} = v^x_{1\phi} - \sum_{k\in\Gamma}(\mathbf{X}_{k,\phi}\mathbf{i}^r_k + \mathbf{R}_{k,\phi}\mathbf{i}^x_k) \tag{1.47}$$

  It is possible to observe that both the real and the imaginary part of the voltage measurement lead to coupling among the different phases of the network. However, both the functions are characterized by linear relationships.

Besides the computation of the measurement functions, it is important to properly model the uncertainty of the rectangular quantities that have been obtained. In fact, these quantities represent indirect measurements whose uncertainty should be calculated duly considering the error propagation coming from the provided magnitude and angle measurements. The rectangular expression of both currents and voltages is obtained by means of the following:

$$y^r = Y \cos\delta \tag{1.48}$$

$$y^x = Y \sin\delta \tag{1.49}$$

where y indicates the generic phasor (either of current or voltage), Y and δ are its magnitude and angle, while y^r and y^x are its real and imaginary parts, respectively.

Indicating with $\mathbf{\Sigma}_{y^{rx}}$ the desired covariance matrix of the phasor measurement in rectangular coordinates and with $\mathbf{\Sigma}_{Y\delta}$ the covariance matrix of the polar version of the phasor, the error propagation law is:

$$\left[\mathbf{\Sigma}_{y^{rx}}\right] = \left[\frac{\partial \mathbf{f}_{yrx}}{\partial \mathbf{x}_{Y\delta}}\right] \left[\mathbf{\Sigma}_{Y\delta}\right] \left[\frac{\partial \mathbf{f}_{yrx}}{\partial \mathbf{x}_{Y\delta}}\right]^T \tag{1.50}$$

where $\mathbf{f}_{y^{rx}}$ is the vector of the functions shown in (1.48) and (1.49) whose derivatives with respect to the starting quantities Y and δ have to be calculated.

Computing the derivative terms in (1.50), the following holds:

$$\begin{bmatrix} \sigma^2_{y^r} & \sigma_{y^r y^x} \\ \sigma_{y^r y^x} & \sigma^2_{y^x} \end{bmatrix} = \begin{bmatrix} \cos\delta & -Y\sin\delta \\ \sin\delta & Y\cos\delta \end{bmatrix} \begin{bmatrix} \sigma^2_Y & \sigma_{Y\delta} \\ \sigma_{Y\delta} & \sigma^2_\delta \end{bmatrix} \begin{bmatrix} \cos\delta & \sin\delta \\ -Y\sin\delta & Y\cos\delta \end{bmatrix} \tag{1.51}$$

where σ^2_Y and σ^2_δ are the variance terms associated to the starting magnitude and angle measurements (which can be obtained from the PMU data sheets, see for example [53]), $\sigma_{Y\delta}$ is the possible covariance term between magnitude and angle measurement, and $\sigma^2_{y^r}$, $\sigma^2_{y^x}$ and $\sigma_{y^r y^x}$ are the equivalent terms associated to the real and imaginary components of the phasor.

Assuming the absence of correlation between magnitude and angle measurement, the following uncertainty terms can be found:

$$\sigma^2_{y^r} = \sigma^2_Y \cos^2\delta + \sigma^2_\delta \; Y^2 \sin^2\delta \tag{1.52}$$

$$\sigma^2_{y^x} = \sigma^2_Y \sin^2\delta + \sigma^2_\delta \; Y^2 \cos^2\delta \tag{1.53}$$

$$\sigma_{y^r y^x} = \cos\delta \sin\delta \; (\sigma^2_Y - \sigma^2_\delta \; Y^2) \tag{1.54}$$

It is possible to observe that the proper modeling of the measurement errors for the rectangular components of the phasor leads to a matrix where a covariance term also exists. As a consequence, the weighting matrix should be built taking into account the presence of such correlation and including the weights resulting from the inversion of the full covariance matrix $\mathbf{\Sigma}_{y^{rx}}$.

1.7.4 Building of PMU Jacobian and functions

In the previous subsection, the measurement functions to be considered for the current and voltage phasor measurements have been presented. Obviously, each one of these measurements implies the presence of two rows in the Jacobian matrix (one for the real component and one for the imaginary one). The details about the derivative terms arising from the phasor measurements are shown in Appendix A.4. Here, some indications about the implementation of Jacobian and measurement functions in the proposed BC-DSSE algorithm are provided. In particular, it is useful to highlight that both current and voltage measurements are characterized by linear functions. This implies that the corresponding Jacobian sub-matrices are constant matrices that can be built outside the iterative WLS process. Moreover, the associated measurement functions can be simply computed, at each iteration of the algorithm, through a matrix multiplication between Jacobian sub-matrix and state vector.

Further simplifications are possible if the measurement system is only composed of PMU measurements (in addition to the power injection pseudo-measurements). In fact, it is possible to observe that, if there are not any voltage or current magnitude measurements, then all the measurements to be considered in the BC-DSSE model are characterized by linear relationships. In such a situation, the whole Jacobian matrix and even the Gain matrix can be computed only once outside of the iterative WLS process, allowing in this way a significant reduction of the execution times.

Chapter 2

Inclusion of equality constraints into BC-DSSE

2.1 Equality constraints

In the previous Chapter, it has been mentioned that SE can be performed following different methods, each one with its strengths and weaknesses. The WLS method is in general the most used technique in transmission systems [4], and some works show that it can be the most convenient choice even for DSSE [26]. Despite the traditional use of voltage magnitudes and angles as state vector of the system, the WLS approach can be implemented in different ways depending on the variables chosen as state vector. The used state vector, obviously, has an impact on the characteristics of the estimator. Besides the SE approach and the choice of the state variables, there is another important aspect affecting implementation, computational burden and performance of the SE algorithm: the way in which the equality constraints are considered and included into the SE model.

The equality constraints are sure information deriving from a priori knowledge on the operating conditions or the topology of the network. The most common case of equality constraints that can be found in electrical systems is given by the so-called zero injections. The zero injections are nodes where there is the certainty that there is neither load consumption nor power generation. For instance, nodes in which there is the branching of an incoming line in more outgoing branches, without the presence of connected loads or generators, are typical examples of zero injection nodes.

The inclusion of the equality constraints in transmission system state estimators has been widely investigated in the literature and different approaches have been proposed to this aim. One of the simplest methods to handle these constraints is to consider them as virtual measurements [4]. Taking into account the previously

mentioned zero injection, the corresponding virtual measurement can be a power or a current injection on the node equal to zero. The problem in such approach is that the uncertainty associated to this information is null and, therefore, the resulting weight for the virtual measurement should be infinite. Obviously, this value cannot be used in the real implementation and then it is replaced by a very large weight in order to emphasize the higher reliability of this information with respect to the reliability of the other measurements. However, the use of very large weights can lead to numerical problems in the running of the SE algorithm and thus other methods have been proposed.

An alternative approach is given by the use of the Lagrangian method (see, for example, [54]). This technique has been conceived to deal with constrained minimization problems and for this reason it is well suited to be used even in the SE context. In [55], to further improve the numerical properties of the SE algorithm, a formulation based on the use of augmented matrices has been proposed: however, such kind of approach leads to large equation systems to be solved at each iteration of the SE algorithm. More recently, in [56], a modified version of the virtual measurement approach has been proposed: the use of very large weights has been avoided by considering low weights even for the zero injections and then re-imposing the constraints between subsequent iterations of the SE algorithm.

In this Chapter, an alternative option for the inclusion of the equality constraints in the proposed BC-DSSE model is presented and tested. It is worth underlining that, in distribution systems, the issue of dealing with the equality constraints can be particularly relevant. In fact, the number of zero injections can be very high, since, in the three-phase model of the distribution network, many nodes may have no loads or generators connected to some of the phases. Moreover, as anticipated in Chapter 1, differently from the voltage based estimators, in the branch-current formulation of the SE algorithm even the Kirchhoff's voltage law along the meshes has to be considered as a constraint. For these reasons, in the BC-DSSE models, an efficient handling of the equality constraints is an important requirement.

2.2 Classical formulation of the equality constraints

Zero injections are the most common case of equality constraints that can be found in distribution networks. They can be generally represented as:

$$\mathbf{c}(\mathbf{x}) = 0 \tag{2.1}$$

where $\mathbf{c}(\mathbf{x})$ is a column vector of the functions expressing the constraints associated to the $2N_c$ zero injections in terms of the state variables ($2N_c$ because each one of the N_c zero injection nodes has constraints on both the active and the reactive component of the power or current injection). It is important to highlight that the

functions involved in $\mathbf{c}(\mathbf{x})$ can be linear or nonlinear, depending on the chosen state vector. In the case of the proposed BC-DSSE model, since the constraints can be considered as zero current injections, $\mathbf{c}(\mathbf{x})$ is a vector of linear functions (see the measurement functions of the equivalent current injection measurements in Section 1.4.2 for details), thus it is:

$$\mathbf{c}(\mathbf{x}) = \mathbf{C}\mathbf{x} \tag{2.2}$$

where the Jacobian $\mathbf{C}$ is a $2N_c \times N$ matrix (N is the number of variables in the state vector) in which the j-th row includes the derivatives of the j-th zero injection function with respect to the variables of the state vector (see Appendix A.1 for details about the creation of the Jacobian matrix associated to equivalent current injections).

As for the mesh constraints, similarly, the Kirchhoff's voltage law along the meshes can be expressed as:

$$\mathbf{m}(\mathbf{x}) = 0 \tag{2.3}$$

where $\mathbf{m}(\mathbf{x})$ is a $2N_{mesh}$ size vector (with N_{mesh} representing the number of meshes in the network) in which each couple of rows j and $j+1$ refers to the constraints associated to the real and imaginary voltage drop along the path of the considered mesh. As in the previous case, the functions associated to the mesh constraints can be linear or nonlinear depending on the chosen state vector. In the case of the BC-DSSE algorithm here proposed, again, the mesh constraints are linear functions (see Section 1.5.7 for the details about the measurement functions associated to the meshes) and they can be expressed as:

$$\mathbf{m}(\mathbf{x}) = \mathbf{M}\mathbf{x} \tag{2.4}$$

where $\mathbf{M}$ is a $2N_{mesh} \times N$ matrix having in each row the derivatives of the corresponding mesh function with respect to the state variables (details about the terms in the Jacobian matrix $\mathbf{M}$ can be found in Appendix A.3)

In the following subsections, the most used methods to deal with the equality constraints, namely the Virtual Measurements (VM) approach and the Lagrange Multipliers (LM) method, will be presented. Such methods are then used as reference for assessing the performance of the proposed approach, which will be presented in Section 2.3.

2.2.1 Virtual Measurements approach

As already anticipated, the simplest method to consider the equality constraints in the SE model is to include them as virtual measurements with very large weights. Indicating with $\mathbf{y_m}$ the column vector of the proper measurements (that is, the vector of the real-time measurements and the pseudo-measurements), with $\mathbf{y_{zi}}$ the

column vector of the virtual measurements given by the zero injections, and with $\mathbf{y_{zm}}$ the column vector of the mesh constraints, the total measurement vector to be considered in the BC-DSSE model is:

$$\mathbf{y} = \begin{bmatrix} \mathbf{y_m} \\ \mathbf{y_{zi}} \\ \mathbf{y_{zm}} \end{bmatrix} = \begin{bmatrix} \mathbf{y_m} \\ \mathbf{0} \\ \mathbf{0} \end{bmatrix} \tag{2.5}$$

In the same way, and using the same subscripts for the notation, the Jacobian, the weighting matrix and the residual vector can be written as:

$$\mathbf{H} = \begin{bmatrix} \mathbf{H}_m \\ \mathbf{H}_{zi} \\ \mathbf{H}_{zm} \end{bmatrix} = \begin{bmatrix} \mathbf{H}_m \\ \mathbf{C} \\ \mathbf{M} \end{bmatrix} \tag{2.6}$$

$$\mathbf{W} = \begin{bmatrix} \mathbf{W}_m & \mathbf{0} & \mathbf{0} \\ \mathbf{0} & \mathbf{W}_{zi} & \mathbf{0} \\ \mathbf{0} & \mathbf{0} & \mathbf{W}_{zm} \end{bmatrix} \tag{2.7}$$

$$\mathbf{r} = \begin{bmatrix} \mathbf{r}_m \\ \mathbf{r}_{zi} \\ \mathbf{r}_{zm} \end{bmatrix} = \begin{bmatrix} \mathbf{y}_m - \mathbf{h}_m(\mathbf{x}) \\ -\mathbf{c}(\mathbf{x}) \\ -\mathbf{m}(\mathbf{x}) \end{bmatrix} \tag{2.8}$$

Taking into account the so-called normal equations to be solved at each iteration of the WLS step in the SE algorithm (see equation (1.4)), the equation system becomes:

$$\begin{aligned} (\mathbf{H}_m^{\mathrm{T}}\mathbf{W}_m\mathbf{H}_m + \mathbf{C}^{\mathrm{T}}\mathbf{W}_{zi}\mathbf{C} + \mathbf{M}^{\mathrm{T}}\mathbf{W}_{zm}\mathbf{M})\Delta\mathbf{x} = \\ \mathbf{H}_m^{\mathrm{T}}\mathbf{W}_m\mathbf{r}_m - \mathbf{C}^{\mathrm{T}}\mathbf{W}_{zi}\mathbf{c} - \mathbf{M}^{\mathrm{T}}\mathbf{W}_{zm}\mathbf{m} \end{aligned} \tag{2.9}$$

which can be rewritten as:

$$(\mathbf{G}_m + \mathbf{G}_{zi} + \mathbf{G}_{zm})\Delta\mathbf{x} = \mathbf{H}_m^{\mathrm{T}}\mathbf{W}_m\mathbf{r}_m - \mathbf{C}^{\mathrm{T}}\mathbf{W}_{zi}\mathbf{c} - \mathbf{M}^{\mathrm{T}}\mathbf{W}_{zm}\mathbf{m} \tag{2.10}$$

where $\mathbf{G}_m = \mathbf{H}_m^{\mathrm{T}}\mathbf{W}_m\mathbf{H}_m$ is a Gain matrix component associated to the measurements and, similarly, $\mathbf{G}_{zi} = \mathbf{H}_{zi}^{\mathrm{T}}\mathbf{W}_{zi}\mathbf{H}_{zi}$ and $\mathbf{G}_{zm} = \mathbf{H}_{zm}^{\mathrm{T}}\mathbf{W}_{zm}\mathbf{H}_{zm}$ are Gain matrix contributes brought by the zero injection and mesh constraints, respectively. It is worth underlining that the size of the obtained equation system is equal to N, where N is the number of variables in the chosen state vector.

Despite its simplicity, the VM approach can lead to numerical problems in the solution of the normal equations shown in (2.10) because of the simultaneous presence of weights with different orders of magnitude. Such issue, well-known in the literature under the name of ill-conditioning (see for example [4] for more details),

brings small errors in the different entries of the equation system to be translated in large errors for the solution vector. Thus, both convergence problems for the SE algorithm and poor accuracy in the estimation results can arise in presence of an ill-conditioned equation system.

This aspect can be particularly critical in distribution systems since, in addition to the large weights of the equality constraints, there is the simultaneous presence of pseudo-measurements that, instead, have to be considered with a very low weight due to their poor reliability. For this reason, it is important to pay due attention to the numerical properties of the DSSE algorithm during its design.

2.2.2 Lagrange Multipliers method

The Lagrange Multipliers (LM) method is a technique used in many different contexts for solving constrained minimization problems. For this reason, it can represent a suitable option also for the SE problem in presence of equality constraints. According to this approach, the objective function to be minimized in the WLS problem (described in Section 1.3.2) has to be extended by including also the equality constraints through suitable Lagrange multipliers. Taking into account the expression of the constraints given by the functions $\mathbf{c}(\mathbf{x})$ and $\mathbf{m}(\mathbf{x})$ for the zero injections and the meshes, respectively, the objective function becomes:

$$J(\mathbf{x}) = [\mathbf{y} - \mathbf{h}(\mathbf{x})]^T \mathbf{W} [\mathbf{y} - \mathbf{h}(\mathbf{x})] + \boldsymbol{\lambda}_{zi}^T \mathbf{c}(\mathbf{x}) + \boldsymbol{\lambda}_{zm}^T \mathbf{m}(\mathbf{x}) \tag{2.11}$$

where $\boldsymbol{\lambda}_{zi}$ and $\boldsymbol{\lambda}_{zm}$ are the column vectors of the Lagrange multipliers associated to the zero injection and mesh constraints, respectively.

Each Lagrange multiplier appearing in the above equation is an unknown and, thus, the derivation of the objective function and the subsequent application of the Gauss-Newton approach to solve the resulting equations lead to the following system to be solved at each iteration of the WLS step:

$$\begin{bmatrix} \mathbf{G}_m & \mathbf{C}^{\mathrm{T}} & \mathbf{M}^{\mathrm{T}} \\ \mathbf{C} & 0 & 0 \\ \mathbf{M} & 0 & 0 \end{bmatrix} \begin{bmatrix} \Delta\mathbf{x} \\ -\boldsymbol{\lambda}_{zi} \\ -\boldsymbol{\lambda}_{zm} \end{bmatrix} = \begin{bmatrix} \mathbf{H}^{\mathrm{T}}\mathbf{W}\mathbf{r} \\ -\mathbf{c}(\hat{\mathbf{x}}) \\ -\mathbf{m}(\hat{\mathbf{x}}) \end{bmatrix} \tag{2.12}$$

where $\mathbf{c}(\hat{\mathbf{x}})$ and $\mathbf{m}(\hat{\mathbf{x}})$ are the constraint functions computed through the estimated state vector $\hat{\mathbf{x}}$.

In (2.12), it is possible to observe that the equality constraints are duly considered in the estimation process and that it is still necessary to compute both the constraint functions $\mathbf{c}(\mathbf{x})$ and $\mathbf{m}(\mathbf{x})$ and the corresponding Jacobian matrices $\mathbf{C}$ and $\mathbf{M}$. However both the zero injections and the meshes are not considered as measurements anymore and thus they do not need to have an associated weight. The

only Gain matrix involved in the equation system is $\mathbf{G}_m$, that is the Gain matrix associated to the set of real measurements and pseudo-measurements.

Such solution allows avoiding the use of large weights and hence relieves the ill-conditioning problem. It is worth noting that in [4], to further reduce the numerical conditioning of the system, the use of a normalization coefficient γ for the weighting matrix is suggested. The normalization coefficient can be chosen as:

$$\gamma = \frac{1}{max(W_{ii})} = min(\sigma_{ii}^2) \tag{2.13}$$

where W_{ii} is the weight of the generic i-th measurement (or pseudo-measurement) and σ_{ii} is its standard deviation.

Introducing the normalization coefficient in equation (2.12), the resulting system to be solved at each iteration of the SE algorithm is:

$$\begin{bmatrix} \gamma\mathbf{G}_m & \mathbf{C}^{\mathrm{T}} & \mathbf{M}^{\mathrm{T}} \\ \mathbf{C} & 0 & 0 \\ \mathbf{M} & 0 & 0 \end{bmatrix} \begin{bmatrix} \Delta\mathbf{x} \\ -\boldsymbol{\lambda}_{zi} \\ -\boldsymbol{\lambda}_{zm} \end{bmatrix} = \begin{bmatrix} \gamma\mathbf{H}^{\mathrm{T}}\mathbf{W}\mathbf{r} \\ -\mathbf{c}(\hat{\mathbf{x}}) \\ -\mathbf{m}(\hat{\mathbf{x}}) \end{bmatrix} \tag{2.14}$$

It is important to highlight that the obtained equation system is expected to have better numerical properties with respect to the one found in equation (2.10), but also implies a larger number of unknowns due to the presence of the Lagrange multipliers. Considering that each constraint has an associated multiplier, the size of the equation system (2.14) is $N + 2N_c + 2N_{mesh}$.

2.3 State Vector Reduction approach

In this Section, a possible alternative approach to deal with the equality constraints in the proposed BC-DSSE algorithm is shown. The proposal is based on a simple State Vector Reduction (SVR): this can be easily obtained thanks to the linearity of the functions expressing the constraints in the proposed BC-DSSE formulation [57].

Firstly, let us consider the case of zero injections. As already mentioned, zero injections can be expressed as equivalent phasor current injections equal to zero. Thus, both for the real and the imaginary part of the current, it is possible to write:

$$\sum_{j\in\Theta_i} \alpha_j i_j^r = 0 \tag{2.15}$$

$$\sum_{j\in\Theta_i} \alpha_j i_j^x = 0 \tag{2.16}$$

where Θ_i is the set of the branches incident to the zero injection node i, and α_j is a coefficient equal to $+1$ or -1 depending on the incoming or outgoing direction

of the j-th branch. From the above relationships, it is easy to observe as a simple state variable elimination can be obtained expressing one of the incident branch currents in terms of the remaining ones (according to the Kirchhoff's current law). The total state vector $\mathbf{x}$ can be, therefore, divided in a reduced state vector $\tilde{\mathbf{x}}$ of length $\tilde{N} = N - 2N_c$ and a set of $2N_c$ removable state variables $\mathbf{x}_{zi}$ (where N_c is the number of zero injection nodes). Since each one of the eliminated variables is linked to the remaining ones through the injection constraints, the following relationship between the starting state vector $\mathbf{x}$ and the reduced version $\tilde{\mathbf{x}}$ can be found:

$$\mathbf{x} = \begin{bmatrix} \tilde{\mathbf{x}} \\ \mathbf{x}_{zi} \end{bmatrix} = \begin{bmatrix} \mathbf{I}_{\tilde{N}} \\ \mathbf{\Gamma}_{zi} \end{bmatrix} \tilde{\mathbf{x}} \tag{2.17}$$

where $\mathbf{I}_{\tilde{N}}$ is a $\tilde{N} \times \tilde{N}$ identity matrix and $\mathbf{\Gamma}_{zi}$ is a $2N_c \times \tilde{N}$ matrix with nonzero elements equal to ± 1 that link the eliminated variables $\mathbf{x}_{zi}$ to the remaining ones.

As for the mesh constraints, in the same way, it is possible to exploit the linear relationship of the constraint function for writing one of the currents involved in the mesh as a function of the other ones. As already seen in Section 1.5.7, the mesh constraint can be expressed as:

$$\sum_{h \in \Psi} \alpha_h \mathbf{Z}_h \mathbf{i}_h = 0 \tag{2.18}$$

where Ψ is the set of the branches involved in the mesh, α_h is ± 1 depending on the direction of the generic h-th current (with respect to the conventional direction of the mesh), and $\mathbf{Z}_h$ and $\mathbf{i}_h$ are the three-phase versions of the impedance and the current of the h-th branch, respectively. From equation (2.18) it is possible to find:

$$\mathbf{i}_k = -\alpha_k \mathbf{Z}_k^{-1} \sum_{\substack{h \in \Psi \\ h \neq k}} \alpha_h \mathbf{Z}_h \mathbf{i}_h \tag{2.19}$$

where k is the index of the branch whose currents $i^r_{k\phi}$ and $i^x_{k\phi}$ will be eliminated from the state variables. The above equation thus allows achieving the expression of the currents in branch k as a function of the remaining branch currents of the mesh.

Considering this additional step, $2N_{mesh}$ state variables $\mathbf{x}_{zm}$ can be eliminated (where N_{mesh} is the number of meshes; in general, if the mesh involves three-phase branches, for each reclosing branch it is $N_{mesh} = 3$) and the state vector $\tilde{\mathbf{x}}$ can be further reduced to a length equal to $\tilde{N} = N - 2N_C - 2N_{mesh}$. Equation (2.17) can be adapted to consider also the variables eliminated due to the mesh constraints as follows:

$$\mathbf{x} = \begin{bmatrix} \tilde{\mathbf{x}} \\ \mathbf{x}_{zi} \\ \mathbf{x}_{zm} \end{bmatrix} = \begin{bmatrix} \mathbf{I}_{\tilde{N}} \\ \mathbf{\Gamma}_{zi} \\ \mathbf{\Gamma}_{zm} \end{bmatrix} \tilde{\mathbf{x}} \tag{2.20}$$

where $\mathbf{\Gamma}_{zm}$ is a $2N_{mesh} \times \tilde{N}$ matrix linking the $2N_{mesh}$ eliminated current variables $\mathbf{x}_{zm}$ to the remaining ones.

In presence of the new state vector $\tilde{\mathbf{x}}$, the only arrangement needed to adapt the BC-DSSE algorithm concerns the normal equations to be considered in the WLS step, which have to be adapted according to the following:

$$\tilde{\mathbf{H}}_m^{\mathrm{T}} \mathbf{W}_m \tilde{\mathbf{H}}_m \Delta\tilde{\mathbf{x}} = \tilde{\mathbf{H}}_m^{\mathrm{T}} \mathbf{W}_m \mathbf{r}_m \tag{2.21}$$

where the new Jacobian $\tilde{\mathbf{H}}_m$ is:

$$\tilde{\mathbf{H}}_m = \mathbf{H}_m \begin{bmatrix} \mathbf{I}_{\tilde{N}} \\ \mathbf{\Gamma}_{zi} \\ \mathbf{\Gamma}_{zm} \end{bmatrix} \tag{2.22}$$

and the residual vector is computed as $\mathbf{r}_m = \mathbf{y_m} - \mathbf{h}(\left[\tilde{\mathbf{x}}^{\mathrm{T}}, \tilde{\mathbf{x}}^{\mathrm{T}}\mathbf{\Gamma}_{zi}^{\mathrm{T}}, \tilde{\mathbf{x}}^{\mathrm{T}}\mathbf{\Gamma}_{zm}^{\mathrm{T}}\right]^{\mathrm{T}})$.

Once the state vector $\tilde{\mathbf{x}}$ is found, it is easy to compute the eliminated branch currents using the matrices $\mathbf{\Gamma}_{zi}$ and $\mathbf{\Gamma}_{zm}$ as shown in equation (2.20). It is important to note that, since the equality constraints are information known a priori, the matrices $\mathbf{\Gamma}_{zi}$ and $\mathbf{\Gamma}_{zm}$ can be built outside the SE algorithm, exploiting the knowledge on the topology and the features of the network. This avoids the computation of such matrices inside the algorithm and thus allows saving computational time.

Among the other characteristics of the proposed method, it is clear that the ill-conditioning problems brought by the VM method are avoided, since the input measurement vector includes only the real-time measurements and the pseudo-measurements. The reduction of the state vector, however, leads to a lower sparsity of the system, reflecting the fact that each eliminated variable is expressed in terms of some remaining quantities. This can represent a drawback for the efficiency of the algorithm, because the fill-ins in the involved matrices can affect the sparse techniques usually adopted for handling the matrices and solving the equation system. At the same time, anyway, the reduction of the state vector also allows having a significantly smaller equation system to be solved. In fact, as can be seen in equation (2.21), the size of the system in this case becomes $N - 2N_c - 2N_{mesh}$, that is significantly smaller than the cases of the VM and LM approaches (in particular considering that the number of zero injections in distribution systems is usually quite high). From a computational standpoint, this aspect counteracts the drawback given by the lower sparsity: the performance of the BC-DSSE algorithm has, thus, to be evaluated in each specific case depending on the particular features of the analyzed network.

A further discussion concerns the applicability of this approach to other WLS DSSE algorithms. From this point of view, it is worth to highlight that the elimination of the state variables, even if possible also with other state vectors, can be implemented with such simplicity and efficiency only when using rectangular branch

currents, thanks to the linearity of the functions associated to the constraints. When different variables are used in the state vector, instead, the non-linearity of the constraints make the application of such approach significantly more complex and less efficient.

2.4 Tests and results

2.4.1 Test assumptions and metrics

Several tests have been performed on the unbalanced IEEE 123-bus network to assess the performance of the SVR approach here proposed for the treatment of the equality constraints. Results are compared to those obtained by means of the traditionally used VM and LM metods in order to highlight the advantages or the possible drawbacks associated to the proposed method. Fig. 2.1 shows the topology of the benchmark grid; the data of the network can be found in [58].

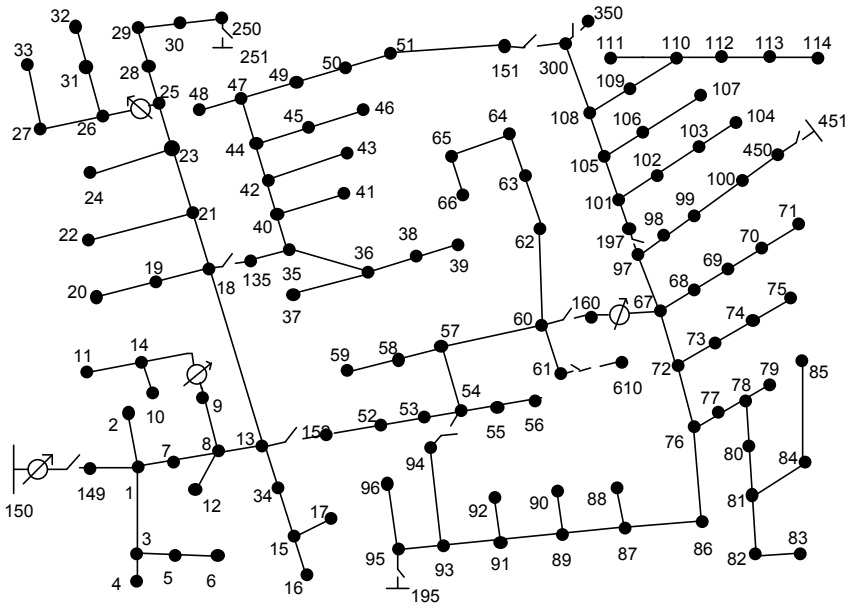

Figure 2.1: IEEE 123-bus test network.

In order to achieve significant results from a statistical point of view, tests have been performed through Monte Carlo simulations. The number of Monte Carlo trials for each simulated scenario is $N_{MC} = 25000$. For each test, first of all, the true conditions of the network are computed by means of a power flow calculation. Then, in each trial, measurements are extracted adding random errors to the corresponding true values according to the assumed uncertainty of the quantities. In particular, the

measurement system has been supposed to be composed of PMUs, with synchronized measurements characterized by normal uncertainty with standard deviation equal to one third of the accuracy value. Accuracies equal to 0.7% and 0.7 crad (i.e. $0.7 \cdot 10^{-2}$ rad) have been considered for the magnitude and angle measurements, respectively, in order to simulate a maximum Total Vector Error (TVE) of 1% (as prescribed by the synchrophasor standard [51] for the measurements in steady state conditions). In addition to the PMU measurements, pseudo-measurements having a Gaussian distributed uncertainty, with a maximum deviation equal to 50% of the nominal value, have been considered for all the loads of the network. Extracted measurements are then provided as input to the BC-DSSE algorithm for the estimation process and the results are stored for the subsequent analysis.

In order to perform a global assessment, the performance of the different approaches is evaluated in terms of accuracy, numerical properties and computational efficiency. To this purpose, the following metrics have been used.

- *Estimation accuracy*: the Root Mean Square Error (RMSE) is an index commonly used in Monte Carlo simulations for assessing the accuracy of an estimated quantity. Given a quantity x, whose true value is x_{true} and the corresponding estimation is $\hat{x}$, the RMSE resulting from N_{MC} Monte Carlo trials is defined as:

$$RMSE_x = \sqrt{\frac{1}{N_{MC}} \sum_{i=1}^{N_{MC}} (\hat{x}_i - x_{true})^2} \tag{2.23}$$

  In this section, however, the focus is not on the accuracy of a specific quantity, but on the overall accuracy performance of the different approaches. For this reason, a mean RMSE, obtained by averaging the RMSEs through all the branches or nodes of the network (depending on the considered quantity), is introduced as overall index for the accuracy assessment.

  Besides the accuracy of the estimated quantities, another parameter will be monitored to evaluate the accuracy of the different approaches in modeling the zero injection constraints. Such parameter is given by the sum of the power injections among all the zero injection nodes and allows evaluating possible issues deriving from an improper modeling of the zero injection constraint. In [56], as an example, it is shown that an unsuitable modeling of the zero injection constraints can also lead to the estimation of significant amounts of injected powers in the zero injection nodes, despite the inclusion of the constraint in the estimation algorithm. Equation (2.24) shows the definition of the indexes concerning both active and reactive power injection (with B representing the set of all the zero injection nodes of the network).

$$P_{0inj} = \sum_{i \in B} |P_i|, \qquad Q_{0inj} = \sum_{i \in B} |Q_i| \tag{2.24}$$

- *Numerical properties*: as already anticipated in the presentation of the VM approach, one possible issue in the modeling of the equality constraints is given by the resulting condition number of the equation system to be solved. The condition number can be defined as the sensitivity of the solution of a linear system of equations to possible errors present in the input data. In particular, a high condition number means that the obtained solution vector can be drastically affected by possible errors (even if small) present in the entries of the equation system, while a low condition number indicates a strong robustness of the solution vector to possible erroneous data. Because of the need to solve an equation system at each iteration of the WLS step in the estimation process, this issue obviously affects also the SE problem [4]. The so-called ill-conditioning of the system can lead to inaccuracies in the estimation results, to possible convergence problems (i.e. a larger number of iterations required to the algorithm to converge) and, in the worst cases, even to numerical instabilities for the algorithm.

  In all the presented approaches, the equation systems to be solved (i.e. (2.10), (2.14) and (2.21) for the VM, LM and SVR methods, respectively) can be rewritten in a common compact form as follows:

$$\mathbf{G_{tot}}\boldsymbol{\Delta}\mathbf{x_{tot}} = \mathbf{u} \tag{2.25}$$

  where $\mathbf{G_{tot}}$ is a coefficient matrix, $\boldsymbol{\Delta}\mathbf{x_{tot}}$ is the total vector of the unknowns (note that this vector includes different variables depending on the approach and, in the case of LM method, also the Lagrange multipliers are included in it) and $\mathbf{u}$ is the vector resulting from the measurement and constraint residuals in the second member of the equation system.

  Given this compact form of the equation system, the condition number K can be computed referring to the coefficient matrix $\mathbf{G_{tot}}$ according to the following:

$$K_{(\mathbf{G_{tot}})} = \|\mathbf{G_{tot}}\| \cdot \|\mathbf{G_{tot}^{-1}}\| \tag{2.26}$$

  where $\|\cdot\|$ stands for the 2-norm of the considered matrix.

  Besides the condition number, other interesting properties are the density and the size of the coefficient matrix: in fact, both of them have a direct impact on the computational burden and the efficiency of the estimation algorithm. The density of a matrix is defined as the ratio between the number of nonzero terms and the total number of elements in the matrix. A low density of the matrix implies a large number of zeros and allows adopting suitable sparse techniques for handling the matrix and solving the equation system. Such techniques can lead to significant benefits for the computational burden of the algorithm. The size of the coefficient matrix is, instead, directly related to the

number of unknowns and equations to be solved. Obviously, a smaller number of unknowns and equations brings advantages from the point of view of the computational burden and, consequently, on the overall execution times.

All these parameters (condition number, density and size of the coefficient matrix) will be duly taken into account in the following tests, in order to highlight differences among the presented approaches and to show their impact on the performance of the BC-DSSE algorithm.

- *Computational efficiency*: the efficiency is a crucial factor in the design of the estimation algorithm, since the real-time running and the reporting rate of the estimator are strictly dependent on it. As a consequence, in the following tests, the overall execution times of the different approaches will be assessed through the monitoring of the average execution time among the different Monte Carlo trials. Moreover, since the execution times are directly affected by the number of iterations needed for the algorithm to converge, the average number of iterations among the N_{MC} Monte Carlo trials, for the different alternative methods, will be also evaluated. It is worth underlining that achievable results can be significantly affected by the hardware, software and implementation technique adopted for developing the SE algorithm. However, here, the implementation of all the versions of the compared methods has been referred to a common and optimized structure of the BC-DSSE algorithm; the only differences concern the implementation details associated to the different inclusion of the equality constraints in the BC-DSSE model, in order to make the comparison as fair as possible. Tests have been performed under Matlab environment and run on a 2.4 GHz quad-core processor with 8 GB RAM.

2.4.2 Impact of the weight on VM approach

Before beginning the comparison of the different methods presented to deal with the equality constraints, a first series of tests, focused only on the VM approach, has been carried out. In fact, in the VM approach, different settings can be used, depending on the particular choice of the weights assigned to the virtual measurements. For this reason, some tests have been performed by using different weights for the virtual measurements, in order to highlight the impact of different choices. In these tests, a measurement system composed of three measurement points, placed at nodes 150, 18 and 67, is assumed to be available in addition to the pseudo-measurements. Each measurement point is supposed to have a voltage synchrophasor measurement on the node and current synchrophasor measurements on all the branches converging to the monitored bus.

Table 2.1 shows the results for the total power injection in the zero injection nodes when weights with increasing orders of magnitude are used. As it can be

expected, the use of larger weights leads to lower values of the power injections estimated in the zero injection nodes, while, if low weights are used, a non-negligible amount of power injection is erroneously assigned to such buses. As a consequence, to strictly fulfil the constraints, the weights to be used should be sufficiently high.

Table 2.1: Variation of P_{0inj} and Q_{0inj} in VM

	Virtual Measurement weight				
	10^8	10^9	10^{10}	10^{11}	10^{12}
$P_{0inj}[kW]$	2.1	$2.2 \cdot 10^{-1}$	$2.2 \cdot 10^{-2}$	$2.2 \cdot 10^{-3}$	$2.2 \cdot 10^{-4}$
$Q_{0inj}[kvar]$	3.2	$3.3 \cdot 10^{-1}$	$3.3 \cdot 10^{-2}$	$3.3 \cdot 10^{-3}$	$3.3 \cdot 10^{-4}$

In any case, it is worth noting that, despite the significant variation of erroneous power injection estimated in the zero injection nodes, in all the cases the mean RMSE for the active powers in the branches is similar (5.4 kW). The reason is twofold: on one hand, the errors in the zero injection estimations are different in sign, and this leads to an overall compensation that limits the effects brought on the branch power estimations; on the other side, the high uncertainty of the pseudo-measurements determines poor accuracy in the estimations of the power flows: thus, the impact of the erroneously estimated zero injections is in any case small with respect to the actual errors in the branch power estimations.

Table 2.2 shows instead the trend for the condition numbers obtained with different weights. As anticipated in previous sections, it is possible to see that larger weights result in increasing values of conditioning. Despite the different orders of magnitude in the obtained condition numbers, the tests here performed (with double precision) do not show any particular deterioration of the accuracy results or of the convergence properties. However, it is important to underline that even larger condition numbers could be obtained if other operating conditions or measurement configurations are considered. Moreover, features of the network (like, for example, the impedance values [4]) significantly affect the conditioning, and their effects are strongly dependent on the used hardware. Therefore, in general, the choice of the weight should be carefully evaluated, searching a trade-off between the requirement to accurately model the equality constraints and the need to avoid ill-conditioning

Table 2.2: Variation of the condition number K in VM

	Virtual Measurement weight				
	10^8	10^9	10^{10}	10^{11}	10^{12}
K	$6.20 \cdot 10^4$	$2.66 \cdot 10^5$	$2.64 \cdot 10^6$	$2.64 \cdot 10^7$	$2.64 \cdot 10^8$

of the system. In the comparison tests shown in the rest of the Chapter, the weight used for the virtual measurements in the VM approach will be conventionally set equal to 10^{10}.

2.4.3 Impact of the zero injection constraints

In this subsection, tests aimed at assessing the impact of the zero injections on the performance of the different approaches are presented. The same measurement system illustrated in the previous subsection (measurement points in nodes 150, 18 and 67) is used as reference configuration.

Performed simulations clearly highlight an important result: all the considered methods exhibit really similar accuracy performance. As an example, the mean of the percent values of RMSE obtained for the voltage and current magnitude estimations are 0.14% and 7.40%, respectively, for all the tested methods. Similar results can be found also for the mean RMSEs of the other electrical quantities. As for the power injection estimation in the zero injection buses, it has been already seen that the VM approach has values of the P_{0inj} and Q_{0inj} indexes slightly different from zero: this reflects the approximation made by using a weight different from infinite, which, theoretically, would properly represent the null uncertainty associated to the constraint. Nevertheless, such approximation does not have significant effects on the accuracy of the other estimated electrical quantities. In case of the LM and SVR methods, instead, since there is no approximation in the modeling of the zero injection constraints, the power injection estimated in the zero injection buses is, as expected, equal to zero.

Since all the methods show a similar behaviour from the point of view of the accuracy, the evaluation of the performance can be focused on their computational efficiency. In this case, significant differences can be found due to the different numerical properties of the presented approaches. Table 2.3 shows the characteristics of the coefficient matrix involved in the equation systems of the different methods. First of all, it is possible to note the significant reduction of the size of the equation system resulting from the elimination of the state variables in the SVR method.

Table 2.3: Numerical properties of the coefficient matrix

Method	Coeff. matrix density	Coeff. matrix size	Condition number
VM	3.26%	454×454	$2.64 \cdot 10^6$
LM	1.48%	692×692	$1.21 \cdot 10^5$
SVR	21.17%	216×216	$2.75 \cdot 10^4$

Such a large reduction derives from the large number of zero injections (119 over 227 total nodes for all the three-phases) that are present in the grid because of the connection of many single-phase loads to three-phase nodes. As it can be observed in Table 2.3, however, this size reduction happens at the cost of a significant increase in the density of the coefficient matrix. On the contrary, in the LM method, the high number of zero injections leads to a larger size and a lower density of the corresponding coefficient matrix.

Table 2.4 shows the obtained results in terms of average number of iterations and execution times. It is possible to observe that the SVR approach clearly results the most efficient method, with an enhancement of the computational performance larger than 20% and 30% with respect to the VM and LM methods, respectively. Moreover, it is worth noting that, given the density of the coefficient matrix and the not too much large size of the equation system, in this specific case, the SVR approach could be also designed without using sparse techniques for handling the coefficient matrix and solving the equation system: in such conditions, the enhancement of the computational performance rises up to more than 30% and 40% with respect to the VM and LM approaches, respectively.

Table 2.4: Average iteration numbers and execution times

Method	Iteration number	Execution time [ms]
VM	3.36	17.6
LM	3.36	20.5
SVR	3.20	14.0

Results also show that the SVR method has better convergence properties: the average iteration number is, in fact, slightly lower than those of the VM and LM approaches. This can be a very important feature, above all for those network (or, in general, those scenarios resulting from the particular measurement system and operating conditions) that require a large number of iterations for the algorithm convergence. An additional advantage guaranteed by the SVR method concerns the conditioning of the coefficient matrix. As it can be seen from Table 2.3, the SVR method has the lowest condition number, while the VM approach, with the chosen weight for the virtual measurements, presents the worst result.

2.4.4 Impact of the measurement configuration

Additional tests have been performed to verify the obtained results even with other measurement system configurations. First of all, the possible use of different measurement devices has been taken into account. To this purpose, PMU measurements

have been replaced with voltage magnitude measurements on the monitored nodes and active and reactive power measurements on the connected branches. Uncertainties with normal distribution and maximum values equal to 1% and 3% have been considered for the voltage and power measurements, respectively.

Performed tests confirm all the results previously found for the case of PMU measurements. In fact, all the approaches show similar accuracy performance, while, from the computational point of view, the SVR method results again the most efficient one. Tables 2.5 and 2.6 show the numerical properties and the efficiency results for the different approaches. In Table 2.5, numerical properties basically replicate the characteristics of the coefficient matrix seen in Table 2.3 for the PMU measurements (it is worth noting that, in this case, due to the lack of synchronized measurements, the size of the equation systems is smaller because of the different formulation of the state vector, and in particular of the slack bus voltage variables). Even in this case, the SVR approach is characterized by a reduced size of the equation system but also by a higher density of the coefficient matrix. Moreover, it exhibits the best properties from the point of view of the system conditioning.

In Table 2.6, the outcomes of the simulations show that, also in this case, the SVR method allows saving computational time, with improvements higher than 15% and 30% with respect to the VM and LM approaches (more than 23% and 37% if the SVR approach is handled without using sparse matrix techniques). Furthermore,

Table 2.5: Numerical properties of the coefficient matrix, traditional measurements

Method	Coeff. matrix density	Coeff. matrix size	Condition number
VM	3.09%	451×451	$4.05 \cdot 10^6$
LM	1.40%	689×689	$4.77 \cdot 10^4$
SVR	20.56%	213×213	$9.98 \cdot 10^3$

Table 2.6: Average iteration numbers and execution times, traditional measurements

Method	Iteration number	Execution time [ms]
VM	4.99	22.9
LM	4.99	27.8
SVR	4.97	19.4

it is possible to observe that the use of traditional measurements leads to a higher number of iterations for the algorithm convergence. The convergence properties of the SVR are, in this case, almost equal to those of the other methods.

Another series of tests has been carried out taking into account again the starting measurement configuration with PMUs. In these tests, additional voltage phasor measurements are supposed to be available besides the measurement points in nodes 150, 18 and 67. Such scenarios have been chosen because the voltage measurements are particularly critical for the BC-DSSE algorithm. In fact, each voltage measurement introduces non-zero quantities in all the Jacobian terms associated to the branch currents in the path between the slack bus and the monitored node. As a result, the following coefficient matrix is also characterized by a larger number of non-zero elements, and this higher density could affect the computational efficiency of the different methods.

To assess such impact, tests have been performed assuming two additional voltage measurements in nodes 86 and 105. Table 2.7 reports the obtained results in terms of both numerical properties and computational efficiency. As expected, the presence of the additional voltages leads to higher densities for the coefficient matrices of all the analyzed methods: this is the main reason for the longer execution times with respect to those shown in Table 2.4. It is important to underline that the obtained increase in the execution times further emphasize the benefits related to the use of the SVR approach. In this case, the improvements in the computational efficiency with respect to VM and LM are larger than 26% and 40%, respectively.

Table 2.7: Numerical properties and computational efficiency, two additional voltage measurements

Method	Coeff. matrix density	Coeff. matrix size	Iteration number	Execution time [ms]
VM	5.95%	454×454	3.24	20.4
LM	2.68%	692×692	3.24	25.0
SVR	24.52%	216×216	3.15	15.0

To check the trend in the improvements brought by the SVR method, another test has been performed adding four supplementary voltage measurements with respect to previous scenario (in nodes 25, 42, 48 and 91). Table 2.8 shows the associated results in terms of density of the coefficient matrix and efficiency of the different methods. As it can be observed, the placement of the additional voltage measurements significantly affects the matrix densities for all the methods and this causes an important rise of the execution times. In these conditions the advantages brought by the use of the SVR approach become still more evident, with saved

times close to 30% and 50% with respect to the VM and LM approaches. It is worth underlining that, as previously mentioned, with these values of density of the coefficient matrix and this size of the equation system, further advantages could be obtained by designing the SVR method without using sparse techniques. In this case, in fact, the enhancement in the computational performance with respect to VM and LM rises up to almost 37% and 50% for the scenario with two additional voltage measurements, and up to more than 45% and 60% for the measurement configuration with six supplementary voltages.

Table 2.8: Coefficient matrix density and computational efficiency, six additional voltage measurements

Method	Coeff. matrix density	Iteration number	Execution time [ms]
VM	10.36%	3.16	25.8
LM	4.64%	3.16	35.8
SVR	31.49%	3.09	18.2

2.4.5 Impact of the mesh constraints

To evaluate the behaviour of the different approaches when dealing with the mesh constraints, some tests have been performed on the benchmark network considering two reclosing branches (between nodes 151 and 300 and between nodes 54 and 94) and taking into account the base monitoring configuration composed of synchronized measurement points in nodes 150, 18 and 67.

The presence of meshes, as shown in Table 2.9, has a remarkable impact on the characteristics of the coefficient matrices for all the approaches. The first effect is on the size of the equation systems to be solved. In case of VM, the presence of the additional branches creating the meshes leads to a larger number of unknowns and, consequently, even to a larger number of equations required to solve the system. This is obviously reflected in the size of the coefficient matrix. In the LM method, this aspect is further exacerbated by the need to have a Lagrange multiplier for each constraint. For this reason, the increase of the size of the coefficient matrix for the LM method (with respect to the size reported in Table 2.3 for the case of radial network) is bigger than the one resulting for the VM approach. As for the SVR method, instead, since each equality constraint leads to the elimination of a state variable, no change appears in the size of the equation system and, thus, in the coefficient matrix.

Table 2.9: Numerical properties of the coefficient matrix, weakly meshed network

Method	Coeff. matrix density	Coeff. matrix size	Condition number
VM	11.42%	466×466	$1.52 \cdot 10^7$
LM	1.78%	716×716	$5.92 \cdot 10^5$
SVR	34.43%	216×216	$7.88 \cdot 10^4$

Also from the point of view of the coefficient matrix density, the effects brought by the mesh constraints are different depending on the specific approach. It is important to observe that each mesh introduces several non-zero entries in the Jacobian matrix $\mathbf{M}$, since it involves all the three-phase currents of the branches belonging to the mesh itself. In the VM and SVR approach, due to the multiplications involving the Jacobian in the computation of the coefficient matrix, this leads to a significant increase of the matrix density. In the LM method, instead, since the constraints are not involved in any matrix multiplication, and given also the important increase in the size of the coefficient matrix, the sparsity properties are not jeopardized.

All these aspects obviously bring direct effects on the computational performance of the different approaches. Table 2.10 shows the obtained results in terms of iteration numbers and execution times. Despite the significant increase of the coefficient matrix density, the SVR approach provides, once again, the best results both from the point of view of the convergence properties and, above all, of the execution times. Moreover, it is also important to highlight that, in this scenario, because of the drastic increase of the density in the VM approach, the LM method provides better computational performance than the VM method. The time saved by using the SVR approach is larger than 25% with respect to both VM and LM methods, with a peak of 43% if no sparse techniques are used.

Table 2.10: Average iteration numbers and execution times, weakly meshed network

Method	Iteration number	Execution time [ms]
VM	3.55	31.7
LM	3.56	31.0
SVR	3.42	23.2

2.4.6 Impact of the size of the network

A last series of tests has been performed to investigate the possible effects brought by different sizes of the network. This analysis is crucial, since actual distribution grids are generally very large networks that can also have thousands of nodes. Thus, it is important to test the performance of the different approaches even for networks with similar dimensions. To this purpose, and to make the comparison with the previous results possible, networks with larger number of nodes have been created by considering an increasing number of feeders, where each feeder replicates the topology of the original 123-bus network. In all the tests, the measurement system is supposed to be composed of a measurement point in the primary substation and, for each feeder, of two measurement points in the nodes corresponding to the buses 18 and 67 of the original version of the grid.

The main effect brought by the increasing sizes of the network is the reduction of the density in the coefficient matrices. Figure 2.2 shows, as an example, the decreasing trend obtained for the density of the coefficient matrices of the different methods when passing from one to ten feeders. It is possible to observe that, despite the increasing number of measurements, the presence of a large number of nodes drastically reduces the matrix density. In this situation, even considering the huge size resulting for the equation systems, the use of sparse techniques is a forced choice for the design of an efficient BC-DSSE algorithm.

Table 2.11 reports the results obtained when ten feeders are considered in the network. In this configuration, the resulting grid has more than two thousands nodes (considering the three phases). From Table 2.11, it is possible to observe that, obviously, the execution times are significantly higher than those of all the previous

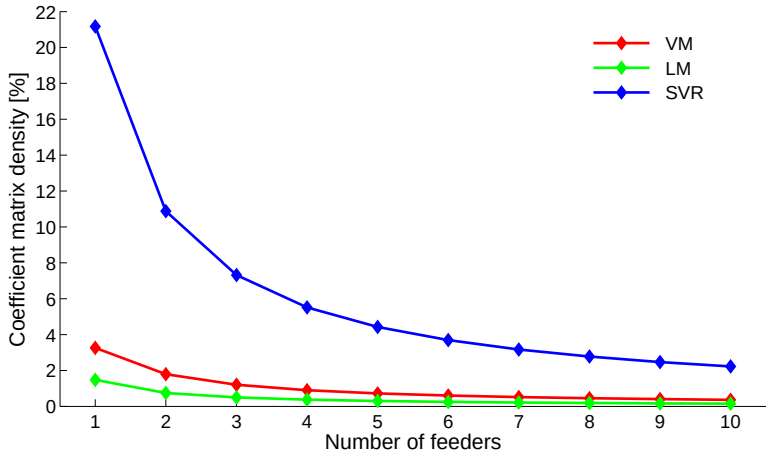

Figure 2.2: Variation in the coefficient matrix density for networks with an increasing number of feeders

tests (given the larger size of the equation system to be solved). Even in this scenario, the SVR method keeps all the aforementioned advantages; its execution times are in fact significantly lower than those of the other methods and it allows saving more than 25% and 38% of the computation time required by the VM and LM approaches, respectively. Similar results and similar considerations also hold for the tests performed with different numbers of feeders.

Table 2.11: Numerical properties and computational efficiency, 10-feeders network

Method	Coeff. matrix density	Coeff. matrix size	Iteration number	Execution time [ms]
VM	0.36%	4486×4486	4.00	185.4
LM	0.15%	6866×6866	4.00	223.1
SVR	2.22%	2106×2106	4.00	137.4

2.5 Final discussion

Tests and results shown in this Chapter clearly highlight that the inclusion of the equality constraints through the elimination of state variables can provide important benefits from the point of view of the computational efficiency of the BC-DSSE algorithm. It is important to underline that such approach, even if well-known in the literature, is usually not implemented in traditional voltage based estimators, since the resulting non-linearity of the constraints does not allow a simple and efficient implementation of this technique. The possibility to express the constraints with linear relationships and to obtain the state vector reduction in a simple way is, thus, a specific feature of the BC-DSSE algorithm.

The achievable improvements on the computational efficiency are, obviously, strictly dependent on the particular features of the considered network. The tests here proposed, for example, refer to a benchmark network having a lot of zero injections, which can be easily handled with the proposed approach. However, it is to be noted that, in a three-phase context, a large number of zero injections should be a common feature, since three-phase nodes often have loads or generators connected to only one of the phases.

The SVR method proved also to be efficient in handling the mesh constraints, despite the increase of computational burden caused by the many fill-ins brought by the meshes. From this standpoint, two aspects have to be underlined. First of all, depending on the size of the considered network, the possibility to design the proposed method without using sparse matrix techniques can be taken into account.

Performed tests show that, if the network is not too large, computations made by using full matrices can be convenient in some scenarios, above all if the density of the coefficient matrix of the equation system is quite high. In this case, the performance of the algorithm are only affected by the size of the equation system and not by the number of fill-ins in the coefficient matrix. Thus, increasing advantages can be obtained even in case of a large number of meshes.

Instead, when the size of the network is very large, the use of sparse matrix techniques is almost a forced choice for obtaining an efficient design of the algorithm. In this situation, the performance of the proposed approach can be adversely affected by the fill-ins appearing with a large number of meshes. However, hybrid solutions combining the advantages of different methods can be also conceived to deal with this possible issue. As an example, the LM method proved to have smaller problems (from the point of view of the density of the coefficient matrix) in presence of mesh constraints. Thus, a solution implementing the SVR method for the zero injection constraints and adopting the LM approach for handling the mesh constraints can be also considered to further improve the efficiency performance. In any case, it is worth noting that distribution grids are usually radial or weakly meshed networks. As a result, possible problems caused by the number of fill-ins in the coefficient matrix of the equation system are generally limited, and the SVR approach can be conveniently adopted to handle all the types of constraints.

Chapter 3

Performance analysis of BC-DSSE

3.1 WLS distribution system state estimators

As described in Chapter 1, the SE problem in power systems is traditionally faced referring to WLS estimation algorithms that use the voltage magnitudes and angles at the different buses of the network as state variables [4]. Several reasons support this choice. First of all, transmission grids are usually highly meshed networks, because this topology ensures a higher reliability for the system. As a consequence, the choice of state variables associated to the nodes, rather than to the branches, allows achieving a smaller size for the equation systems to be solved inside the algorithm. Moreover, transmission systems are usually characterized by very low R/X ratios. This feature can be duly exploited in practical applications by neglecting the resistance terms. In this way, the SE algorithm can be decoupled, separating the computation of the voltage magnitudes from the estimation of the voltage angles.

In distribution systems, because of the different features of the network, these advantages do not hold anymore. In most of the cases, distribution grids are radial or only weakly meshed; thus, the number of branches and nodes in the network is similar. As for the line parameters, R/X ratios close to 1 or even higher are quite common; therefore, the decoupling of the traditional state estimators is not possible. As a result, different formulations of the WLS algorithm could be more convenient than the traditional one and, in general, the electrical quantities related to the branches become a possible alternative as state variables of the system.

For these reasons, in the literature, two main classes of WLS algorithms have been developed to deal with the DSSE problem: state estimators based on the node voltages (as, for example, in [28–30, 54, 59]) and estimators using the branch currents as state variables (like, for example, [31–34, 36, 60]). Each one of these categories can be further divided depending on the implementation of the state variables in polar or rectangular coordinates.

This Chapter aims at assessing the performance of the proposed DSSE algorithm. The goal is to highlight the strengths and weaknesses of the presented proposal, providing a comprehensive and as fair as possible evaluation of the performance through the comparison with other types of WLS estimators available in the literature, based on different state variables. In fact, for example, the type of variables directly estimated through the DSSE algorithm could affect the final estimation accuracy. Moreover, the need to consider different mathematical relationships in the algorithm can imply a different computational burden, and thus, also a different efficiency for the alternative approaches [61]. Besides the global performance of the proposed DSSE formulation in terms of accuracy, efficiency, computational burden and numerical properties, the possibility to design a phase-decoupled version of the algorithm will be also investigated. Furthermore, the impact brought by the network parameter uncertainties, due to the mathematical model used in the algorithm, will be analyzed.

3.2 Node voltage based estimators

As aforementioned, voltage based estimators are well known in the literature since they are commonly used in transmission systems. Their main advantage is the handling of the meshed networks: in fact, they guarantee a constant number of state variables regardless of the radial, weakly or highly meshed topology of the network. Moreover, the constraints associated to the application of the Kirchhoff voltage law along the meshes are inherently considered in the model and do not require a specific implementation. Since in distribution systems the traditional decoupling of the state estimator, obtained by neglecting the resistance component of the line parameters, is not possible, both polar and rectangular coordinates have been proposed as a possible choice for the state variables of the system.

3.2.1 Polar voltage DSSE formulation

Referring to the three-phase model of the distribution systems, if the node voltages in polar form are assumed as state variables of the DSSE algorithm, the state vector can be written as $\mathbf{x} = [\mathbf{x}_A, \mathbf{x}_B, \mathbf{x}_C]$, where the generic component $\mathbf{x}_\phi$ referred to phase ϕ is:

$$\mathbf{x}_\phi = [\delta_{2\phi}, ..., \delta_{N\phi}, V_{1\phi}, ..., V_{N\phi}] \tag{3.1}$$

where $\delta_{i\phi}$ and $V_{i\phi}$ are the angle and the magnitude of the voltage at the i-th node of the phase ϕ and N_ϕ is the number of buses belonging to the phase ϕ of the network.

This state vector is usually implemented when only conventional measurements are deployed in the grid: in fact, the voltage angle of the first node (namely the

slack bus of the system) is chosen as angle reference, fixed equal to zero (or $\pm 120°$ depending on the considered phase of the system) and thus it can be removed from the set of variables within the state vector. Instead, if synchronized measurements provided by PMUs are also available, as shown in [52], the reference is given by the UTC time and thus the voltage angle of the slack bus should be also included in the state vector for being estimated, leading to:

$$\mathbf{x}_\phi = [\delta_{1\phi}, ..., \delta_{N\phi}, V_{1\phi}, ..., V_{N\phi}] \tag{3.2}$$

The main differences among the different formulations are basically focused on the mathematical relationships needed to express the measurement functions and, consequently, the Jacobian matrix involved in the estimation process. Considering [28] as reference for the mathematical details involved in the computation of the functions associated to the conventional measurements, and [49] for the inclusion of the syncrophasor measurements, the following relationships have been considered.

- **Active and reactive power flow**

  Indicating with $h_{P_{l\phi}}$ and $h_{Q_{l\phi}}$ the measurement functions associated to the active and reactive power flow measurement on the phase ϕ of branch l, it is possible to write (see [28] for details):

$$\begin{aligned} h_{P_{l\phi}} = V_{s\phi} \sum_{\psi=A}^{C} \{ & g_{l,\phi\psi} \left[V_{s\psi} \cos(\delta_{s\phi} - \delta_{s\psi}) - V_{r\psi} \cos(\delta_{s\phi} - \delta_{r\psi}) \right] \\ & + b_{l,\phi\psi} \left[V_{s\psi} \sin(\delta_{s\phi} - \delta_{s\psi}) - V_{r\psi} \sin(\delta_{s\phi} - \delta_{r\psi}) \right] \} \end{aligned} \tag{3.3}$$

$$\begin{aligned} h_{Q_{l\phi}} = V_{s\phi} \sum_{\psi=A}^{C} \{ & g_{l,\phi\psi} \left[V_{s\psi} \sin(\delta_{s\phi} - \delta_{s\psi}) - V_{r\psi} \sin(\delta_{s\phi} - \delta_{r\psi}) \right] \\ & - b_{l,\phi\psi} \left[V_{s\psi} \cos(\delta_{s\phi} - \delta_{s\psi}) - V_{r\psi} \cos(\delta_{s\phi} - \delta_{r\psi}) \right] \} \end{aligned} \tag{3.4}$$

  where $V_{s\psi}$ and $V_{r\psi}$ are the voltage magnitudes of the generic phase ψ at the sending and the receiving node of branch l, respectively; $\delta_{s\psi}$ and $\delta_{r\psi}$, similarly, are the voltage angles of the generic phase ψ at the sending and the receiving nodes of the line, respectively; $g_{l,\phi\psi}$ and $b_{l,\phi\psi}$ are, respectively, the real and imaginary parts of the admittance in branch l: if $\psi = \phi$ the components refer to the self-admittance of the branch, while if $\psi \neq \phi$ the terms represent the mutual admittance between the different phases of the three-phase model. From (3.3) and (3.4) it is possible to observe that the found relationships are non-linear and involve the voltage states of both magnitudes and angles of all the three phases of the sending and the receiving node of the considered line. As a consequence, the derivatives required in the Jacobian matrix, if computed

without using approximations, are also nonlinear and would need to be updated at each iteration of the estimation process. Moreover, coupling among the different phases exists because of the presence of the mutual admittance terms.

- **Active and reactive power injection**

  The power injection on the phase ϕ of node i can be seen as the sum of the branch powers converging to the considered node. As a result, the measurement functions $h_{P_{inj,i\phi}}$ and $h_{Q_{inj,i\phi}}$, related to the active and reactive components of the power injection, respectively, can be written as:

$$\begin{aligned} h_{P_{inj,i\phi}} = V_{i\phi} \sum_{k\in\Omega} \sum_{\psi=A}^{C} \{ & g_{k,\phi\psi} \left[V_{i\psi} \cos(\delta_{i\phi} - \delta_{i\psi}) - V_{r_k\psi} \cos(\delta_{i\phi} - \delta_{r_k\psi}) \right] \\ & + b_{k,\phi\psi} \left[V_{i\psi} \sin(\delta_{i\phi} - \delta_{i\psi}) - V_{r_k\psi} \sin(\delta_{i\phi} - \delta_{r_k\psi}) \right] \} \end{aligned} \tag{3.5}$$

$$\begin{aligned} h_{Q_{inj,i\phi}} = V_{i\phi} \sum_{k\in\Omega} \sum_{\psi=A}^{C} \{ & g_{k,\phi\psi} \left[V_{i\psi} \sin(\delta_{i\phi} - \delta_{i\psi}) - V_{r_k\psi} \sin(\delta_{i\phi} - \delta_{r_k\psi}) \right] \\ & - b_{k,\phi\psi} \left[V_{i\psi} \cos(\delta_{i\phi} - \delta_{i\psi}) - V_{r_k\psi} \cos(\delta_{i\phi} - \delta_{r_k\psi}) \right] \} \end{aligned} \tag{3.6}$$

  where Ω is the set of branches converging to node i, $V_{i\psi}$ and $\delta_{i\psi}$ are the voltage magnitude and angle of the generic phase ψ of the considered node i, $V_{r_k\psi}$ and $\delta_{r_k\psi}$ are the corresponding voltage magnitudes and angles of the ending nodes of the k-th branch and $g_{k,\phi\psi}$ and $b_{k,\phi\psi}$ are, similarly to the previous case, the real and imaginary parts of the admittances in branch k. As in the case of power flows, it is possible to note that the relationships describing the power measurements, and the associated derivative terms, if considered without any approximation are nonlinear and introduce coupling among the different phases.

- **Current magnitude**

  The function associated to a current magnitude measurement $I_{l\phi}$ on the phase ϕ of a generic line l can be obtained as follows:

$$h_{I_{l\phi}} = \sqrt{{i^r_{l\phi}}^2 + {i^x_{l\phi}}^2} \tag{3.7}$$

  where $i^r_{l\phi}$ and $i^x_{l\phi}$ are the real and imaginary parts of the considered current, which can be computed as follows:

$$\begin{aligned} i^r_{l\phi} = \sum_{\psi=A}^{C} \{ & g_{l,\phi\psi} \left[V_{s\psi} \cos(\delta_{s\psi}) - V_{r\psi} \cos(\delta_{r\psi}) \right] \\ & - b_{l,\phi\psi} \left[V_{s\psi} \sin(\delta_{s\psi}) - V_{r\psi} \sin(\delta_{r\psi}) \right] \} \end{aligned} \tag{3.8}$$

$$i_{l\phi}^{x} = \sum_{\psi=A}^{C} \{ g_{l,\phi\psi} \left[V_{s\psi} \sin(\delta_{s\psi}) - V_{r\psi} \sin(\delta_{r\psi}) \right] + b_{l,\phi\psi} \left[V_{s\psi} \cos(\delta_{s\psi}) - V_{r\psi} \cos(\delta_{r\psi}) \right] \} \tag{3.9}$$

where, similarly to the case of the branch power flows, $V_{s\psi}$ and $V_{r\psi}$ are the voltage magnitudes of the generic phase ψ at the sending and the receiving nodes of branch l, $\delta_{s\psi}$ and $\delta_{r\psi}$ are the voltage angles at the same nodes, and $g_{l,\phi\psi}$ and $b_{l,\phi\psi}$ are, respectively, the real and imaginary parts of the admittance in branch l. As clear from the shown relationships, the current magnitude measurement functions are nonlinear and involve all the three phases of the sending and receiving nodes of the considered branch. The calculation of the derivatives with respect to the generic variable x of the state vector, computed by using the rule of differentiation [28], yield:

$$\frac{\partial I_{l\phi}}{\partial x} = \frac{\partial I_{l\phi}}{\partial i_{l\phi}^{r}} \cdot \frac{\partial i_{l\phi}^{r}}{\partial x} + \frac{\partial I_{l\phi}}{\partial i_{l\phi}^{x}} \cdot \frac{\partial i_{l\phi}^{x}}{\partial x} \tag{3.10}$$

$$\frac{\partial I_{l\phi}}{\partial x} = \frac{\partial i_{l\phi}^{r}}{\partial x} \cos(\theta_{l\phi}) + \frac{\partial i_{l\phi}^{x}}{\partial x} \sin(\theta_{l\phi}) \tag{3.11}$$

where $\theta_{l\phi}$ is the current angle that can be obtained from the calculated real and imaginary currents as follows:

$$\theta_{l\phi} = \tan^{-1} \left(\frac{i_{l\phi}^{x}}{i_{l\phi}^{r}} \right) \tag{3.12}$$

As it can be observed from equations (3.7)-(3.12), if the proper computation of the measurement functions and the Jacobian sub-matrix related to the current magnitude measurements is performed, several steps are needed. Moreover, the Jacobian has to be updated at each iteration of the estimation process.

- **Voltage magnitude**

  The measurement functions related to a voltage magnitude measurement $V_{i\phi}$ on the phase ϕ of the node i is trivial, since it corresponds to a state variable of the system. Thus, it is:

  $$h_{V_{i\phi}} = V_{i\phi} \tag{3.13}$$

  The presence of voltage magnitude measurements does not introduce coupling among the different phases of the system. Moreover, the corresponding Jacobian sub-matrix is constant and, hence, it can be computed outside the iterative part of the DSSE algorithm to reduce the computational burden and speed up the estimation process.

- **Current and voltage phasors**

  Following what demonstrated in [49], the more convenient way to include the current PMU measurements in a voltage based estimator is by considering them in rectangular coordinates. The reference functions are thus the same indicated in (3.8) and (3.9) for the real and the imaginary components of the current, respectively. It is worth noting that, similarly to what shown in Chapter 1 for the BC-DSSE estimator, the inclusion of the synchrophasors in rectangular coordinates leads to correlations between real and imaginary parts of the phasor, which should be duly considered for a proper modeling of the measurement errors. It is also worth noting that the derivatives to be considered in the Jacobian are not constant and need to be computed at each iteration of the WLS algorithm. As for the voltage phasor measurements, instead, their inclusion in the mathematical model of the polar voltage based estimator is straightforward, since both magnitudes and angles are variables of the used state vector. In this case, therefore, the Jacobian sub-matrix is constant and can be computed only once outside the iterative part of the estimation algorithm.

In comparison to the BC-DSSE proposed in Chapter 1, it is important to underline that in this model all the measurement functions are directly considered (while in the rectangular BC-DSSE formulation the power measurements were converted in equivalent current measurements). As a result, the polar Node Voltage DSSE (NV-DSSE) does not require the computation of equivalent measurements and the consequent calculation of the related full covariance matrix of the measurement errors. Furthermore, it is worth noting that, differently from the branch current estimator, the other electrical quantities of the network (in this case, for example, the currents) do not need to be computed at each iteration of the WLS algorithm, but, if required, they can be calculated at the end of the iterative process (in the proposed branch current estimator, instead, a forward sweep step was necessary at each iteration to compute the node voltages to be used in the calculation of the equivalent current measurements). This allows reducing the computational costs in the polar NV-DSSE. At the same time, however, the presence of many nonlinear measurement functions and the need to update at each iteration the associated Jacobian sub-matrices, lead to the opposite effect of increasing the computational burden.

3.2.2 Rectangular voltage DSSE formulation

The rectangular version of the voltage based DSSE is an alternative that allows a more straightforward implementation of many of the measurement functions. In particular, similarly to the proposed BC-DSSE, power measurement functions can

be linearized by using equivalent current measurements. This allows an easier implementation of many of the measurements available in a distribution system, namely the pseudo-measurements related to the power injections of loads or generators. Referring to the three-phase model of the distribution systems, and indicating with $\mathbf{x} = [\mathbf{x}_A, \mathbf{x}_B, \mathbf{x}_C]$ the three-phase state vector, if only traditional measurements are available in the field, the generic component $\mathbf{x}_\phi$ referred to phase ϕ is:

$$\mathbf{x}_\phi = [v^r_{1\phi}, ..., v^r_{N\phi}, v^x_{2\phi}, ..., v^x_{N\phi}] \tag{3.14}$$

where $v^r_{i\phi}$ and $v^x_{i\phi}$ are, respectively, the real and the imaginary parts of the voltage at node i. If also PMU synchrophasors are present in the measurement system, instead, the vector $\mathbf{x}_\phi$ is:

$$\mathbf{x}_\phi = [v^r_{1\phi}, ..., v^r_{N\phi}, v^x_{1\phi}, ..., v^x_{N\phi}] \tag{3.15}$$

where the imaginary part of the slack bus voltage is introduced because of the use of the UTC time as reference for the angle measurements.

The indications shown in [30] are used as reference for the implementation of the measurement functions for this DSSE model. In the following, for the sake of convenience, the measurement functions used in the implementation are reported.

- **Active and reactive power flow**

  As aforementioned, in the rectangular NV-DSSE model, power measurements are converted in equivalent current measurements (see Section 1.4 for details on the computation of the equivalent measurements). As a consequence, the active and reactive power flow in branch l are converted in real and imaginary currents on the line, which can be expressed in terms of the rectangular voltages used in the state vector as follows:

$$h^{eq}_{i^r_{l\phi}} = \sum_{\psi=A}^{C} \{ g_{l,\phi\psi} \left[v^r_{s\psi} - v^r_{r\psi} \right] - b_{l,\phi\psi} \left[v^x_{s\psi} - v^x_{r\psi} \right] \} \tag{3.16}$$

$$h^{eq}_{i^x_{l\phi}} = \sum_{\psi=A}^{C} \{ g_{l,\phi\psi} \left[v^x_{s\psi} - v^x_{r\psi} \right] + b_{l,\phi\psi} \left[v^r_{s\psi} - v^r_{r\psi} \right] \} \tag{3.17}$$

  where $v^r_{s\psi}$ and $v^x_{s\psi}$ are the real and the imaginary parts of the voltage at the sending node of the considered branch l, respectively, $v^r_{r\psi}$ and $v^x_{r\psi}$ are the analogous voltages at the receiving node of the line, and $g_{l,\phi\psi}$ and $b_{l,\phi\psi}$are the real and imaginary terms of the admittance for branch l. From the reported equations, it is possible to observe that the conversion of the powers in equivalent currents allows achieving linear relationships. As a consequence, the resulting Jacobian sub-matrix is constant and can be computed only once at the beginning of the estimation process. The presence in the functions of the self and

mutual terms of branch admittance, instead, leads to the coupling among the different phases of the system.

- **Active and reactive power injection**

  Also for the power injections, the conversion in equivalent current measurements is generally performed. Considering the equivalent measurements deriving from a power injection on the phase ϕ of node i, the following holds:

$$h^{eq}_{i^r_{inj,i\phi}} = \sum_{k\in\Omega}\sum_{\psi=A}^{C}\{g_{k,\phi\psi}\left[v^r_{i\psi} - v^r_{r_k\psi}\right] - b_{k,\phi\psi}\left[v^x_{i\psi} - v^x_{r_k\psi}\right]\} \tag{3.18}$$

$$h^{eq}_{i^x_{inj,i\phi}} = \sum_{k\in\Omega}\sum_{\psi=A}^{C}\{g_{k,\phi\psi}\left[v^x_{i\psi} - v^x_{r_k\psi}\right] + b_{k,\phi\psi}\left[v^r_{i\psi} - v^r_{r_k\psi}\right]\} \tag{3.19}$$

  where Ω is the set of the branches converging to node i, $v^r_{i\psi}$ and $v^x_{i\psi}$ are the real and the imaginary parts of the voltage of the generic phase ψ at the considered node i, $v^r_{r_k\psi}$ and $v^x_{r_k\psi}$ are the real and imaginary parts of the voltages on the phase ψ of the ending node of the k-th branch, and $g_{k,\phi\psi}$ and $b_{k,\phi\psi}$ are the real and imaginary parts of the admittances in branch k. Similarly to the previous case, it is possible to note that the measurement functions are characterized by linear relationships (and consequently by a constant Jacobian) and that they imply the coupling among the different phases of the system.

- **Current magnitude**

  In [30], the current magnitude measurements are converted in equivalent current phasors exploiting the phase-angle computed starting from the rectangular components of the current calculated as in (3.16) and (3.17). Here, to have a fair comparison with the other approaches, such a conversion is not performed and the current magnitude is implemented in its original form. Similarly to what shown in the previous subsection for the polar NV-DSSE, the current magnitude measurement in a generic branch l is computed as:

$$h_{I_{l\phi}} = \sqrt{{i^r_{l\phi}}^2 + {i^x_{l\phi}}^2} \tag{3.20}$$

  where $i^r_{l\phi}$ and $i^x_{l\phi}$ are the real and imaginary parts of the considered current calculated as in (3.16) and (3.17). Even in this case, the rule of differentiation can be used to compute the derivatives to be included in the Jacobian matrix and, thus, the following holds:

$$\frac{\partial I_{l\phi}}{\partial x} = \frac{\partial i^r_{l\phi}}{\partial x}\cos(\theta_{l\phi}) + \frac{\partial i^x_{l\phi}}{\partial x}\sin(\theta_{l\phi}) \tag{3.21}$$

where x is the generic state variable of the state vector and $\theta_{l\phi}$ is the current angle in the considered branch, whose tangent is equal to the ratio between the computed real and imaginary components of the current phasor. It is worth noting that proper consideration of the current magnitude measurement implies a nonlinear function involving also the other phases of the grid and, therefore, lead to the coupling among the three-phases of the system.

- **Voltage magnitude**

  A voltage magnitude measurements on the phase ϕ of a generic node i of the grid can be included in the model of the rectangular NV-DSSE algorithm according to the following:

$$h_{V_{i\phi}} = \sqrt{{v_{i\phi}^r}^2 + {v_{i\phi}^x}^2} \tag{3.22}$$

  where $V_{i\phi}$ is the considered voltage magnitude and $v_{i\phi}^r$ and $v_{i\phi}^x$ are the real and imaginary components of the same voltage. It is possible to observe that (3.22) is a nonlinear function but it does not introduce any coupling among the different phases of the system (thus, only state variables belonging to the same phase of the measured voltage are involved in the calculations).

- **Current and voltage phasors**

  The inclusion of the current and voltage phasors in the rectangular NV-DSSE is straightforward. As for the currents, the linear relationships shown in (3.16) and (3.17) can be used to consider the real and imaginary part of the phasor, respectively. As for the voltage phasors, the implementation is also easy, since the measurements can be converted in rectangular coordinates in order to have a full correspondence with the chosen state variables of the algorithm. In both cases, it is worth noting that the conversion in rectangular coordinates of the synchrophasors provided by the PMUs requires the computation of the resulting full covariance matrix, starting from the original measurement errors associated to the magnitude and phase-angle measurements. The procedure to calculate this covariance matrix is the same indicated in Section 1.7.3 for the rectangular BC-DSSE. It is also important to note that both current and voltage phasors, being characterized by linear measurement functions, allows the computation of their constant sub-matrices only once in the estimation algorithm.

In this formulation of the DSSE, similarly to the proposed rectangular BC-DSSE, equivalent current measurements are introduced in place of the original power measurements. This allows the achievement of linear functions (and constant Jacobians) for the branch power measurements and above all for the pseudo-measurements of

power injections, which are the majority of measurements in the distribution system context. Differently from the rectangular BC-DSSE, however, the voltages needed to update at each iteration the equivalent current measurements are directly estimated into the state vector, and thus they do not need any other dedicated step. As for the estimation of the currents (or the powers) in the branches, if needed, it can be carried out at the end of the algorithm, outside of the iterative part, exploiting the estimation of the node voltages and the consequent knowledge of the voltage drop along the lines.

3.3 Branch current based estimators

As illustrated in Chapter 1, the idea to use the rectangular branch currents as state variables in the DSSE has been conceived because of the radial topology of many of the distribution networks and the simplicity in the definition of the measurement functions (in particular for the power measurements, when converted in equivalent current measurements). As already described, besides the computation of the equivalent current measurements, this procedure also requires the execution of a forward sweep step at each iteration of the WLS algorithm, in order to obtain the updated values of the voltages at the nodes. Some years later, the possibility to implement a DSSE algorithm using the branch currents in polar coordinates was advanced by Wang and Schulz [60]. The main reason for this proposal was associated to the consequent easiness in the handling of possible current magnitude measurements. In fact, this kind of measurements can bring issues in traditional state estimators and, for this reason, sometimes they are also discarded in case of high redundancy of the measurements. Since in distribution systems the measurements are only few, the possible presence of current magnitude measurements cannot be disregarded. As a consequence, they should be duly taken into account and properly introduced into the DSSE model. The use of the polar BC-DSSE, thanks to the use of the current magnitudes as state variables of the system, represents of course the most straightforward solution for the management of these measurements.

3.3.1 Polar current DSSE formulation

Similarly to the polar version of the NV-DSSE, the polar BC-DSSE does not take particular advantages from a possible definition of equivalent current measurements in place of the powers. For this reason, power measurements can be defined in their original form. Despite the lack of this calculation, similarly to the rectangular version of the BC-DSSE, a forward sweep step is required at each iteration of the estimation algorithm to compute the updated values of the voltages at the nodes. In fact (as it will be shown in the following description of the measurement functions) the

knowledge of the node voltages is necessary to calculate the measurement functions and the Jacobian terms needed in the estimator. It is worth noting that, similarly to what described in Chapter 1 for the rectangular BC-DSSE, the original version of the polar BC-DSSE presented in [60] is based on the use of only currents in the state vector. However, such a choice does not allow the achievement of any knowledge about the voltage profile of the network. To deal with this issue, in [36], a modified version of this estimator has been proposed, where the slack bus voltages are included within the state vector. As shown also for the rectangular BC-DSSE (Section 1.6), the extended state vector with the additional slack bus voltages allows a suitable estimation of the voltage profile and to properly exploit the presence of the voltage measurements available in the network. Referring to this extended model, and taking into account the three-phase scheme of the distribution systems, the state vector $\mathbf{x} = [\mathbf{x}_A, \mathbf{x}_B, \mathbf{x}_C]$ has, for each phase ϕ, the following form:

$$\mathbf{x}_\phi = [V_{slack,\phi}, I_{1\phi}, ..., I_{N_{br}\phi}, \theta_{1\phi}, ..., \theta_{N_{br}\phi}] \tag{3.23}$$

where $V_{slack,\phi}$ is the voltage magnitude of the phase ϕ of the slack bus, $I_{l\phi}$ and $\theta_{l\phi}$ are the magnitude and phase-angle, respectively, of the current in the same phase ϕ of the generic branch l, and N_{br} represents the total number of branches present in the network. The state vector formulation shown in (3.23) can be used when only conventional measurements are available on the field. Similarly to the other estimators, if PMU measurements are also present, then the phase-angle of the slack bus voltage has also to be estimated and thus it has to be included in the state vector. In this case, the inclusion of the slack bus voltage is more convenient if performed by referring to its rectangular components (the measurement functions deriving from this choice are simpler, see [36] for additional details). As a consequence, the state vector when synchrophasor measurements are present is:

$$\mathbf{x}_\phi = [v^r_{slack,\phi}, v^x_{slack,\phi}, I_{1\phi}, ..., I_{N_{br}\phi}, \theta_{1\phi}, ..., \theta_{N_{br}\phi}] \tag{3.24}$$

where $v^r_{slack,\phi}$ and $v^x_{slack,\phi}$ are the real and imaginary parts of the slack bus voltage on the considered phase ϕ. In the following, referring to the considerations presented in [60], the measurement functions used for the implementation of the polar BC-DSSE algorithm are reported for the sake of convenience.

- **Active and reactive power flow**

  The active and reactive power measurements on the phase ϕ of a generic branch l can be expressed in terms of the polar coordinates of the branch currents as follows:

$$h_{P_{l\phi}} = \alpha V_{s\phi} I_{l\phi} \cos(\delta_{s\phi} - \theta_{l\phi}) \tag{3.25}$$

$$h_{Q_{l\phi}} = \alpha V_{s\phi} I_{l\phi} \sin(\delta_{s\phi} - \theta_{l\phi}) \tag{3.26}$$

where $V_{s\phi}$ and $\delta_{s\phi}$ are the voltage magnitude and angle, respectively, of the phase ϕ of the sending node of branch l, $I_{l\phi}$ and $\theta_{l\phi}$ are the current magnitude and angle of the same phase ϕ of branch l, and α is ± 1 depending on whether the measured power has the same direction of the one chosen as conventionally positive for the branch or not. From (3.25) and (3.26) it is possible to observe that the measurement functions describing the branch power flows are nonlinear and they require the knowledge of the voltages in the considered node. This emphasize the importance to perform the forward sweep step at each iteration of the DSSE algorithm (in order to have the updated values of voltage) and above all to include the slack bus voltages within the state vector in order to have a proper estimation of the voltage profile of the network. As shown in [60], the Jacobian terms can be conveniently calculated using the same calculations needed for the definition of the measurement functions. It is also worth noting that, similarly to the rectangular BC-DSSE, power measurements do not imply the coupling among the different phases of the system.

- **Active and reactive power injection**

  As seen in the previous cases, the power injection in a generic node i can be defined as the sum of the powers of the branches converging to the considered node. Indicating with Ω and Λ, respectively, the sets of the branches incoming and outgoing from the considered node i, the searched measurement functions can be expressed as:

$$h_{P_{inj,i\phi}} = \alpha V_{i\phi} \left[\sum_{k \in \Omega} I_{k\phi} \cos(\delta_{i\phi} - \theta_{k\phi}) - \sum_{m \in \Lambda} I_{m\phi} \cos(\delta_{i\phi} - \theta_{m\phi}) \right] \tag{3.27}$$

$$h_{Q_{inj,i\phi}} = \alpha V_{i\phi} \left[\sum_{k \in \Omega} I_{k\phi} \sin(\delta_{i\phi} - \theta_{k\phi}) - \sum_{m \in \Lambda} I_{m\phi} \sin(\delta_{i\phi} - \theta_{m\phi}) \right] \tag{3.28}$$

  where $V_{i\phi}$ and $\delta_{i\phi}$ are the voltage magnitude and angle at the considered node i, respectively, $I_{k\phi}$ and $\theta_{k\phi}$ are the current magnitude and angle of the generic branch k (the same notation also holds for the currents of the branches m) and α is a constant equal to ± 1 depending on the direction of the power injection (load consumption or power generation). As in the previous case, it is possible to observe that power injections are characterized by nonlinear measurement functions that require the knowledge of the voltage profile of the network for their calculation. Moreover, they involve multiple branches but do not imply any coupling among the different phases of the three-phase system.

- **Current magnitude**

  The definition of the current magnitude measurements is obviously trivial since such measurements correspond to state variables of the system. Therefore, for the generic measurement on branch l, it is possible to simply write:

$$h_{I_{l\phi}} = I_{l\phi} \tag{3.29}$$

  where $I_{l\phi}$ is the current magnitude of the considered branch. In this case, the measurement functions are linear and the related constant Jacobian matrices can be computed only once at the beginning of the estimation process.

- **Voltage magnitude**

  A voltage magnitude measurement on the phase ϕ of a generic node i can be treated by considering the voltage drops along the lines, starting from the estimated slack bus voltage. In particular, indicating with Γ the path between the slack bus and node i, it is possible to write:

$$v_{i\phi} = v_{slack\phi} - \sum_{k\in\Gamma} \mathbf{Z}_{k,\phi}\mathbf{i}_k \tag{3.30}$$

  where $v_{i\phi}$ is the voltage phasor on the phase ϕ of the measured node i, $v_{slack\phi}$ is the voltage phasor on the same phase of the slack bus, $\mathbf{Z}_{k,\phi}$ is the row of the three-phase impedance matrix of branch k including the self and mutual impedances for phase ϕ, and $\mathbf{i}_k$ is the three-phase vector of the currents in branch k. Starting from (3.30), it is possible to define the voltage magnitude measurement function in node i as:

$$h_{V_{i\phi}} = Re\left\{\left[v_{slack\phi} - \sum_{k\in\Gamma} \mathbf{Z}_{k,\phi}\mathbf{i}_k\right] e^{-j\delta_{i\phi}}\right\} \tag{3.31}$$

  where $\delta_{i\phi}$ is the voltage angle on the phase ϕ of node i. From (3.31) it is possible to obtain:

$$h_{V_{i\phi}} = V_{slack\phi}\cos(\delta_{slack\phi} - \delta_{i\phi}) - \sum_{k\in\Gamma}\sum_{\psi=A}^{C} Z_{k,\phi\psi} I_{k\psi}\cos(\zeta_{k,\phi\psi} + \theta_{k\psi} - \delta_{i\phi}) \tag{3.32}$$

  where $V_{slack\phi}$ and $\delta_{slack\phi}$ are the magnitude and the angle of the slack bus voltage, $Z_{k,\phi\psi}$ and $\zeta_{k,\phi\psi}$ are the magnitude and the angle of the impedance in branch k (the self impedance of phase ϕ if $\psi = \phi$ or the mutual term between phases ϕ and ψ if $\psi \neq \phi$), and $I_{k\psi}$ and $\theta_{k\psi}$ are the magnitude and angle of the current on phase ψ of the k-th branch. As it can be observed from (3.32), the voltage magnitude measurement function involves the currents of all the

branches (and phases) in the path between slack bus and measured node. The function is nonlinear and implies the coupling among the different phases of the system.

- **Current and voltage phasors**

  The inclusion of the current phasors in the polar BC-DSSE algorithm is straightforward, since PMUs provide the currents in terms of their magnitude and phase-angle, thus in the same form of the variables within the state vector. As for the voltage phasors, instead, a convenient implementation can be obtained by implementing the phasors in rectangular coordinates (see [36] for further details). Considering a voltage synchrophasor measurement on the phase ϕ of a generic node i, the associated measurement function can be obtained by computing the real and the imaginary parts of the voltage measurement function reported in (3.30) as follows:

$$h_{v^r_{i\phi}} = v^r_{slack\phi} - \sum_{k\in\Gamma}\sum_{\psi=A}^{C} Z_{k,\phi\psi} I_{k\psi} \cos(\zeta_{k,\phi\psi} + \theta_{k\psi}) \tag{3.33}$$

$$h_{v^x_{i\phi}} = v^x_{slack\phi} - \sum_{k\in\Gamma}\sum_{\psi=A}^{C} Z_{k,\phi\psi} I_{k\psi} \sin(\zeta_{k,\phi\psi} + \theta_{k\psi}) \tag{3.34}$$

  where $v^r_{slack\phi}$ and $v^x_{slack\phi}$ are the real and imaginary parts of the phase ϕ of the slack bus voltage, and the impedance and current terms are the same presented for the case of voltage magnitude measurements. As it can observed, current phasor measurements are linear, with a constant Jacobian, and do not introduce any coupling among the phases of the system, while voltage phasor measurements are nonlinear and imply the coupling of the phases of the network.

- **Meshes**

  As described in Chapter 1, DSSE algorithms based on branch current state variables require the explicit implementation of the mesh constraints brought by the Kirchhoff's voltage law along the meshes. As a consequence, even for the polar BC-DSSE it is necessary to define the equivalent measurements associated to the mesh constraints to be included in the DSSE model. As seen in Section 1.5.7, the mesh constraint can be expressed in the following terms:

$$\sum_{h\in\Psi} \alpha_h \mathbf{Z}_h \mathbf{i}_h = 0 \tag{3.35}$$

  where Ψ is the set of the branches belonging to the considered mesh, α_h is ± 1 depending on the mesh direction with respect to the conventional direction assumed for the h-th branch current, and $\mathbf{Z}_h$ and $\mathbf{i}_h$ are the three-phase

impedance matrix and the three-phase current vector associated to the h-th branch, respectively. Expressing (3.35) in terms of the polar currents of the polar BC-DSSE state vector, and considering that the Kirchhoff's voltage law holds for both the real and imaginary voltage drops, it is possible to find:

$$h^r_{mesh,\phi} = \sum_{h\in\Psi}\sum_{\psi=A}^{C} \alpha_h Z_{h,\phi\psi} I_{h\psi} \cos(\zeta_{h,\phi\psi} + \theta_{h\psi}) \tag{3.36}$$

$$h^x_{mesh,\phi} = \sum_{h\in\Psi}\sum_{\psi=A}^{C} \alpha_h Z_{h,\phi\psi} I_{h\psi} \sin(\zeta_{h,\phi\psi} + \theta_{h\psi}) \tag{3.37}$$

where $Z_{h,\phi\psi}$, $\zeta_{h,\phi\psi}$, $I_{h\psi}$ and $\theta_{h\psi}$ are the same terms of impedance and current used also for the voltage measurement functions. As clear from (3.36) and (3.37), measurement functions associated to the mesh constraints are nonlinear and imply the coupling among the different phases of the grid.

3.4 Tests and results

3.4.1 Test assumptions and metrics

Several tests have been performed to analyze the performance and characteristics of the presented WLS formulations in different scenarios. The balanced 95-bus network depicted in Fig. 3.1[1] is used as benchmark grid to assess the performance of the WLS models in presence of changing measurement system configurations and in case of meshed topology of the network (obtained by connecting some nodes as described in the following). The presence of either conventional or synchrophasor measurements has been supposed to investigate possible differences of the impact brought on the WLS algorithms performance. Data of the 95-bus network can be found in [62]. Further simulations are then carried out on the unbalanced IEEE 123-bus network shown in Fig. 3.2 [58]. The focus in this case is on the impact brought by the three-phase model of the network (with the consequent presence of mutual terms for the branch impedances) on the numerical properties of the different WLS formulations. Moreover, the possibility to achieve the phase-decoupling of the different WLS algorithms is also studied.

Tests have been performed by means of Monte Carlo simulations using a number of Monte Carlo trials $N_{MC} = 25000$. In all the tests, a load flow, referring to the nominal conditions of the network, is performed to find the operating conditions of the grid to be considered as reference. Then, starting from these reference conditions,

[1] As for the numeration of the branches, each branch index is given by the node number of its end node (the largest one), decreased by one.

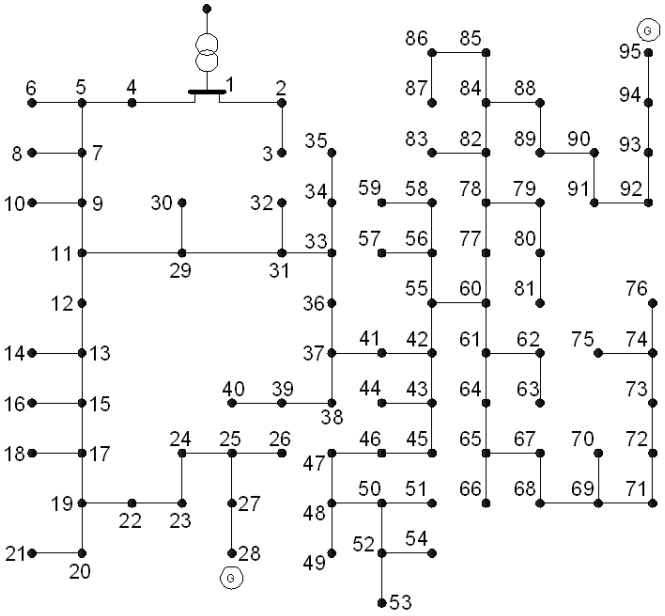

Figure 3.1: Balanced 95-bus test network

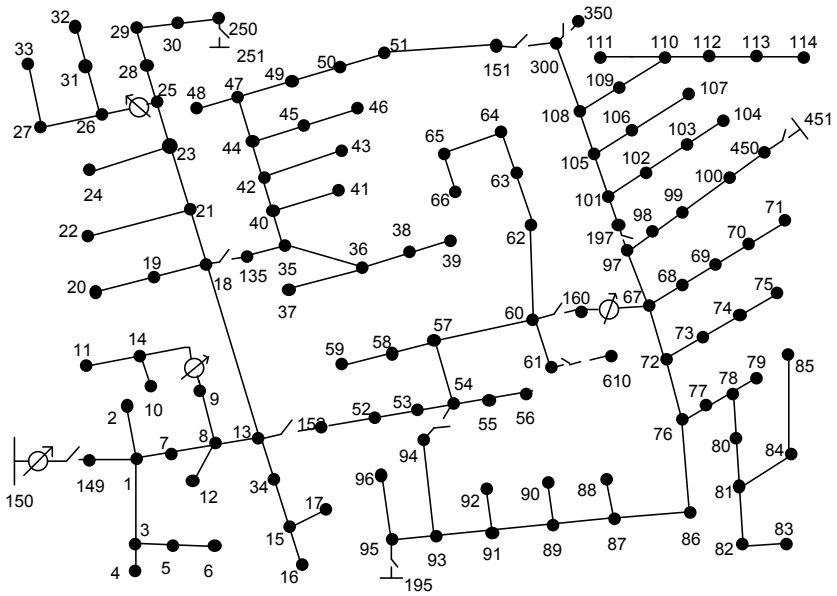

Figure 3.2: Unbalanced IEEE 123-bus test network

measurements and pseudo-measurements are extracted according to their assumed uncertainty distribution. In particular, the following assumptions have been used in all the tests.

- Pseudo-measurements are assumed to be available for all the load and generation nodes, and are considered as random variables with a Gaussian probability distribution having expanded uncertainty (with coverage factor equal to three) equal to 50% of their rated value.

- Real measurements are assumed as random variables with a Gaussian probability distribution having standard deviation equal to one third of their accuracy. As for the conventional measurements, an accuracy of 1% and 2% is considered for voltage and current magnitude measurements, respectively. As for the synchrophasors provided by PMUs, instead, an accuracy equal to 0.7% and 0.7 crad has been taken into account for the measurements of magnitude and phase-angle, respectively; such a choice allows obtaining a maximum TVE of 1% as prescribed by the standard for the synchrophasors [51] for the measurements in steady state conditions.

- Equality constraints are handled in all the methods by means of virtual measurements with a weight equal to 10^{10}. As seen in Chapter 2, some benefits could be achieved for the rectangular BC-DSSE by including the equality constraints through a state vector reduction; however, here, the same approach has been adopted for all the algorithms in order to obtain a fair comparison through the use of the same settings.

- The same convergence criterion has been used for all the algorithms. To achieve a comparable behaviour even from this point of view, in branch current based estimators the stop criterion has been fixed on the voltage variables, considering at each iteration the difference between the actual voltage state (as obtained from the forward sweep) and the voltage state of the previous iteration. Similarly to the voltage estimators, the maximum absolute value among these voltage differences is compared to a predefined threshold (10^{-6} for all the estimators).

As for the metrics used to assess the performance of the different WLS algorithms, similarly to Chapter 2, the mean RMSE has been adopted as global index for the evaluation of the estimation accuracy. Together with the accuracy performance, the computational efficiency of the different WLS formulations has been evaluated through the average of the execution times in the different Monte Carlo trials. In addition, the average number of the iterations and the numerical properties of the different WLS formulations, in terms of density of the Gain matrix, are also monitored. The number of iterations is considered since the convergence properties of the algorithm have an obvious impact on the execution times. As for the Gain matrix, its density can affect the execution times when sparse matrix methods are used, as usual, to handle the matrices and to solve the equation systems within

the WLS algorithm. In the following sections, a detailed analysis is carried out to investigate the impact of these aspects on the overall performance of the different WLS formulations.

3.4.2 Results on the 95-bus network

The first series of tests has been performed referring to a realistic measurement system scenario, where only few measurement devices are placed on the network. To this purpose, three measurement points have been assumed to be available at nodes 1, 11 and 55. Each measurement point is composed of the voltage measurement at the node and of current measurements in two of the branches connected to the node. The test has been carried out considering the possibility to have either conventional or synchrophasor measurements (thus considering magnitudes or phasors of voltage and current). A first important result is obtained looking at the accuracies provided by the tested algorithms. In fact, all the WLS formulations provide the same accuracy results regardless of the used state variables. This is a relevant result since it highlights that the different choice of the state variables does not affect the estimation accuracy. Moreover, it also proves that the conversion of the power measurements in equivalent currents, into the rectangular formulations of both the node voltage and the branch current estimators, does not lead to any degradation of the accuracy performance of the corresponding estimators. As a consequence, the choice of the most suitable algorithm to be used in a specific context can be addressed by other factors, like, for example, the computational efficiency. Table 3.1 shows the results of mean RMSE obtained for all the WLS formulations.

Table 3.1: Test with starting measurement configuration, current and voltage estimations: mean Root Mean Square Errors (RMSEs)

Measurement type	Current magnitude [%]	Current angle [crad]	Voltage magnitude [%]	Voltage angle [crad]
Conventional	9.26	3.94	0.20	0.09
PMU	8.30	2.59	0.14	0.01

As for the computational efficiency, instead, different results have been obtained depending on the adopted formulation. Table 3.2 shows the comparison of the results in terms of execution times, together with the convergence properties and the numerical characteristics of the Gain matrix of each one of the tested algorithms. It is possible to observe that significantly lower execution times can be obtained

Table 3.2: Test with starting measurement configuration, computational and numerical properties

Estimator	Measurement type	Avg Execution Time [ms]	Avg Iteration Number	Gain matrix density [%]
rect. BC-DSSE	Conventional	7.5	6.4	3.7
	PMU	4.5	3.5	3.8
polar BC-DSSE	Conventional	25.8	6.3	5.3
	PMU	18.3	4.2	5.4
rect. NV-DSSE	Conventional	9.3	6.4	5.8
	PMU	5.3	3.5	5.8
polar NV-DSSE	Conventional	23.3	6.3	5.8
	PMU	14.4	3.6	5.8

through the rectangular versions of the estimators. The main reason is the presence of a larger number of linear measurement functions. In particular, the conversion of the pseudo-measurements, which represent the majority of the measurements to be processed, in equivalent currents allows only one computation of the related constant Jacobian sub-matrix, thus saving computational time. It is also important to note that, in the measurement scenario with synchrophasor measurements, since all the measurements involved in the estimation process are linear (only for the rectangular estimators), then the whole Jacobian matrix can be built only once and also the Gain matrix can be factorized outside the iterative part of the WLS procedure. This, obviously, allows saving additional computation time. In general, it is also interesting observing that, in case of PMU measurements, the availability of phasor measurements allows improving the convergence properties of all the algorithms. From this point of view (convergence properties), all the compared formulations exhibit a similar behaviour. In the comparison between the two best formulations, namely the proposed BC-DSSE and the rectangular NV-DSSE, it is possible to observe that the branch current version provides slightly better efficiency performance. This is also due to a more straightforward management of the pseudo-measurements that, as seen in Chapter 1, can be expressed as a simple sum of the used state variables. In this way, in fact, only a reduced number of state variables are involved in the associated Jacobian sub-matrix and this leads to a lower density of the Gain matrix. As discussed also in Chapter 2, this allows obtaining important advantages, in particular considering the common use of sparse matrix methods for the execution of the mathematical operations within the algorithms.

Impact of the measurement system configuration

Further tests have been performed by considering different configurations of the measurement systems. The aim is to highlight possible differences with respect to the previous test scenario, or possible drawbacks for some of the WLS algorithms, in presence of specific configurations of the measurement infrastructure. In particular, looking at the mathematical relationships describing the measurement functions of the different WLS formulations, it could be expected that voltage measurements are critical for the branch current estimators and, on the contrary, current measurements could be troublesome for voltage based estimators.

Following this criterion, and to emphasize possible drawbacks, a test has been performed adding seven voltage measurements with respect to the starting measurement system scenario used in the previous test. Voltage measurements have been placed at nodes: 28, 40, 54, 76, 81, 87 and 95. Even in this case, obtained results show that all the estimators provide the same accuracy performance, thus confirming the previous comments on this aspect. As for the computational performance, Table 3.3 shows the results in terms of execution times, average iteration number and Gain matrix density. It is possible to note that, again, the rectangular versions of the estimators provide results largely better than the polar ones (the execution times are more than halved). At the same time, in the comparison between BC-DSSE and NV-DSSE, it is possible to observe that voltage measurements bring a clear degradation of the efficiency performance of the branch current based estimators. In particular, the sparsity properties of both the rectangular and polar BC-DSSE are significantly worsened due to the considered voltage measurements.

Table 3.3: Test with additional voltage measurements, computational and numerical properties

Estimator	Measurement type	Avg Execution Time [ms]	Avg Iteration Number	Gain matrix density [%]
rect. BC-DSSE	Conventional	11.1	6.3	22.6
	PMU	6.2	3.5	23.1
polar BC-DSSE	Conventional	29.7	6.2	23.4
	PMU	21.9	4.2	23.9
rect. NV-DSSE	Conventional	9.3	6.3	5.8
	PMU	5.5	3.5	5.8
polar NV-DSSE	Conventional	23.1	6.2	5.8
	PMU	13.4	3.2	5.8

This is an expected result since, in the branch current formulations, each voltage measurement involves the current variables of all the branches in the path between the chosen slack bus and the measured node. The important increase of density of the Gain matrix is clearly reflected in the efficiency performance of the algorithms and in fact, in this case, the rectangular NV-DSSE exhibits execution times lower than the proposed BC-DSSE.

A similar test has been performed replacing the voltage measurements with currents in the branches adjacent to the previously considered nodes. Thus, seven additional current measurements have been considered in branches 27, 39, 53, 75, 80, 86 and 94. Focusing on the computational properties of the algorithms (the accuracy results are the same for all the estimators even in this case), Table 3.4 shows an overview of the different results. As it can be observed, the same scenario presented in Table 3.2 has been obtained. In fact, rectangular estimators provide significantly better execution times and, in particular, the proposed BC-DSSE has the lowest execution times. In general, however, it is possible to observe that, differently from the previous test, in this case the addition of current measurements does not cause any particular degradation of the performance of voltage estimators.

Table 3.4: Test with additional current measurements, computational and numerical properties

Estimator	Measurement type	Avg Execution Time [ms]	Avg Iteration Number	Gain matrix density [%]
rect. BC-DSSE	Conventional	7.1	5.7	3.8
	PMU	4.4	3.0	3.9
polar BC-DSSE	Conventional	23.5	5.6	5.3
	PMU	18.2	4.1	5.4
rect. NV-DSSE	Conventional	8.8	5.7	5.8
	PMU	5.2	3.0	5.8
polar NV-DSSE	Conventional	21.0	5.6	5.8
	PMU	15.5	3.8	5.8

Impact of the network topology

An important difference between voltage and current based estimators is given by the need to explicitly introduce the mesh constraints in the branch current formulations. Moreover, it is worth noting that, when radial networks are considered, the number of unknowns in the different estimators is the same; instead, if meshed

Table 3.5: Nodes connected by branches to simulate the presence of meshes

Mesh 1	Mesh 2	Mesh 3	Mesh 4	Mesh 5	Mesh 6	Mesh 7	Mesh 8
3-35	26-47	35-59	76-81	26-40	51-66	35-87	76-92

topologies are assumed, the number of state variables for the branch current estimators automatically increases (if, as in this analysis, virtual measurements are used to handle the mesh constraints) as a direct consequence of the additional branches (with respect to a generic radial tree of the network) creating the meshes. For this reason, it is important to assess the behaviour of the proposed BC-DSSE algorithm in case of meshed networks.

To this purpose, meshed topologies have been designed, starting from the radial 95-bus network, adding some branches in order to create the meshes. Tests have been carried out on the resulting meshed grids, by considering the starting measurement configuration with measurement points in nodes 1, 11 and 55. All the simulations prove, once again, that all the different estimators have equivalent performance from the point of view of the estimation accuracy. Different results are obtained, instead, for the efficiency of the WLS algorithms. Fig. 3.3 shows the execution times achieved for the rectangular versions of BC-DSSE and NV-DSSE, when a growing number of meshes is assumed. The considered meshes and the nodes connected by the additional branches creating the mesh are indicated in Table 3.5.

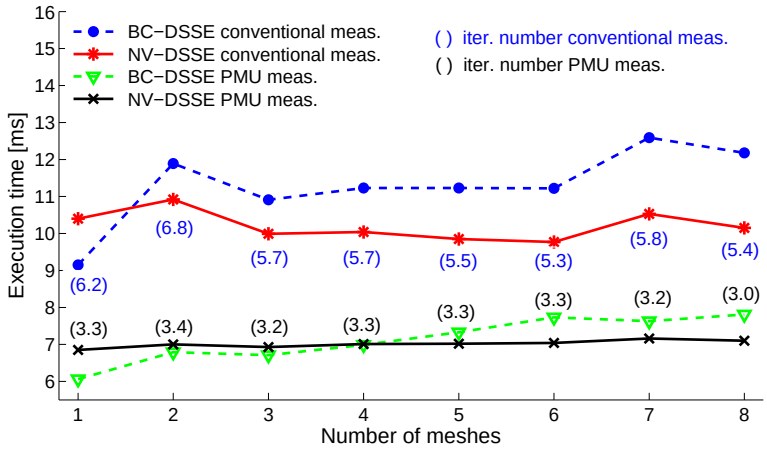

Figure 3.3: Impact of the meshed topology on the execution times of rectangular estimators

The shown results highlight that the performance of the NV-DSSE are practically not affected by the presence of meshes in the network, while the proposed BC-DSSE shows a degradation of its performance with an increasing number of

meshes. It is also worth noting that the presence of the meshes, obviously, creates completely different conditions for the powers and currents flowing in the network. These different conditions affect the number of iterations required by the algorithms to converge. In Fig. 3.3, the average number of iterations required by the tested algorithm (both BC-DSSE and NV-DSSE have exhibited always the same convergence properties), when considering the different network topologies, is reported (between parenthesis). Such information allows explaining the slight ripple observable for the execution times.

As for the motivations leading to the degradation of the BC-DSSE performance, the main reason is related to the large number of state variables involved in the measurement function describing the mesh constraint. As it can be observed in Section 1.5.7, in fact, each constraint involves all the branches in the path of the mesh. As a consequence, the numerical properties of the Gain matrix are significantly affected, as clearly shown in Fig. 3.4. Similar discussions can be done also for the polar versions of BC-DSSE and NV-DSSE, but considering that, as in the previous tests, significantly higher execution times are provided by these formulations.

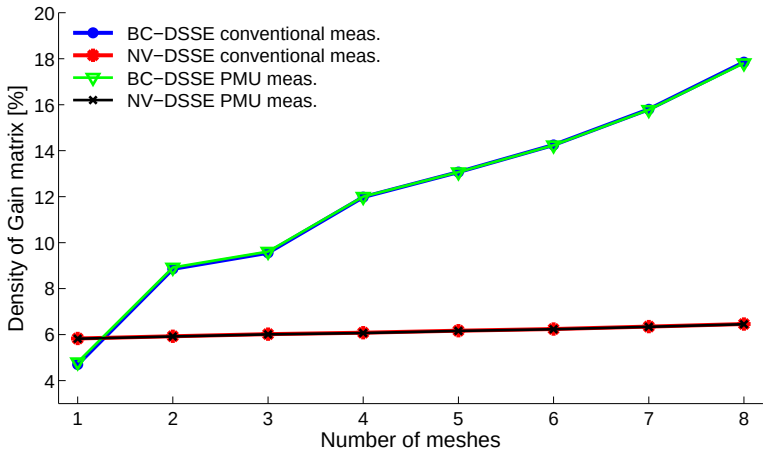

Figure 3.4: Impact of the meshed topology on the Gain matrix density of rectangular estimators

Impact of network parameters uncertainty

Additional tests have been performed to evaluate the impact of the network parameters uncertainty on the estimation results of the proposed BC-DSSE algorithm in comparison to the other WLS formulations. The uncertainty of the network parameters is an aspect often neglected in the solution of the SE problem. Usually, in fact, line parameters are considered using their nominal values and no attention is paid to the possible uncertainty in the knowledge of such values. However, some

works are available in the literature showing the effects brought by the network parameters uncertainty on the accuracy of the SE results [63–66]. Such issue could be also particularly relevant in distribution systems [67], where the lines can be quite old and the network information can refer to manufacturers' data that do not take into account possible variations brought by the environmental conditions or by the normal aging of the lines.

In this subsection, the main aim is to assess the possible different effects arising due to the different model of the WLS formulations. In fact, from a mathematical point of view, the propagation of the network uncertainty is quite different for current and voltage based estimators. In particular, in NV-DSSE, the network parameters appear in the Jacobian matrix and thus they are directly involved in the WLS procedure. In BC-DSSE, instead, due to the majority of equivalent currents associated to the pseudo-measurements, only few Jacobian terms (namely those related to voltage measurements or mesh constraints) involve the line parameters. However, network data strongly affect the result of the forward sweep, since this step is based on the computation of the voltage drops along the lines. As a consequence, it could be interesting to understand if the different WLS formulations are characterized by a different impact of this additional component of uncertainty that, in practical cases, is always present and should be properly taken into account.

To this purpose, several tests have been performed on the benchmark 95-bus test network by considering the starting measurement configuration composed of measurement points in nodes 1, 11 and 55. Network parameters uncertainty has been considered assuming both Gaussian and uniform distributions. Results of the simulations clearly show that this additional component of uncertainty lead to a worse accuracy of the estimation results. As an example, Figs. 3.5 and 3.6 show the expanded uncertainty (with a coverage factor equal to three) obtained for the estimations of voltage magnitudes and angles (expressed as differences with respect to the slack bus voltage angle), respectively, when uniformly distributed network parameters, with a maximum deviation of 10%, are taken into account. Synchronized measurements have been considered for this test. In particular, the results achievable by considering or not the network parameters uncertainty are pointed out. For the sake of clarity in the presentation of the results, the estimations of the proposed BC-DSSE are compared only to those of the polar NV-DSSE, but analogous results have been achieved even for the other two types of estimator. As clear in the figures, a slight worsening of the estimation accuracy has been obtained for the voltage magnitude, while the degradation of the results is more evident for the voltage angles. However, it can be observed that, regardless of the different propagation of the uncertainty, the same impact is brought by the line parameters uncertainty both on the current and the voltage based estimator results. Such result is also confirmed by the other performed simulations. As a consequence, even

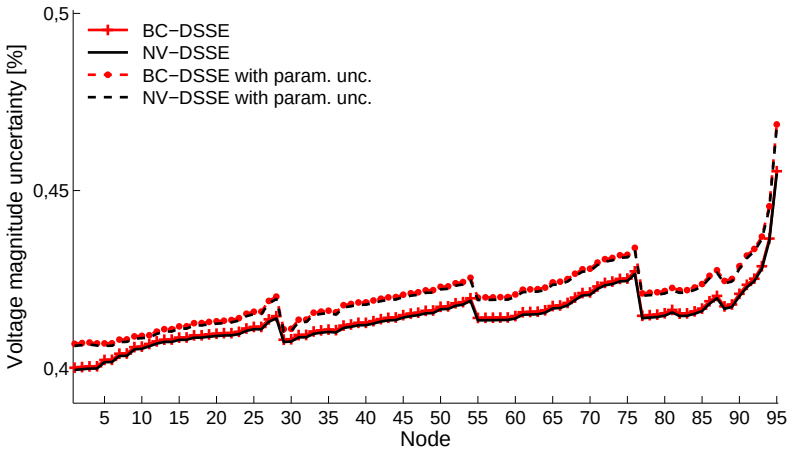

Figure 3.5: Expanded uncertainty of voltage magnitude estimation, impact of network parameters uncertainty

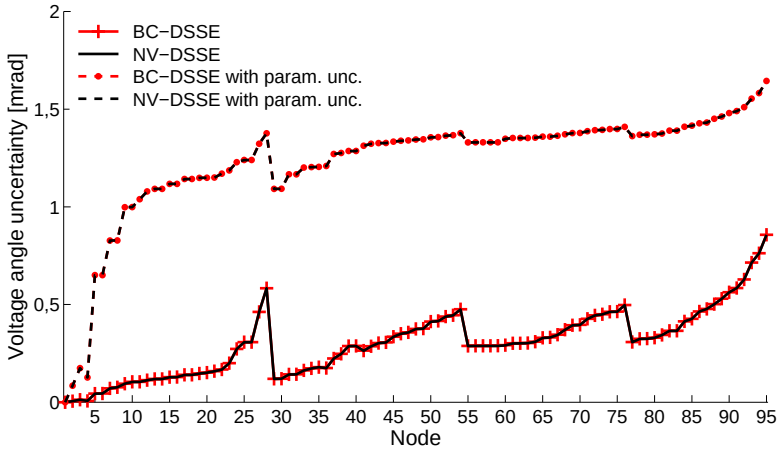

Figure 3.6: Expanded uncertainty of voltage angle estimation, impact of network parameters uncertainty

when network data uncertainty is duly taken into account, all the different WLS formulations provide equivalent results from the point of view of the estimation accuracy.

3.4.3 Results on the 123-bus network

All the considerations made in the previous test scenario, referring to the balanced 95-bus grid, have been verified even in an unbalanced network scenario. To this purpose, tests have been performed on the unbalanced IEEE 123-bus network (Fig.

Table 3.6: Test with unbalanced network, current and voltage estimations: mean Root Mean Square Errors (RMSEs)

Measurement type	Current magnitude [%]	Current angle [crad]	Voltage magnitude [%]	Voltage angle [crad]
Conventional	7.82	6.74	0.20	0.07
PMU	7.60	5.51	0.19	0.02

3.2). A measurement system configuration composed of measurement points in nodes 18, 67 and 149 has been considered for the tests. As presented in Chapter 1 for the rectangular BC-DSSE and in this Chapter for the other formulations of WLS estimator, in unbalanced conditions the three-phase model of the distribution system has to be considered. This implies to duly consider all the mutual terms of impedance arising among the different phases of the system. Mutual impedances appear both in the computation of the measurement functions and in the Jacobian matrix used within the WLS procedure. Moreover, in case of BC-DSSE, mutual terms have to be duly considered also during the forward sweep step.

Table 3.6 shows the accuracy results obtained for voltage and current estimations in terms of mean RMSE. Confirming the previously found results, even in this case, all the tested algorithms provide estimations with exactly the same accuracy. As expected, instead, significantly different results have been obtained for the computational performance. Table 3.7 shows the results in terms of execution times, iteration numbers and density of the Gain matrix. As it can be seen, the rectangular versions of the WLS estimators are the fastest ones even in this context and, in particular, the proposed BC-DSSE exhibits significantly better performance than the other ones. In fact, it is important to note that, when unbalanced networks are considered, the need to use the three-phase models and, consequently, to consider the mutual impedance terms emphasizes the differences between current and voltage based estimators. In the branch current formulations, all the pseudo-measurements (thus, the majority of the available measurements) do not imply the coupling among the different phases of the system and this simplifies the computation of the related measurement functions and, above all, of the Jacobian terms (each pseudo-measurement is associated only to state variables belonging to the same phase of the system). Instead, in case of NV-DSSE, the coupling brought by the pseudo-measurements requires the proper consideration of all the mutual terms, thus increasing the computational burden of the algorithms (pseudo-measurements involve the state variables of all the phases of the system). The effects of this coupling is clear looking at the density of the Gain matrices. In this case, in fact, the difference between current and voltage estima-

Table 3.7: Test with unbalanced network, computational and numerical properties

Estimator	Measurement type	Avg Execution Time [ms]	Avg Iteration Number	Gain matrix density [%]
rect. BC-DSSE	Conventional	40.4	4.8	3.1
	PMU	29.7	3.0	3.3
polar BC-DSSE	Conventional	68.8	4.7	3.6
	PMU	61.3	3.8	3.7
rect. NV-DSSE	Conventional	57.6	4.8	6.5
	PMU	34.2	3.0	6.5
polar NV-DSSE	Conventional	161.0	4.4	6.5
	PMU	147.8	3.9	6.5

tors is larger with respect to a similar balanced network scenario (see for example Table 3.2). The consequent increase of the computational burden is relevant in particular for the polar version of NV-DSSE: in this case, in fact, execution times are significantly higher than all the other estimators.

Phase-decoupling of the WLS estimators

As additional analysis, the possibility to design phase-decoupled versions of the proposed BC-DSSE and the other WLS estimators has been investigated. Such possibility, advanced even in some other papers in the literature (for example [32]), has been considered taking into account that, usually, self impedances are larger than the mutual terms. The performed tests have shown that it is possible to achieve the same accuracy results of the fully coupled estimators if mutual impedances are neglected only in the Jacobian matrix, but not in the computation of the measurement functions. In case of the branch current estimators, mutual terms have also to be duly considered during the forward sweep step. Neglecting the mutual impedances in the Jacobian allows achieving three different Jacobian and Gain matrices for each phase. As a result, the WLS procedure can be performed separately for the different phases, thus relying on smaller equation systems to be solved. Moreover, parallel computing can be exploited to further speed up the estimation process.

From a computational point of view, different results have been obtained for the tested WLS algorithms. Table 3.8 shows the execution times and the iteration numbers obtained for the different estimators. It is worth underlining that the reported execution times have been obtained without considering any parallelization

Table 3.8: Test with phase-decoupled estimators, computational performance

Estimator	Measurement type	Avg Execution Time [ms]	Avg Iteration Number
rect. BC-DSSE	Conventional	22.6	5.5
	PMU	19.6	4.9
polar BC-DSSE	Conventional	62.3	5.4
	PMU	58.0	4.9
rect. NV-DSSE	Conventional	118.9	16.4
	PMU	102.6	16.3
polar NV-DSSE	Conventional	307.9	16.7
	PMU	325.7	16.4

in the estimation process. In case of parallel computing, thus, execution times approximately equal to one third of those reported could be expected. Looking at Table 3.8, some important considerations can be drawn. First of all, it is possible to observe that significant differences have been obtained, between the current and voltage based estimators, in terms of number of iterations required to converge. The reason for such outcome is the different impact of the made approximation in the two classes of estimator. In fact, as already highlighted, in current estimators only few measurements (the voltage ones) bring coupling among the phases of the system. As a consequence, the mutual terms neglected in the Jacobian matrix are few and their approximation do not significantly affect the convergence properties of the algorithm. Instead, in case of voltage estimators, the approximation involves a large number of measurements (all the pseudo-measurements) and Jacobian terms. For this reason, the convergence properties of the algorithm are drastically affected and the number of iterations is very high. As clear from the shown results, in case of voltage formulations, the advantages brought by the phase-decoupling of the estimator are thus adversely balanced by a significantly larger number of iterations required from the algorithm to converge.

As additional consideration, it is possible to note that, in case of current estimators (where the degradation of the convergence properties is limited), the execution of three WLS procedures based on smaller equation systems brings important advantages even if no parallelization is used. This emphasizes the benefits coming from the possible use of a decoupled version in the proposed estimator. Finally, it is worth noting that, when different measurement system configurations or network topologies (i.e. meshed topologies) are considered, even the proposed BC-DSSE can

be characterized by a larger number of coupled measurements (both voltage measurements and meshes introduce coupling among the phases). As a consequence, there could be scenarios where the convergence properties of the estimator could be more significantly affected, thus leading to smaller benefits, but, in general, results prove that the phase-decoupling of the proposed BC-DSSE is possible and can significantly enhance the overall efficiency of this estimator.

3.5 Final discussion

The choice of a suitable DSSE algorithm is important for the proper management of the distribution systems. In particular, the accuracy of the estimation results plays a crucial role for the decisions taken by the DMS. Furthermore, the computational efficiency of the estimation algorithm is essential to allow the real-time execution of the DMS tasks with, possibly, high reporting rates.

For this reason, in this Chapter, the attention has been focused on the performance of the proposed BC-DSSE algorithm, providing a comparison with respect to different formulations of the WLS estimators. The analysis has been made designing all the algorithms with the same settings in order to achieve a comparison as fair as possible. Performed tests prove that, regardless of the choice of the state variables, WLS algorithms provide always the same accuracy results. Such feature has been confirmed even when considering the effects brought by the network parameters uncertainty. This is an important result, since it proves that the equivalent measurements introduced in the proposed BC-DSSE model do not affect the estimation accuracy. From the point of view of the computational efficiency, instead, different results have been obtained depending on the implementation details of the algorithms. In general, performed tests show that the proposed BC-DSSE and the rectangular NV-DSSE are the most efficient, thanks to the presence of many linear measurement functions (in some cases obtained by means of equivalent current measurements). In particular, the proposed BC-DSSE results the best option in actual scenarios where few real measurements are available and the networks usually have radial or weakly meshed topology. However, in case of different scenarios (if many voltage measurements or meshes are present), the performance of the BC-DSSE can be slightly deteriorated and the use of the rectangular NV-DSSE could become more convenient.

In a three-phase context, the estimators performance are affected also by the presence of the mutual impedances. In this case, the phase coupling introduced by the measurement functions leads to a degradation of the performance of voltage based estimators, emphasizing the advantages related to the proposed BC-DSSE formulation. The possibility to use phase-decoupled versions of the BC-DSSE estimator, neglecting the mutual impedances in the Jacobian, has been also studied. In

general, it is possible to say that such approximation is feasible and brings to the same accuracy results of the fully coupled estimator. From the computational point of view, this solution brings advantages for the computational burden required at each iteration of the algorithm. In fact, the decoupling allows dividing the estimation of each phase, achieving smaller equation systems to be solved and using parallel computing for the estimation process. However, at the same time, it can also lead to a degradation of the convergence properties of the algorithm, thus demanding a larger number of iterations to converge. For this reason, the possible use of the decoupled version of the estimator should be carefully evaluated depending on the considered scenario. In general, performed tests show that, in realistic scenarios, the proposed BC-DSSE has only a limited deterioration of the convergence properties and thus significant improvements can be obtained for the computation times.

As final consideration, it is worth noting that many different versions of the BC-DSSE estimator could be obtained by changing the implementation details. As an example, in the literature common approximations are to consider the phase-angle differences between different nodes equal to zero (for example, in the computation of the Jacobian terms) or to convert the voltage or current magnitude measurements in equivalent phasor measurements exploiting the angle estimations of the previous iteration. Such approximations can be introduced in the proposed estimator. In the presented algorithm, however, the introduction of possible approximations has been avoided in order to achieve estimation results as accurate as possible or, when they have been introduced (as in the case of the three-phase decoupled formulation), the achievement of equivalent accuracies has been tested. Moreover, it is also worth noting that, in this Chapter, in the perspective to test the algorithm with settings equal to those of the other WLS formulations, the proposed BC-DSSE has been implemented by using virtual measurements to handle the equality constraints. However, as shown in Chapter 2, large benefits can be obtained by adopting the proposed state vector reduction. Obviously, this should be an additional feature to be duly taken into account in the overall evaluation of the proposed estimator.

Chapter 4

Impact of measurements on DSSE

4.1 Role of the measurements in DSSE

Until now, the analysis of the DSSE issue has been mainly focused on the development of an estimation algorithm tailored for distribution systems and able to combine accuracy and efficiency properties. However, the main requirement needed to achieve accurate estimation results is, of course, the availability of a suitable measurement system on the field. As already mentioned in the first Chapter, this represents a particularly critical aspect, since distribution systems have been traditionally managed without the extensive use of measurement devices. However, recent changes in the distribution system scenario, like the increasing penetration of DG or the growing presence of other DERs, have brought significant modifications to the traditional operation of these networks, adding higher uncertainty and variability to the operating conditions. For this reason, and because of the more advanced functions needed to manage such a complex scenario, actual distribution systems have to necessarily rely on a upgraded configuration of the measurement system in order to achieve the required targets of estimation accuracy needed for the proper operation of the control and management functions.

The main obstacle to the deployment of measurement devices in distribution grids is obviously given by the involved costs. It is worth noting that related costs are not only those associated to the measurement instruments and the required transducers, but also those concerning the communication system and all the infrastructure needed to transmit, acquire, elaborate and store the measurement data. In the literature, many research works have investigated the problem of finding a proper trade-off between the need to enforce the measurement system and the necessity to minimize the financial investments. To this purpose, several criteria have been proposed aimed at defining measurement systems able to achieve the desired technical goals with limited costs. The different proposals mainly differ for the type

of the optimization process used to define type, number and placement of the measurement devices, for the technical requirements to be fulfilled, and for the different parameters and features of the network taken into account.

In [68], as an example, the enhancement of the voltage magnitude estimation is addressed by deploying additional voltage magnitude measurements in the nodes having the highest standard deviation as a result of the DSSE process. The sequential placement of the voltage measurements is performed until the attainment of a prefixed accuracy goal for the voltage magnitude estimation in all the buses of the network. In [69], similarly, the focus is on the accuracy of the voltage magnitude estimations. A two-step process is proposed to detect the best candidates for the placement of a new measurement point, which, in this case, relies on a branch power measurement in addition to the voltage magnitude one. Accuracy requirements also for the voltage angles, besides the voltage magnitudes, are instead considered in [70]. The meter placement technique here proposed is based on the analysis of the covariance matrix of the voltage magnitudes and angles for each bus. Nodes with the worst matrix determinant are selected for the placement of voltage magnitude measurements. Once the target for the voltage magnitude accuracy is achieved, a similar criterion is adopted for defining the placement of power measurements, in order to fulfil the accuracy target also for the voltage angles. Further refinements to this meter placement technique have been presented in [71].

More complex scenarios, with additional features of the distribution grids, have been taken into account in some other papers. In [72], the installation of measurement points near to switches, tap changer transformers and large industrial loads or generation plants is suggested. Starting from this base configuration, additional devices, if needed, are added to satisfy the accuracy targets required by the control functions designed for voltage regulation, switching consequence assessment and loss estimation. In [73], instead, a meter placement approach based on dynamic programming has been proposed. The allocation of the measurements aims at achieving the desired accuracy goals with minimum costs, and also takes into account the economic advantages deriving from the installation of multiple devices in the same measurement point. Moreover, the unavoidable presence of uncertainty in the knowledge of the network parameters is also considered in the meter placement procedure. The same technique, based on the Bellman's principle, has been adapted in [74] to consider also the decay of the metrological characteristics of the measurement system and to guarantee, in this way, the robustness of the accuracy results with respect to possible lost or malfunctioning of the measurement devices.

The possible impact of modern measurement instruments is also considered in different papers. In [50], for instance, a meter placement technique that involves also smart meters and PMUs, and that takes into account the different accuracies and costs of these devices, has been proposed. Such approach has been further

extended in [75] to consider the possibility of different network configurations and the presence of changing operating conditions brought by the variable behaviour of loads and generators over the time.

Despite the existence of a large number of proposals, which could provide useful advices about typology, number and position of the measurement devices to be installed, a clear idea of the impact of the different types of measurement on the DSSE results is still necessary, in order to properly design (or to improve) the meter placement techniques and to address them to achieve the desired technical requirements. Several papers report general comments about the impact of specific kinds of measurements, and their placement, on the DSSE results (for example, [60, 76]). Only few works, however, provide detailed analysis on this aspect. In [77], some generalizable rules are provided. In particular, interesting considerations concern the global effect brought by the voltage magnitude measurements on the voltage magnitude estimation, and the local impact of the power measurements for the branch power estimation. Empirical analysis of the impact of different types of measurements can be found also in [78].

This Chapter aims at performing a more detailed analysis on the impact of both traditional and modern measurement devices on the accuracy of the DSSE results. The analysis is developed through tests specifically conceived to highlight how the estimation of the different electrical quantities is affected by type and placement of the instruments constituting the measurement system. In the case of the voltage magnitude estimation, considerations obtainable by means of experimental tests are also supported by a theoretical explanation, which is derived from the mathematical analysis of the propagation of the uncertainty towards the voltage magnitude estimation in the DSSE. It is important to underline that all the considerations drawn in this Chapter, which refer to results achieved through the branch current version of the DSSE, can be easily extended to all the WLS based estimators, since, as shown in Chapter 3, all the DSSE algorithms provide practically the same accuracy results independently of the chosen state vector. Shown results aim at providing a clear picture of the possible effects obtainable through the installation of a specific measurement device and, thus, are intended to give support for the choice of the measurement system to be installed in future distribution grids.

4.2 Test assumptions

Tests performed to analyze the measurement impact on the accuracy of the DSSE results have been carried out on the 95-bus network depicted in Fig. 4.1. As already seen in Chapter 3, this is a balanced network: for the study here proposed, this is not a problem since the results obtainable on the equivalent single-phase model can be generalized to each one of the three-phases in an unbalanced context. The grid is also

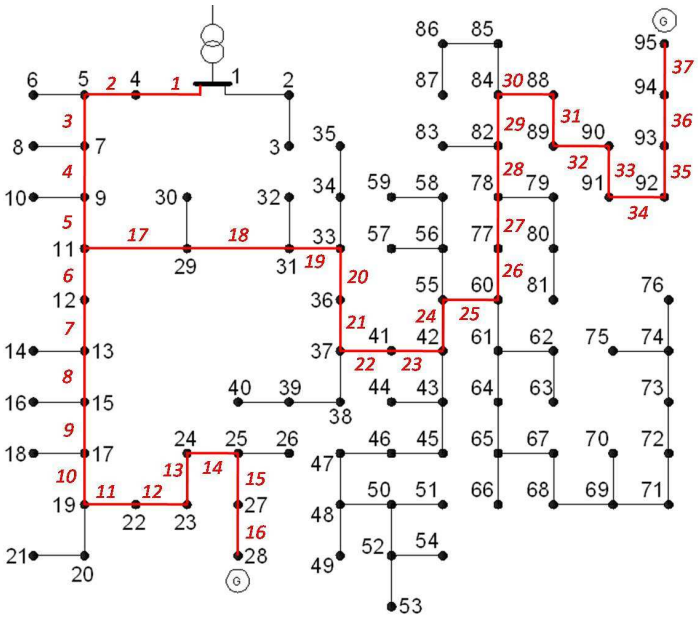

Figure 4.1: 95-bus test network, with indication of the main feeders

characterized by two large sources of DG in nodes 28 and 95. This allows assessing the impact of the measurements in a realistic scenario with an active behaviour of the network. Fig. 4.1 also shows, in red, the branches that compose the main feeders of the network[1]. Some of the results will be presented focusing only on these branches, for the sake of clarity.

Tests have been carried out following the same approach used in the previous Chapters. Monte Carlo simulations have been run to obtain statistical information about the estimation results, with a number of trials $N_{MC} = 25000$. Each Monte Carlo trial is performed extracting the measurements by adding random errors to the reference values (achieved through a power flow calculation) according to the assumed uncertainty. Pseudo-measurements are supposed to be always available for all the node injections, and are considered to be characterized by uncertainty with Gaussian distribution having, if not differently indicated, maximum uncertainty equal to 50%. Real measurements are instead considered and placed differently depending on the specific test case. In general, however, all the real measurements are supposed to have Gaussian uncertainty with standard deviation equal to one third of the accuracy value.

As for the parameters used to assess the impact of the measurements on the estimation results, the main focus is, obviously, on the accuracy of the results. Therefore,

[1] As for the numeration of the branches, each branch index is given by the node number of its end node (the largest one), decreased by one. If results refer only to the branches of the feeder, the numeration of the branches is the one reported in red in the Figure.

the expanded uncertainty (with a coverage factor equal to 3) of the estimated quantities will be monitored to evaluate the effects deriving from each specific measurement configuration.

4.3 Impact of measurements on voltage estimation

The accurate estimation of the voltage profile of a network plays a fundamental role for the efficient management of the network itself. In fact, many of the control functions envisaged in future DMSs rely on the knowledge of the voltage magnitude at the different nodes of the grid. A high accuracy in such knowledge is crucial, since it allows the DSO to operate the network with a better awareness and confidence on the operating conditions. In this way, possible decisions oriented to keep a too large safety margin can be avoided, allowing a more efficient and reliable operation of the network.

The analysis of the impact of the different measurements on the estimation of the voltage profile can be handled conveniently, from a mathematical point of view, by referring to the BC-DSSE algorithm [79]. In the following, first of all, the theoretical analysis is presented, in order to highlight the main sources of uncertainty affecting the accuracy of the voltage estimation. Then, tests and results performed on the 95-bus network are presented, in order to prove the validity of the developed analysis and to highlight the impact of the measurement configuration on the voltage estimation results.

4.3.1 Mathematical analysis of the voltage estimation uncertainty

The analysis here performed refers to the use of the BC-DSSE algorithm presented in Chapter 1. However, since the estimation results given by WLS estimators having different state vectors are the same, the outcomes of this analysis have general validity for all the DSSE algorithms based on the WLS approach. In this section, just the presence of traditional measurements is taken into account. The effects resulting from the possible use of synchronized measurements provided by PMUs is the focus of Section 4.5.

Recalling what was shown in Chapter 1, the structure of the state vector $\mathbf{x}$ used in the BC-DSSE algorithm, when no PMU measurements are available, is:

$$\mathbf{x} = [V_s, i_1^r, ..., i_{N_{br}}^r, i_1^x, ..., i_{N_{br}}^x] \tag{4.1}$$

where V_s is the voltage magnitude of the chosen slack bus, i_j^r and i_j^x are the real and imaginary parts of the current on the generic branch j, and N_{br} is the total number

of branches in the network. The resulting size of the state vector is, therefore, $N = 2N_{br} + 1$.

As known from the literature (see, for example, [4] or [26]), WLS based estimators allow obtaining the covariance matrix associated to the estimated state variables, by means of the inversion of the Gain matrix $\mathbf{G}$ used in the last iteration of the estimation process (see equation (1.4)). As a consequence, the estimation covariance matrix $\mathbf{G}^{-1}$ is a $N \times N$ matrix having the variances related to the estimated state variables on the diagonal and the covariance terms outside the diagonal. Referring to the assumed structure of the state vector in equation (4.1), thus, the term $\mathbf{G}^{-1}(1,1)$ of this covariance matrix is associated to the resulting variance of the voltage magnitude estimation $\hat{V}_s$ in the slack bus. The following analysis is carried out by focusing on the factors affecting this variance term. However, since the reference node can be chosen arbitrarily, the final results of this study can be extended to deduce the factors affecting the uncertainty of the voltage magnitude estimation of all the nodes of the network.

Variance of the slack bus voltage

To detect the sources leading to the resulting uncertainty for the slack bus voltage estimation $\hat{V}_s$, the Gain matrix can be divided as follows:

$$\mathbf{G} = \mathbf{A} + \mathbf{B} \tag{4.2}$$

with:

$$\mathbf{A} = \begin{bmatrix} \mathbf{G}_{11} & \mathbf{G}_{12} \\ \mathbf{0} & \mathbf{G}_{22} \end{bmatrix}, \quad \mathbf{B} = \begin{bmatrix} \mathbf{0} & \mathbf{0} \\ \mathbf{G}_{21} & \mathbf{0} \end{bmatrix} \tag{4.3}$$

where $\mathbf{G}_{11}$ is a scalar, $\mathbf{G}_{12}$ is a row vector of size $1 \times 2N_{br}$, $\mathbf{G}_{22}$ is a $2N_{br} \times 2N_{br}$ matrix and $\mathbf{G}_{21}$ is a column vector of size $2N_{br} \times 1$. Since the Gain matrix is symmetric, it is: $\mathbf{G}_{21} = \mathbf{G}_{12}^T$ (where the superscript T indicates the transpose operator).

In [80], it is shown that, when $\mathbf{B}$ is a rank one matrix (as in this case), the inverse of the sum $\mathbf{A} + \mathbf{B}$ can be written as:

$$\mathbf{G}^{-1} = (\mathbf{A} + \mathbf{B})^{-1} = \mathbf{A}^{-1} - k\mathbf{C} \tag{4.4}$$

where:

$$k = \frac{1}{1 + tr(\mathbf{B}\mathbf{A}^{-1})} \tag{4.5}$$

$$\mathbf{C} = \mathbf{A}^{-1}\mathbf{B}\mathbf{A}^{-1} \tag{4.6}$$

with $tr(\cdot)$ representing the trace of the considered matrix (that is the sum of the elements on the main diagonal of the matrix).

According to [81], instead, the inverse of the upper block triangular matrix $\mathbf{A}$ can be expressed as:

$$\mathbf{A}^{-1} = \begin{bmatrix} \mathbf{G}_{11}^{-1} & -\mathbf{G}_{11}^{-1}\mathbf{G}_{12}\mathbf{G}_{22}^{-1} \\ \mathbf{0} & \mathbf{G}_{22}^{-1} \end{bmatrix} \tag{4.7}$$

Using (4.7) to calculate $\mathbf{C}$, the following block matrix can be found:

$$\mathbf{C} = \begin{bmatrix} -\frac{\mathbf{G}_{12}\mathbf{G}_{22}^{-1}\mathbf{G}_{12}^{T}}{\mathbf{G}_{11}^{2}} & \frac{\mathbf{G}_{12}\mathbf{G}_{22}^{-1}\mathbf{G}_{12}^{T}\mathbf{G}_{12}\mathbf{G}_{22}^{-1}}{\mathbf{G}_{11}^{2}} \\ \frac{\mathbf{G}_{22}^{-1}\mathbf{G}_{12}^{T}}{\mathbf{G}_{11}} & -\frac{\mathbf{G}_{22}^{-1}\mathbf{G}_{12}^{T}\mathbf{G}_{12}\mathbf{G}_{22}^{-1}}{\mathbf{G}_{11}} \end{bmatrix} \tag{4.8}$$

It is worth noting that the sub-matrices present in $\mathbf{C}$, as expressed in (4.8), have the same size of the sub-matrices previously defined in $\mathbf{A}$ and $\mathbf{B}$.

Since our focus is on the variance of $\hat{V}_s$, let us consider only the element $(1,1)$ of the estimation covariance matrix $\mathbf{G}^{-1}$. Using (4.4), and exploiting (4.5) and the block matrices obtained in (4.7) and (4.8), it is possible to find:

$$\mathbf{G}^{-1}(1,1) = \frac{1}{G_{11}} + \frac{1}{(G_{11})^2}\frac{\mathbf{G}_{12}\mathbf{G}_{22}^{-1}\mathbf{G}_{12}^{T}}{1 + tr(\mathbf{B}\mathbf{A}^{-1})} \tag{4.9}$$

The trace of $\mathbf{B}\mathbf{A}^{-1}$ is:

$$tr(\mathbf{B}\mathbf{A}^{-1}) = -\frac{1}{G_{11}}\mathbf{G}_{12}\mathbf{G}_{22}^{-1}\mathbf{G}_{12}^{T} \tag{4.10}$$

Thus, (4.9) becomes:

$$\mathbf{G}^{-1}(1,1) = \frac{1}{G_{11}} + \frac{1}{(G_{11})}\frac{\mathbf{G}_{12}\mathbf{G}_{22}^{-1}\mathbf{G}_{12}^{T}}{G_{11} - \mathbf{G}_{12}\mathbf{G}_{22}^{-1}\mathbf{G}_{12}^{T}} \tag{4.11}$$

With some arithmetics, it is possible to write:

$$\mathbf{G}^{-1}(1,1) = \frac{1}{G_{11}} + \frac{1}{(G_{11})^2}\frac{G_{11}\mathbf{G}_{12}\mathbf{G}_{22}^{-1}\mathbf{G}_{12}^{T} - k_2 + k_2}{G_{11} - \mathbf{G}_{12}\mathbf{G}_{22}^{-1}\mathbf{G}_{12}^{T}} \tag{4.12}$$

where:

$$k_2 = \mathbf{G}_{12}\mathbf{G}_{22}^{-1}\mathbf{G}_{12}^{T}\mathbf{G}_{12}\mathbf{G}_{22}^{-1}\mathbf{G}_{12}^{T} \tag{4.13}$$

Then:

$$\mathbf{G}^{-1}(1,1) = \frac{1}{G_{11}} + \frac{1}{(G_{11})^2}(\mathbf{G}_{12}\mathbf{G}_{22}^{-1}\mathbf{G}_{12}^{T} + \frac{k_2}{G_{11} - \mathbf{G}_{12}\mathbf{G}_{22}^{-1}\mathbf{G}_{12}^{T}}) \tag{4.14}$$

Writing the last member of the above equation as a function of k, the following holds:

$$\mathbf{G}^{-1}(1,1) = \frac{1}{G_{11}} + \frac{1}{(G_{11})^2}[\mathbf{G}_{12}(\mathbf{G}_{22}^{-1} + k\frac{\mathbf{G}_{22}^{-1}\mathbf{G}_{12}^T\mathbf{G}_{12}\mathbf{G}_{22}^{-1}}{G_{11}})\mathbf{G}_{12}^T] \tag{4.15}$$

Looking at the starting equation in (4.4) and considering the blocks in matrix $\mathbf{C}$ (equation (4.8)), it is possible to note that the term between the parenthesis is:

$$\mathbf{G}_{22}^{-1} + k\frac{\mathbf{G}_{22}^{-1}\mathbf{G}_{12}^T\mathbf{G}_{12}\mathbf{G}_{22}^{-1}}{G_{11}} = \mathbf{G}_{22}^{-1} - k\mathbf{C}_{22} = \mathbf{\Sigma}_I \tag{4.16}$$

where $\mathbf{\Sigma}_I$ represents the block of the covariance matrix $\mathbf{G}^{-1}$ associated to the estimations of the currents included in the state vector (it can be obtained deleting the first row and the first column of $\mathbf{G}^{-1}$).

Then, the final result is:

$$\mathbf{G}^{-1}(1,1) = \frac{1}{G_{11}} + \frac{1}{G_{11}^2}[\mathbf{G}_{12}\mathbf{\Sigma}_I\mathbf{G}_{12}^T] \tag{4.17}$$

Analysis of the elements of the Gain matrix

To fully understand the meaning of the relationship found in (4.17), it is necessary to analyze the sub-matrices that compose the Gain matrix. In particular, the focus will be on the blocks $\mathbf{G}_{11}$ and $\mathbf{G}_{12}$, since they are those involved in equation (4.17).

As seen in Chapter 1, the Gain matrix is calculated as:

$$\mathbf{G} = \mathbf{H}^T\mathbf{W}\mathbf{H} \tag{4.18}$$

where the Jacobian $\mathbf{H}$ and the weighting matrix $\mathbf{W}$ are involved in this computation.

For the purposes of this analysis, it is useful to analyze the Gain matrix by separating the contributions coming from the voltage measurements and the other remaining measurements (powers and currents). It is worth recalling that, in the BC-DSSE formulation, all the power measurements (both branch powers and power injections) are converted in equivalent current measurements. As a result, the measurement vector used as input for the estimation algorithm is composed only of voltage or current measurements. Grouping these two sets of measurements, Jacobian and weighting matrix can be divided in the following way:

$$\mathbf{H} = \begin{bmatrix}\mathbf{H}_V \\ \mathbf{H}_I\end{bmatrix} \qquad \mathbf{W} = \begin{bmatrix}\mathbf{W}_V & \mathbf{0} \\ \mathbf{0} & \mathbf{W}_I\end{bmatrix} \tag{4.19}$$

where $\mathbf{H}_V$ and $\mathbf{H}_I$ are the Jacobian sub-matrices associated to the voltage and current measurements, respectively, and $\mathbf{W}_V$ and $\mathbf{W}_I$ are, similarly, the corresponding weighting sub-matrices.

Computing the Gain matrix through the above formulation of Jacobian and weighting matrix, it is possible to find:

$$\begin{aligned}\mathbf{G} &= \begin{bmatrix}\mathbf{H}_V^T & \mathbf{H}_I^T\end{bmatrix}\begin{bmatrix}\mathbf{W}_V & \mathbf{0}\\ \mathbf{0} & \mathbf{W}_I\end{bmatrix}\begin{bmatrix}\mathbf{H}_V\\ \mathbf{H}_I\end{bmatrix} = \\ &= \mathbf{H}_V^T\mathbf{W}_V\mathbf{H}_V + \mathbf{H}_I^T\mathbf{W}_I\mathbf{H}_I = \mathbf{G}_V + \mathbf{G}_I\end{aligned} \tag{4.20}$$

where $\mathbf{G}_V$ and $\mathbf{G}_I$ are the independent contributions brought to the Gain matrix by the voltage and current measurements, respectively.

Obviously, both $\mathbf{G}_V$ and $\mathbf{G}_I$ are $N \times N$ matrices and, similarly to what has been done in (4.3), they can be divided in four sub-matrices having the same size and notation of the blocks of the Gain matrix. Since all the current measurements have null derivatives with respect to the slack bus voltage variable (see Appendix A), the sub-matrices $\mathbf{G}_{I_{11}}$, $\mathbf{G}_{I_{12}}$ and $\mathbf{G}_{I_{21}}$ are null matrices and, therefore, it is possible to obtain:

$$\mathbf{G} = \begin{bmatrix}\mathbf{G}_{V11} & \mathbf{G}_{V12}\\ \mathbf{G}_{V12}^T & \mathbf{G}_{V22} + \mathbf{G}_{I22}\end{bmatrix} \tag{4.21}$$

As it can be observed, the sub-matrices $\mathbf{G}_{11}$ and $\mathbf{G}_{12}$, which are those of interest in this analysis, are only dependent on the voltage measurements, while no contribution is brought by the currents. As a result, their computation is reduced to the analysis of the elements involved in the matrix multiplication $\mathbf{H}_V^T\mathbf{W}_V\mathbf{H}_V$. To this purpose, considering the derivative terms appearing in $\mathbf{H}_V$ (i.e. in the Jacobian sub-matrix related to the voltage magnitude measurements, whose elements are reported in Appendix A.1), the following results can be found:

$$G_{11} = \sum_i W_{V_i}(\cos\delta_i)^2 \tag{4.22}$$

$$\mathbf{G}_{12(1,j)} = \begin{cases}\sum_i \lambda_{ji} R_{ji} W_{V_i}\cos\delta_i & \text{if } j \le N_{br}\\ \sum_i \lambda_{ji} X_{ji} W_{V_i}\cos\delta_i & \text{if } j > N_{br}\end{cases} \tag{4.23}$$

where: i is the index of the node where the voltage measurement is placed; δ_i is the difference between the angle of the voltage in node i and the reference angle in the slack bus; W_{V_i} is the weight associated to the voltage measurement in node i; λ_{ji} is a logic value equal to 1 if the branch j is in the path, considered in the Jacobian, between node i and the slack bus, while it is equal to 0 otherwise; $R_{ji} = (-r_j\cos\delta_i - x_j\sin\delta_i)$ and $X_{ji} = (x_j\cos\delta_i - r_j\sin\delta_i)$ are the derivatives of the voltage magnitude measurement in node i with respect to the real and imaginary parts of the current in branch j, respectively, with r_j and x_j representing the resistance and reactance of branch j.

Sources of uncertainty for the voltage magnitude estimation

The main factors affecting the accuracy of the voltage magnitude estimation are obtained by combining the mathematical results found in (4.17), (4.22) and (4.23). Some approximations commonly made in distribution systems can be supposed in order to identify the uncertainty sources having a larger impact. For example, since distribution systems usually have short lines with low impedances, the voltage angles δ_i are generally very small and they can be considered, in first approximation, equal to 0. In this case, considering the resulting value of $\mathbf{G}_{11}$ in (4.22), and introducing it into (4.17), the variance of the slack bus voltage estimation becomes:

$$\sigma^2_{\hat{V}_s} = \sigma^2_1 + \sigma^2_2 = \frac{1}{\sum_i W_{V_i}} + \frac{1}{(\sum_i W_{V_i})^2}[\mathbf{G}_{12}\mathbf{\Sigma}_I\mathbf{G}^T_{12}] \tag{4.24}$$

Equation (4.24) highlights the presence of two different contributions to the overall variance of the voltage estimation. In particular, the first term is a constant contribution that only depends on the number and the accuracy of the voltage measurements available on the network. If, for the sake of simplicity, the hypothesis to have voltage measurements with the same uncertainty is considered, the following holds:

$$\sigma^2_1 = \frac{1}{M_V W_V} = \frac{\sigma^2_V}{M_V} \tag{4.25}$$

where M_V is the total number of voltage measurements available on the network and W_V and σ^2_V are, respectively, the common weight and variance assumed for the voltage measurements.

As for the second term in equation (4.24), the presence of the matrix multiplication leads to a long sum of elements, making the achievement of a clear relationship difficult. However, just as an example, it is possible to suppose that the covariance matrix of the current estimations $\mathbf{\Sigma}_I$ is diagonal. In this case, and always under the hypothesis to have voltage measurements with the same uncertainty, the following relationship can be found:

$$\sigma^2_2 = \frac{1}{M^2_V}\sum_i \sum_{j=1}^{N_{br}} \lambda_{ji}(r^2_j\sigma^2_{i^r_j} + x^2_j\sigma^2_{i^x_j}) \tag{4.26}$$

where i, as before, represents the index of the node where each voltage measurement is placed, while $\sigma^2_{i^r_j}$ and $\sigma^2_{i^x_j}$ are the variances of the real and imaginary parts of the current in branch j. In real cases the covariance matrix $\mathbf{\Sigma}_I$ cannot be considered as diagonal, since the presence of many pseudo-measurements leads to a strong correlation among the different current estimations. Nevertheless, equation (4.26) can be useful to obtain a better understanding: in fact, it shows that the component σ^2_2 is basically given by the sum, for each voltage measurement, of the uncertainty

terms related to the voltage drops between the measured node and the considered bus.

Finally, as already mentioned at the beginning, it is worth remarking that the analysis here performed, even if developed by referring to the slack bus voltage, can be easily extended to the voltage estimation in each bus of the network, because the choice of the slack bus is arbitrary. In particular, from the obtained results, it is possible to state that:

- each bus has a common and constant term of uncertainty that depends only on the number and the accuracy of the voltage measurements deployed on the network; moreover, since the other contribution is an additional term of uncertainty, this represents the lowest value of uncertainty that can be achieved with the considered measurement system;

- each bus has a second contribution of uncertainty, which mainly depends on the knowledge of the voltage drops present, for each voltage measurement, in the path between the measured and the considered node; as a result, this term is strictly dependent on the accuracy of the current estimations (as it can be seen in equation (4.26)) and on the placement of the voltage measurements (because this affects the number of terms involved in the sum of equation (4.26)).

4.3.2 Validation of the mathematical analysis

Several tests have been performed on the 95-bus network to validate the theoretical analysis and to highlight the implications arising from the found results. The first series of tests has been carried out to demonstrate the goodness of the proposed analysis. A reference measurement system composed of four voltage magnitude measurements, placed at nodes 1, 11, 28 and 37, and with accuracy equal to 1%, has been taken into account for these tests.

Fig. 4.2 shows the results concerning the expanded uncertainty (with coverage factor equal to 3) of the voltage magnitude estimations. In particular, both the theoretical and the statistical uncertainty are reported. The theoretical uncertainty is obtained extracting the voltage slack bus variance from the estimation covariance matrix $\mathbf{G}^{-1}$ and then computing the remaining voltage uncertainties using the covariance matrix $\mathbf{\Sigma}_I$ of the current estimations and applying the uncertainty propagation law. The statistical uncertainty, instead, is the simple result achieved by means of the Monte Carlo simulation. It is possible to observe that a really good matching exists: this confirms the reliability of the information associated to the matrix $\mathbf{G}^{-1}$ for expressing the uncertainty of the estimation results.

Besides this aspect, Fig. 4.2 also allows a first assessment of the reliability of the results found in the previous mathematical analysis. As aforementioned,

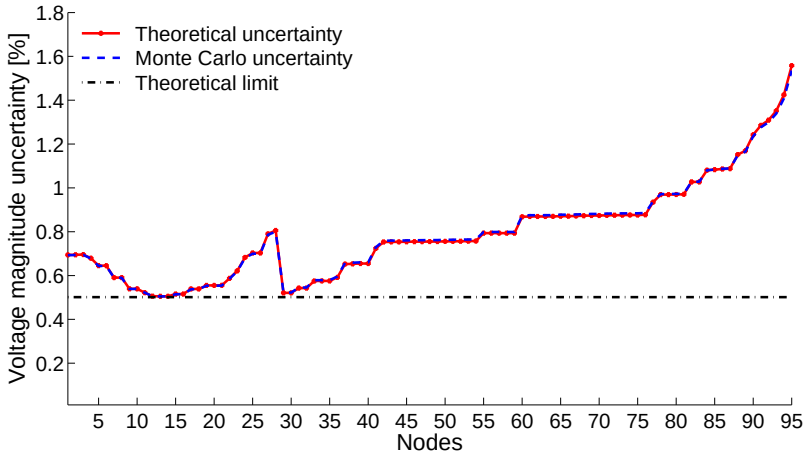

Figure 4.2: Expanded uncertainty of voltage magnitude estimation with theoretical approach and Monte Carlo simulations

the constant term of uncertainty σ_1^2 represents the lowest limit of uncertainty that can be achieved with a given measurement system. The value obtained for the considered measurement scenario is indicated in Fig. 4.2 as “theoretical limit". It can be observed that the uncertainty of all the voltage estimations is higher than this limit. Moreover, the impact brought by the second component of uncertainty σ_2^2 can be also evaluated. The best estimations are around node 11: in fact, this area is quite close to all the assumed voltage measurements and this allows minimizing the number of voltage drops contributing to the overall uncertainty. On the contrary, the worst estimation is on node 95. This is justified by the long distance of this node from the buses having the voltage measurements and by the high uncertainty associated to the large current injected by the generator on this node.

As a confirmation of the role played by the branch current uncertainty (and, thus, by the voltage drops) on the resulting uncertainty of the voltage profile, another test has been performed considering different loading conditions for the network. In particular, a scenario with the power injections (both load consumptions and generator injections) scaled at 125%, 100%, 75% and 50% is taken into account. Fig. 4.3 shows the obtained results, always considering the previous base measurement configuration. It is worth recalling that pseudo-measurements are supposed to be known with an uncertainty expressed in relative terms. For this reason, a lower loading condition leads to a lower uncertainty, in absolute terms, on the knowledge of the branch currents. As a result, it is possible to observe that, for lower values of the loading conditions, the contribution of the uncertainty term σ_2^2 is reduced and this leads to a consequent improvement of the voltage estimation, in general, for all the nodes of the network.

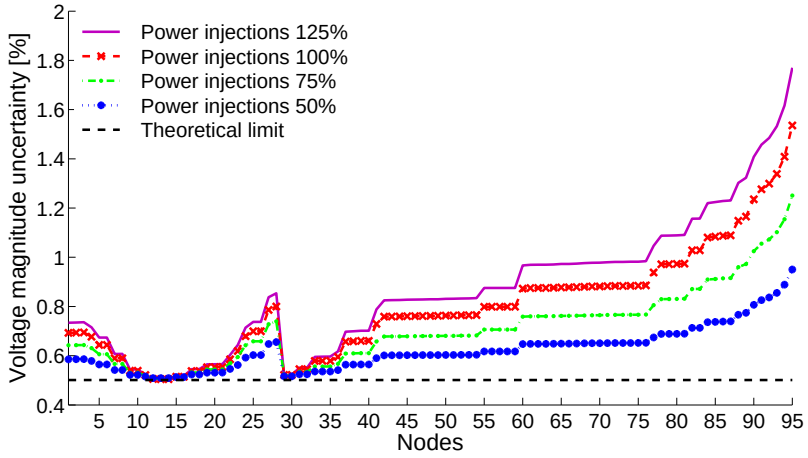

Figure 4.3: Expanded uncertainty of voltage magnitude estimation for different loading conditions in the network

Another test has been performed, instead, considering the original values of power injections, but assuming different uncertainties in the knowledge of the pseudo-measurements. In this case, the expected result is to have better estimations of the branch currents by assuming an improved knowledge of the prior information and, in these conditions, to achieve a reduction of the uncertainty term σ_2^2. Test results shown in Fig. 4.4 confirm all the provided considerations. In particular, it is possible to observe as, with a quite low pseudo-measurement uncertainty (10%), the impact brought by the voltage drops is significantly reduced and the uncertainty of all the voltage profile is very flat and close to the theoretical limit given by σ_1^2. In general, this emphasizes the potential benefits coming from an accurate modeling of the loads and generators behaviour.

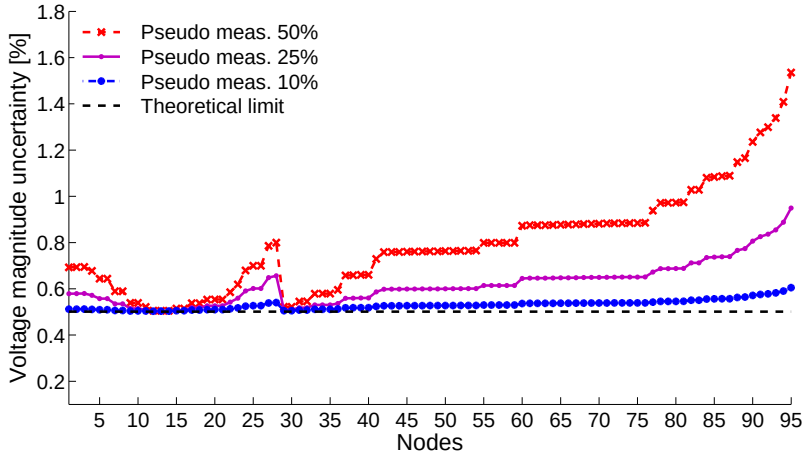

Figure 4.4: Expanded uncertainty of voltage magnitude estimation for different uncertainties in the knowledge of the pseudo-measurements

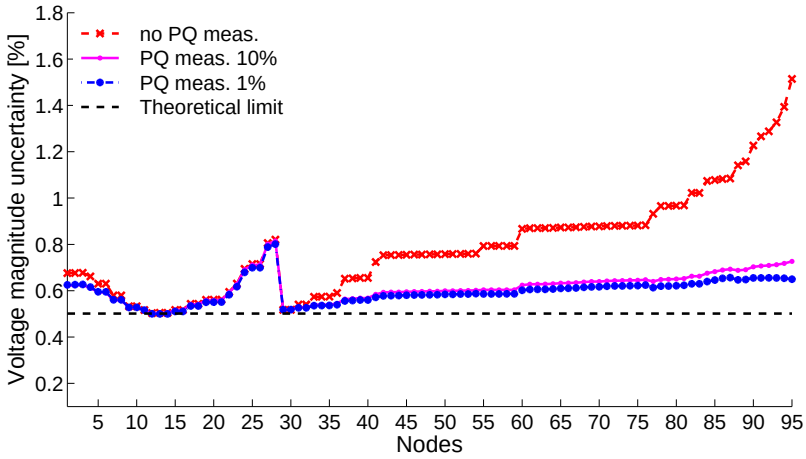

Figure 4.5: Expanded uncertainty of voltage magnitude estimation in presence of branch power measurement

All the previous tests refer to modifications of the scenario involving all the nodes of the network. This can be a motivation for the global effects found on the changing uncertainties of the voltage profile. For this reason, a further test has been performed to highlight possible benefits coming from just one additional measurement. In particular, the installation of a power measurement on the branch connected to the generation node 95 has been supposed. Fig. 4.5 shows the impact of such measurement when considering a quite large or a very low uncertainty (10% and 1%, respectively). It is possible to observe that, even in the worst case, when the power measurement has low accuracy, the presence of only one additional measurement, if suitably chosen, can provide significant benefits to the voltage estimation of a large number of nodes. In this case, the found result is strongly related to the choice of monitoring a very large current, which is associated to the high power injected by the generator at node 95. By measuring this large current, it is possible to improve the knowledge of the current estimations in many of the adjacent branches and, thus, to reduce the consequent effects of the voltage drop uncertainties involved in σ_2^2.

4.3.3 Impact of the analysis on a meter placement perspective

As further discussion, a test highlighting the impact of the presented analysis in a meter placement perspective is proposed. The test has been performed starting from the same configuration (with four voltage measurements at nodes 1, 11, 28 and 37) used in the previous simulations. As it can be observed in the previously shown results, such configuration does not allow an accurate estimation of the voltage

magnitude for all the nodes of the network. To solve this issue and to improve the estimation accuracy of the voltage profile, if the knowledge brought by the pseudo-measurements cannot be enhanced, the only choice is to deploy additional measurement devices on the network.

Several meter placement techniques deal with this issue by detecting the buses with the highest voltage uncertainty and placing an additional measurement in these nodes [68, 70]. In the following, the case of six additional voltage measurements (in nodes 4, 25, 27, 93, 94 and 95), placed according to this approach, will be taken into account; such solution will be indicated as "Solution A". On the other hand, a possible alternative solution is chosen here by taking into account the results of the performed analysis and looking at the operating conditions of the network. In particular, an additional voltage measurement has been added in node 95, in order to reduce the theoretical limit of voltage uncertainty given by σ_1^2. Moreover, three power measurements (in branches 3, 26 and 94[2]) are chosen to improve the accuracy of some of the largest currents of the network. The goal is, in this case, to reduce the contribution of uncertainty given by σ_2^2. This measurement configuration is indicated in the following as "Solution B".

Fig. 4.6 shows the uncertainty results obtained through the two different measurement systems. It is possible to observe that Solution A allows a significant enhancement of the voltage estimation in many of the nodes, due to the large number of voltage measurements and the consequent reduction of the uncertainty contribution σ_1^2. Despite this improvement, there are still some nodes exhibiting a significantly high uncertainty. In case of Solution B, instead, the best achievable uncertainty is higher, since the number of used voltage measurements is lower. However, all the nodes show a similar behaviour and the achieved uncertainty for the voltage profile is very flat. This solution, therefore, even if using a lower number of measurement devices with respect to the meter placement of Solution A, could be able to fulfil a possible accuracy target of 0.5% for all the nodes of the network.

As a final consideration, it is worth noting that, in general, the marginal benefits arising from the installation of an additional voltage measurement decrease with increasing number of such measurements. In Fig. 4.7, as an example, the values of the theoretical limit of uncertainty that can be achieved by using an increasing number of voltage measurements is reported. The dependence of such limit on the accuracy of the measurement devices is also shown. As it can be observed, it is clear that the reported trends are proportional to $1/\sqrt{M_V}$. These trends, in grids without too heavy loading conditions and with a suitable monitoring of the main currents, can provide a good reference for the expected uncertainty of the voltage estimations depending on number and accuracy of the available voltage measurements.

[2]As for the numeration of the branches, each branch index is given by the node number of its end node (the largest one), decreased by one.

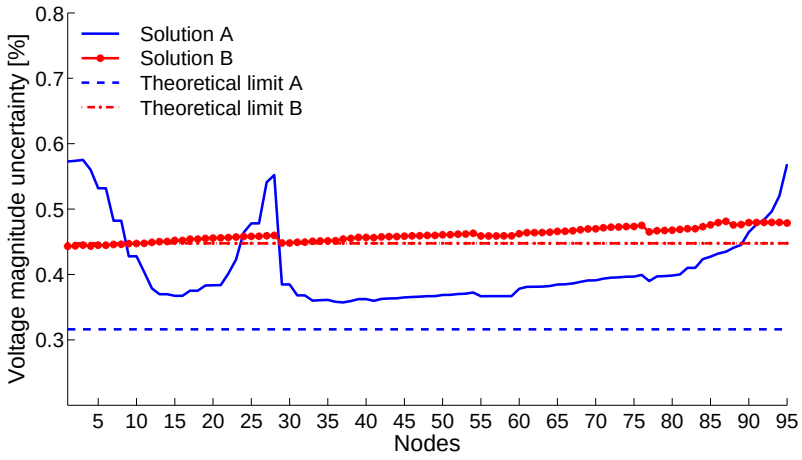

Figure 4.6: Expanded uncertainty of voltage magnitude estimation for different measurement configurations

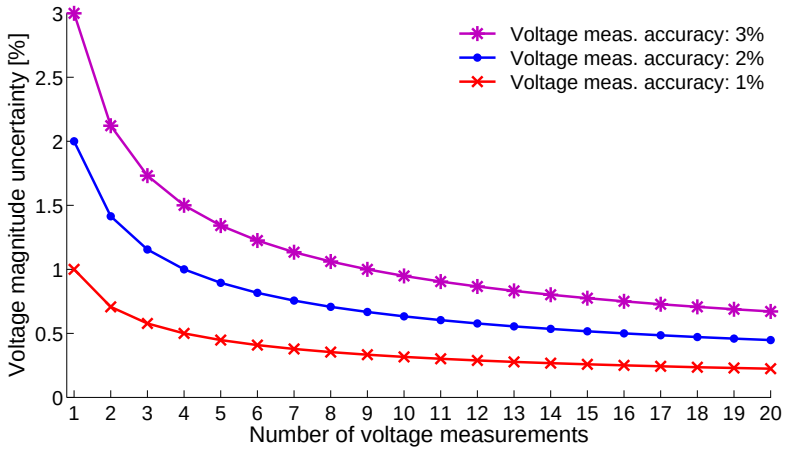

Figure 4.7: Theoretical limit of the expanded uncertainty of voltage magnitude estimation for increasing number of voltage measurements

4.4 Impact of measurements on flow estimation

In the literature, many of the works dealing with the issue of the accuracy of the estimation focus their attention on the voltage magnitude estimation. In fact, above all in active scenarios with strong penetration of DG, the particular behaviour of loads and generators in specific periods of the day can easily lead to under or over voltage issues. The regulation of the voltage profile through the controlled injection of reactive power in the grid, the generation curtailment or the demand-side management is one of the main tasks in the DMS. For this reason, many of the

meter placement techniques are designed to fulfil prefixed targets of accuracy in the voltage estimation.

Nevertheless, the accurate estimation of the flows in the different branches of the grid is, in the same way, equally important. The knowledge of the flows, intended as powers or currents, is in fact essential for several management functions, like, for instance, loss evaluation and optimal power flow, or to relieve possible over loading conditions. Some works underline the importance of the power flows estimation. In [13], as an example, the reference measurement configuration used in the tests is obtained through a meter placement technique designed to guarantee a minimum accuracy in the knowledge of the branch active powers. In [82], instead, the importance to have a suitable measurement configuration for achieving accurate energy flow estimations is highlighted. Furthermore, as already seen in the previous Section, it is useful to remind that the uncertainty in the knowledge of the branch currents has direct effects also on the voltage profile estimation. As a consequence, understanding the main factors affecting the estimation of the branch flows is important both for the power/current estimation itself and for the achievement of an accurate voltage knowledge.

In the following, tests aimed at highlighting the impact of different measurement configurations on the accuracy of the current and power estimations are carried out.

4.4.1 Impact of power measurements

One of the main peculiarities of distribution systems is the lack of real measurements installed on the field and the consequent necessity to use pseudo-measurements to achieve the observability of the network. A large source of uncertainty is, doubtless, the poor reliability associated to the information deduced from the historical or statistical data used to create the pseudo-measurements. Suitable methods aimed at enhancing the accuracy of the pseudo-measurements are increasingly required and represent a hot research topic. To show the possible impact deriving from a more accurate knowledge of the loads and generators behaviour, a first series of tests has been performed assuming different values of accuracy for the pseudo-measurements. Figs. 4.8 and 4.9 show the results obtained for the active power and the current magnitude estimation, respectively, by considering only one voltage measurement in the substation (with accuracy of 1%) and pseudo-measurements in all the load and generation nodes. It is worth noting that the state estimation performed on such scenario is equivalent to the execution of a power flow calculation, since the number of measurements is equal to the number of unknown state variables (there is no redundancy in the measurements).

From the figures it is possible to observe that, since the accuracy of all the power injections has been changed, the whole profile of uncertainty is scaled with respect to the reference case of pseudo-measurements with uncertainty equal to

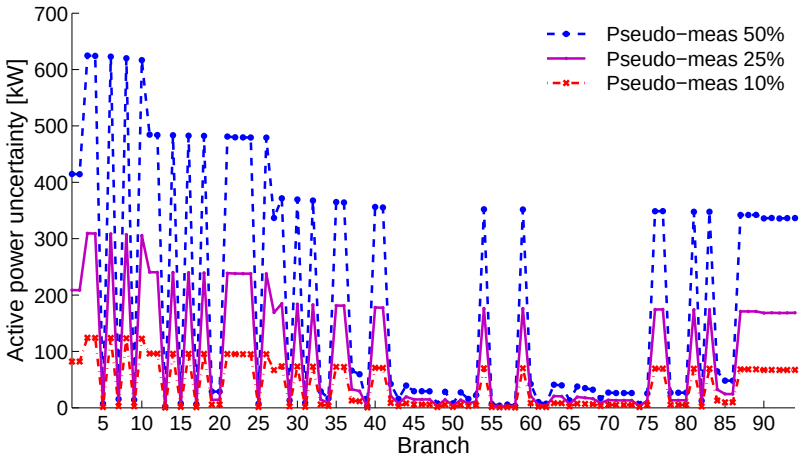

Figure 4.8: Impact of the pseudo-measurements accuracy on the power flows estimation

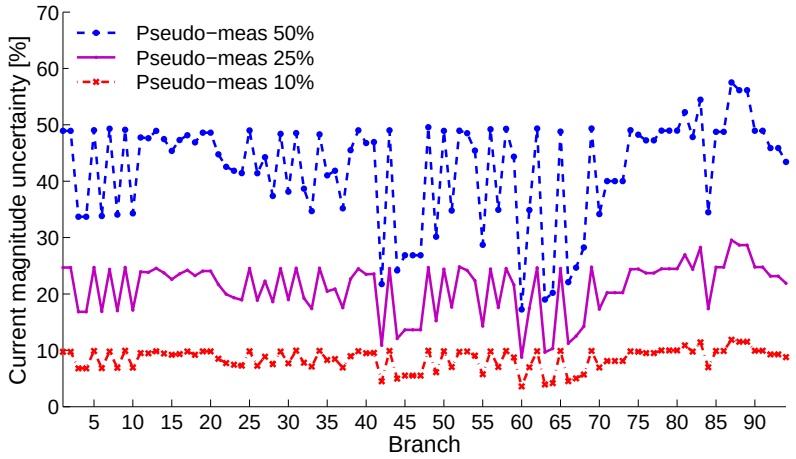

Figure 4.9: Impact of the pseudo-measurements accuracy on the current magnitude estimation

50%. As in the case of the voltage magnitude estimations, this outcome, even if trivial, emphasizes the importance to perform an accurate and detailed modeling of the pseudo-measurements for improving the confidence on their knowledge. An alternative option could be to use the smart meters to telemeter accurate real-time measurements of power injection to the control center. This solution could bring significant advantages, but it is not easily feasible because the consequent massive amount of data implies hard requirements from the point of view of the communication.

Considering a more realistic scenario with pseudo-measured injections having low reliability (assumed uncertainty equal to 50%), the following tests show the

impact brought by branch power measurements. The first test has been performed assuming, in addition to the voltage measurement in substation, the measurement of the powers in the branches departing from such node. An accuracy of 3% is supposed for both the active and the reactive power measurements. Results achieved for the current magnitude estimation are reported in Fig. 4.10. They are compared to those obtained by considering, as reference scenario, the only voltage measurement in substation, in order to highlight the impact brought by the additional power measurements.

Fig. 4.10 shows that a very large enhancement of the estimation accuracy is present in the measured branches (1 and 3) and in all the branches of the main feeder that are close to the measured ones (in particular, in the path between the substation and node 11). For these branches, the expanded uncertainty of the current magnitude estimation is lower than 3%. Moving away from the monitored branches, the improvements in the estimation accuracy are less prominent but still evident: for the branches in the feeders between nodes 11 and 28 and between nodes 11 and 42 (see Fig. 4.1), the resulting uncertainty is around 30% (with respect to an uncertainty larger than 40% for the reference scenario without power measurements). Effects of the power measurements can be seen even in the branches of the feeder arriving at node 95 (very far from the substation). A similar behaviour has been obtained also for the expanded uncertainties of active and reactive power.

For a better understanding of the obtained results, it is important to specify that the monitored branches in the substation (in particular branch 3) carry a very large current. This can be the reason of such a large impact on so many branches. To further investigate this aspect, another test has been performed removing the power measurements from substation and placing them at branch 75 (which carries

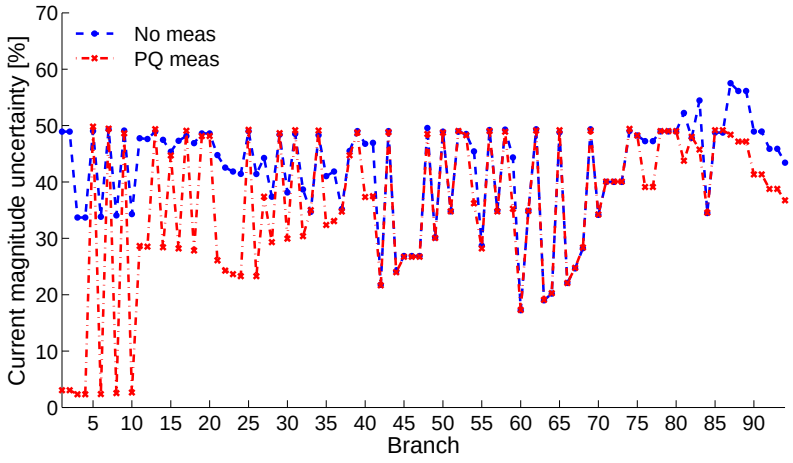

Figure 4.10: Impact of power measurements in substation on the current magnitude estimation

a significantly lower current). Results shown in Fig. 4.11 for the current magnitude estimation clearly indicate that the size of the monitored current plays a key role for the resulting impact. In fact, in this case, the only estimations affected by the additional power measurement are those of the branches close to branch 75, i.e. the branches in the path between nodes 61 and 76. For all the other current estimations, the impact of this power measurement is negligible.

As a result, some important considerations can be drawn from these two performed tests. The main consideration is that the impact brought by the power measurements strictly depends on the size of the measured quantity. In fact, obviously, the main impact of the measurement is on the uncertainty of current and power in the measured branch. In the adjacent branches, the uncertainty of the corresponding currents/powers is also related to the additional contributions of uncertainty coming from the possible injections or from the currents/powers carried by connected laterals. If the power in the measured branch is very large with respect to the other ones, these additional contributions of uncertainty can be relatively small and do not jeopardize the estimation uncertainty in the adjacent branches. On the contrary, if the measured power is very small, its accurate knowledge does not bring any benefit to the estimation in the adjacent branches, since their accuracy will be affected by the larger contributions of uncertainty coming from the power injections or the powers of the other connected branches.

Possible implications, in a meter placement perspective, arising from these considerations are shown in the following test. Two different measurement configurations, each one composed of four measurement points, are taken into account. In the first one (indicated in the following as "Configuration A"), measurement points have been assumed at nodes 1, 11, 37 and 60: this choice has been made to test

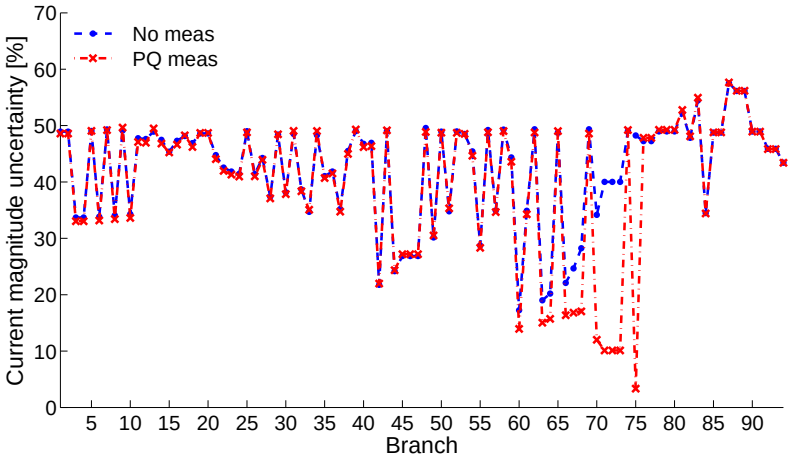

Figure 4.11: Impact of power measurements in branch 75 on the current magnitude estimation

a scenario where the monitored quantities are in the central nodes of the network. As for the second configuration (indicated in the following as "Configuration B"), measurement points are placed at nodes 1, 28, 37 and 95: this choice has been made to assure the monitoring of the largest currents in the network, i.e. those coming from the substation and the generation nodes. Each one of the measurement points is composed of power measurements in two of the branches connected to the bus (obviously, only one measurement is possible for nodes 28 and 95). Moreover, the measurement of the voltage in the substation is always available.

Fig. 4.12 shows the results obtained for the expanded uncertainty of the active power estimations with the two different measurement systems. The attention can be focused on the branches constituting the main feeders of the 95-bus network (see Fig. 4.1), because the powers involved in the lateral branches are smaller and, thus, also their uncertainties in absolute terms are low. As in the previous tests, it is possible to observe that the effects of the power measurements are clearly larger in the branches close to the measurement points. For example, in case of Configuration A, very low uncertainties have been obtained for the power estimations of the branches close to the measurement points in nodes 11 and 60 (see Fig. 4.1 for the numbering of the branches of the feeder). Nevertheless, due to missing monitoring of the DG, a high uncertainty is still present in the branches near to generation nodes. With the measurement system assumed in Configuration B, instead, several branches exhibit a worse estimation accuracy. However, a flatter profile of uncertainty has been obtained, thanks to the measurement of the largest currents. As a consequence, in this scenario, all the branch powers are estimated with an uncertainty lower than 70 kW. Such a solution, thus, proves to be suitable for minimizing the maximum uncertainty among the power estimations of all the branches of the network.

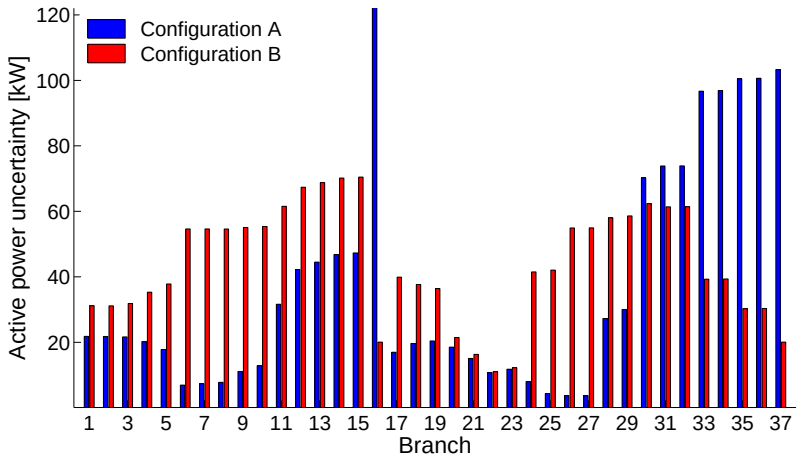

Figure 4.12: Expanded uncertainty of active power estimation with different measurement configurations

4.4.2 Impact of current magnitude measurements

Together with the use of enhanced power injections or the deployment of branch power measurements, the other direct way to improve the uncertainty of the flows in the network is the use of current magnitude measurements. In this subsection, tests aimed at assessing the impact brought by these measurements, and highlighting possible differences with respect to the use of power measurements, have been performed.

The first test has been carried out by considering the installation of current magnitude measurements (with uncertainty equal to 2%) in the branches departing from the substation. Moreover, in the substation, the presence of the voltage measurement is assumed. Results of this test are compared to those obtained in the previous subsection with the same placement of the power measurements, and with the reference scenario where only the voltage measurement is considered.

Fig. 4.13 shows the results for the uncertainty in the active power estimation. As expected, it can be observed that the impact brought by the current measurements is similar to that of the power measurements. In fact, the measurement of the large currents departing from the substation allows achieving a significant improvement in the estimation of the power flowing in the branches close to the substation bus. Moreover, because of the large size of the measured currents, the estimation enhancement, even if less prominent, is also propagated to the farthest branches in the main feeders of the network. In comparison to the results obtained by using power measurements, Fig. 4.13 shows that the direct measurement of power leads to larger advantages, above all in the branches closer to the substation bus.

Fig. 4.14 reports, instead, the results obtained for the relative uncertainties of current magnitude estimation. Even in this case, it is possible to note the significant benefits brought by the monitoring of the substation branches: in the feeder between nodes 1 and 11 the estimation uncertainty is reduced to values smaller than 4%. Another interesting aspect arising from the results shown in Fig. 4.14 is that, in this case, differently from what seen for the active power estimations, the direct measurement of the considered quantity (that is, of current magnitude) brings only slightly larger benefits (with respect to the use of power measurements) and basically only in the measured branches. On the contrary, in the farthest branches of the feeders, better current magnitude estimations are obtained considering the deployment of power measurements. This demonstrates, in general, the larger impact associated to the combined measurement of active and reactive power.

As a final consideration about the use of current magnitude measurements, it is important to underline that their use has been always particularly critical in the state estimation context. In fact, their presence in an active scenario (with bi-directional power flows) can lead to multiple solutions of the SE problem, causing possible convergence issues and consequent inaccuracies in the estimation results. This problem

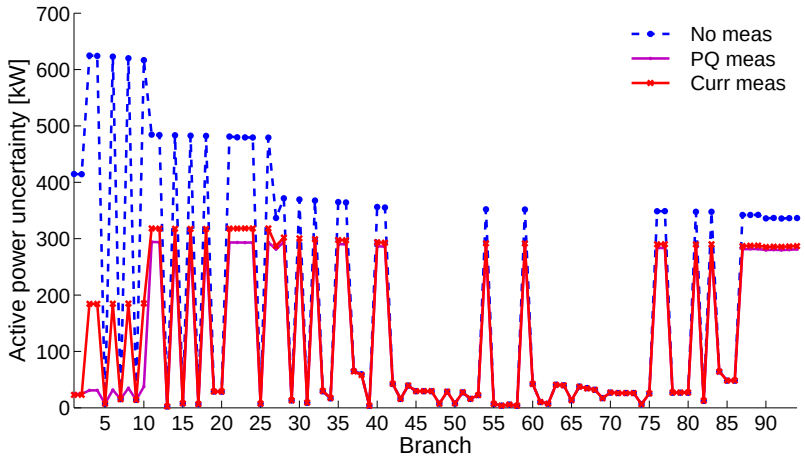

Figure 4.13: Impact of current magnitude measurements in substation on the active power estimation

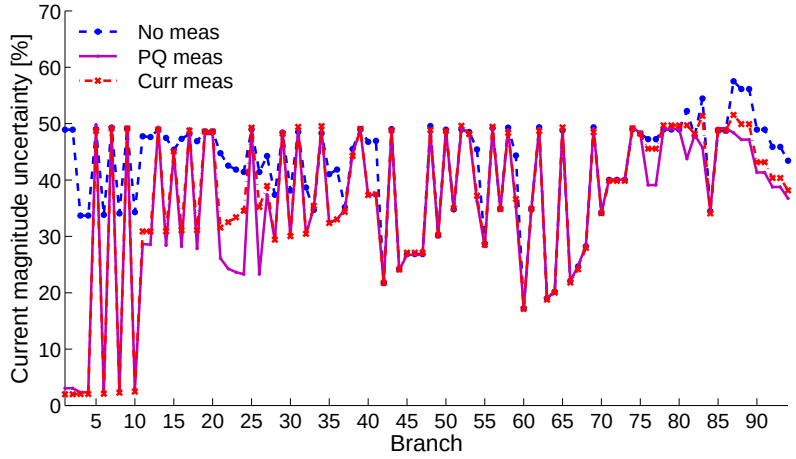

Figure 4.14: Impact of current magnitude measurements in substation on the current magnitude estimation

is well known in the literature [4, 83] and in fact, in transmission systems, current magnitude measurements are often disregarded. In distribution systems, given the low redundancy of the available real-time measurements, the possible presence of current magnitude measurements is an essential additional source of information and, thus, they cannot be disregarded as well. However, in the decisional stage for the choice of the measurement devices to be used in the upgrade of the actual measurement system, this aspect should be duly taken into account.

4.4.3 Impact of voltage measurements

As final analysis of the impact of the different types of measurement on the flow estimations, the possible effects brought by the deployment of voltage measurements are investigated. As first test, a measurement system composed of four voltage measurements (with uncertainty equal to 1%) in nodes 1, 28, 37 and 95 has been considered. In Fig. 4.15, the active power estimation results obtained with this measurement configuration are compared to those related to the presence of only a voltage measurement in the substation. It is possible to observe that, in this case, an evident enhancement of the accuracy of the active powers can be obtained. The reason for this outcome is strongly connected to the absence of power or current measurements. In fact, each couple of voltage measurements provides a sort of constraint on the voltage drops along the branches and, thus, on the flowing currents. Because of the poor accuracy associated to the pseudo-measurements, and without any better information available, these constraints are able to enhance the highly uncertain knowledge on the branch powers.

As a confirmation, another test has been performed considering the availability of measurement points in the same nodes (1, 28, 37 and 95). In one case, the presence of power measurements (with uncertainty equal to 3%) on all the branches converging to each monitored nodes has been considered. In the second scenario, this measurement configuration is integrated with the addition of the voltage measurements on the nodes. Fig. 4.16 shows the obtained results. It is possible to note that, in this case, the effects brought by the same voltage measurements are practically negligible. The reason is due to the presence of the power measurements, which already provide an important information concerning the overall power flow-

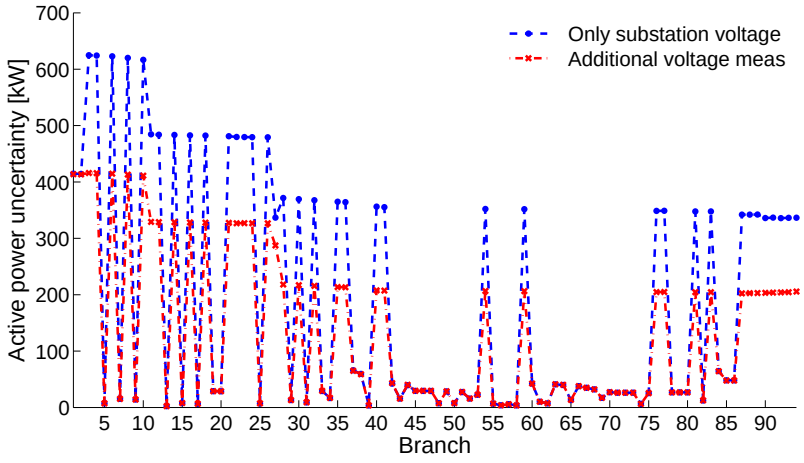

Figure 4.15: Impact of voltage magnitude measurements on the active power estimation, when no flow measurements are available

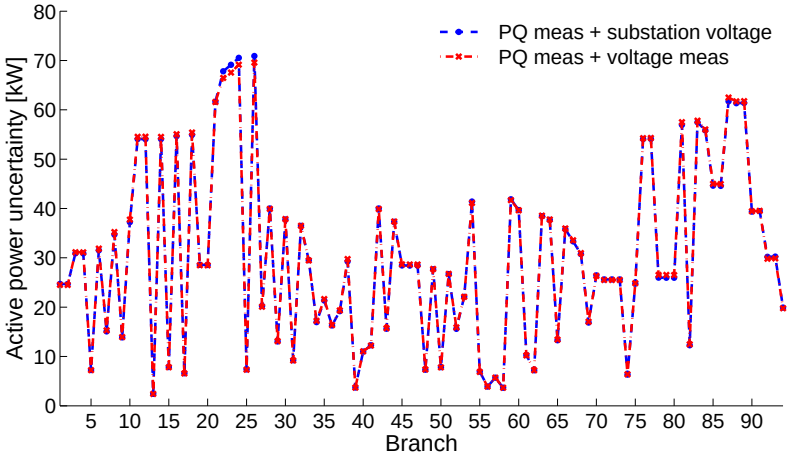

Figure 4.16: Impact of voltage magnitude measurements on the active power estimation, when power measurements are also available

ing in the paths between the measured nodes. In such a situation, the "constraint" given by the voltage measurements can bring some additional advantages but not so important as in the previous test.

4.5 Impact of synchronized measurements

As already discussed in the first Chapter, PMUs are modern measurement instruments that are becoming increasingly widespread in transmission systems. The capability to provide very accurate measurements of current and voltage phasors, and the synchronization with respect to an absolute time reference, are the main reasons for the spread of these measurement devices. In distribution systems, despite the necessity to foresee a measurement system upgrade, the deployment of PMUs is strongly limited by their high costs.

In this Section, regardless of the economic aspects involved in the choice of the measurements systems, some tests have been performed to analyze, technically, the possible advantages coming from the use of PMUs. It is important to underline that PMUs are measurement devices very different from the other conventional measurements, under many points of view. As an example, PMUs are designed to give time tagged measurements that refer to a specific instant of time. The compliance requirements provided by the standard for the sysnchrophasors [51] set accuracy limits referred to both steady-state and dynamic conditions. As a result, compliant PMUs provide instantaneous measurements whose accuracy is guaranteed under most of the practical operating conditions (except for the presence of large step changes, which are, however, suitably marked). Moreover, it is worth noting

that there are devices able to provide synchrophasor measurements with significantly higher accuracy. On the other side, however, the upstream presence of transducers leads to the unavoidable degradation of such accuracy. As a result, to obtain the real accuracy of the PMU measurements, a detailed analysis of all the contributions of uncertainty arising from the whole measurement chain would be necessary.

Conventional instruments, instead, use a specific time window to perform their measurements. Their accuracy is generally provided for steady-state conditions, while their behaviour under dynamic conditions could be not well known. In the distribution system scenario, where high dynamics can be expected (due for example to the unpredictable and intermittent operation of the DG based on renewable sources), the accuracy characteristics of the traditional measurements could be significantly degraded. Another aspect affecting the overall accuracy of a measurement system based on conventional devices is the lack of synchronization among the different measurements collected from the grid.

An extensive analysis of all the possible sources of uncertainty for traditional or synchronized measurements is out of the scope of this thesis. The tests presented here, basically, aims at highlighting the different effects on the estimation results achievable when using phasor measurements in place of the conventional measurements of voltage and power. To compare the results, in the following, a measurement system composed of four measurement points at nodes 1, 28, 37 and 95 is considered. In case of conventional measurements, voltage and power measurements are assumed to have uncertainties equal to 1% and 3%, respectively. As for the PMUs, instead, magnitude and angle measurements are supposed to have uncertainty equal to 1% and 1 crad (10^{-2} rad), respectively. These accuracies have been chosen referring to the worst case scenario possible for the PMUs, according to the limit of 1% imposed by the synchrophasor standard [51] for the TVE in steady state conditions.

A first test has been performed by considering only voltage measurements in the monitored nodes. In this scenario, each PMU provides an additional voltage angle measurement with respect to the traditional measurements. Therefore, it is possible to roughly assess the additional contribution brought by the voltage angle measurements on the estimation of the different quantities. Results show that the knowledge of the voltage angles is useful to improve the estimation of both active and reactive powers. As an example, Fig. 4.17 shows the results obtained for the estimations of active power in the branches belonging to the main feeders of the network (indicated in red in Fig. 4.1). It is possible to observe that PMUs allow a clear improvement, which in some branches is larger than 60 kW. Similar enhancements have been achieved even for the current magnitude estimations. Fig. 4.18 reports the corresponding percent results, always focusing on the branches of the main feeders. As for the voltage magnitude estimation, both conventional instruments and PMUs rely on voltage magnitude measurements with the same

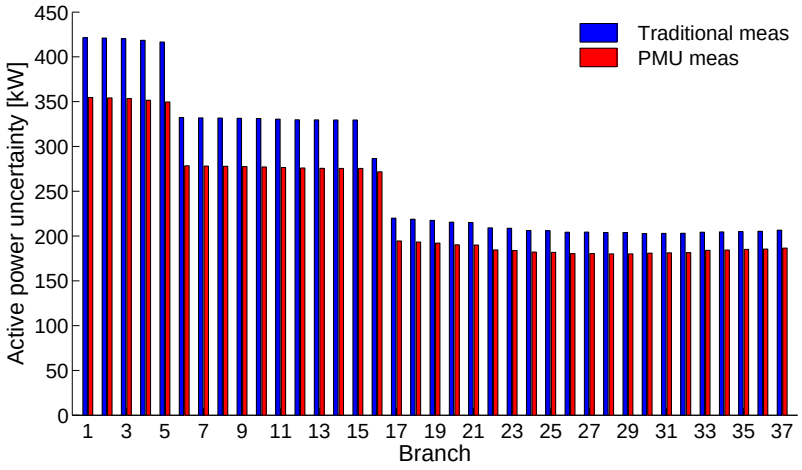

Figure 4.17: Uncertainty on the active power estimation in case of voltage measurements

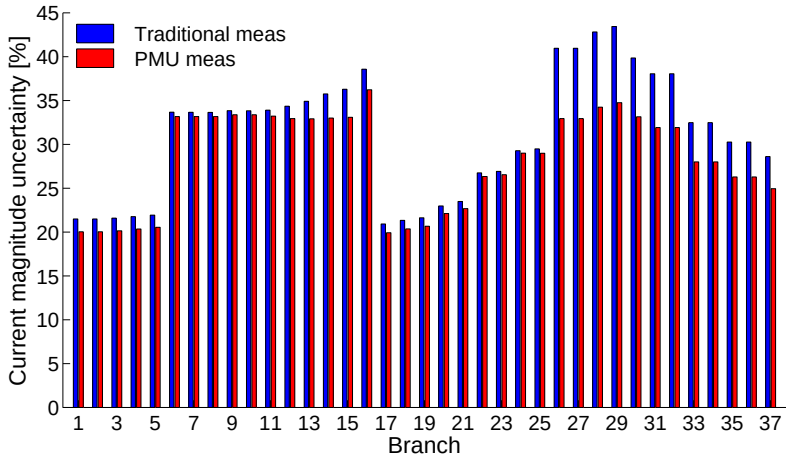

Figure 4.18: Uncertainty on the current magnitude estimation in case of voltage measurements

uncertainty. However, since, as seen in Section 4.3, the voltage magnitude estimation is affected also by the voltage drops, the better estimation of the flows allowed by the PMUs leads also to a slightly better estimation for the voltage magnitude profile.

Another test has been carried out by taking into account only the flow measurements in the branches adjacent to the considered nodes and the voltage measurement in the substation. In this case, both the measurement typologies rely on two informations: active and reactive power for the traditional measurements and current magnitude and angle for the PMUs. This test allows comparing the different impact of such measurements on the estimations of the electrical quantities of the

network. Even in this case, PMUs lead to a higher accuracy for the power estimations. However, since the presence of flow measurements allows better estimations with respect to the previous test, in this case the enhancements are lower in absolute terms (around 10 kW for several branches). Similar reasoning also holds for the current estimations. Fig 4.19 shows the results obtained for the current magnitude estimation. It is possible to see that, in general, a significant enhancement of the accuracy has been obtained with respect to the previous measurement test-case (see the corresponding results in Fig. 4.18). Even in this scenario with enhanced estimations, PMUs still allow improving the knowledge on the current magnitudes. Such enhancement in the flow estimations, even if not too large, is clearly reflected also in the voltage magnitude estimations, whose results are shown in Fig. 4.20

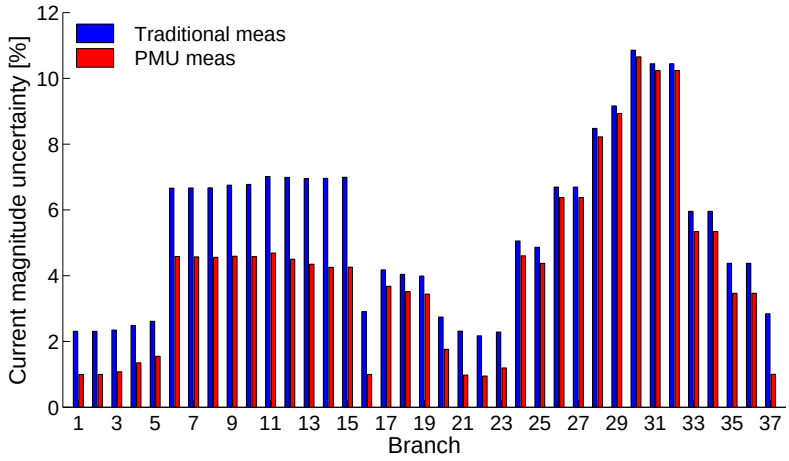

Figure 4.19: Uncertainty on the current magnitude estimation in case of flow measurements

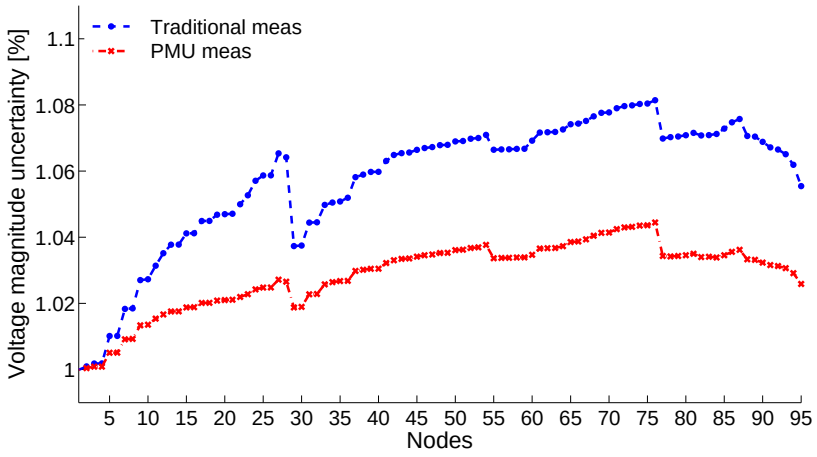

Figure 4.20: Uncertainty on the voltage magnitude estimation in case of flow measurements

As final test, the simultaneous use of all the measurements (voltage magnitude and powers for the traditional meters and voltage and current phasors for the PMUs) has been considered. In case of traditional measurements, with respect to the previous test, the only addition of the voltage magnitude measurements is provided. As already seen in the previous sections, such addition has clear effects on the uncertainty of the voltage magnitude estimation, while it is not particularly useful to enhance the estimation of currents and powers in the network (see Fig. 4.16). In case of PMUs, besides the voltage magnitudes, even the voltage angle measurements are added to the set of the input measurements. The presence of voltage angle measurements proves to have an impact on the power estimations and, in this case, in particular for the reactive powers. Fig. 4.21 shows the enhancement in the reactive power estimations obtained by adding voltage phasor measurements to the measurement scenario of the previous test. It is possible to observe that a slight enhancement has been obtained for all the branches of the main feeder. Since the same enhancement has not been obtained in case of traditional measurements (thus, with the only addition of voltage magnitude measurements), this estimation improvement can be totally attributed to the presence of the voltage angle measurements.

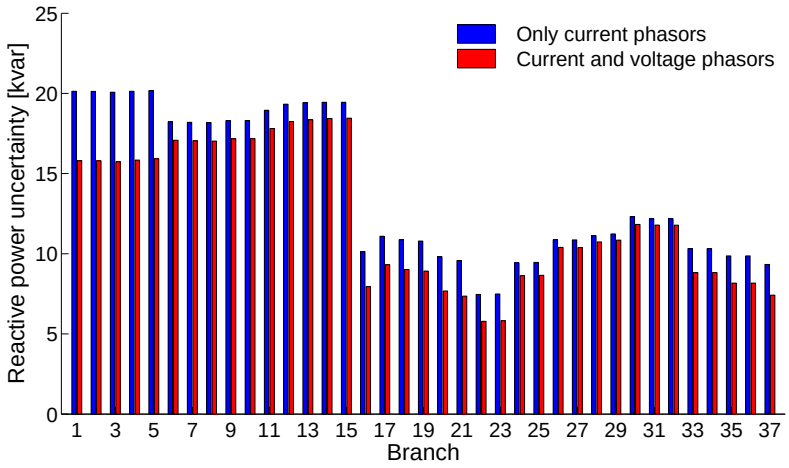

Figure 4.21: Uncertainty on the reactive power estimation in the cases of only current or current and voltage phasor measurements

4.6 Final discussion

The choice of a measurement system aimed at enabling the accurate estimation of the electrical quantities of a grid is one of the most challenging issues in distribution systems. This Chapter presented an analysis of the impact brought by different measurements on the estimation of the different electrical quantities of a network.

Results of this analysis allow some important considerations, which can be helpful in a meter placement perspective.

First of all, it has been shown that the voltage profile estimation is basically determined by two factors. The first one is the number and the accuracy of the voltage measurements deployed on the network. The second one is linked to the accuracy in the knowledge of the flows in the network (and, thus, of the voltage drops along the branches). If the largest currents in the network are monitored, then, the uncertainty on the voltage profile estimation is similar for all the nodes and it basically depends only on number and accuracy of the available voltage measurement devices. This means that the position of the voltage measurements is not decisive and can be adapted according to other requirements (like, for example, the necessity to connect voltage and current or power measurements in the same measurement point in order to reduce the costs).

As for the branch flows estimation, test results show that significant enhancements can be obtained only by installing current or power measurements. The impact of these measurements is in general dependent on the size of the measured quantity. If the measured power or current is large, then the positive effects of such measurement can be propagated even to the power and current estimation of other connected branches. Instead, if the measured quantity is not so large, than the effects are only local and limited to the measured branch and, maybe, to few other very close branches. This aspect emphasizes the necessity to monitor, in particular, the branches belonging to the main feeders or those connected to large loads or generators (in general, those branches that can be reasonably expected to carry large currents).

Finally, further analysis has been proposed to investigate the possible technical benefits coming from the use of PMUs. Such analysis has been limited to consider the impact brought by the additional angle measurements. It has been shown that the knowledge of the angles can provide some benefits, in a context characterized by low redundancy of the measurements, above all for the power estimations. Other additional benefits could be provided by the higher accuracy of these devices and the availability of the synchronization to an absolute time reference, but the detailed analysis of these aspects is out of the scope of this thesis.

Chapter 5

Impact of correlations on DSSE

5.1 Measurement correlation in DSSE

The deployment of a suitable measurement system is essential for the effective management and control of future distribution systems. Nevertheless, the number of measurement devices that will be installed in the near future is not expected to be too large, due to obvious economic reasons. As a consequence, a careful choice of type and placement of the measurements is necessary to achieve specific requirements in the DSSE results. In any case, it is clear that economic constraints bring limitations to the design of the measurement system and this, in turn, leads to limits also for the accuracy achievable in the DSSE. As a consequence, solutions able to enhance the accuracy of the DSSE results are strongly required. A way to enhance the estimation results is to provide a very accurate modeling of the measurements used in the SE process. In [84], as an example, the importance of considering the uncertainty contribution brought by the instrument transformers, in the modeling of the measurement uncertainties provided to the WLS estimator, has been highlighted. In [85], it is shown that proper consideration of the uncertainty sources present in the whole measurement chain, thus including both measurement devices and instrument transformers, allows improving the accuracy performance of WLS state estimators.

Besides the accurate definition of the uncertainty of each single measurement, a proper modeling of the measurement uncertainties should also take into account possible correlations existing among different measurements. In general, correlations are usually neglected in the SE models. In the literature, only a few works deal with this issue and investigate the impact brought by possible correlations. In [86], the estimation of the operating conditions is performed by means of a probabilistic power flow using the measured values as constraints; in this approach, correlations among the power injections of similar loads are considered to improve the estima-

tion results. A probabilistic power flow including correlations is also used in [87]; in this case the considered correlations are among the loads belonging to the same geographical area and among similar generation sources. Some works show also the possibility to take into account the correlations in the weighting matrix of the WLS estimators. In [88], for example, the WLS model includes the correlations among the pseudo-measurements of different loads and generators, and between active and reactive power injection of the same node. Possible correlations existing in real measurements are considered in the WLS estimators in [89] and [90]. In [89], a point estimate method is used to compute the correlations arising among voltage and active and reactive power provided by multifunction meters. In [90], instead, unscented transformations are used to consider the possible correlations among instrument transformer signals and to calculate the resulting covariance matrix for the power meter outputs. More recently, [91] has investigated the impact, over long execution periods of SE, brought by the time correlation in PMU measurements provided with high reporting rate.

In this Chapter, an overall analysis of the most important sources of correlation that can affect the DSSE is performed [92]. In particular, possible correlations arising in the measurements provided by power meters and PMUs are investigated. Moreover, correlations in pseudo-measurements associated to loads and generators with similar behaviour, or belonging to the same geographical area, are discussed. Finally, tests aimed at highlighting the effects deriving from the inclusion of such correlations in the WLS model of the DSSE are presented and discussed.

5.1.1 Inclusion of correlation in DSSE

This subsection shows how to consider correlations in the mathematical model of the estimators based on the WLS approach. The inclusion of the correlations follows the same pattern for all the types of input data. Thus, the following considerations hold for all the types of measurement correlations and the presented scheme serves as a general reference for all the cases analyzed below.

As already described in Chapter 1, WLS estimators use a weighting matrix $\mathbf{W}$ to assign a different level of confidence to the input measurements. The proper implementation of the WLS approach is obtained generating the weighting matrix through the inversion of the covariance matrix $\mathbf{\Sigma_y}$ of the measurement errors. In the traditional approach, all the measurements are considered as independent and the covariance matrix $\mathbf{\Sigma_y}$ is a diagonal matrix, where the i-th element of the diagonal is the variance $\sigma^2_{y_i}$ of the i-th measurement y_i. In this case, the resulting weighting matrix is also diagonal and the i-th weight (associated to the i-th measurement) is the inverse of the variance $\sigma^2_{y_i}$. More in general, if the correlations among different measurements are considered, the expression of the covariance matrix is:

$$\boldsymbol{\Sigma}_{\mathbf{y}} = \begin{bmatrix} \sigma_{y_1}^2 & \dots & \rho_{1,j}\sigma_{y_1}\sigma_{y_j} & \dots & \rho_{1,M}\sigma_{y_1}\sigma_{y_M} \\ \vdots & \sigma_{y_2}^2 & & & \vdots \\ \rho_{i,1}\sigma_{y_i}\sigma_{y_1} & & \ddots & & \vdots \\ \vdots & & & \ddots & \vdots \\ \rho_{M,1}\sigma_{y_M}\sigma_{y_1} & \dots & \dots & \dots & \sigma_{y_M}^2 \end{bmatrix} \tag{5.1}$$

where σ_{y_i} is the standard deviation of the i-th measurement, $\rho_{i,j}$ is the correlation factor between measurements i and j, and M is the total number of measurements. In this case, obviously, the weighting matrix resulting from the inversion of $\boldsymbol{\Sigma}_{\mathbf{y}}$ is not diagonal anymore. However, it is worth noting that, in general, not all the measurements are correlated and only some covariance terms are different from zero. As an example, in case of real measurements, the measurements provided by different devices can be reasonably considered as independent. Possible correlations can be found, instead, among the measurements provided by the same instrument. In this scenario, indicating with $\mathbf{Y}_k$ the set of all the measurements coming from the k-th device, and with $\mathbf{Y}_{pseudo}$ the set of all the pseudo-measurements, the covariance matrix $\Sigma_{\mathbf{y}}$ can be written as the following diagonal block matrix:

$$\boldsymbol{\Sigma}_{\mathbf{y}} = \begin{bmatrix} \boldsymbol{\Sigma}_{\mathbf{y}_1} & \mathbf{0} & \dots & \mathbf{0} \\ \mathbf{0} & \boldsymbol{\Sigma}_{\mathbf{y}_2} & & \vdots \\ \vdots & & \ddots & \mathbf{0} \\ \mathbf{0} & \dots & \mathbf{0} & \boldsymbol{\Sigma}_{\mathbf{y}_{pseudo}} \end{bmatrix} \tag{5.2}$$

where $\boldsymbol{\Sigma}_{\mathbf{y}_k}$ and $\boldsymbol{\Sigma}_{\mathbf{y}_{pseudo}}$ are the covariance sub-matrices associated to the sets of the measurements in the k-th device and of the pseudo-measurements, respectively. It is worth noting that the weighting matrix resulting from (5.2) is also a diagonal block matrix, which can be obtained through the inversion of the single covariance sub-matrices. From a computational point of view, this allows avoiding the inversion of the full covariance matrix and, thus, can lead to a reduction of the computational burden.

5.2 Analysis of correlation in multifunction meters

As anticipated in the previous Section, measurements provided by different instruments can be reasonably considered as decorrelated, since they do not have common sources of uncertainty. Instead, measurements coming from the same device can share one or more sources of uncertainty and, thus, they can be correlated. In the analysis developed here, the focus is on the correlations arising in multifunction meters. In this context, multifunction meters are intended as instruments able to

provide measurements of both voltage magnitude and active and reactive power. To assess the possible presence of correlation in such measurements, the connection scheme depicted in Fig. 5.1 (which is derived from [89]) is considered. According to Fig. 5.1, multifunction meters provide the three-phase measurements of voltage and power relying on the acquisition of the voltage and current signals at the monitored point. For each phase, the measurements of voltage magnitude V, active power P and reactive power Q are, therefore, obtained through the elaboration of the corresponding inputs of the phase, i.e. the voltage magnitude V (the same provided as output), the current magnitude I and the phase-angle difference $\alpha = \delta - \theta$, where δ and θ are the phase-angles of voltage and current, respectively.

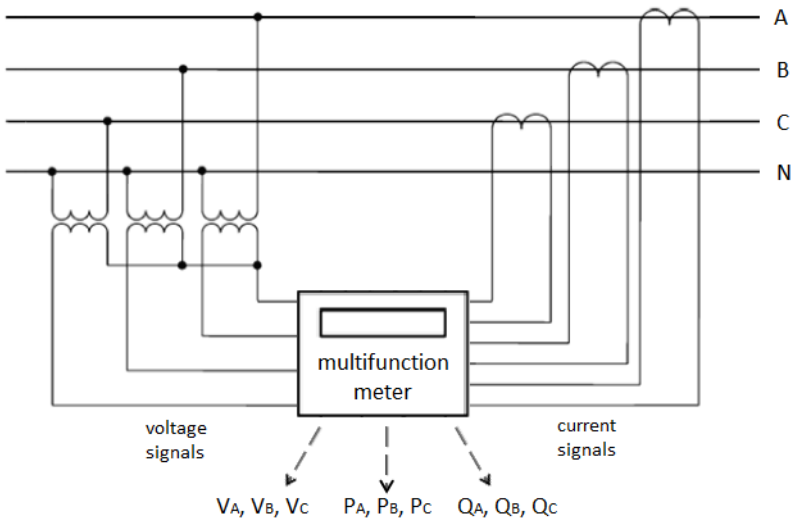

Figure 5.1: Measurement scheme of a multifunction meter

Focusing, for the sake of simplicity, only on one phase of the system, and taking into account only the fundamental components of the input signals of voltage and current, it is possible to express the measured active and reactive powers as:

$$\begin{aligned} P &= P(V, I, \alpha) = VI\cos(\alpha) \\ Q &= Q(V, I, \alpha) = VI\sin(\alpha) \end{aligned} \tag{5.3}$$

Equation (5.3) indicates that both the powers are indirect measurements obtained through the elaboration of all the input variables. As a result, since the input uncertainties are the same, it is clear that consequent correlations arise. In [89], the full covariance matrix of the output measurements is obtained by means of a point estimation method that is performed after the first iteration of the SE algorithm. It is worth noting that, besides the computational burden associated to execution of this technique, the covariance matrix obtained in this way is only an estimation of the

real covariance matrix. Here, instead, the law of propagation of the uncertainty [93] is applied to achieve the proper covariance matrix.

Indicating with $\mathbf{f}_{vpq}$ the vector of the mathematical functions associated to the output measurements, it is:

$$\mathbf{f}_{vpq} = \begin{pmatrix} V \\ P(V, I, \alpha) \\ Q(V, I, \alpha) \end{pmatrix} \tag{5.4}$$

Then, indicating with $\mathbf{x}_{vi\alpha}$ and $\mathbf{\Sigma}_{vi\alpha}$ the vector and the covariance matrix of the input variables, respectively, it is possible to express the covariance matrix $\mathbf{\Sigma}_{vpq}$ of the output measurements as:

$$\left[\mathbf{\Sigma}_{vpq}\right] = \left[\frac{\partial \mathbf{f}_{vpq}}{\partial \mathbf{x}_{vi\alpha}}\right] \left[\mathbf{\Sigma}_{vi\alpha}\right] \left[\frac{\partial \mathbf{f}_{vpq}}{\partial \mathbf{x}_{vi\alpha}}\right]^T \tag{5.5}$$

where the derivative matrix is the Jacobian of the functions associated to the output measurements with respect to the input variables:

$$\left[\frac{\partial \mathbf{f}_{vpq}}{\partial \mathbf{x}_{vi\alpha}}\right] = \begin{bmatrix} \frac{\partial V}{\partial V} & \frac{\partial V}{\partial I} & \frac{\partial V}{\partial \alpha} \\ \frac{\partial P}{\partial V} & \frac{\partial P}{\partial I} & \frac{\partial P}{\partial \alpha} \\ \frac{\partial Q}{\partial V} & \frac{\partial Q}{\partial I} & \frac{\partial Q}{\partial \alpha} \end{bmatrix} = \begin{bmatrix} 1 & 0 & 0 \\ I\cos\alpha & V\cos\alpha & -VI\sin\alpha \\ I\sin\alpha & V\sin\alpha & VI\cos\alpha \end{bmatrix} \tag{5.6}$$

and the input covariance matrix, considering all the input measurements as independent, is:

$$\mathbf{\Sigma}_{vi\alpha} = \begin{bmatrix} \sigma_V^2 & & \\ & \sigma_I^2 & \\ & & \sigma_\alpha^2 \end{bmatrix} \tag{5.7}$$

where σ_V, σ_I and σ_α are the standard deviations associated to voltage magnitude, current magnitude and phase-angle difference, respectively.

Solving the matrix multiplication in (5.5), the following variances of the output measurements can be found:

$$\sigma_V^2 = \sigma_V^2 \tag{5.8}$$

$$\sigma_P^2 = \sigma_V^2 I^2 \cos^2\alpha + \sigma_I^2 V^2 \cos^2\alpha + \sigma_\alpha^2 V^2 I^2 \sin^2\alpha \tag{5.9}$$

$$\sigma_Q^2 = \sigma_V^2 I^2 \sin^2\alpha + \sigma_I^2 V^2 \sin^2\alpha + \sigma_\alpha^2 V^2 I^2 \cos^2\alpha \tag{5.10}$$

As for the covariances terms, the following results can be obtained:

$$\sigma_{VP} = \sigma_V^2 I \cos\alpha \tag{5.11}$$

$$\sigma_{VQ} = \sigma_V^2 I \sin\alpha \tag{5.12}$$

$$\sigma_{PQ} = \frac{1}{2}\sin 2\alpha(\sigma_V^2 I^2 + \sigma_I^2 V^2 - \sigma_\alpha^2 V^2 I^2) \tag{5.13}$$

Since the information provided by the multifunction meter only refers to the voltage and power measurements, it is necessary to convert the found relationships in terms of these output variables and of the independent uncertainty contributions. Considering that uncertainties are usually expressed in terms of their relative values, it is more convenient to present the variances terms in (5.8 - 5.10) divided by the squared measured quantities, thus obtaining:

$$\frac{\sigma_V^2}{V^2} = \frac{\sigma_V^2}{V^2} \tag{5.14}$$

$$\frac{\sigma_P^2}{P^2} = \left(\frac{\sigma_V^2}{V^2} + \frac{\sigma_I^2}{I^2} + \sigma_\alpha^2 \tan^2\alpha\right) \tag{5.15}$$

$$\frac{\sigma_Q^2}{Q^2} = \left(\frac{\sigma_V^2}{V^2} + \frac{\sigma_I^2}{I^2} + \sigma_\alpha^2 \cot^2\alpha\right) \tag{5.16}$$

As for the covariance terms, the conversion of equations (5.11 - 5.13) leads to:

$$\frac{\sigma_{VP}}{VP} = \frac{\sigma_V^2}{V^2} \tag{5.17}$$

$$\frac{\sigma_{VQ}}{VQ} = \frac{\sigma_V^2}{V^2} \tag{5.18}$$

$$\frac{\sigma_{PQ}}{PQ} = \frac{\sigma_V^2}{V^2} + \frac{\sigma_I^2}{I^2} - \sigma_\alpha^2 \tag{5.19}$$

Relationships found in (5.8 - 5.13) are those to be considered in the DSSE model if the input measurements used in the estimation algorithm are voltage and power measurements. Instead, if power measurements are converted in equivalent currents, as in the case of the BC-DSSE algorithm presented in this thesis, an additional elaboration must be performed to achieve the final covariance matrix $\mathbf{\Sigma}_{vi}$ related to the voltage magnitude and the equivalent current measurements.

As in the previous case, the law of propagation of the uncertainty can be used to compute the resulting variance and covariance terms arising due to the presence

of the indirect current measurements. Retrieving equations (1.29) and (1.30) from Chapter 1, the real and imaginary parts i^r and i^x of the equivalent currents are:

$$i^r = P\cos\delta + Q\sin\delta \tag{5.20}$$

$$i^x = P\sin\delta - Q\cos\delta \tag{5.21}$$

where δ is the voltage angle in the considered node. It is worth noting that, to have a faster computation of the BC-DSSE algorithm, it is more convenient to build the weighting matrix only once, before the iterative part of the estimator; thus, a constant covariance matrix is needed. For this reason, the voltage angle δ can be assumed, in first approximation, equal to 0 or $\pm 120°$, depending on the phase, if the overall measurement system includes only traditional measurements. In case of presence of PMUs, instead, since the angles have to be referred to the UTC reference, the voltage angle measured (on the considered phase) by one of the available PMUs can be used as reference. In both cases (measurement system with only traditional devices or with the presence of PMUs), this choice lead to an approximation. However, since in distribution systems the lines are usually short and the impedances are low, the differences in the phase-angles for the different nodes of the network are generally quite small. For this reason, the introduced approximation is in general acceptable and, as also shown in Chapter 3, it does not affect the accuracy performance of the BC-DSSE algorithm.

Considering the relationship functions shown in (5.20) and (5.21), the vector $\mathbf{f}_{vi}$ of the measurement functions associated to the quantities to be provided as input to the BC-DSSE algorithm can be defined as:

$$\mathbf{f}_{vi} = \begin{pmatrix} V \\ i^r(P,Q) \\ i^x(P,Q) \end{pmatrix} \tag{5.22}$$

Then, applying the law of propagation of the uncertainty, the following covariance matrix can be obtained:

$$\left[\boldsymbol{\Sigma}_{vi}\right] = \left[\frac{\partial \mathbf{f}_{vi}}{\partial \mathbf{x}_{vpq}}\right] \left[\boldsymbol{\Sigma}_{vpq}\right] \left[\frac{\partial \mathbf{f}_{vi}}{\partial \mathbf{x}_{vpq}}\right]^T \tag{5.23}$$

where $\mathbf{x}_{vpq}$ is the set of the variables V, P and Q, and the Jacobian involved in the matrix multiplication is:

$$\left[\frac{\partial \mathbf{f}_{vi}}{\partial \mathbf{x}_{vpq}}\right] = \begin{bmatrix} \frac{\partial V}{\partial V} & \frac{\partial V}{\partial P} & \frac{\partial V}{\partial Q} \\ \frac{\partial i^r}{\partial V} & \frac{\partial i^r}{\partial P} & \frac{\partial i^r}{\partial Q} \\ \frac{\partial i^x}{\partial V} & \frac{\partial i^r}{\partial P} & \frac{\partial i^x}{\partial Q} \end{bmatrix} = \begin{bmatrix} 1 & 0 & 0 \\ 0 & \cos\delta & \sin\delta \\ 0 & \sin\delta & -\cos\delta \end{bmatrix} \tag{5.24}$$

It is worth underlining that, since the covariance matrix $\mathbf{\Sigma}_{vpq}$ to be used in (5.23) is the full matrix obtained through (5.5), the final covariance matrix $\mathbf{\Sigma}_{vi}$ is a full matrix as well. Therefore, covariance terms arise, indicating the presence of resulting correlations among voltage magnitude, real and imaginary currents.

5.3 Analysis of correlation in PMUs

Similarly to the case of the multifunction meters, even when considering PMUs, it is reasonable to assume that measurements provided by different devices are independent. The focus is, thus, on the measurements provided by the same PMU. Fig. 5.2 provides an illustration of the general measurement scheme of a PMU, with the indication of the main blocks involved in the computation of the output synchrophasors. As described in [94], each one of these blocks is a source of uncertainty for the final synchrophasor measurement. In particular:

- *Transducers*: voltage and current transformers (VTs and CTs, respectively) are usually employed, whose uncertainty depends on their accuracy class, as defined in the standards [95] and [96]. Some PMUs provide the possibility to compensate the transducer errors. However, this would require a very accurate characterization of each single transducer, which could be impractical; moreover, the behaviour of the transducers depends on the operating and environmental conditions, thus, a total compensation of their errors is, in any case, impossible.

- *Synchronization system*: it allows the time synchronization to the UTC reference through the acquisition of the GPS signal; such synchronization is affected by a given uncertainty depending on the characteristics of the GPS receiver. It is worth noting that this uncertainty contribution plays an essential role in

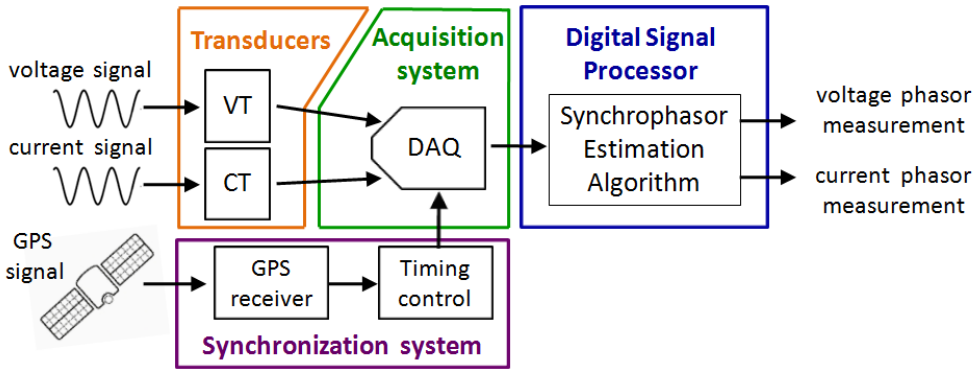

Figure 5.2: Uncertainty sources in the measurement scheme of a PMU

the final accuracy of the synchrophasor, since a time synchronization error is directly translated in a phase-angle error.

- *Acquisition system*: it includes both the analog signal conditioning and the analog to digital converters. Here, uncertainties arise because of noise, nonlinearity and gain errors in the signal conditioning and due to the quantization error in the analog to digital conversion.

- *Synchrophasor algorithm*: is the mathematical core of the PMU, that is the algorithm designed to estimate the synchrophasor by using the acquired signals of voltage and/or current and the time information coming from the previous stages. The uncertainty introduced in this step is highly dependent on the type of implemented algorithm and the characteristics of the input signal (presence of harmonics and/or interharmonics, frequency of the signal, etc.)

The uncertainty contributions coming from transducers, acquisition system and synchrophasor algorithm should be accurately characterized to find out if there are common errors affecting different signals. In general, correlations can arise from these stages, but their study would require a deep analysis (which should be specific for each single PMU) that it is out of the scope of this thesis. Instead, as for the uncertainty contribution associated to the synchronization system, the same component of error can be attributed to all the signals processed simultaneously by the PMU, since all the channels refer to the same time information provided by the timing controller. Consequently, in the following, the analysis will be focused on the correlations brought by the presence of this common component of time error.

5.3.1 Correlation factor between angle measurements

As aforementioned, the uncertainty coming from the synchronization system has a direct impact on the angle measurements, since time errors are directly translated into errors on the angle estimations. As a consequence, the magnitude measurements provided by the PMU can be still assumed as decorrelated, while correlations arise among the different angle measurements.

To evaluate the correlation between two generic angle measurements A and B, the previously described sources of uncertainty can be taken into account through the sum of the following three contributions:

$$\epsilon_A = \epsilon_{T_A} + \epsilon_{S_A} + \epsilon_{tb} \tag{5.25}$$

$$\epsilon_B = \epsilon_{T_B} + \epsilon_{S_B} + \epsilon_{tb} \tag{5.26}$$

where ϵ_A and ϵ_B are the angle deviations resulting in the two measurements A and B; ϵ_{T_i} $(i = A, B)$ is the effect of the transducer angle error (or of the residual uncertainty,

if a compensation of the transducer errors is performed); ϵ_{S_i} is the component of error associated to the elaboration of the signal inside the PMU (which comprises both the contribution related to the acquisition system and the effects brought by the particular synchrophasor estimation algorithm implemented in the digital processor); ϵ_{tb} is the common component of time base error, which is related to the achieved synchronization level.

Indicating with σ_{T_i}, σ_{S_i} and σ_{tb} the standard deviations associated to the three uncertainty contributions, and assuming all these components as decorrelated, the variance of each measurement can be expressed as:

$$\sigma_i^2 \triangleq E[\epsilon_i^2] = \sigma_{T_i}^2 + \sigma_{S_i}^2 + \sigma_{tb}^2 \tag{5.27}$$

As for the covariance, instead, since the time base error is the only common component, it is:

$$E[\epsilon_A \epsilon_B] = E[(\epsilon_{T_A} + \epsilon_{S_A} + \epsilon_{tb})(\epsilon_{T_B} + \epsilon_{S_B} + \epsilon_{tb})] = E[\epsilon_{tb}^2] = \sigma_{tb}^2 \tag{5.28}$$

Exploiting the knowledge of variance and covariance, it is possible to obtain the resulting correlation factor, which is:

$$\rho_{A,B} = \frac{E[\epsilon_A \epsilon_B]}{\sigma_A \sigma_B} = \frac{\sigma_{tb}^2}{\sqrt{\left(\sigma_{T_A}^2 + \sigma_{S_A}^2 + \sigma_{tb}^2\right)\left(\sigma_{T_B}^2 + \sigma_{S_B}^2 + \sigma_{tb}^2\right)}} \tag{5.29}$$

Equation (5.29) shows that the correlation factor depends on the ratio between the common component of uncertainty and the total ones. It is worth noting that all the contributions of uncertainty are generally indicated in the data sheets as maximum angle deviations, thus in degrees or radians. As a consequence, they are expressed in absolute values and do not depend on the particular measured quantity. As an example, in [96], the maximum angle deviation indicated for voltage transducers compliant with the 0.5-class accuracy is $5.8 \cdot 10^{-3}$ rad. Thus, for two different voltage angle measurements (for example referred to different phases of the node) it is: $\epsilon_{T_A} = \epsilon_{T_B} = \epsilon_T$. Assuming that also the system error inside the PMU has similar uncertainty properties for all the channels, then it would be: $\epsilon_{S_A} = \epsilon_{S_B} = \epsilon_S$. With these assumptions, (5.29) becomes:

$$\rho_{A,B} = \frac{\sigma_{tb}^2}{(\sigma_T^2 + \sigma_S^2 + \sigma_{tb}^2)} \tag{5.30}$$

In equation (5.30), the impact brought by the common component of uncertainty on the resulting correlation factor is clear.

Just as an example, the data sheets of a commercial PMU [53] have been used to assess the value of the correlation factor in a real scenario. In [53], it is possible to

find that the maximum deviation brought by the system error ϵ_S is equal to $0.03° = 0.52 \cdot 10^{-3}$ rad, while the maximum deviation associated to the time base error ϵ_{tb}, is 1 μs. Considering the period of an electrical quantity at the nominal frequency of 50 Hz, the time base deviation can be automatically translated in an angle deviation equal to $0.018° = 0.31 \cdot 10^{-3}$ rad. Finally, considering the standards [96] as reference for the voltage transducers, and taking into account the requirements provided for the 0.5-class accuracy, the maximum deviation of the transducer errors is assumed equal to $5.8 \cdot 10^{-3}$ rad. With these data, the resulting correlation factor between two voltage angle measurements is $\rho_{A,B} = 2.8 \cdot 10^{-3}$, which is a very low value. Looking at the considered deviations, it is clear that such result is strictly affected by the presence of the large uncertainty associated to the transducer. Just as an example, if the possibility to perfectly compensate the transducer error is supposed, then the resulting correlation factor is $\rho_{A,B} = 0.26$. Even in this case, the correlation factor is not particularly high, however, such value could be able to affect the accuracy performance of the DSSE algorithm. In the following, this result will be taken into account for the analysis of the impact of the PMU correlation on the DSSE accuracy.

5.3.2 Covariance matrix of PMU measurements

To include the correlations among the angle measurements simultaneously performed by a PMU in the WLS formulation, it is necessary to properly build the covariance matrix of the PMU measurement errors. This covariance matrix strictly depends on the way in which PMU measurements are introduced in the DSSE model. As an example, in [97], the covariance matrix has been obtained for a traditional voltage based estimator, where PMU measurements are included in polar coordinates for the voltages, and in rectangular coordinates for the current phasors.

In the BC-DSSE model proposed here, as described in Chapter 1, both voltage and current phasors can be conveniently included by using their rectangular coordinates. Considering this aspect, and indicating with y_A and y_B two generic phasors measured by the same PMU (can be either voltage or current phasors), whose magnitude and angle measurements are Y_i and α_i (with $i = A, B$) and the real and imaginary parts are y_i^r and y_i^x, respectively, the following vector $\mathbf{f}_{pmu}$ of the input measurements to the estimation algorithm can be defined:

$$\mathbf{f}_{pmu} = \begin{pmatrix} y_A^r\ (Y_A, \alpha_A) \\ y_A^x\ (Y_A, \alpha_A) \\ y_B^r\ (Y_B, \alpha_B) \\ y_B^x\ (Y_B, \alpha_B) \end{pmatrix} \tag{5.31}$$

Indicating with $\mathbf{x}_{pmu}$ the set of PMU measurements Y_i, α_i, and with σ_{Y_i} and σ_{α_i} the corresponding values of standard deviation, the covariance matrix $\mathbf{\Sigma}_{\mathbf{y_{pmu}}}$ of

the rectangular phasors can be obtained by applying the law of propagation of the uncertainty as follows:

$$\mathbf{\Sigma_{ypmu}} = \left[\frac{\partial \mathbf{f}_{pmu}}{\partial \mathbf{x}_{pmu}}\right] \begin{bmatrix} \sigma^2_{Y_A} & 0 & 0 & 0 \\ 0 & \sigma^2_{\alpha_A} & 0 & \rho\sigma_{\alpha_A}\sigma_{\alpha_B} \\ 0 & 0 & \sigma^2_{Y_B} & 0 \\ 0 & \rho\sigma_{\alpha_A}\sigma_{\alpha_B} & 0 & \sigma^2_{\alpha_B} \end{bmatrix} \left[\frac{\partial \mathbf{f}_{pmu}}{\partial \mathbf{x}_{pmu}}\right]^T \tag{5.32}$$

where ρ is the correlation factor between the angle measurements α_A and α_B and the Jacobian matrix, involving the derivatives of the vector $\mathbf{f}_{pmu}$ with respect to the set of PMU measurements $\mathbf{x}_{pmu}$, is:

$$\left[\frac{\partial \mathbf{f}_{pmu}}{\partial \mathbf{x}_{pmu}}\right] = \begin{bmatrix} \cos\alpha_A & -Y_A\sin\alpha_A & 0 & 0 \\ \sin\alpha_A & Y_A\cos\alpha_A & 0 & 0 \\ 0 & 0 & \cos\alpha_B & -Y_B\sin\alpha_B \\ 0 & 0 & \sin\alpha_B & Y_B\cos\alpha_B \end{bmatrix} \tag{5.33}$$

Making the matrix multiplication in equation (5.32), it is possible to observe that all the variances and the covariance terms related to the same phasor measurement (for example, the terms related to the correlation between y^r_A and y^x_A) are the same already obtained in Section 1.7.3 (Chapter 1) and they only depend on the conversion of the phasors in rectangular coordinates. However, in addition to these terms, also covariances between the rectangular components of different phasor measurements arise. In particular, it is possible to find:

$$\sigma_{y^r_A y^r_B} = y^x_A \; y^x_B \; \rho \; \sigma_{\alpha_A}\sigma_{\alpha_B} \tag{5.34}$$

$$\sigma_{y^r_A y^x_B} = -y^x_A \; y^r_B \; \rho \; \sigma_{\alpha_A}\sigma_{\alpha_B} \tag{5.35}$$

$$\sigma_{y^x_A y^r_B} = -y^r_A \; y^x_B \; \rho \; \sigma_{\alpha_A}\sigma_{\alpha_B} \tag{5.36}$$

$$\sigma_{y^x_A y^x_B} = y^r_A \; y^r_B \; \rho \; \sigma_{\alpha_A}\sigma_{\alpha_B} \tag{5.37}$$

where the subscripts of σ in the left term indicate the quantities involved in the covariance.

Obtained results clearly show that the resulting covariance matrix is full and that correlations arise among all the rectangular components of the different phasors. It is important to note that the found relationships are valid for each couple of phasors and, thus, the same covariance terms can be obtained also when considering more simultaneous phasor measurements. For example, in case of measurement of a three-phase voltage and a three-phase current, the found relationships have to be used to express all the covariances between each possible combination of the six phasor measurements.

5.4 Analysis of correlation in pseudo-measurements

Pseudo-measurements are a particular case of input data where the presence of correlation is highly possible [86–88,92,98]. Since the prior information on the power injections provides the largest number of input data for the DSSE, and since such information is in general poorly reliable, additional details associated to a correlated behaviour could be particularly useful to enhance the estimation results.

Different types of correlation can be detected in pseudo-measurements. A possible correlation is among the power consumptions at different nodes of the network; such correlation can arise, for example, because of load similarity or due to the weather conditions. In a smart grid scenario, operations carried out by the DSO (for instance, in a demand side management context) can provide an additional source of correlation. This kind of correlation can be quite high above all for the loads belonging to the same geographical area [87,88]. In a similar way, correlation can exist among the power injections at different generation nodes. As an example, it is easy to imagine the presence of high correlation degrees among generation plants of the same typology based on renewable energy sources. For instance, the power production of photovoltaic and wind plants is strongly dependent on the weather conditions: consequently, plants located in the same area can be expected to have a correlated behaviour during the day. Even in this case, management interventions performed by the DSO (like, for example, reactive generation control or active power curtailment for voltage control purposes) can play an additional role in correlating DG nodes. This type of correlation, which involves different nodes of the network, will be indicated in the following as "inter-node correlation". It is worth underlining that, in a three-phase context, the power injections on the different phases of the same node can be seen as injections at three different buses. As a result, the same considerations made for the inter-node correlation can be applied also to the case of power injections concerning the different phases of the same node.

Another kind of correlation that is likely to be present is between the active and the reactive power injected at the same node. This correlation can exist as a consequence of the degree of knowledge about the power factor of the injection and can be quite relevant. In some works, indeed, the power factor of the loads is assumed to be perfectly known [88]: in this case, the resulting correlation factor would be equal to ± 1 (one of the two powers could be also expressed in terms of the other one). In the following, this correlation will be referred to as "intra-node correlation".

The tests performed in the next Section take into account the possible presence of both inter-node and intra-node correlation. It is worth noting that, when these two types of correlation are simultaneously present, also cross-correlation factors arise. As an example, if the active power consumptions of two loads are correlated, and the

active and reactive powers of each node are also related, then spurious correlation arises between the active power of one node and the reactive power of the other one. This aspect has to be carefully considered in the design of the covariance matrix. In the following tests, spurious correlations are computed through the multiplication of the different factors involved in the cross-correlation.

5.5 Tests and results

5.5.1 Test assumptions

Several tests have been performed on the 95-bus network (already used in the previous chapters, but reported again in Fig. 5.3 [1] for the sake of convenience) to analyze the impact deriving from the inclusion of possible correlations in the DSSE model. Tests refer to the equivalent single-phase model of the 95-bus network, in order to make easier the evaluation of the correlation impact and to obtain a clearer presentation of the results. However, as highlighted in previous sections, correlations can arise also between electrical quantities belonging to different phases. In particular, both PMU angle measurements and active power pseudo-measurements can introduce a given degree of correlation among quantities related to different phases. As pointed out in the analysis, the way to deal with these correlations is exactly the same to be used for the correlations between quantities belonging to the same phase. Thus, the same considerations and effects highlighted through the single-phase model can be reasonably extended also to the three-phase scenario.

Tests have been performed by using a Monte Carlo approach with a number of trials $N_{MC} = 50000$. In the simulations, first of all, true reference operating conditions are computed by means of a power flow calculation. Then, for each Monte Carlo trial, measurements are extracted through the addition of random errors to the reference values. It is important to underline that here, differently from the tests performed in the other chapters, the generation of the random errors has to duly consider, besides the assumed uncertainty for the considered quantities, also the assumed correlations. The following assumptions have been used in all the performed tests:

- pseudo-measurements are considered to be available on all the load and generation nodes of the network with an expanded uncertainty (three times the standard deviation of a Gaussian distribution) equal to 50%;
- real-time measurements are assumed to be random variables with a standard deviation equal to one third of their accuracy value.

[1] As for the numeration of the branches, each branch index is given by the node number of its end node (the largest one), decreased by one.

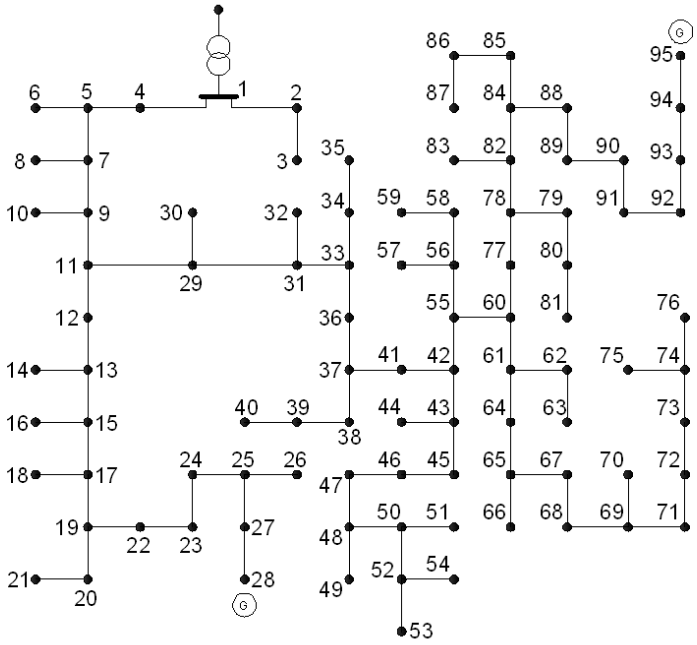

Figure 5.3: 95-bus test network

For each kind of correlation, several tests have been performed using different measurement configurations. In the presented results, however, a reference measurement configuration is used, which is composed of four measurement points at nodes 1, 11, 37 and 60. Each measurement point is assumed to have a device able to measure the voltage at the node (the magnitude or the phasor depending on the use of conventional meters or PMUs, respectively) and the flows in two of the branches connected to the considered bus (the current magnitude or the active and reactive power in case of traditional measurement devices or the current phasors in case of PMUs). Table 5.1 shows the overall set of real-time measurements considered in the reference measurement scenario. As for the assumed correlations, different assumptions are made depending on the specific test. Therefore, details on this aspect will be provided separately for each test.

Once extracted, the measurements are provided as input to two different estimators. In the first one, the DSSE algorithm is designed with the traditional

Table 5.1: Measurement point positions

Nodes	1	11	37	60
Branches	1 (1-2)	11 (11-12)	36 (37-36)	60 (60-61)
(Start-End node)	3 (1-4)	28 (11-29)	40 (37-41)	76 (60-77)

assumption of having independent measurements: thus, the covariance matrix of the measurement errors, and the consequent weighting matrix, do not include the correlations. In the second one, instead, correlations are duly considered in the covariance matrix of the measurement errors and, in this way, are introduced in the DSSE model. Results provided by the two different estimators are finally compared to assess the impact brought by the proper modeling of the correlations in the DSSE model. To this purpose, the accuracy results of the different estimation algorithms are evaluated by comparing the expanded uncertainties (with a coverage factor equal to three) of voltage and current estimations. In some tests, if the results do not require a detailed plot of the estimations at each node or branch, an overall index for the whole network is used, that is the mean of the expanded uncertainties (with a coverage factor equal to three) through all the nodes or branches of the network (depending on the considered quantity).

5.5.2 Impact of multifunction meter correlation

As shown in Section 5.2, the covariance terms and correlation factors arising in the output measurements of a multifunction meter are strictly dependent on the values of the measured quantities. Thus, it is not possible to simply define a specific value of the correlation factor to be used in the simulations. The tests are hence performed referring to the real behaviour of these meters. Starting from the true values of voltage and current in the considered measurement point, the corresponding measurements are extracted and then used to compute the resulting outputs of voltage and active and reactive power. Accuracies equal to 1% and $5.8 \cdot 10^{-3}$ rad have been assumed for the magnitude and angle measurements of both voltage and current, respectively, thus considering a main error contribution coming from the transducers. The procedure described in Section 5.2, based on the law of propagation of the uncertainty, is then used for the computation of the covariance matrix of the multifunction meter measurement errors. Finally, the corresponding weighting submatrix to be included in the DSSE model is obtained through the inversion of the above mentioned covariance matrix.

A first test has been performed considering the multifunction meters placed in the measurement points indicated in Section 5.5.1. As previously claimed, correlation factors arising in each multifunction meter can be highly variable, depending on the size of the measured quantities. Table 5.2 shows, as an example, the correlation factors among the measurement errors for the multifunction meter placed in node 1. It is possible to observe that correlation varies from low values (0.10 for the correlation factor between the active power P_3 in branch 3 and the reactive power Q_1 in branch 1) to quite high factors (0.71 for the correlation between voltage V_1 and active power P_1).

Performed test shows that considering the presence of the correlations in the

Table 5.2: Matrix of the correlation factors among the measurement errors of the multifunction meter at node 1

	V_1	P_1	Q_1	P_3	Q_3
V_1	1.00	0.71	0.21	0.62	0.61
P_1	0.71	1.00	0.20	0.46	0.40
Q_1	0.21	0.20	1.00	-0.10	0.38
P_3	0.62	0.46	-0.10	1.00	0.50
Q_3	0.61	0.40	0.38	0.50	1.00

DSSE model allows achieving better accuracy performance of the estimator. Table 5.3 shows the results of mean expanded uncertainty for both voltages and currents. It is possible to observe that slight improvements are present for the estimations of all the electrical quantities. However, a different impact is obtained for the different quantities. In fact, for the voltage estimations, the benefits coming from the introduction of the correlations in the DSSE model are basically spread among all the nodes. Fig. 5.4 shows, as an example, the results obtained for the expanded uncertainty of the voltage magnitude: it is clear that all the nodes exhibit an improved estimation when considering the correlations in the estimator model. In the case of the branch currents, instead, the effects brought by the correlation are mainly local and focused on the branches close to the measurement points. As a consequence, several branches are practically not affected by the considered correlation, while other branches (close the multifunction meters) show a more evident impact (as an example, in the considered scenario, the expanded uncertainty for the current magnitude in branch 7 decreases from 42.8% to 40.9%).

Similar results have been obtained also considering different measurement placements. In general, therefore, it is possible to say that proper consideration of the multifunction meter correlation can be useful to slightly enhance the accuracy performance of the DSSE. The impact of such correlations is usually not too large; however,

Table 5.3: Impact of multifunction meter correlation on the mean of the expanded uncertainty of voltage and current estimations

Model	Current magnitude [%]	Current angle [crad]	Voltage magnitude [%]	Voltage angle [crad]
no corr. in weights	22.66	6.79	0.51	$1.9 \cdot 10^{-2}$
with corr. in weights	22.54	6.76	0.50	$1.8 \cdot 10^{-2}$

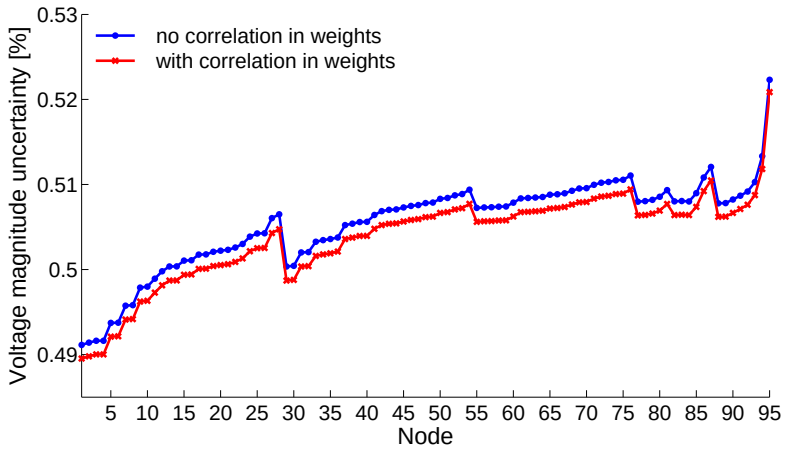

Figure 5.4: Expanded uncertainty of voltage magnitude estimation with multifunction meter correlation

all the electrical quantities can achieve some benefits from the correct consideration of these correlations in the modeling of the measurement errors.

5.5.3 Impact of PMU correlation

In Section 5.3, it has been shown that possible correlations can arise among the different angle measurements provided by a PMU, due to the presence of a common component of error associated to the time synchronization. In the most general cases, the resulting correlation factors are almost negligible because of the presence of a larger uncertainty contribution brought by the transducers. However, if an accurate compensation of the transducer errors is performed (it is worth noting that a perfect compensation is actually not possible), then the correlation factors rise up to more significant values.

In this subsection, taking into account the results found in Section 5.3, some tests have been performed by considering a correlation factor ρ equal to 0.26 among all the angle measurements provided by each PMU. The accuracies are assumed equal to 0.7% and 0.7 crad for the magnitude and angle measurements, respectively, in order to obtain a maximum TVE of 1% as prescribed by the standard of synchrophasors [51] for the tests in steady-state conditions. The measurement placement described in Section 5.5.1 has been adopted in the tests. Results show that, in this scenario, proper consideration of the PMU correlation in the DSSE model brings only very small enhancements on the accuracy performance of the estimator. In fact, almost the same estimation uncertainties have been obtained both neglecting and considering the correlations in the estimator. The same kind of results can be obtained also considering different placements for the PMUs. The possible reasons for such a very small impact can be both the low value of correlation and the

Table 5.4: Impact of PMU correlation on the mean of the expanded uncertainty of voltage and current estimations

Model	Current magnitude [%]	Current angle [crad]	Voltage magnitude [%]	Voltage angle [crad]
no corr. in weights	22.42	6.70	0.36	$1.4 \cdot 10^{-2}$
with corr. in weights	22.36	6.62	0.36	$1.3 \cdot 10^{-2}$

simultaneous high accuracy of the PMU measurements. Indeed, in this situation, the additional information associated to the measurement correlations can be not so valuable to further improve the already good estimations determined by the highly accurate PMU measurements.

To further investigate this aspect, additional tests have been carried out by raising the correlation factors up to 0.9. Table 5.4 shows the consequent results for the mean expanded uncertainty of both voltage and current estimations. It is possible to note that, in this case, thanks to the presence of very large correlation factors, some slight improvements on the estimation accuracy can be observed, in particular for the currents. In fact, similarly to the case of multifunction meters, the large correlation allows refining the estimation accuracy for the branches closest to the measurement points. As an example, in this case, when PMU correlations are duly considered, the uncertainty of the current magnitude estimation in branch 7 goes from 39.5% to 37.4%. Similar results and similar considerations can be achieved also when considering different measurement configurations. In general, thus, it is possible to say that the impact brought by the PMU measurement correlations in realistic scenarios is usually limited; however, if additional sources of correlation are present and the correlation factors rise up to larger values, then some more significant enhancement can be achieved, in particular on the current estimations of the branches closest to the measurement points.

5.5.4 Impact of pseudo-measurement correlation

As described in Section 5.4, two different types of correlation can be defined for the pseudo-measurements. The first one is an inter-node correlation, that is a correlation among the power consumptions (or generations) at different nodes. The second one is an intra-node correlation, that is the correlation between the active and reactive power injection at the same bus. In this section, tests have been performed to highlight the possible effects coming from the proper consideration of these correlations

in the measurement model of the DSSE. At the beginning, several tests have been performed by considering separately inter-node and intra-node correlations, in order to point out the impact brought by each one of them. Then, the overall impact deriving from the simultaneous presence of both the types of correlation has been investigated.

Simulations have been carried out considering the presence of multifunction meters, PMUs or voltage and current magnitude measurements in the monitored points indicated in Table 5.1. To avoid the superimposition of the effects brought by the real-time measurement correlations, both the multifunction meter and the PMU measurements are assumed as decorrelated. In particular, accuracies of 1% and 3% have been assumed for the voltage magnitude and the active and reactive power measurements provided by the multifunction meters, respectively, while accuracies of 0.7% and 0.7 crad have been assumed for the magnitude and angle measurements provided by the PMUs. In case of voltage and current magnitude measurements, instead, the assumed accuracy is 1% for both the measurements.

Inter-node correlation

The first test has been performed by taking into account a strong inter-node correlation between the generation nodes (correlation factor equal to 0.9) and among the active power consumptions at nodes 3, 21, 53 and 76 (correlation factor equal to 0.8). Figures 5.5 and 5.6 show the results for the expanded uncertainty of the current magnitude and angle estimations, respectively, when considering multifunction meters in the measurement points. It is possible to observe that the inclusion of the correlations in the weighting matrix of the DSSE model clearly leads to significant benefits on the estimation results. In particular, assumed correlations prove to be useful for enhancing the current estimation in the branches close to the correlated nodes. As an example, in branches 19 and 20, which are adjacent to the correlated load in node 21, the uncertainty of the current magnitude estimation decreases from 48.8% to 28.8% when correlations are duly considered. In the same way, with a proper measurement error modeling, branch 27 is able to exploit the correlation between the generators for reducing the estimation uncertainty of its current magnitude from 32.2% to 20.8%. Similar considerations also hold for the current angle estimations: for instance, in branch 27, the estimation improvement is equal to almost 6 crad.

The particular choice of the measurement placement and of the correlated nodes also highlights that the impact is not always the same in all the branches adjacent to the correlated nodes. For example, it is worth noting that branches 1 and 2 (which connect the substation bus to the correlated node 3) do not exhibit any enhancement on the estimation accuracy, despite the presence of the near correlated bus. The reason in this case is due to the presence of a very close measurement point (in substation): in this situation, the currents in branches 1 and 2 are already

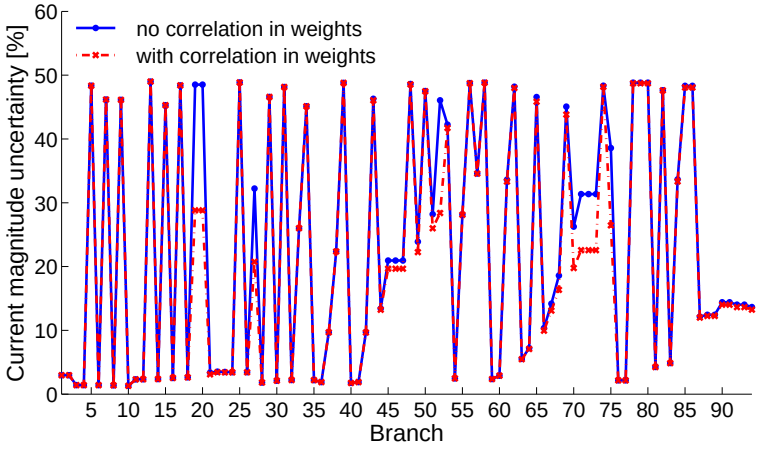

Figure 5.5: Expanded uncertainty of current magnitude estimation with inter-node correlation in nodes 3, 21, 53 and 76

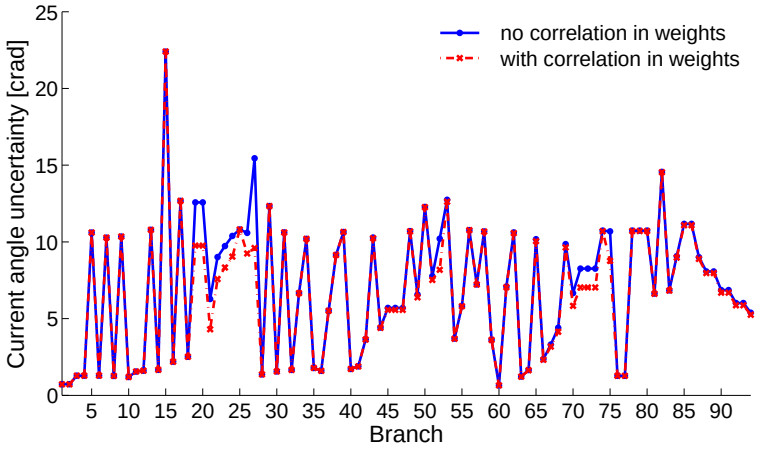

Figure 5.6: Expanded uncertainty of current angle estimation with inter-node correlation in nodes 3, 21, 53 and 76

accurately estimated (because of the power measurements in branch 1) and, thus, the additional contribution brought by the load correlation does not further improve the estimation accuracy. More in general, it is worth noting that the effects of the considered correlations are mainly on the current estimations of the lateral branches. Such estimations are generally characterized by very large relative uncertainties, but usually refer to small size currents. For this reason (taking also into account the impact of the current estimations on the resulting voltage profile, as described in Chapter 4), the benefits on the voltage estimations are less evident and, in general, are mainly focused on few nodes.

Very similar results have been obtained even when considering PMUs or voltage

and current magnitude measurements in place of the multifunction meters. Thus, obtained results are not dependent on the particular type of real-time measurements deployed on the network. In general, this first test shows that inter-node correlations can be particularly useful for enhancing the estimation accuracy of those currents that cannot be accurately estimated due to the lack of a close measurement point. This is a very important result for two reasons. From one hand, this implies that the knowledge of the correlations is able to refine the poorly accurate information included in the pseudo-measurements. On the other hand, the presence of large effects in the unmonitored areas can be a significant benefit in the distribution system scenario, since several areas can be totally unobserved due to the limited deployment of measurement instruments.

Additional tests have been performed to confirm the results obtained in the previous test. Following the assumptions used in [88], different groups of correlated loads have been identified in order to simulate the presence of correlation among the loads belonging to the same geographical area. In particular, four correlated zones have been considered:

- zone A: loads included between nodes 12 and 27;
- zone B: loads included between nodes 38 and 54;
- zone C: loads included between nodes 62 and 76;
- zone D: loads included between nodes 81 and 94.

In each area, a correlation factor equal to 0.8 has been assumed among the active power consumptions of the loads. Moreover, the correlation between the generation nodes (with correlation factor equal to 0.9) has been always assumed to be present.

A series of tests has been carried out considering the presence of correlation in only one of the aforementioned correlated areas. Fig. 5.7 shows, as an example, the results obtained for the current magnitude estimation when considering the inter-node correlation in zone A (in case of PMU measurement points). It is possible to observe that, in the branches corresponding to the correlated area, a significant enhancement of the estimation results has been obtained by including the correlations in the estimator model. In particular, estimations are significantly refined in all the lateral branches, where the uncertainty has been reduced to values around 30% (with respect to uncertainties very close to 50% when correlations are not taken into account). Moreover, thanks to the correlation among all the loads of the area (and the consequent enhancement of all the lateral branch current estimations), an evident impact has been found even for the branch currents of the feeder: for example, in branch 21 the estimation uncertainty decreases from 2.8% to 1.9%. Similar considerations also hold for the current angle estimations and for the cases of different measurement instruments installed on the network.

The local impact of the correlations is confirmed also by the other simulations performed with only one group of correlated loads. Fig. 5.8 shows, instead, the

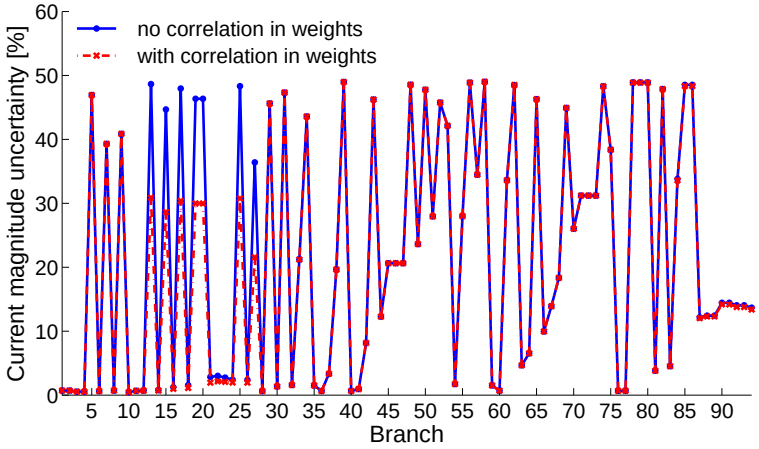

Figure 5.7: Expanded uncertainty of current magnitude estimation with inter-node correlation in zone A

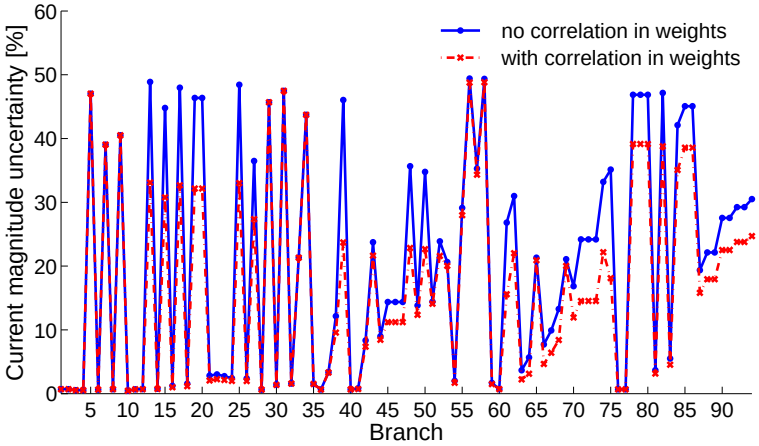

Figure 5.8: Expanded uncertainty of current magnitude estimation with inter-node correlation in all the zones

results obtained when the load correlations are assumed for all the aforementioned zones. In this case, as it can be expected, the results combine the local impacts brought by the correlations of each area. As a consequence, the improvement in the current estimations can be seen for a larger number of branches. Basically, however, the same considerations highlighted for the previous scenarios still hold.

Intra-node correlation

The following test aims at assessing the impact of the intra-node correlation. To this purpose, a correlation factor equal to 0.8 has been assumed between the active and the reactive power injection of each load. Results of this test show a different

impact depending on the type of measurement devices used in the network. In fact, the introduction of the intra-node correlations brings additional information about the power factor of the loads. The main effects are hence on the current angle estimations and, as a consequence, this knowledge is particularly useful when other information on the phase-angles is missing. As a confirmation, Figs. 5.9 and 5.10 show the different results obtained for the current angle estimations when considering voltage and current magnitude measurements, or when PMUs are used. It is possible to observe that, in the first case, since both the voltage and current measurements do not provide any kind of information about the phase-angles, the inclusion of the intra-node correlation in the estimator model allows significantly

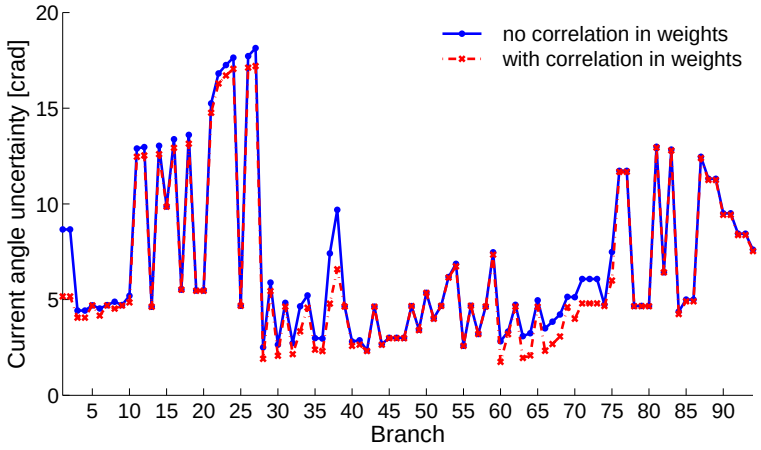

Figure 5.9: Expanded uncertainty of current angle estimation with intra-node correlation in case of voltage and current magnitude measurements

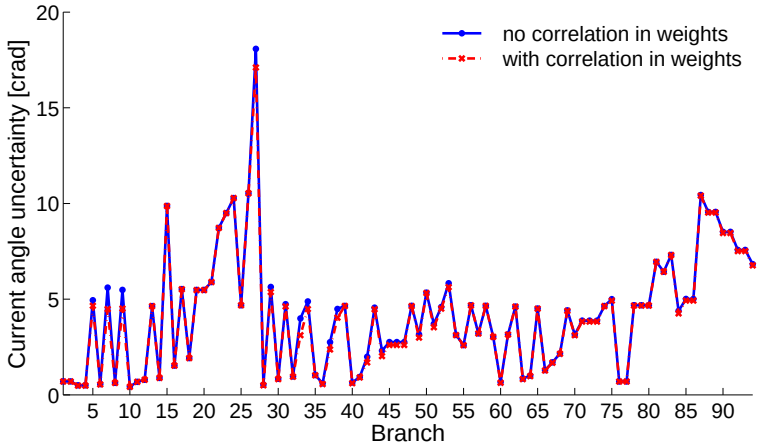

Figure 5.10: Expanded uncertainty of current angle estimation with intra-node correlation in case of PMU measurements

enhancing the current angle estimations for several branches. In particular, it is worth noting that the improvements are mainly concentrated on the branches close to the measurement points: this demonstrates that the intra-node correlation allows integrating the information coming from the measurement devices. Instead, when PMU measurements are considered, since both voltage and current phasors already have highly accurate information on the phase-angles, the additional contribution brought by the intra-node correlation allows only slight improvements on the current angle knowledge. In case of multifunction meters, basically the same considerations made for the PMUs hold, since the simultaneous measurements of active and reactive power allows achieving a good knowledge on the phase-angles of the electrical quantities.

Inter-node and intra-node correlation

Another series of tests has been performed to evaluate the impact brought by the simultaneous presence of both inter-node and intra-node correlation. In the presented test, inter-node correlations have been assumed among the loads of all the previously identified areas (with a correlation factor equal to 0.8) and between the generators in nodes 28 and 95 (with correlation factor equal to 0.9). Moreover, intra-node correlation between the active and the reactive power injection of each load (with correlation factor equal to 0.8) has been considered. It is worth recalling that in this case, besides the assumed correlations, even indirect correlations arise (for example between the active and the reactive power of different loads interested by inter-node correlation), thus leading to a larger number of variable correlations. Test results show a cumulative effect of the two kinds of correlation. As a consequence, in the current magnitude estimations, the proper modeling of the correlations in the DSSE basically leads to the same results highlighted in the inter-node correlation tests (since the intra-node correlation has practically no impact on the current magnitude estimations). Instead, in the case of current angle estimations, different results can be observed, because of the different effects obtained by using different measurement instruments. In Fig. 5.11, as an example, the results obtained when considering voltage and current magnitude measurements are shown. It is possible to note that, in this case, the overall impact obtained by properly considering the correlations in the estimator model is quite large, since both the inter-node and the intra-node correlation bring significant benefits to the estimation accuracy. As additional consideration, it is also worth noting that, in such a scenario, the large improvements achievable on the current estimations are also reflected on the voltage estimations. Fig. 5.12 shows, for example, the uncertainty resulting for the voltage magnitude estimation: it is possible to see that, in this case, proper consideration of the input data correlations in the measurement model of the DSSE leads to clear improvements for several nodes.

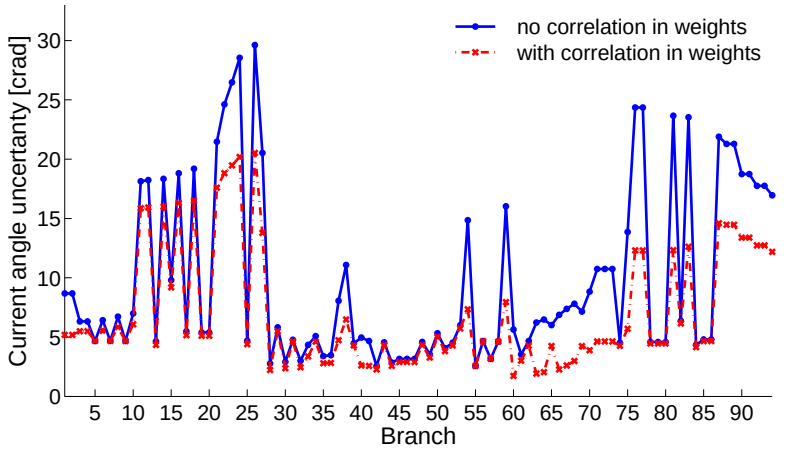

Figure 5.11: Expanded uncertainty of current angle estimation with inter and intra-node correlation in case of voltage and current magnitude measurements

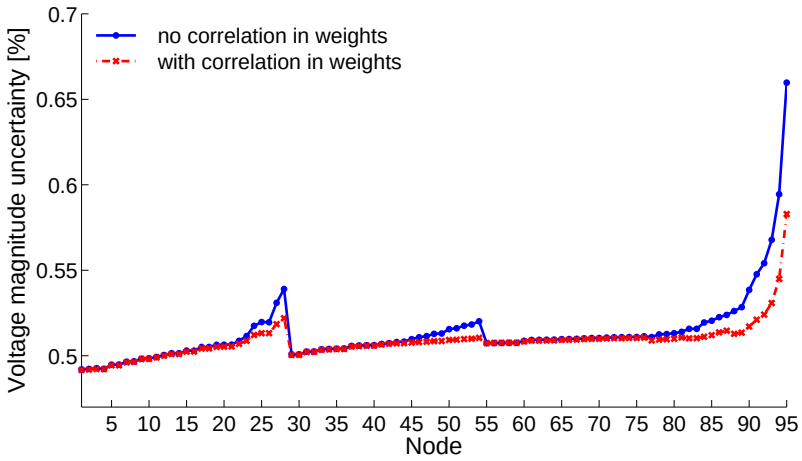

Figure 5.12: Expanded uncertainty of voltage magnitude estimation with inter and intra-node correlation in case of voltage and current magnitude measurements

As further analysis, additional tests have been carried out to assess the impact of different levels of correlation. To this purpose, the assumptions considered in the previous test have been assumed as reference and correlation factors have been proportionally reduced with respect to the values used in that scenario. As it can be expected, the enhancements deriving from the proper inclusion of the correlations in the DSSE model are strongly related to the correlation factor values. Table 5.5 shows, as an example, the improvements achievable on the current magnitude estimation of some branches when assuming different levels of correlation. Obviously, increasing values of correlation factors lead to larger improvements. Moreover, it is

also worth noting that the impact is nonlinear, even because of the presence of spurious correlations. Thus, increasing values of correlation factors lead to more and more important improvements on the accuracy of the estimation results.

Table 5.5: Impact of different levels of correlation

Correlation level	Expanded uncertainty improvement [%]		
	Branch 25	Branch 39	Branch 75
25%	1.7	5.7	5.1
50%	6.8	15.4	14.7
75%	16.2	29.4	28.0
100%	33.0	48.4	46.7

Effects of possible mismatch in correlation values

In this subsection, additional tests have been performed to analyze the impact of a possible mismatch in the knowledge of the correlation factors. In fact, until now, all the tests have been performed by considering the presence of a given correlation among the pseudo-measurements and assessing the benefits coming from the proper inclusion of such correlation in the DSSE model. In practical scenarios, however, the exact knowledge of the correlation values is unrealistic. Thus, tests performed here aim at assessing the impact brought by the inclusion of a non-perfectly matching value of correlation in the measurement model of the estimator.

To this purpose, some tests have been carried out by considering: an inter-node correlation (with correlation factor equal to 0.6) in all the four zones previously defined for the inter-node correlation tests; an inter-node correlation (correlation factor equal to 0.675) between the active power injected by the generators in nodes 28 and 95; an intra-node correlation (correlation factor equal to 0.6) between the active and reactive powers of each load injection. Obviously, the indirect correlations arising in this context have also to be taken into account. The choice of these correlation values allows assessing the effects deriving from the consideration in the DSSE model of both underestimated and overestimated correlations. Starting from this reference scenario, in fact, tests have been performed using the above mentioned correlations for the measurement extractions, but introducing in the estimator model correlation factors ranging from 1/4 to 5/4 of the actual values. In this way, the effect of possible errors in the knowledge of the correlations can be evaluated.

Test results clearly show that, even when considering a not perfectly matched value of correlation factor in the DSSE, significant benefits on the estimation accuracy can be still achieved. As an example, Fig. 5.13 reports the results obtained for

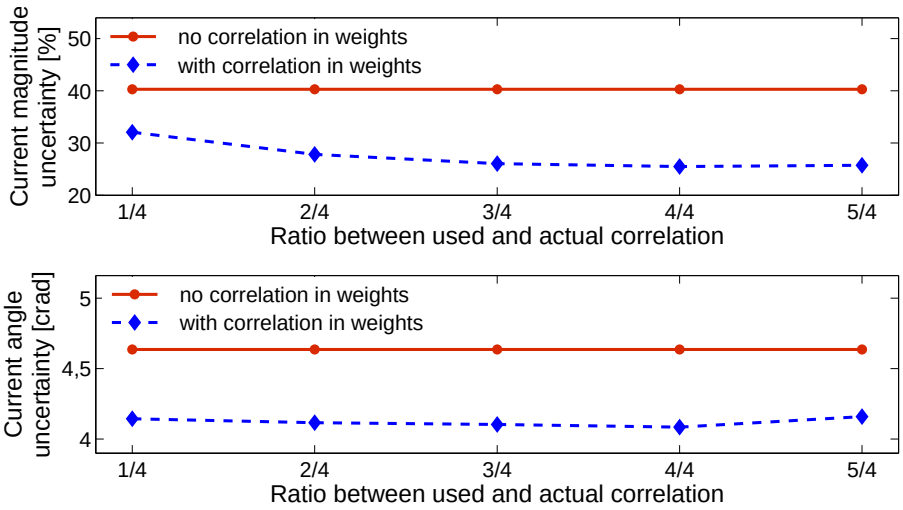

Figure 5.13: Expanded uncertainty of current magnitude and angle estimation in branch 45 in presence of correlation mismatch

the current estimation in branch 45 when considering voltage and current magnitude measurements in the network. It is possible to observe that, obviously, the largest improvements are obtained considering a perfect knowledge of the correlation factor. Nevertheless, even when the correlation factors introduced in the DSSE model are significantly different from the actual ones, large enhancement on the estimation accuracy can be still obtained. For example, in this case, the uncertainty of the current magnitude estimation decreases from more than 40% to around 25% by considering the proper correlation factors. However, also when the correlations considered in the DSSE are halved, the current magnitude uncertainty can be still reduced to a value lower than 28%. Similar considerations hold also for the current angle estimations and for the results found in the other branches of the network. Such results have been also confirmed by considering different measurement configurations (with different meter placement) in the network. Thus, it is possible to conclude that a proper inclusion of pseudo-measurement correlations in the model allows enhancing the accuracy of the DSSE results and can provide important benefits even when correlation values are not perfectly known.

5.6 Final discussion

This Chapter shows the importance of a proper measurement modeling for achieving an enhanced estimation of the electrical quantities of the network. In particular, the possible correlations existing among the measurements provided as input to the DSSE algorithm can represent an important, additional source of information when

only a limited number of measurement instruments is available on the field. The developed analysis shows that, differently from the common assumptions used in SE, correlations can exist among the real-time measurements provided by the same device. Moreover, in the distribution system scenario, additional correlations are highly possible among the pseudo-measurements. For instance, loads with similar behaviour or generation plants based on renewable energy sources are likely to have a strong correlation in their power injections.

Performed tests show that the proper consideration of these correlations in the modeling of the measurement errors allows improving the accuracy of the DSSE results. However, a different impact is obtained when considering the correlation of real-time measurements and pseudo-measurements. In the first case, correlations arising both in multifunction meters and in PMUs, if suitably considered in the DSSE model, can provide some advantages, above all in the estimation of the branch currents closest to the considered measurements. However, these advantages are usually not very strong. As a consequence, the possible use of these correlations should be carefully assessed, even considering that their use implies an increase of the computational burden, with the consequent effects on the estimator efficiency. In case of pseudo-measurements, instead, the benefits provided by the proper implementation of the correlations in the measurement model of the DSSE are significant. In particular, large improvements can be achieved for all the branch currents close to the correlated nodes. Consequently, such correlation, when present, is a valuable information that should be duly exploited, since it allows improving the knowledge about the pseudo-measurements and, in this way, it leads to enhanced estimations even in those unmonitored areas of the network that cannot rely on any close measurement device.

In a realistic environment, the pseudo-measurement correlations could be obtained from historical data, from the knowledge on the loads or generators behaviour, or also from the results of the run-time estimations. As a consequence, it is important to note that the correlation degrees are, in general, not perfectly known. Nevertheless, performed tests show that, even if the assumed correlations do not perfectly match the actual ones, their introduction in the DSSE model still allows obtaining significant advantages. Such a result proves that benefits related to the use of the pseudo-measurement correlations can be achieved also in practical scenarios.

Chapter 6

Multi-area DSSE

6.1 Multi-area state estimation

One of the most important issues in distribution systems is the size of these networks. As already described in Chapter 1, the high number of nodes, together with the need to consider the three-phase model of the grid, significantly affects the estimator efficiency, leading to long computation times for the solution of the DSSE problem. This aspect is particularly critical, above all considering that actual distribution grids need to deal with an increasing penetration of renewable sources, which are highly intermittent and characterized by a quickly variable behaviour. In this context, in fact, the real-time management and control of the network (and thus also the execution of the DSSE) should be performed with high reporting rates, in order to make the detection of fast dynamics affecting the network possible. Thus the development of an efficient and fast DSSE is essential. Moreover, additional issues can also arise, as for the communication system or for the storage requirements, because of the large amount of data to be managed.

A possible way to tackle this problem can be the employment of scalable solutions by means of a multi-area partition of the network. It is worth noting that multi-area techniques have been also proposed to enable wide-area management and control in transmission systems. However, the objectives pursued at the transmission and distribution side are different. In transmission systems, the goal is basically to aggregate state estimations performed on different sub-networks, usually managed by different Transmission System Operators, in order to have integrated data on a wide area. In distribution systems, instead, the aim is to decompose the DSSE problem in order to have smaller systems to be handled. In this way, storage and communication requirements could be distributed in the system and the DSSE process can be performed on smaller networks, allowing the reduction of the overall execution times. It is also worth highlighting that distribution systems include grids operated

at different voltage levels: then, a multi-area solution can be useful also to handle, separately, networks with different technical features.

Despite the large number of works dealing with the Multi-Area State Estimation (MASE) issue in transmission systems, the possibility to employ a similar solution also at the distribution level has not been deeply investigated so far. Several issues prevent an easy implementation of the multi-area approach in distribution systems. The main problem is given by the limited number of measurement instruments installed on the field. As an example, the possibility to split the grid in reduced areas can be strictly conditioned by the availability of measurements allowing the observability, or a minimum redundancy, for each sub-network. Thus, the design of the multi-area partition has to duly consider the configuration of the actual measurement system, or, in a perspective of measurement system upgrade, the choice of the meter placement. Another severe issue is that, because of the low number of real measurements, an important deterioration of the DSSE accuracy performance can arise by using multi-area approaches. To this purpose, suitable procedures could be used to integrate the results of the local estimations in order to increase the overall accuracy of the DSSE. Several solutions have been proposed, for the same purposes, for transmission systems. Thus, some of these methods could be adapted for being used in a distribution scenario, or, alternatively, techniques specifically designed for the distribution systems should be conceived. From this point of view, it is important to underline that different solutions could provide different effects both on the resulting accuracy performance and on the communication requirements. Both these aspects should be duly taken account for the development of a multi-area approach well suited to the distribution systems.

In general, for the proper design of a multi-area scheme, it is clear that a reasonable trade-off among the contrasting features of accuracy, efficiency, and communication and storage requirements has to be found. In the next subsection, some different ways to approach the MASE problem are shown in order to highlight strengths and weaknesses of each method. Then, in the following, a proposal specifically conceived for the distribution networks, taking into account the peculiarities of these systems, is presented and tested.

6.2 Multi-area approaches

Several MASE approaches are available in the literature, usually conceived for the transmission system scenario. The different proposals can be classified according to several criteria, like, for example: the level of area overlapping, the timing of the estimation processes, the used computing architecture or the adopted solution methodology [99]. The knowledge of pros and cons of the alternative solutions within each category can be useful to identify the types of approach more suited to

the features and requirements of the distribution networks.

6.2.1 Level of area overlapping

The possible approaches to the MASE problem can be discerned depending on the way in which the network is partitioned. The typologies of multi-area partition can be basically classified in three main groups: no overlapping, minimum overlapping and extended overlapping. Fig. 6.1 shows a schematic overview of the different criteria.

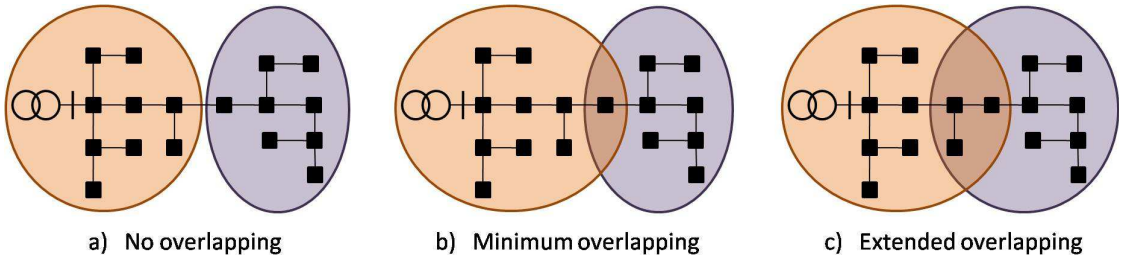

Figure 6.1: Main types of multi-area partition

The partition without any overlapping implies a decomposition of the network where no buses are shared between different areas. In this case each node belongs to only one sub-network and the size of each area is minimized. In transmission systems, since the state vector of the conventional estimators is usually composed of the voltages at the nodes, such a solution leads to independent local estimations for the different sub-networks. The refinement of the SE accuracy of each area is usually obtained by including the border information of the neighboring areas (the voltage estimations at the border nodes and/or the powers at the branches connecting the considered area to the adjacent ones) in specifically designed integration procedures. As an example, in [100], independent local estimations are performed at the first step of the MASE algorithm. Then, the voltage estimations at the border buses and the power measurements at the tie-lines connecting the different areas are included in a second step to obtain consistent results among the areas. In [101], instead, information related to the border buses is considered at each iteration of the MASE process in order to improve the accuracy of the estimation results. Other MASE approaches using a multi-area partition with no overlapping can be found, for example, in [102, 103].

In the solution with minimum overlapping, instead, one node is shared between adjacent areas. This allows also sharing some measurements between the local SEs of adjoining areas. Moreover, such partition leads to the presence of more voltage estimations, brought by the overlapped sub-networks, on the common buses. The

different voltage estimations on the shared nodes can be duly exploited to refine the SE results. For example, in [104], the MASE problem is tackled through an optimization technique, where the different voltage estimations on the shared node (given by adjacent areas) are handled by means of an equality constraint. For the solution of the optimization problem, each local SE updates the information about the shared node voltage estimation coming from the adjacent areas at each iteration of the estimation process. Similarly, in [105], the local SEs involve the voltage state of a shared bus; even in this case, the information about this voltage estimation is exchanged between the neighboring areas at each iteration of the MASE process in order to achieve consistent and enhanced results.

In a multi-area decomposition with extended overlapping, more nodes are shared between different areas. In this case, hence, the amount of measurements and node voltage estimations shared between different areas is larger than the previous schemes. This option can provide some benefits for the integration of the local SE results, but also implies a larger size for the sub-networks, with a possible impact on the MASE efficiency (in terms of overall execution times). Examples of MASE approaches relying on extended overlapping partitions can be found in [106, 107]. In [107], for instance, the partition is performed detecting independent areas separated by connecting tie-lines; however, each local SE includes in its state vector also the voltage variables of all the border nodes belonging to the adjoining areas.

In distribution systems, as aforementioned, it is important to remark that the choice of the network partition is significantly affected by the available configuration of the measurement system. In particular, due to the low number of measurement devices deployed on the field, it is essential to pay due attention to possible observability problems and to the achievement of minimum redundancy levels depending on the desired targets of robustness for the MASE.

6.2.2 Timing of the estimation processes

The timing used for the execution of the local SE in each area of the network is an essential element characterizing the MASE approaches. In transmission systems, usually, all the proposals refer to a parallel running of the local estimations. However, in general, as indicated also in [108], two different options are possible: in series or in parallel estimation of the areas. Fig. 6.2 shows a schematic overview of the two possible alternatives.

In the series implementation of the MASE, local SEs are performed sequentially and each area exploits the estimation results provided by the neighboring upstream areas. It is worth noting that such a solution could be particularly interesting in the distribution system scenario, because it could allow a more flexible partition of the network with the possibility to create areas that become observable thanks to the information provided by the upstream areas. Additional benefits concern

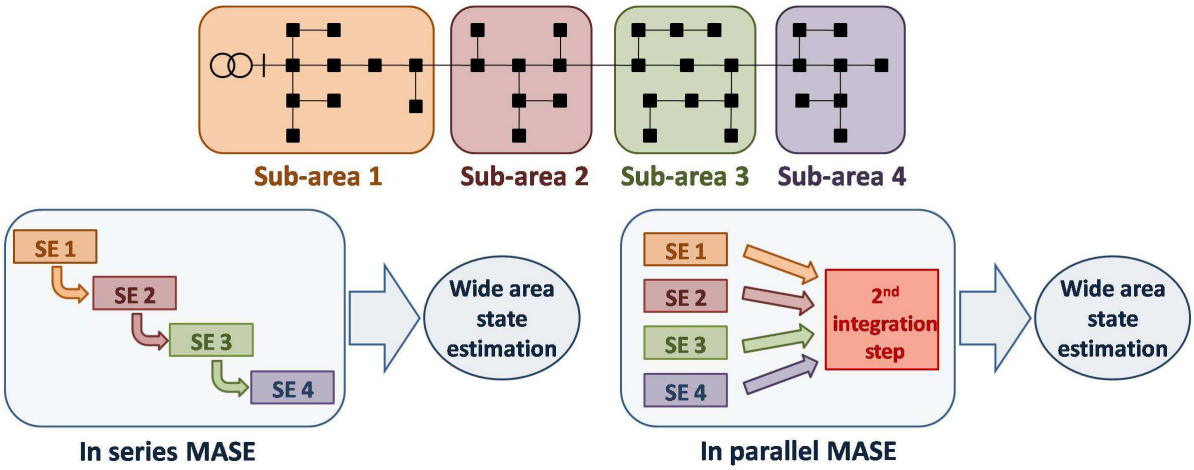

Figure 6.2: In series and in parallel Multi-Area State Estimation

the storage requirements (each area has to consider only its own data plus possible information about the border nodes and the connecting lines of the adjoining areas) and the communication costs (which are quite low, since the communication between adjacent areas can be limited to the only final estimation results of the border quantities). The major drawback of such approach, instead, is on the efficiency. In fact, the sequential run of the local estimations leads to long execution times; in any case, it is worth underlining that the sequential execution of the SE in smaller networks allows saving computation time with respect to the estimation process carried out on the whole network.

In case of parallel estimation of the areas, the local SEs are performed simultaneously in all the sub-networks. The main benefit provided by this approach is clearly on the execution times, which can be significantly lowered thanks to the parallel running of the local SEs. In order to enhance the estimation results provided by the area SEs, suitable procedures of integration of the local estimation results are usually employed. The communication costs, the storage requirements and the accuracy results of the final estimation are strictly dependent on the particular methodology used for this integration procedure. It is also important to underline that, in general, parallel execution of the local SEs requires the observability of all the areas. As a consequence, such solution is possible only if it is supported by the presence of a suitable measurement infrastructure.

In practical cases, obviously, hybrid solutions can be also designed. In fact, it is possible to conceive schemes where the local SEs are performed in parallel only in some areas, while other zones are enabled to run the SE only after the acquisition of the estimation results from the upstream sub-networks.

6.2.3 Computing architecture

A very important feature for the multi-area approaches is the type of computing architecture used to perform the MASE. Possible options can be classified in two main categories: centralized architecture (in the literature, often referred also to as hierarchical) and decentralized architecture. Fig. 6.3 shows a simple scheme of the two options together with the indication of the main features for each one.

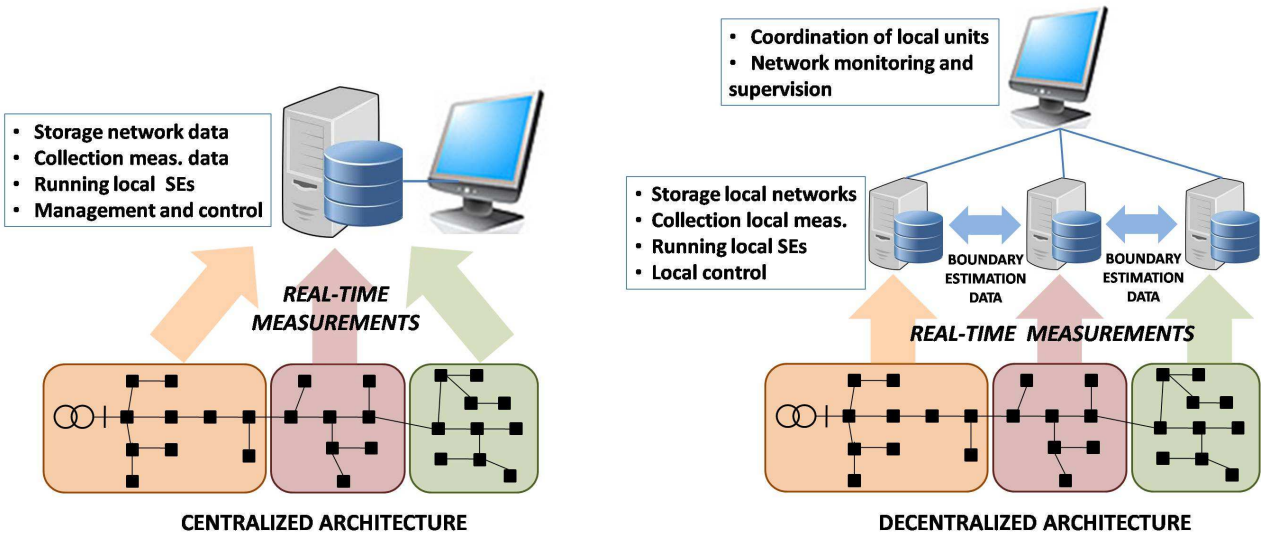

Figure 6.3: Centralized and decentralized architecture

A hierarchical solution is characterized by the presence of a control center gathering all the data and performing all the main functions. In this architecture, each area communicates only with the central unit. This unit, in addition to the collection of the real-time measurements coming from the different areas, has also to handle the pseudo-measurements for the whole grid and to store the network data of all the sub-networks. As a consequence, high communication costs and storage requirements can derive from this solution. At the same time, the execution and coordination of the different area SEs in a single computing center can facilitate the implementation of advanced MASE techniques, with consequent benefits for the accuracy of the estimation results. Moreover, the concentration of all the data in a central station can provide additional advantages in terms of a more straightforward management and control of the network.

In a decentralized architecture, instead, the computing centers are distributed over the network. Each area has a dedicated unit, which is responsible for the execution of the local SE and for the communication with the neighboring areas of the data needed for the refinement of the local estimation results. In this scheme, each

area handles its own real-time measurements, pseudo-measurements and network data. This allows a reduction of the communication and storage requirements in each computing node, but at the cost of having a dedicated center in each area and with possible limitations for the design of the MASE technique. Management and control function can be implemented either on a central computing center or locally in the sub-network units. In the last case, a central master could exist in any case, but with functions that can be limited to the coordination and supervision of the local units and to the monitoring of the network operation.

It is worth noting that, even in this case, hybrid solutions, combining some of the benefits of both the centralized and decentralized approaches, can be also conceived. As an example, the architecture could be designed to have a hierarchical configuration for the management of the MASE process but with computing nodes distributed over the network. In this case, each node handles the measurements and pseudo-measurements of its area and performs the local SE. Then, the sub-network SE results are sent to a central master that operates the additional steps of refinement of the estimation. In such scheme, the advantages are in the distribution of the processing tasks and in the reduction of the data to be communicated to the central station (for example, the acquisition of the measurements from the field is performed locally by the sub-network units).

In transmission systems, most of the proposals refer to a hierarchical design of the MASE [100, 102, 107]; in some cases, the approach is explicitly conceived to allow a distributed architecture [103, 105]. Some decentralized schemes have been also proposed in [101, 104] to distribute the processing, communication and storage requirements. In the distribution system scenario, given the large amount of data to be managed, a decentralized solution can provide important benefits for the communication and storage requirements. At the same time, centralized solutions allow larger flexibility for the design of the MASE technique and this can be crucial to limit the deterioration of the estimation accuracy brought by the low number of available measurement devices. As a result, the choice of the architecture has to achieve a proper trade-off among these different requirements.

6.2.4 Solution methodology

The MASE issue can be tackled by using a large variety of mathematical techniques. The aspect common to all the possible approaches is the need to coordinate the estimations of the different areas in order to improve the accuracy of the final results. Regardless of the details of the different techniques, two main categories can be distinguished depending on the coordination level used in the MASE process: MASE algorithms with integration of the results at the SE level, and algorithms with coordination at the iteration level. In the first case, the algorithms are usually composed of two steps: in the first one, SE is performed in each area; in the second

one, the estimations provided by the local areas are integrated in order to refine the results. In the second category, instead, the MASE algorithms are designed to have an exchange of data between adjoining zones (generally about the estimations of the border quantities) at each iteration of the estimation process. Thus, the local estimators have to include in their model the information coming from the neighboring areas and have to update it at each iteration of the MASE.

The two approaches have significantly different features in terms of accuracy, efficiency and communication costs. The most evident impact is on the communication requirements. In fact, it is clear that the MASE algorithms with coordination at the iteration level imply high communication costs, since the exchange of data is required many times during a single estimation. Moreover, a good level of synchronization is also needed (between the iterations in the different sub-network SEs) in order to efficiently perform the estimation process. Despite these strict requirements on communication and synchronization, the algorithms with coordination at the iteration level can provide very good performance from an accuracy point of view. In several cases, the mathematical model provided in these algorithms allows the achievement of an optimum solution, i.e. an estimation solution equal to the results obtainable by performing the SE on the whole network. In general, however, a large number of iterations of the MASE algorithm can be needed to achieve such result, with the obvious consequences on the overall execution times. As for the two-step MASE approaches, instead, the opposite considerations can be made. In fact, these techniques generally provide only sub-optimal solutions (with a consequent deterioration of the accuracy performance with respect to the case of SE on the whole network), but also demand low communication costs and allow achieving largely reduced execution times.

Even in this case, the choice of the best algorithm should be carefully assessed, also by taking into account the features of the grid to be monitored, the computing architecture to be used and the specific targets to be satisfied.

6.3 Multi-area proposal for DSSE

In the literature, only few works deal with the problem of the Multi-Area Distribution System State Estimation (MA-DSSE). In [108], a hierarchical two-step estimator has been proposed, where a central coordinator refines the local estimations to achieve the overall voltage profile of the network. In [109], instead, the MA-DSSE problem is tackled by means of a differential evolution algorithm having distributed local estimators coordinated at the iteration level. Here, in the following, a decentralized MA-DSSE approach, based on a two-step procedure and designed to have accurate estimations, low communication costs and distributed storage requirements, is presented.

The first issue in the development of the multi-area scheme is, obviously, the definition of the different network areas. As already mentioned in the previous sections, in distribution systems the partition of the grid has to be duly coordinated with the available measurement system, in order to avoid possible observability problems in the created areas. Assuming a distribution network with measurements only in the main substation, and designing the multi-area scheme in parallel with the upgrade of the measurement infrastructure of the grid, the proposed solution is based on the following assumptions.

- The decomposition into areas can be addressed by both topological and geographical criteria; however, when possible, the partition should be performed so to create areas having a similar number of nodes.
- Adjacent areas are overlapped and share one node (minimum overlapping); this node has to be monitored with a suitable measurement point and can be shared by more than two areas.
- Each measurement point has to monitor all the electrical quantities available in the bus; thus, it has to include the voltage measurement at the node and as many flow measurements (powers or currents) as the branches converging to the node.

The solution here proposed, schematically depicted in Fig. 6.4, provides several advantages. The creation, when possible, of zones with a similar number of nodes aims at avoiding the presence of areas acting as bottlenecks for the execution times and is thus conceived to maximize the efficiency of the MA-DSSE. The choice of the minimum overlapping and the placement of a measurement point in the shared node is instead thought to ensure the observability for each area. In fact, if the pseudo-measurements of the power injections for all the load and generation nodes are available, then the presence of these measurement points guarantees the observability in all the areas. Moreover, the presence of at least one measurement point in each zone is crucial also for the robustness to possible communication failures. In fact, also in case of communication problems, each area can achieve the estimation

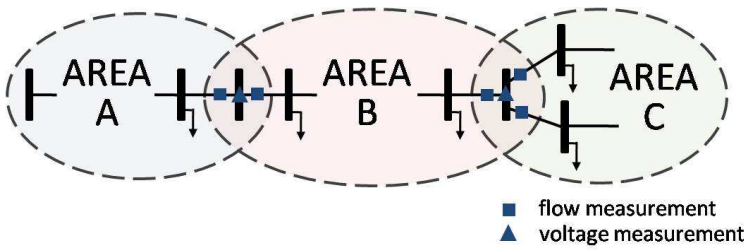

Figure 6.4: Scheme of the multi-area partition of the network

of its own operating conditions (even if with a lower accuracy) and it can enable possible management and control tools. It is important also to note that each overlapped node could be shared by more than two areas: in this way, the number of created areas can be maximized, keeping low, at the same time, the number of measurement points to be installed (in a perspective of strict economic constraints for the network upgrade). The full monitoring of all the electrical quantities associated to the overlapped node, instead, allows exploiting the measurements on the branches connected to the shared node, but not belonging to the area of interest, as equivalent injections for the considered area. This leads to a higher redundancy in the measurement of the flows incoming or outgoing from each area. Finally, in case of traditional measurements (in this case, each area has its own slack bus angle reference), the phase-angles of the different zones can be sequentially shifted, by using the difference in the voltage angle estimation on the overlapped node, to obtain consistent phase-angle information for the whole network. In this way, an overall picture of the operating conditions of the entire grid can be obtained.

The proposed MA-DSSE approach is based on a two-step estimation procedure. In the first step, all the measurements internal to the considered area are exploited to perform a local DSSE. As anticipated, the flow measurements on the branches converging to the overlapped nodes of the area, which are external to the area itself, are lumped all together and introduced in the local DSSE as equivalent injection for the node. The local estimations can be performed in parallel among the different areas of the network, and in a totally independent way. Their results are then used as input for the second step. Besides the estimated values, each area has to provide to the second step also the corresponding variances associated to the estimations. In the algorithm used here, local estimations are carried out by means of the BC-DSSE algorithm presented in Chapter 1; the needed estimation variances can be thus obtained through the inversion of the Gain matrix used in the last iteration of the WLS process. However, it is worth noting that other WLS estimators based on different state variables can be also used (the estimation variances can be always obtained by inverting the corresponding Gain matrix).

The design of the second step plays a key role for the final accuracy of the estimation results. In [110], a study of possible alternative solutions, with different levels of complexity and computational burden, has been presented. The analysis emphasizes that different accuracy results can be obtained depending on the goodness of the adopted method. In the proposal here presented, the second step is performed through a new BC-DSSE in each sub-network, which uses the estimation results of the first step as input measurements. In particular, for each area i, defining as Γ_i the set of the adjoining areas, the following equivalent measurements are used:

- the output $\hat{\mathbf{x}}_i$ of the first step estimation in area i;
- for each area j belonging to Γ_i, its voltage estimation on the shared node

between areas i and j;

- for each overlapped node of the area i, the current estimations in the branches of the neighboring areas converging to such node are lumped up to a single equivalent current injection on the common bus.

For the proper implementation of the second step, due attention must be paid to the phase-angles of the estimated quantities coming from the neighboring areas. In particular, if the measurement system is composed of traditional measurements, it is necessary to consider that each sub-network has its own angle reference. In this case, as for the voltage estimations provided by the adjacent areas, only their magnitude is taken into account. Instead, as for the equivalent current injections, a realignment of each branch current involved in the computation of the injection has to be done exploiting the mismatch (between the considered area i and the adjoining area j) of the voltage angle estimation on the shared node. In case of measurement system composed of PMUs, instead, since the phase-angles of all the sub-networks have the same reference given by the UTC time, no phase-angle realignment is needed for the currents. Moreover, the complex voltage estimations coming from the adjacent areas can be included in rectangular coordinates and they can contribute, in this way, to the refinement of the final phase-angle estimations.

Starting from this set of inputs, the second step is thus implemented by applying, in each area i, the BC-DSSE to the following equivalent measurement model:

$$\mathbf{y}_{2^{nd}} = \begin{bmatrix} \hat{\mathbf{x}}_i \\ \hat{\mathbf{x}}_j^B \end{bmatrix} = \begin{bmatrix} \mathbf{x}_i \\ \mathbf{f}_j(\mathbf{x}_i) \end{bmatrix} + \begin{bmatrix} \boldsymbol{\epsilon}_i \\ \boldsymbol{\eta}_j \end{bmatrix} \tag{6.1}$$

where $\mathbf{y}_{2^{nd}}$ is the vector of the equivalent measurements used in the second step; $\mathbf{x}_i$ and $\hat{\mathbf{x}}_i$ are the state vector of the considered area i and its estimation, respectively; $\hat{\mathbf{x}}_j^B$ is the set of the equivalent measurements resulting from the estimated border quantities in the neighboring areas j; $\mathbf{f}_j(\mathbf{x}_i)$ is the vector of the measurement functions linking the equivalent measurements from areas j to the state variables of area i; $\boldsymbol{\epsilon}_i$ and $\boldsymbol{\eta}_j$ are, respectively, the error vectors associated to the first step estimations coming from area i and to the equivalent input measurements provided by the adjoining area j. Similarly to the first step, these errors can be modeled through a covariance matrix $\boldsymbol{\Sigma}_{\mathbf{y}}$ and its inverse should be considered as weighting matrix for the second step.

The results arising from this second DSSE are the final estimations for each sub-network. Since the communication required to perform this second step is limited to the exchange, among the adjacent areas, of the border quantity estimations, this MA-DSSE technique can be easily implemented in a decentralized way. Therefore, in the designed architecture, each area has a mini-control center where the local estimations are carried out; such computing nodes work in parallel and communicate only with the intelligent nodes of the neighboring zones. This allows distributing the storage

requirements (for example, the sub-network data can be stored in the computing center of the associated area) and minimizing the communication requirements (each area collects its own measurements and communicates only with the intelligent nodes of the adjoining zones to exchange few border quantity estimations).

6.4 Data correlation in the proposed multi-area approach

The proposed multi-area approach is based on the execution of DSSEs relying on WLS algorithms. As a consequence, coherently with the discussions made in the previous chapters of this thesis, due attention has to be paid to the modeling of the measurements used as input to the estimator, in order to achieve estimation results as accurate as possible. Since the first step estimations are obtained by means of a normal DSSE, based on the real-time measurements and pseudo-measurements available for the considered sub-network, all the aspects highlighted in the previous chapters about the proper modeling of these measurements still hold. For this reason, the focus of this Section is on the modeling of the equivalent measurements used as input for the DSSE of the second step. In particular, it is important to note that, because of the chosen multi-area partition with overlapped nodes and the presence of measurement points shared by different sub-networks, correlations can arise between the estimation results obtained in adjacent sub-networks [111]. Thus, in the following of this Section, the analysis of the correlations among the states estimated by adjoining areas during the first step is presented, and the way to properly consider it into the measurement model of the second step DSSE is shown.

6.4.1 Covariance among the state estimations of adjoining areas

Since the correlations among the estimated states of adjoining areas arise because of the presence of shared measurements, to formalize this correlation it is necessary to highlight the relationship between final estimation and starting measurements. Considering only the last iteration n of the DSSE algorithm and linearized measurement functions, the solution of the normal equations used in the WLS process yields:

$$\Delta\hat{\mathbf{x}}_n = \mathbf{G}_n^{-1}\mathbf{H}_n^T\mathbf{W}(\mathbf{y} - \mathbf{h}(\hat{\mathbf{x}}_{n-1})) \tag{6.2}$$

where $\Delta\hat{\mathbf{x}}_n$ is the updating state vector $\mathbf{x}$ at iteration n, $\mathbf{G}_n = \mathbf{H}_n^T\mathbf{W}\mathbf{H}_n$ is the Gain matrix, $\mathbf{H}_n$ is the Jacobian of the measurement functions, $\mathbf{W}$ is the weighting matrix,

$\mathbf{y}$ is the set of available measurements and $\mathbf{h}(\hat{\mathbf{x}}_{n-1})$ is the vetor of the measurement functions computed through the state vector estimated at the previous iteration.

Grouping the terms in (6.2), it is possible to write:

$$\Delta\hat{\mathbf{x}}_n = \mathbf{B} \cdot \Delta\mathbf{y} \tag{6.3}$$

where $\mathbf{B} = (\mathbf{H}^{\mathrm{T}}\mathbf{W}\mathbf{H})^{-1}\mathbf{H}^{\mathrm{T}}\mathbf{W}$ is the pseudoinverse matrix linking the update of the estimated state $\hat{\mathbf{x}}$ to the measurement residuals $\Delta\mathbf{y}$.

Considering the link between estimations and measurements expressed in (6.3), it is possible to analyze the correlation arising in the estimations of two areas sharing some measurements. To this purpose, let us consider two generic areas A and B, characterized by N_i state variables and M_i measurements, (with $i = [A, B]$), and with a consequent $[N_i \times 1]$ state vector $\mathbf{x}_i$ and an $[M_i \times 1]$ measurement vector $\mathbf{y}_i$. Hence, each area has an $[M_i \times N_i]$ Jacobian matrix $\mathbf{H}_i$ and an $[M_i \times M_i]$ weighting matrix $\mathbf{W}_i$.

If the measurements shared between areas A and B are M_{AB}, then the overall number of measurements available in the two areas is: $M = M_A + M_B - M_{AB}$. Considering areas A and B together, it is possible to create an $[M \times 1]$ measurement vector $\mathbf{y}_{TOT}$ and an $[M \times M]$ weighting matrix $\mathbf{W}_{TOT}$ including all the available measurements. The measurement vector $\mathbf{y}_{TOT}$ can be written as:

$$\mathbf{y}_{TOT} = \begin{bmatrix} \mathbf{y}_{AA} \\ \mathbf{y}_{AB} \\ \mathbf{y}_{BB} \end{bmatrix} \tag{6.4}$$

where $\mathbf{y}_{AA}$ and $\mathbf{y}_{BB}$ are the sub-vectors of the measurements belonging only to area A or B, respectively, while $\mathbf{y}_{AB}$ is the vector of the measurements shared between the two sub-networks. Coherently with the construction of the measurement vector $\mathbf{y}_{TOT}$, the weighting matrix $\mathbf{W}_{TOT}$ can be expressed as follows:

$$\mathbf{W}_{TOT} = \begin{bmatrix} \mathbf{W}_{AA} & \mathbf{0} & \mathbf{0} \\ \mathbf{0} & \mathbf{W}_{AB} & \mathbf{0} \\ \mathbf{0} & \mathbf{0} & \mathbf{W}_{BB} \end{bmatrix} \tag{6.5}$$

where $\mathbf{W}_{AA}$, $\mathbf{W}_{AB}$, and $\mathbf{W}_{BB}$ are the diagonal sub-matrices composed of the weights associated to the M_{AA}, M_{AB}, and M_{BB} measurements (considered as uncorrelated), respectively.

For each area, it is also possible to build an expanded Jacobian matrix $\mathbf{H}_{i_{TOT}}$ involving the relationship among the vector $\mathbf{y}_{TOT}$ of all the measurements of the network and the state of the considered area: for the measurements not belonging to the area itself, the corresponding rows of the Jacobian will have null elements and thus it is:

$$\mathbf{H}_{A_{TOT}} = \begin{bmatrix} \mathbf{H}_A \\ \mathbf{0} \end{bmatrix}, \ \mathbf{H}_{B_{TOT}} = \begin{bmatrix} \mathbf{0} \\ \mathbf{H}_B \end{bmatrix} \tag{6.6}$$

Considering the null elements of the expanded Jacobians $\mathbf{H}_{i_{TOT}}$, it is possible to verify that the following relationship holds:

$$\mathbf{G}_i = \mathbf{H}_i^{\mathrm{T}} \mathbf{W}_i \mathbf{H}_i = \mathbf{H}_{i_{TOT}}^{T} \mathbf{W}_{TOT} \mathbf{H}_{i_{TOT}} \tag{6.7}$$

Considering (6.7), it is possible to write a matrix $\mathbf{B}_{i_{TOT}}$ that links the estimates of the area i to the vector $\mathbf{y}_{TOT}$, which is:

$$\mathbf{B}_{i_{TOT}} = \mathbf{G}_i^{-1} \mathbf{H}_{i_{TOT}}^{T} \mathbf{W}_{TOT} \tag{6.8}$$

Since, as known, the inverse of the Gain matrix is the covariance matrix of the estimated states, (6.8) can be rewritten as:

$$\mathbf{B}_{i_{TOT}} = \mathbf{\Sigma}_i \mathbf{H}_{i_{TOT}}^{T} \mathbf{W}_{TOT} \tag{6.9}$$

where $\mathbf{\Sigma}_i$ is the covariance matrix of the estimates of area i.

Considering the structure shown in (6.5) for the overall weighting matrix and in (6.6) for the Jacobian matrices, the matrix $\mathbf{B}_{i_{TOT}}$ can be decomposed in the following way for the two areas A and B:

$$\mathbf{B}_{A_{TOT}} = \begin{bmatrix} \mathbf{B}_A & \mathbf{0} \end{bmatrix}, \ \mathbf{B}_{B_{TOT}} = \begin{bmatrix} \mathbf{0} & \mathbf{B}_B \end{bmatrix} \tag{6.10}$$

where $\mathbf{B}_A$ and $\mathbf{B}_B$ are, respectively:

$$\mathbf{B}_A = \mathbf{\Sigma}_A \mathbf{H}_A^{\mathrm{T}} \mathbf{W}_A, \ \ \mathbf{B}_B = \mathbf{\Sigma}_B \mathbf{H}_B^{\mathrm{T}} \mathbf{W}_B \tag{6.11}$$

Considering the relationship shown in (6.3), and applying the law of propagation of the uncertainty, the covariance between the state variables estimated in areas A and B can be written as follows:

$$\mathbf{\Sigma}_{\hat{\mathbf{x}}_A, \hat{\mathbf{x}}_B} = \mathbf{B}_{A_{TOT}} \mathbf{\Sigma}_{\mathbf{y}_{TOT}} \mathbf{B}_{B_{TOT}}^{\mathrm{T}} \tag{6.12}$$

where $\mathbf{\Sigma}_{\mathbf{y}_{TOT}}$ is the covariance matrix of all the measurement errors. Considering that the weighting matrix is chosen as the inverse of the measurement error covariance matrix, (6.12) becomes:

$$\mathbf{\Sigma}_{\hat{\mathbf{x}}_A, \hat{\mathbf{x}}_B} = \mathbf{B}_{A_{TOT}} \mathbf{W}_{TOT}^{-1} \mathbf{B}_{B_{TOT}}^{\mathrm{T}} \tag{6.13}$$

Considering (6.10) for the matrices $\mathbf{B}_{i_{TOT}}$, equation (6.13) becomes:

$$\mathbf{\Sigma}_{\hat{\mathbf{x}}_A, \hat{\mathbf{x}}_B} = \begin{bmatrix} \mathbf{B}_A & \mathbf{0} \end{bmatrix} \mathbf{W}_{TOT}^{-1} \begin{bmatrix} \mathbf{0} & \mathbf{B}_B \end{bmatrix}^{\mathrm{T}} \tag{6.14}$$

and, taking into account (6.11), it results:

$$\boldsymbol{\Sigma}_{\hat{\mathbf{x}}_A,\hat{\mathbf{x}}_B} = \begin{bmatrix}\boldsymbol{\Sigma}_A\mathbf{H}_A^{\mathrm{T}}\mathbf{W}_A & \mathbf{0}\end{bmatrix}\mathbf{W}_{TOT}^{-1}\begin{bmatrix}\mathbf{0} & \boldsymbol{\Sigma}_B\mathbf{H}_B^{\mathrm{T}}\mathbf{W}_B\end{bmatrix}^{\mathrm{T}} \tag{6.15}$$

Since the weighting and covariance matrices are symmetric, it is possible to rewrite (6.15) as follows:

$$\boldsymbol{\Sigma}_{\hat{\mathbf{x}}_A,\hat{\mathbf{x}}_B} = \begin{bmatrix}\boldsymbol{\Sigma}_A\mathbf{H}_A^{\mathrm{T}}\mathbf{W}_A & \mathbf{0}\end{bmatrix}\mathbf{W}_{TOT}^{-1}\begin{bmatrix}\mathbf{0}\\ \mathbf{W}_B\mathbf{H}_B\boldsymbol{\Sigma}_B\end{bmatrix} \tag{6.16}$$

In the Jacobians of the areas A and B indicated in (6.16), it is possible to separate the contributions of the measurements belonging only the considered area from those coming from the shared measurements as follows:

$$\mathbf{H}_A = \begin{bmatrix}\mathbf{H}_{AA}\\ \mathbf{H}_{AB}\end{bmatrix}, \quad \mathbf{H}_B = \begin{bmatrix}\mathbf{H}_{BA}\\ \mathbf{H}_{BB}\end{bmatrix} \tag{6.17}$$

and, thus, it is possible to rewrite (6.16) as follows:

$$\begin{aligned}\boldsymbol{\Sigma}_{\hat{\mathbf{x}}_A,\hat{\mathbf{x}}_B} &= \begin{bmatrix}\boldsymbol{\Sigma}_A\mathbf{H}_{AA}^{T}\mathbf{W}_{AA} & \boldsymbol{\Sigma}_A\mathbf{H}_{AB}^{\mathrm{T}}\mathbf{W}_{AB} & \mathbf{0}\end{bmatrix}\times\\ &\times\begin{bmatrix}W_{AA} & \mathbf{0} & \mathbf{0}\\ \mathbf{0} & W_{AB} & \mathbf{0}\\ \mathbf{0} & \mathbf{0} & W_{BB}\end{bmatrix}^{-1}\times\begin{bmatrix}\mathbf{0}\\ \mathbf{W}_{AB}\mathbf{H}_{BA}\boldsymbol{\Sigma}_B\\ \mathbf{W}_{BB}\mathbf{H}_{BB}\boldsymbol{\Sigma}_B\end{bmatrix}\end{aligned} \tag{6.18}$$

Finally, performing the matrix multiplication in (6.18), it is possible to obtain the following expression for the covariance matrix:

$$\boldsymbol{\Sigma}_{\hat{\mathbf{x}}_A,\hat{\mathbf{x}}_B} = \boldsymbol{\Sigma}_A\mathbf{H}_{AB}^{\mathrm{T}}\mathbf{W}_{AB}\mathbf{H}_{BA}\boldsymbol{\Sigma}_B \tag{6.19}$$

6.4.2 Covariance between the voltage estimation of adjoining areas

The relationship expressed in (6.19) provides the covariances existing between each state variable of area A and area B. As shown in Chapter 4, the impact of the measurements on the final estimation results is different depending on their typology. In particular, it has been shown that voltage measurements have a global effect on the accuracy of the voltage magnitude profile of the network, while the currents usually have only a local impact that is highly dependent on the size of the measured current. For this reason, in the case of interest, the attention can be focused on the covariance brought by the shared voltage measurement placed at the overlapped node on the voltages to be exchanged by the two different areas.

As shown in Chapter 1, the state vector in the BC-DSSE model is composed by the currents of all the branches and the voltage in the slack bus. Referring, for

the moment, to the case of only traditional measurements available on the field, the voltage magnitude of the slack bus has to be considered in the state vector. Since the uncertainty obtained in the estimation process is not dependent on the particular choice of the slack bus of the area, then, without any loss of generality, the overlapped node can be considered as slack bus for both the areas A and B. Assuming, as made in Chapter 1, that the slack bus voltage magnitude is the first element of the state vectors $\mathbf{x}_A$ and $\mathbf{x}_B$, the analysis can be consequently reduced to the computation of the element $(1,1)$ of the covariance matrix $\mathbf{\Sigma}_{\hat{\mathbf{x}}_A,\hat{\mathbf{x}}_B}$. It is possible to observe that this calculation involves only the first row of $\mathbf{\Sigma}_A$ and the first column of $\mathbf{\Sigma}_B$ in (6.19). Furthermore, since the only shared measurement is the voltage magnitude at the overlapped node (indicated in the following as V_s), it is:

$$\mathbf{W}_{AB} = \frac{1}{\sigma^2_{V_s}} = w_{V_s} \tag{6.20}$$

where $\sigma^2_{V_s}$ is the variance associated to the voltage magnitude measurement at the shared node, and w_{V_s} is the corresponding weight considered in the weighting matrix. As for the Jacobian matrix, the derivative of the measurement function associated to the voltage V_s with respect to the elements of the state vectors $\mathbf{x}_A$ and $\mathbf{x}_B$ yields:

$$\mathbf{H}_{AB} = \mathbf{H}_{BA} = [1, 0, ..., 0] \tag{6.21}$$

As a result, it is possible to find that the only contribution to the sought covariance between the first step estimation of the slack bus voltages in areas A and B is given by:

$$\mathbf{\Sigma}_{\hat{\mathbf{x}}_A,\hat{\mathbf{x}}_B}(1,1) = \sigma^2_{\hat{V}_{sA}} w_{V_s} \sigma^2_{\hat{V}_{sB}} \tag{6.22}$$

where $\sigma^2_{\hat{V}_{sA}}$ and $\sigma^2_{\hat{V}_{sB}}$ are the resulting variances in the estimation of the slack bus voltage provided by areas A and B.

Equation (6.22) shows that the covariance between the voltages to be included in the second step of the multi-area estimation process can be computed without the communication of additional data by the adjoining area (the only needed information is the variance of the voltage estimation in the overlapped node, which has to be communicated in any case). Such covariance term can be included in the matrix of the measurement errors used in the second estimation step to calculate the weighting matrix to be adopted in the second BC-DSSE run.

When PMUs are used in place of the conventional measurements, the approach to compute the arising covariances is similar to the previous case, but it has to take into account the presence of two shared measurements (both the real and the imaginary part of the voltage at the overlapped node, which are indicated in the following as v_s^r and v_s^x, respectively) and the different formulation of the state vectors $\mathbf{x}_A$ and $\mathbf{x}_B$ (the slack bus voltage is, in this case, included in rectangular coordinates within the state vector).

In this case, the elements of interest in the covariance matrix $\mathbf{\Sigma}_{\hat{\mathbf{x}}_A,\hat{\mathbf{x}}_B}$ are those included in the sub-matrix (h,k), with $h = 1,2$ and $k = 1,2$: such sub-matrix includes the covariance terms associated to all the possible combinations among the rectangular components of the voltage slack bus estimations of area A and the same estimations provided by area B.

As for the weighting matrix $\mathbf{W}_{AB}$, since the PMUs provide the voltage phasor measurements in polar coordinates, but these measurements are included in rectangular coordinates in the BC-DSSE model, a full weighting matrix has to be considered for including the correlations arising between real and imaginary components of the measured voltage (see Section 1.7.3 in Chapter 1 for the details). Thus, it is:

$$\mathbf{W}_{AB} = \begin{bmatrix} w_{v_s^r} & w_{v_s^r v_s^x} \\ w_{v_s^x v_s^r} & w_{v_s^x} \end{bmatrix} \tag{6.23}$$

Instead, as for the Jacobian matrices $\mathbf{H}_{AB}$ and $\mathbf{H}_{BA}$, the two rows related to the derivatives of the measurements v_s^r and v_s^x with respect to the variables of the state vector (considering the state vector built as indicated in Chapter 1 for the case of PMU measurements) are:

$$\mathbf{H}_{AB} = \mathbf{H}_{BA} = \begin{bmatrix} 1, 0, \ldots, 0 \\ 0, 1, \ldots, 0 \end{bmatrix} \tag{6.24}$$

Referring to this structure of the Jacobian matrices, and considering the matrix multiplications involved in equation (6.19), the following holds:

$$[\mathbf{\Sigma}_A \mathbf{H}_{AB}^{\mathrm{T}}] \Big|_{h=1,2} = \begin{bmatrix} \sigma^2_{\hat{v}^r_{sA}} & \sigma_{\hat{v}^r_{sA}\hat{v}^x_{sA}} \\ \sigma_{\hat{v}^x_{sA}\hat{v}^r_{sA}} & \sigma^2_{\hat{v}^x_{sA}} \end{bmatrix} \tag{6.25}$$

$$[\mathbf{H}_{BA}^{\mathrm{T}} \mathbf{\Sigma}_B] \Big|_{k=1,2} = \begin{bmatrix} \sigma^2_{\hat{v}^r_{sB}} & \sigma_{\hat{v}^r_{sB}\hat{v}^x_{sB}} \\ \sigma_{\hat{v}^x_{sB}\hat{v}^r_{sB}} & \sigma^2_{\hat{v}^x_{sB}} \end{bmatrix} \tag{6.26}$$

where the notation $\mathbf{P}|_{h=..;k=..}$ indicates the rows h or columns k to be considered in the resulting matrix $\mathbf{P}$, the terms $\sigma_{\hat{v}^r_{si}}$ and $\sigma_{\hat{v}^x_{si}}$ (with $i = A, B$) are, respectively, the standard deviations of the real and the imaginary part of the slack bus voltage estimated by area i, and $\sigma_{\hat{v}^r_{si}\hat{v}^x_{si}}$ is the resulting covariance.

Using the same kind of notation, the sub-matrix of interest achievable from (6.19) is:

$$\begin{aligned} \mathbf{\Sigma}_{\hat{\mathbf{x}}_A,\hat{\mathbf{x}}_B} \Big|_{h=1,2;k=1,2} &= \begin{bmatrix} \sigma^2_{\hat{v}^r_{sA}} & \sigma_{\hat{v}^r_{sA}\hat{v}^x_{sA}} \\ \sigma_{\hat{v}^x_{sA}\hat{v}^r_{sA}} & \sigma^2_{\hat{v}^x_{sA}} \end{bmatrix} \begin{bmatrix} w_{v_s^r} & w_{v_s^r v_s^x} \\ w_{v_s^x v_s^r} & w_{v_s^x} \end{bmatrix} \begin{bmatrix} \sigma^2_{\hat{v}^r_{sB}} & \sigma_{\hat{v}^r_{sB}\hat{v}^x_{sB}} \\ \sigma_{\hat{v}^x_{sB}\hat{v}^r_{sB}} & \sigma^2_{\hat{v}^x_{sB}} \end{bmatrix} \\ &= \begin{bmatrix} \sigma_{\hat{v}^r_{sA}\hat{v}^r_{sB}} & \sigma_{\hat{v}^r_{sA}\hat{v}^x_{sB}} \\ \sigma_{\hat{v}^x_{sA}\hat{v}^r_{sB}} & \sigma_{\hat{v}^x_{sA}\hat{v}^x_{sB}} \end{bmatrix} \end{aligned} \tag{6.27}$$

where $\sigma_{\hat{v}^r_{sA}\hat{v}^r_{sB}}$ is the covariance between the real part of the voltage estimated in A and the real part of the voltage estimated in B and the other elements have analogous interpretations.

Equation (6.27) points out that, for the computation of the covariances between the voltages estimated on the overlapped node by areas A and B, the only data to be received by the neighboring area i are the variances $\sigma^2_{\hat{v}^r_{si}}$ and $\sigma^2_{\hat{v}^x_{si}}$ (related to the real and imaginary parts, respectively) and the covariance term $\sigma_{\hat{v}^r_{si}\hat{v}^x_{si}}$. It is worth noting that these data should be communicated in any case and, therefore, even in this case, there are no additional costs in the communication between adjoining areas. Finally, equation (6.27) also shows that, in general, the resulting covariance matrix is full and covariance terms arise for all the possible combinations of the rectangular voltage terms.

6.5 Tests and results

6.5.1 Test assumptions

The performance of the proposed multi-area approach has been evaluated through several tests performed on the unbalanced IEEE 123-bus network. Fig 6.5 shows the network topology and chosen multi-area partition. Following the indications

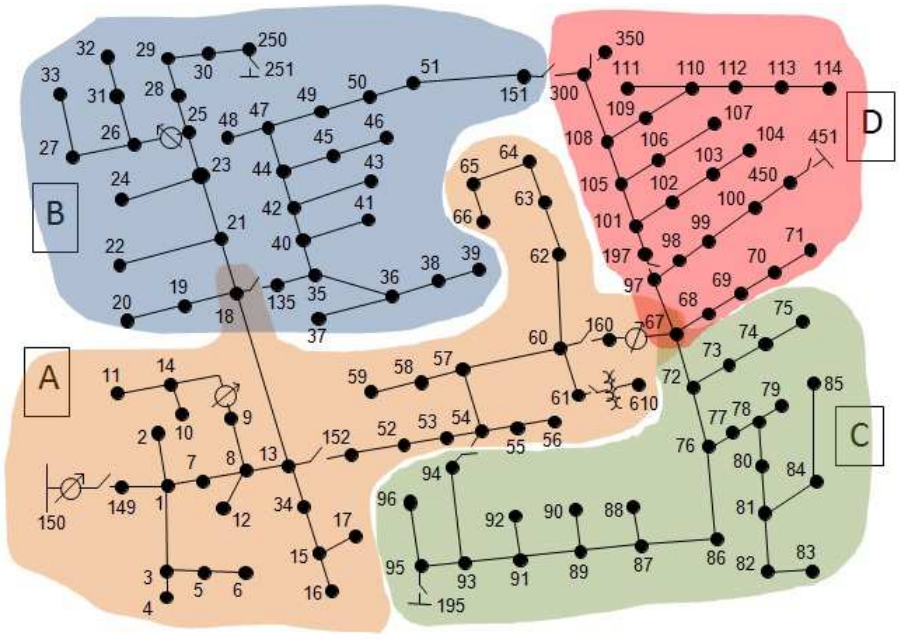

Figure 6.5: Multi-area partition of the IEEE 123-bus network

reported in Section 6.3, the decomposition has been carried out aiming to achieve sub-networks with a similar number of nodes, in order to enhance the efficiency of the multi-area solution. Moreover, the use of areas with overlapped nodes has been exploited to create more observable sub-networks starting from a limited number of measurement points. As an example, node 67 is shared by three areas and the corresponding measurement point allows the observability for both areas C and D.

According to the proposed method (and the chosen multi-area partition), measurement points are considered in the shared nodes 18 and 67 in addition to the measurement point in substation (node 150). Each measurement point includes a voltage magnitude measurement at the node and power measurements in all the converging branches. The alternative of having PMU measurements has been also analyzed, and in this case voltage and current phasor measurements are considered in the measurement system. In addition to the real-time measurements, the availability of pseudo-measurements for all the load consumptions has been also considered, in order to obtain the observability for all the identified areas.

As in the previous chapters, tests have been performed by means of Monte Carlo simulations ($N_{MC} = 50000$ Monte Carlo trials have been used in each test). In all the tests, true reference operating conditions are obtained through a power flow calculation. The resulting electrical quantities are then used for the random extraction of measurements and pseudo-measurements, according to their probability distribution. In particular, the following assumptions have been considered.

- Pseudo-measurements are assumed as random variables having a Gaussian probability distribution and an expanded uncertainty equal to 50% (three times the standard deviation).

- Real-time measurements are assumed as random variables with Gaussian distribution and standard deviation equal to one third of their accuracy value. As for the traditional measurements, accuracies equal to 1% and 3% have been considered for the voltage magnitude and the power measurements, respectively; as for the synchronized measurements, accuracies of 0.7% and 0.7 crad have been assumed for the magnitude and phase-angle measurements of both voltage and current phasors.

The properties of the proposed multi-area solution have been evaluated with particular attention to the accuracy performance. To this purpose, the estimation results obtained with the presented approach (henceforth indicated as MA-DSSE) are compared to those achievable by using different methods. A first term of comparison is given by the results obtained through the estimation carried out on the whole network (indicated in the following as Integrated State Estimation (ISE)). The estimation on the overall system represents, in fact, the optimum solution that can be obtained with the assumed measurement configuration. As a consequence, such

comparison allows assessing the degradation arising in the accuracy of the results due to the implementation of the multi-area scheme. Another used term of comparison is the estimation obtained through the local BC-DSSE performed in each area (indicated in the following as Local State Estimation (LSE)). These results, which are the outputs of the first step estimation in the proposed MA-DSSE algorithm, are useful to evaluate the impact brought by the second BC-DSSE run envisioned in the second step of the MA-DSSE process.

The goodness of the second step has been also analyzed evaluating the accuracy performance obtainable through other possible approaches. In particular, in the following tests, the first of the methods presented in [110] (henceforth indicated as MASE-1) is used to see the differences achievable with alternative second step implementations. The method MASE-1 operates the second step by comparing the voltage estimations in the shared nodes, as computed by the local estimators of the different overlapping areas, and uses the most accurate one to correct the voltage profile of the areas with worse estimations. Such correction is performed by means of a simple shift, according to the difference in the voltage estimation between the most accurate estimation and the considered one, for the voltages of all the nodes of the corrected areas. This kind of approach is taken into account since it is very simple and it demands only minimum processing costs to be carried out.

Finally, the accuracy performance of the proposed MA-DSSE method are also analyzed assessing the impact deriving from the inclusion in the measurement model of the covariance terms between the voltage estimations performed by the local estimators of different areas. To this purpose, in some tests, the MA-DSSE approach has been also tested by neglecting these correlation terms, in order to assess the differences in the results obtained in the two different cases (including or not the correlations in the estimator model).

6.5.2 Test results

Starting measurement configuration

The first series of tests has been performed referring to the starting measurement configuration composed of the measurement points in nodes 150, 18 and 67. First of all, the validity of the mathematical approach developed in Section 6.4 to calculate the covariance between the voltage estimations on the shared nodes obtained by different local estimators has been verified. This check has been performed by comparing the correlation factors obtained through the theoretical formulation (using the covariances calculated with (6.22) and (6.27) for the traditional and synchrophasor measurements, respectively) and those obtained by means of the Monte Carlo simulations. Table 6.1 shows, as an example, the correlation factors obtained for the voltages to be included in the second step estimation for area A when consid-

Table 6.1: Correlation between first step voltage estimations

Voltage estimations	Theoretical calculation	Monte Carlo calculation
V_{150}^{A} - V_{18}^{B}	0.581	0.581
V_{150}^{A} - V_{67}^{C}	0.585	0.583
V_{150}^{A} - V_{67}^{D}	0.585	0.583
V_{67}^{C} - V_{67}^{D}	1.000	1.000

ering traditional measurements (reported results refer only to the first phase of the network, but analogous results have been achieved even for the other phases). According to the proposed method, the voltages to be taken into account are the slack bus voltage of the considered area (V_{150}^{A}) and the voltage estimations on the shared nodes performed by the neighboring zones (V_{18}^{B}, V_{67}^{C} and V_{67}^{D} for areas B, C and D, respectively). From Table 6.1 it is possible to observe that the correlations between the slack bus voltage estimation in area A and the voltage estimations coming from the adjacent areas are not negligible. Moreover, a full correlation exists between the voltage estimations on node 67 provided by areas C and D. It is worth noting that, if some of the inputs to the second step estimation are fully correlated, as in this case, then, only one of them is considered in order to avoid singularity problems for the matrices involved in the subsequent estimation process. In all the cases, the correlation factors calculated through the proposed mathematical formulation exhibit a very good matching with the values resulting from the Monte Carlo simulation, confirming thus the validity of the presented approach. In a similar way, a very good matching has been found also for the correlations among the voltages to be included in the second step estimation of the other areas of the network.

As for the accuracy performance of the proposed method, Fig. 6.6 shows the results obtained for the expanded uncertainty (with a coverage factor equal to three) of the voltage magnitude estimation in the different areas. The results reported in Fig. 6.6 and in the following tests refer only to the first phase of the system, but the shown uncertainty levels and the following considerations hold always for all the phases. It is worth noting that the node numeration reported in the figures does not correspond to the node indexes shown in Fig. 6.5. In fact, for clarity in the presentation of the results, the nodes have been renumbered so to have the aggregation of the buses related to the same areas. Moreover, it should be observed that the overall number of nodes is only 80 because several of the laterals in the network are single-phase branches. In order to avoid a complex representation, the estimation uncertainty shown for the shared nodes is always the one coming from

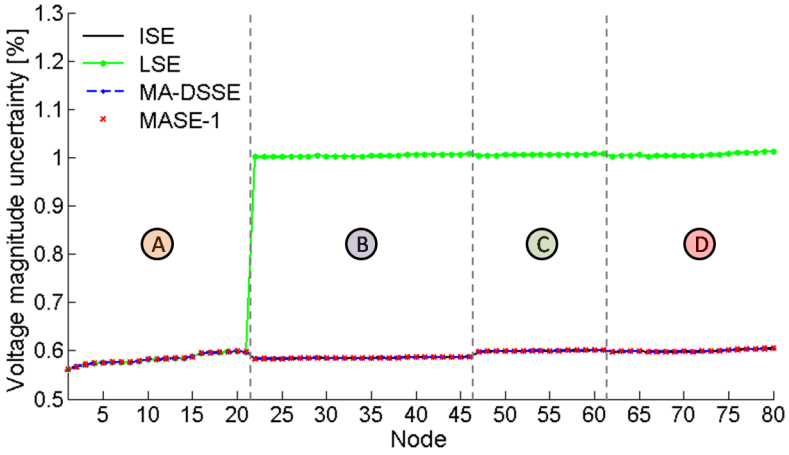

Figure 6.6: Expanded uncertainty for the voltage magnitude estimation in case of starting measurement configuration with traditional measurements

area A: in the other areas the resulting uncertainty is usually different, but, in general, the uncertainty level can be easily deduced by the results on the other buses since the profile is always quite flat.

Some interesting considerations can be drawn by the results shown in Fig. 6.6. First of all, it is important to note the difference in the uncertainty levels obtained with the local estimations. This is an expected result: in fact, as already pointed out in Chapter 4, the accuracy of the voltage estimations is strictly associated to the number of voltage measurements available on the network. As a result, the local estimation in area A is the best one, since it relies upon a larger number of voltage measurements. Furthermore, since area A includes all the measurement points installed in the network, the results of the LSE in this sub-network are practically the same as the ISE. On the contrary, in areas B, C and D, due to the presence of only one voltage measurement, the accuracy of the voltage profile is significantly worse than the ISE and it is limited by the accuracy of the voltage measurement itself.

The results obtained through the first step estimations emphasize the importance to conceive suitable approaches to refine the LSEs. With the assumed measurement scenario, both MASE-1 and the proposed MA-DSSE allow improving the estimation results and achieving accuracies very similar to those provided by the ISE. In case of MASE-1, this can be obtained considering, in the shared nodes, the optimum estimations provided by area A. In fact, the subsequent shift of the voltages in the other nodes of the worse estimated zones leads to the propagation of the smaller uncertainty of area A to all the sub-networks. In case of MA-DSSE, in the same way, the equivalent measurements included in the second run of the BC-DSSE lead to similar benefits. However, it is worth noting that such results can be obtained

only by considering a proper modeling of the measurements to be included in the second step estimation. As a confirmation, Fig. 6.7 shows the results obtained with the MA-DSSE method when considering or neglecting the correlation between the voltage estimations provided by different areas. It is clear that, if existing correlations are disregarded, the results can be adversely affected, leading to less accurate estimations.

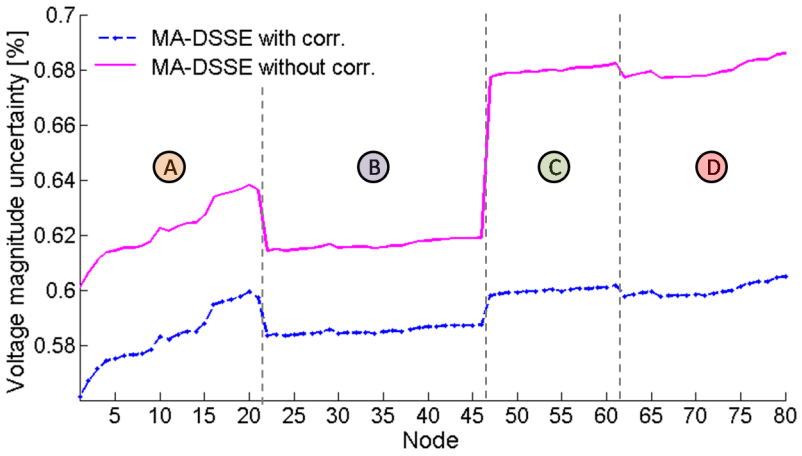

Figure 6.7: MA-DSSE with or without correlations, expanded uncertainty for the voltage magnitude estimation with starting measurement configuration

The considerations reported for the voltage magnitude estimations in case of traditional measurements are also valid when considering the deployment of PMUs. The use of the different types of measurement implies, instead, some differences in the considerations for the voltage angle estimations. In the case of conventional measurements, each area has its own slack bus angle reference. To achieve consistent results for the whole network, it is necessary to consider an absolute reference bus and to refer the angles of all the areas to this reference. This phase-angle alignment, as aforementioned, can be done by exploiting the mismatch on the voltage angle information provided by the different areas in the shared nodes. The results obtained in this way, referred to the entire grid, show that all the estimators (thus including also the LSEs) give very similar estimation outcomes, with an expanded uncertainty of the voltage angles lower than 2 mrad for all the nodes. When PMU measurements are considered, instead, all the areas already have a common reference given by the UTC time. Therefore, in this case, no alignment procedures are needed. The voltage angle uncertainties achieved in this case, as shown in Fig. 6.8, exhibit a trend very similar to the one seen for the voltage magnitudes. Indeed, the LSE results in areas B, C and D are characterized by a significantly lower accuracy, due to the presence of only one PMU in the sub-network. However, the execution of suitable second step approaches allows refining the results and achieving estimation accuracies very

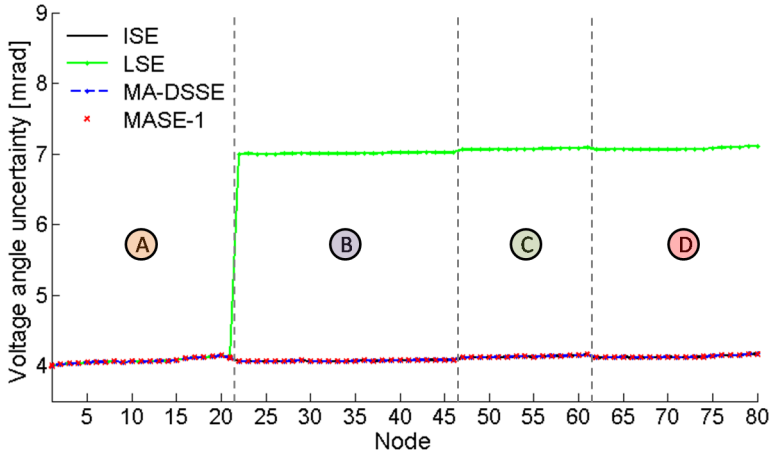

Figure 6.8: Expanded uncertainty for the voltage angle estimation in case of starting measurement configuration with synchronized measurements

close to those provided by the ISE. Moreover, it is worth highlighting that if, instead of the absolute phase-angles, the angle differences with respect to a reference node are calculated (as it is for the conventional measurements), even in this case the achievable uncertainties would be similar for all the estimators and largely lower than 2 mrad.

Final considerations concern the estimation results obtained for the branch currents. In this case, it is interesting to observe how the chosen measurement configuration, with the monitoring of the flows in all the branches converging to the overlapped nodes, allows a good estimation of the branch currents since the first step. This result is a consequence both of the accurate monitoring of the flows in the border branches and, in general, of the local impact brought by the flow measurements. In fact, the local effect of the flow measurements leads to a sort of decoupling in the branch current estimations of the different areas. Moreover, since the border quantities are already accurately known (thanks to the presence of the real-time measurements), the data exchange performed in the second step does not lead to further improvements in the knowledge of the incoming and outgoing flows from each area. The benefits associated to this meter placement, in a current estimation perspective, are also confirmed by the very similar results obtained for all the estimators: in fact, both local and multi-area estimators exhibit accuracy performance very close to the reference ones provided by the ISE.

Since one of the main advantages brought by the use of multi-area approaches is the reduction of the execution times, Table 6.2 shows the comparison of the computation times achieved by means of the ISE and the multi-area techniques. In the multi-area approaches the overall execution times are obtained by summing the longest times among the one required by the different local estimations (first step)

and the one associated to the second step, thus simulating the parallel running of the different area estimations. Tests are performed in Matlab environment using a 2.4 GHz Quad Core Processor with 8 GB RAM. As clear from the shown results, the use of the multi-area approaches allows a significant reduction of the execution times. In case of MASE-1, obviously, resulting computation times are better than those provided by the MA-DSSE, since the second step only requires a simple shift of the voltage estimations. It is worth underlining that such results are only indicative and do not take into account the time consumption of additional tasks like the acquisition of the data, the communication between areas, etc.

Table 6.2: Average execution times for ISE and MASE approaches

Measurements	ISE [ms]	MASE-1 [ms]	MA-DSSE [ms]
Conventional	98.8	15.4	21.0
PMU	71.2	10.3	15.7

Measurement configuration with additional measurement points

The previous series of tests basically showed that, if one of the sub-networks includes all the measurement points available on the grid, then the proposed MA-DSSE approach is able to provide the same results achievable by means of the ISE. To assess the performance of the proposed method even in presence of different measurement scenarios, other tests have been performed assuming additional measurements in the network. In particular, the following tests show the case of two additional measurement points installed in nodes 86 and 105 (in area C and D, respectively).

Fig 6.9 shows the results for the voltage magnitude estimation in case of conventional measurements. It is possible to observe that the ISE clearly provides the best estimation results, since it is the only approach to process simultaneously all the measurements available on the field. The impact brought by the number of processed voltage measurements can be clearly observed looking at the results for the LSEs in the different areas. Area A provides the best results among the different sub-networks, since it can rely upon three measurement points; area B, instead, has the worst accuracy results (only one measurement point available), while areas C and D significantly enhance their accuracy with respect to the results obtained with the previous measurement configuration, thanks to the presence of the additional measurement point. However, in all the cases, a significant difference exists with respect to the results provided by the ISE.

Large enhancements with respect to the local estimation results can be obtained

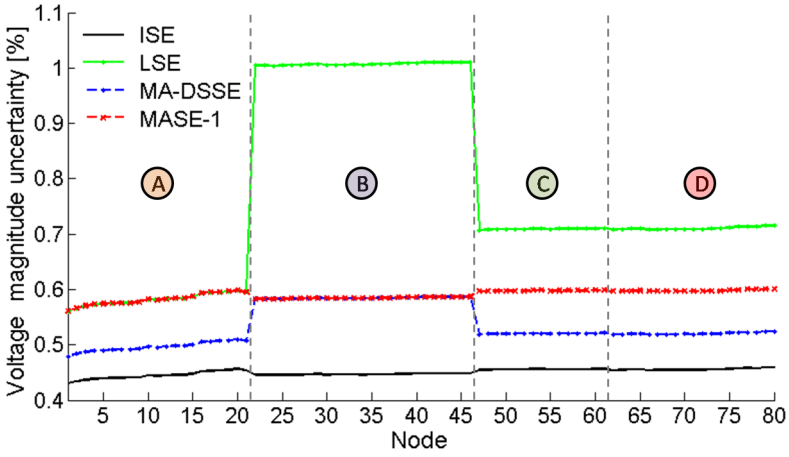

Figure 6.9: Expanded uncertainty for the voltage magnitude estimation in case of additional measurement points with traditional measurements

through the multi-area approaches. In this scenario, however, significant differences can be found depending on the design of the second step. In particular, the MASE-1 approach clearly shows its limits on the refinement of the estimation results. As evident from Fig. 6.9, the voltage correction performed through this approach only allows propagating the uncertainty level of the areas with the better local estimations towards the adjoining zones. In this case, since the LSE in area A is the best one, its uncertainty level can be spread to all the sub-networks (all the other areas are adjacent to area A). However, no improvements can be obtained in area A. With the proposed MA-DSSE technique, instead, the use of a second step including the information provided by the adjacent areas allows refining the estimation results in all the zones. In particular, it can be observed that the estimation of area A can be significantly improved, since the second step allows integrating the useful information provided by areas C and D. In the same way, areas C and D can refine their estimations exploiting the estimation coming from area A and D or C (depending on the case). Instead, as for area B, it should be noted that the final uncertainty level is higher than the other zones because this sub-network cannot integrate the voltage information provided by areas C and D. Similar results and considerations also hold for the case of measurement points based on PMUs.

As for the estimation of the other electrical quantities, considerations similar to those reported for the previous measurement scenario can be done. The estimation of the voltage angles has to be differentiated depending on the presence of traditional or synchronized measurements. In the case of traditional measurements, the estimation on the whole grid, obtained by shifting the voltage angle estimations in areas B, C and D so to consider the slack bus of area A (node 150) as unique reference, leads to very similar results for all the monitored estimators, with estimation

uncertainties lower than 2 mrad for all the buses. In case of PMU measurements, instead, the voltage angle estimations referred to the UTC time exhibit a trend of the uncertainty levels analogous to the one shown in Fig. 6.9 for the voltage magnitudes. However, if the phase-angle differences with respect to the slack bus in node 150 are computed, as it happens for the conventional measurements, even in this case the estimation results are very close for all the estimators, with estimation uncertainties lower than 1.5 mrad for all the nodes. As for the current estimations, again, the same considerations made for the previous tests with the starting measurement configuration can be done. In fact, the local impact of the flow measurements and the already accurate monitoring of the incoming and outgoing flows of each area lead to estimations very similar to those provided by the ISE since the first step of the multi-area estimation.

Since important differences can be found for the estimations of the voltage magnitudes, an additional test has been carried out to confirm the different behaviour of the multi-area approaches when considering the presence of multiple measurement points. To this purpose, a possible future scenario with an enhanced measurement system has been taken into account. With respect to the measurement configuration considered in the previous test, additional measurement points have been placed in nodes 25, 42, 48 (area B) and 91 (area C). Summarizing, in this augmented measurement system, four measurement points are present in area B, three are in areas A and C, and two are in area D.

Focusing on the results obtained for the voltage magnitude estimations, Figs. 6.10 and 6.11 show the uncertainty levels obtained when considering traditional or syncrophasor measurements, respectively. As it can be observed, the ISE provides the best accuracy performance, while the results associated to the LSEs are significantly less accurate and strictly dependent on the number of measurement points available on each sub-network. As for the multi-area approaches, shown results confirm the considerations highlighted in the previous tests. The MASE-1 method allows propagating the uncertainties of the best LSEs to the adjoining zones. In particular, in this scenario, the highest accuracy of area B can be propagated to area A, while the LSE in area D can be enhanced exploiting the more accurate estimation coming from area A or C. However, large improvements can be obtained by using the proposed MA-DSSE method. In fact, the integration of the information provided by the adjoining areas leads to significant enhancements for the estimation accuracy of all the areas. In particular, in this case, it is interesting to observe that area A, even if it does not have the largest number of measurement points, becomes the most accurate sub-network thanks to the acquisition of the information coming from all the other zones. This clearly demonstrates the beneficial effect brought by the estimations of the neighboring zones included in the second step of the proposed MA-DSSE approach.

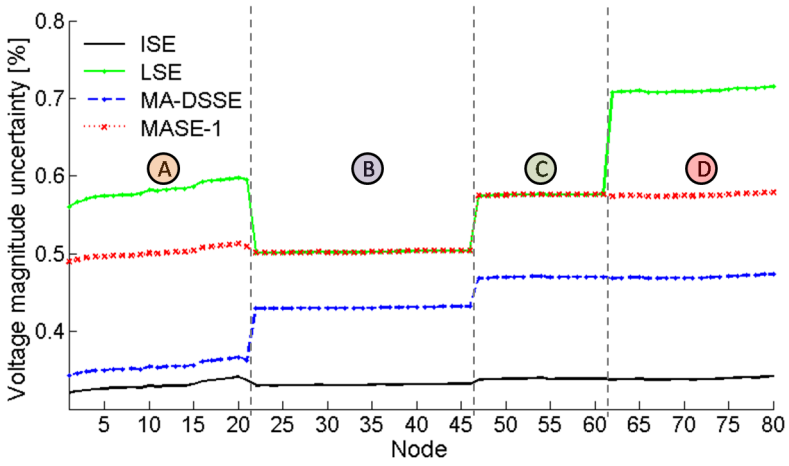

Figure 6.10: Expanded uncertainty for the voltage magnitude estimation in case of augmented measurement system with traditional measurements

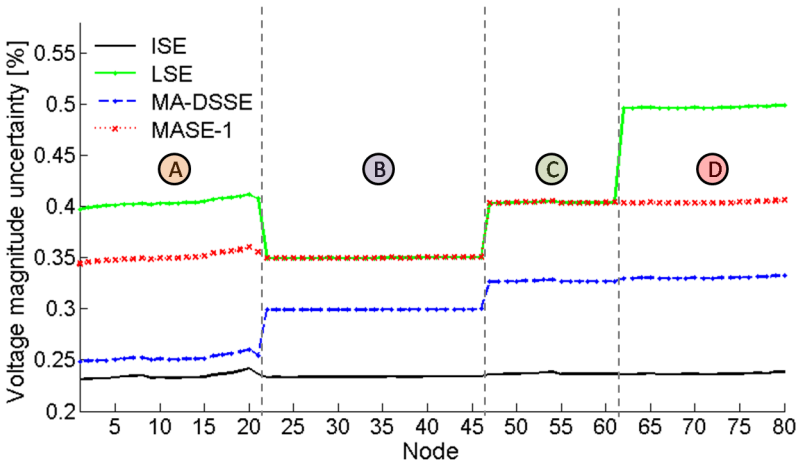

Figure 6.11: Expanded uncertainty for the voltage magnitude estimation in case of augmented measurement system with synchronized measurements

6.6 Final discussion

The development of suitable multi-area approaches is almost a mandatory task in distribution systems, given the very large number of nodes present in these networks and the need to consider three-phase models of the system. Nevertheless, the design of multi-area techniques for the distribution level is particularly challenging, mainly because of the scarcity of measurement devices usually available in these grids. In spite of this issue, the design of the multi-area method should be able to fulfil

the desired requirements of accuracy, speed and efficiency, while keeping low the computational burden and the communication costs.

In this Chapter, a multi-area state estimation algorithm taking into account the main features of the distribution networks, and thus tailored to these systems, has been presented. The proposed MA-DSSE algorithm is designed to allow a decentralized scheme of the architecture and to distribute, in this way, the processing, storage and communication requirements. Several tests have been performed to assess the goodness of the proposed method. Simulation results show that the two-step formulation of the MA-DSSE algorithm allows a significant enhancement of the voltage magnitude estimations with respect to the results given by the local estimations. On the contrary, instead, the voltage magnitude estimations provided by the MA-DSSE are in general worse than those achievable through the estimation on the whole network; however, this an expected cost to be paid for speeding up the estimation process (the execution times resulting for the MA-DSSE, in the proposed test cases, are about five times smaller than those obtainable through the ISE). Moreover, the particular configuration chosen for the measurement system and the multi-area partition allows achieving optimum results, similar to those provided by the ISE, for the estimations of currents (both in magnitude and angle) and voltage angle differences.

As described also in the other Chapters of this thesis, important enhancements on the accuracy performance can be obtained by considering a proper model of the measurements used in the estimation algorithms. In this case, the focus has been on the modeling of the equivalent measurements provided as input to the second-step estimation process. The developed analysis showed that, because of the chosen partition of the network, correlations can arise between the voltage estimations provided by different sub-networks. As confirmed by the performed tests, proper consideration of these correlations in the second-step of the MA-DSSE algorithm allows enhancing the final accuracy of the estimation results. Moreover, the developed analysis showed that the computation of these covariance terms does not require the exchange of additional data between adjacent areas. Thus, existing correlations can be duly considered in the MA-DSSE measurement model without any increase in the communication costs.

In general, several different multi-area approaches can be conceived. The technique here proposed provides, however, a good trade-off among the requirements of reducing the size of the DSSE problem, speeding up the estimation process, and providing estimation results as accurate as possible with only minimum communication costs and reduced computational burden.

Conclusions

The changes occurring in electrical systems, due to technical and economic reasons, and the requirements of a reliable and efficient delivery of the power supply to the customers demand a smarter management of the current grids at all the levels. In particular, the distribution level, until now managed without a detailed monitoring of its operating conditions, requires significant reinforcements, in terms of both measurement infrastructure and control functionalities, to deal with the changes in act. In this context, Distribution System State Estimation tools play a key role, since they allow the estimation of the operating conditions of the distribution grid, representing the essential link between the measurements gathered from the field and the control functions envisaged in future Distribution Management Systems.

In this thesis, the focus has been on the development of appropriate procedures to accurately perform DSSE. Several goals have been pursued. First of all, a DSSE algorithm specifically conceived for the distribution systems and tailored to the features of these networks has been designed. The proposed estimator allows the proper processing of all the types of measurement, including both conventional measurements and new generation synchrophasors provided by Phasor Measurement Units. Particular attention has been paid to the measurement model to be used within the DSSE algorithm, since its implementation can strongly affect the accuracy achievable in the estimation results. Moreover, a simple method to handle the equality constraints, well suited to the proposed estimator, has been presented to improve its computational efficiency. The proposed estimator has been critically analyzed and compared to other approaches available in the literature, in order to highlight strengths and weaknesses of the conceived solution.

In the second part of the thesis, the problem of DSSE has been analyzed from a wider perspective, aiming at highlighting the impact of different measurement aspects on the estimation results. The impact of measurement type and placement on the estimation accuracy of the different electrical quantities has been deeply investigated, supporting the empirical results through a detailed mathematical analysis. Such study can provide important guidelines for the choice of the measurement infrastructure to be deployed in future distribution systems in order to achieve specific accuracy targets for the estimation of the different electrical quantities. The possi-

bility to enhance the estimation accuracy by properly considering the measurement correlations has also been investigated. Developed analysis shows that different sources of correlation can exist in the measurements used as input to the DSSE algorithm. Performed simulations prove that the inclusion of these correlations in the DSSE model can lead to significant benefits on the estimation accuracy.

Finally, a possible decentralized multi-area architecture, designed to handle large distribution networks, has been proposed. Such a solution has been conceived duly taking into account the opposite requirements of accuracy, computational efficiency and low communication costs desirable in realistic scenarios. Even in this case, particular attention has been focused on the proper modeling of the measurements in order to achieve estimation results as accurate as possible. To this purpose, a mathematical analysis has been developed to assess the correlations arising in the proposed multi-area approach. Test results confirm the validity of the developed analysis and, above all, prove the importance of a proper consideration of all the measurement aspects for enhancing the accuracy of the estimations.

In conclusion, in this thesis, the problem of state estimation in future distribution system has been deeply analyzed, focusing in particular on the issues related to the measurement modeling and processing. The analysis and the results presented in this thesis shows how the achievement of a really smart management and control of future distribution grids (as expected in the Smart Grid scenario) is strictly dependent on the smart deployment, processing and management of the measurements in the network.

Appendix A

Jacobian of BC-DSSE

A.1 Jacobian of original BC-DSSE

The Jacobian of the original BC-DSSE includes all the derivatives of the traditional measurements with respect to the real and imaginary components of the branch currents. Following the same scheme used in Section 1.4.2 for the measurement functions, the relationships associated to the different Jacobian terms are here reported.

- **Active and reactive power flow**

$$\frac{\partial h^{eq}_{i^r_{l\phi}}}{\partial i^r_{j\psi}} = \begin{cases} 0 & \text{for phase } \psi \neq \phi \\ 0 & \text{for phase } \psi = \phi \text{ and branch } j \neq l \\ \alpha & \text{for phase } \psi = \phi \text{ and branch } j = l \end{cases} \tag{A.1}$$

$$\frac{\partial h^{eq}_{i^r_{l\phi}}}{\partial i^x_{j\psi}} = 0 \qquad \text{for each phase } \psi \text{ and branch } j \tag{A.2}$$

$$\frac{\partial h^{eq}_{i^x_{l\phi}}}{\partial i^r_{j\psi}} = 0 \qquad \text{for each phase } \psi \text{ and branch } j \tag{A.3}$$

$$\frac{\partial h^{eq}_{i^x_{l\phi}}}{\partial i^x_{j\psi}} = \begin{cases} 0 & \text{for phase } \psi \neq \phi \\ 0 & \text{for phase } \psi = \phi \text{ and branch } j \neq l \\ \alpha & \text{for phase } \psi = \phi \text{ and branch } j = l \end{cases} \tag{A.4}$$

where α is $+1$ or -1 depending on the direction of the measured power with respect to the conventional direction assumed for the branch current.

- **Active and reactive power injection**

$$\frac{\partial h^{eq}_{i^r_{inj,i\phi}}}{\partial i^r_{j\psi}} = \begin{cases} 0 & \text{for phase } \psi \neq \phi \\ 0 & \text{for phase } \psi = \phi \text{ and branch } j \text{ not converging in node } i \\ \alpha & \text{for phase } \psi = \phi \text{ and branch } j \text{ incoming in node } i \\ -\alpha & \text{for phase } \psi = \phi \text{ and branch } j \text{ outgoing from node } i \end{cases} \tag{A.5}$$

$$\frac{\partial h^{eq}_{i^r_{inj,i\phi}}}{\partial i^x_{j\psi}} = 0 \qquad \text{for each phase } \psi \text{ and branch } j \tag{A.6}$$

$$\frac{\partial h^{eq}_{i^x_{inj,i\phi}}}{\partial i^r_{j\psi}} = 0 \qquad \text{for each phase } \psi \text{ and branch } j \tag{A.7}$$

$$\frac{\partial h^{eq}_{i^x_{inj,i\phi}}}{\partial i^x_{j\psi}} = \begin{cases} 0 & \text{for phase } \psi \neq \phi \\ 0 & \text{for phase } \psi = \phi \text{ and branch } j \text{ not converging in node } i \\ \alpha & \text{for phase } \psi = \phi \text{ and branch } j \text{ incoming in node } i \\ -\alpha & \text{for phase } \psi = \phi \text{ and branch } j \text{ outgoing from node } i \end{cases} \tag{A.8}$$

where α is $+1$ for positive powers drawn by loads and -1 for positive power generations.

- **Current magnitude**

$$\frac{\partial h_{I_{l\phi}}}{\partial i^r_{j\psi}} = \begin{cases} 0 & \text{for phase } \psi \neq \phi \\ 0 & \text{for phase } \psi = \phi \text{ and branch } j \neq l \\ \cos\theta_{l\phi} & \text{for phase } \psi = \phi \text{ and branch } j = l \end{cases} \tag{A.9}$$

$$\frac{\partial h_{I_{l\phi}}}{\partial i^x_{j\psi}} = \begin{cases} 0 & \text{for phase } \psi \neq \phi \\ 0 & \text{for phase } \psi = \phi \text{ and branch } j \neq l \\ \sin\theta_{l\phi} & \text{for phase } \psi = \phi \text{ and branch } j = l \end{cases} \tag{A.10}$$

where $\theta_{l\phi}$ is the angle of the current in branch l and for phase ϕ.

- **Voltage magnitude**

Indicating with Γ the set of branches linking the chosen slack bus to the node i where there is the voltage measurement, it is:

$$\frac{\partial h_{V_{i\phi}}}{\partial i^r_{j\psi}} = \begin{cases} 0 & \text{for } j \notin \Gamma \\ -r^{\phi\phi}_j \cos\delta_{i\phi} - x^{\phi\phi}_j \sin\delta_{i\phi} & \text{for phase } \psi = \phi \text{ and branch } j \in \Gamma \\ -r^{\phi\psi}_j \cos\delta_{i\phi} - x^{\phi\psi}_j \sin\delta_{i\phi} & \text{for phase } \psi \neq \phi \text{ and branch } j \in \Gamma \end{cases} \tag{A.11}$$

$$\frac{\partial h_{V_{i\phi}}}{\partial i^x_{j\psi}} = \begin{cases} 0 & \text{for } j \notin \Gamma \\ x_j^{\phi\phi}\cos\delta_{i\phi} - r_j^{\phi\phi}\sin\delta_{i\phi} & \text{for phase } \psi = \phi \text{ and branch } j \in \Gamma \\ x_j^{\phi\psi}\cos\delta_{i\phi} - r_j^{\phi\psi}\sin\delta_{i\phi} & \text{for phase } \psi \neq \phi \text{ and branch } j \in \Gamma \end{cases} \tag{A.12}$$

where $r_j^{\phi\phi}$ and $x_j^{\phi\phi}$ are the real and the imaginary part of the self-impedance of branch j; $r_j^{\phi\psi}$ and $x_j^{\phi\psi}$ are the real and the imaginary part of the mutual impedance in branch j between phases ϕ and ψ; $\delta_{i\phi}$ is the voltage angle of node i for phase ϕ (where there is the considered voltage measurement).

A.2 Additional terms for traditional measurements

Because of the inclusion of the slack bus voltage in the state vector of the BC-DSSE model, the resulting derivative terms with respect to the voltage state variable must be computed. Looking at the measurement functions reported in Section 1.4.2, it is easy to observe that only the voltage magnitude measurements depend on the slack bus voltage state. As a result, power measurements (both the equivalent currents associated to power injections and branch power flows) and current magnitude measurements have derivative terms with respect to the voltage state variable equal to zero. As for the voltage magnitude measurements, considering with i the node where the voltage measurement is installed, and with $V_{s\psi}$ the slack bus voltage magnitude included in the state vector for phase ψ, it is:

$$\frac{\partial h_{V_{i\phi}}}{\partial V_{s\psi}} = \begin{cases} \cos(\delta_{1\phi} - \delta_{i\phi}) & \text{if phase } \phi = \psi \\ 0 & \text{if phase } \phi \neq \psi \end{cases} \tag{A.13}$$

A.3 Jacobian for the mesh virtual measurements

The Jacobian sub-matrix for the mesh constraints has to be computed when such constraints are included in the BC-DSSE model as virtual measurements. Indicating with Ψ the set of branches involved in the considered mesh, it is:

$$\frac{\partial h^r_{mesh}}{\partial V_{s\psi}} = \quad 0 \qquad \text{for each phase } \psi \tag{A.14}$$

$$\frac{\partial h^r_{mesh}}{\partial i^r_{j\psi}} = \begin{cases} 0 & \text{for } j \notin \Psi \\ \alpha_j r_j^{\phi\phi} & \text{for phase } \psi = \phi \text{ and branch } j \in \Psi \\ \alpha_j r_j^{\phi\psi} & \text{for phase } \psi \neq \phi \text{ and branch } j \in \Psi \end{cases} \tag{A.15}$$

$$\frac{\partial h^r_{mesh}}{\partial i^x_{j\psi}} = \begin{cases} 0 & \text{for } j \notin \Psi \\ -\alpha_j x_j^{\phi\phi} & \text{for phase } \psi = \phi \text{ and branch } j \in \Psi \\ -\alpha_j x_j^{\phi\psi} & \text{for phase } \psi \neq \phi \text{ and branch } j \in \Psi \end{cases} \tag{A.16}$$

$$\frac{\partial h^x_{mesh}}{\partial i^r_{j\psi}} = \begin{cases} 0 & \text{for } j \notin \Psi \\ \alpha_j x_j^{\phi\phi} & \text{for phase } \psi = \phi \text{ and branch } j \in \Psi \\ \alpha_j x_j^{\phi\psi} & \text{for phase } \psi \neq \phi \text{ and branch } j \in \Psi \end{cases} \tag{A.17}$$

$$\frac{\partial h^x_{mesh}}{\partial i^x_{j\psi}} = \begin{cases} 0 & \text{for } j \notin \Psi \\ \alpha_j r_j^{\phi\phi} & \text{for phase } \psi = \phi \text{ and branch } j \in \Psi \\ \alpha_j r_j^{\phi\psi} & \text{for phase } \psi \neq \phi \text{ and branch } j \in \Psi \end{cases} \tag{A.18}$$

where $r_j^{\phi\phi}$, $x_j^{\phi\phi}$, $r_j^{\phi\psi}$ and $x_j^{\phi\psi}$ have the same meaning as in the previous case for the voltage magnitude measurements, and α_j is $+1$ or -1 depending on the direction of the mesh in branch j with respect to the conventional direction assumed for the corresponding branch current.

A.4 Jacobian in case of PMU measurements

Considering the inclusion of both the real and the imaginary components of the slack bus voltage when PMU measurements are available on the field, the following derivative terms can be found for the current and voltage phasors.

- **Current phasors - real component**

  Considering the measurement of the current phasor on the phase ϕ of the generic branch l, it is:

$$\frac{\partial h_{i^r_{l\phi}}}{\partial v^r_{s\psi}} = 0 \qquad \text{for each phase } \psi \tag{A.19}$$

$$\frac{\partial h_{i^r_{l\phi}}}{\partial v^x_{s\psi}} = 0 \qquad \text{for each phase } \psi \tag{A.20}$$

$$\frac{\partial h_{i^r_{l\phi}}}{\partial i^r_{j\psi}} = \begin{cases} 0 & \text{for phase } \psi \neq \phi \\ 0 & \text{for phase } \psi = \phi \text{ and branch } j \neq l \\ \alpha & \text{for phase } \psi = \phi \text{ and branch } j = l \end{cases} \tag{A.21}$$

$$\frac{\partial h_{i^r_{l\phi}}}{\partial i^x_{j\psi}} = 0 \qquad \text{for each phase } \psi \text{ and branch } j \tag{A.22}$$

  where α is $+1$ or -1 depending on the direction of the measured current with respect to the conventional verse assumed for the branch current.

- **Current phasors - imaginary component**

  Considering the measurement of the current phasor on the phase ϕ of the generic branch l, it is:

$$\frac{\partial h_{i^x_{l\phi}}}{\partial v^r_{s\psi}} = 0 \qquad \text{for each phase } \psi \tag{A.23}$$

$$\frac{\partial h_{i^x_{l\phi}}}{\partial v^x_{s\psi}} = 0 \qquad \text{for each phase } \psi \tag{A.24}$$

$$\frac{\partial h_{i^x_{l\phi}}}{\partial i^r_{j\psi}} = 0 \qquad \text{for each phase } \psi \text{ and branch } j \tag{A.25}$$

$$\frac{\partial h_{i^x_{l\phi}}}{\partial i^x_{j\psi}} = \begin{cases} 0 & \text{for phase } \psi \neq \phi \\ 0 & \text{for phase } \psi = \phi \text{ and branch } j \neq l \\ \alpha & \text{for phase } \psi = \phi \text{ and branch } j = l \end{cases} \tag{A.26}$$

  where α is $+1$ or -1 depending on the direction of the measured current with respect to the conventional verse assumed for the branch current.

- **Voltage phasors - real component**

  Indicating with Γ the set of branches linking the chosen slack bus to the node i where there is the voltage measurement, it is:

$$\frac{\partial h_{v^r_{l\phi}}}{\partial v^r_{s\psi}} = \begin{cases} 1 & \text{for phase } \phi = \psi \\ 0 & \text{for phase } \phi \neq \psi \end{cases} \tag{A.27}$$

$$\frac{\partial h_{v^r_{l\phi}}}{\partial v^x_{s\psi}} = \quad 0 \qquad \text{for each phase } \psi \tag{A.28}$$

$$\frac{\partial h_{v^r_{i\phi}}}{\partial i^r_{j\psi}} = \begin{cases} 0 & \text{for } j \notin \Gamma \\ -r^{\phi\phi}_j & \text{for phase } \psi = \phi \text{ and branch } j \in \Gamma \\ -r^{\phi\psi}_j & \text{for phase } \psi \neq \phi \text{ and branch } j \in \Gamma \end{cases} \tag{A.29}$$

$$\frac{\partial h_{v^r_{i\phi}}}{\partial i^x_{j\psi}} = \begin{cases} 0 & \text{for } j \notin \Gamma \\ x^{\phi\phi}_j & \text{for phase } \psi = \phi \text{ and branch } j \in \Gamma \\ x^{\phi\psi}_j & \text{for phase } \psi \neq \phi \text{ and branch } j \in \Gamma \end{cases} \tag{A.30}$$

  where $r^{\phi\phi}_j$ and $x^{\phi\phi}_j$ are the real and the imaginary parts of the self-impedance of branch j, and $r^{\phi\psi}_j$ and $x^{\phi\psi}_j$ are the real and the imaginary parts of the mutual impedance in branch j between phases ϕ and ψ.

- **Voltage phasors - imaginary component**

  Indicating with Γ the set of branches linking the chosen slack bus to the node i where there is the voltage measurement, it is:

$$\frac{\partial h_{v^x_{l\phi}}}{\partial v^r_{s\psi}} = \quad 0 \qquad \text{for each phase } \psi \tag{A.31}$$

$$\frac{\partial h_{v^x_{l\phi}}}{\partial v^x_{s\psi}} = \begin{cases} 1 & \text{for phase } \phi = \psi \\ 0 & \text{for phase } \phi \neq \psi \end{cases} \tag{A.32}$$

$$\frac{\partial h_{v^x_{i\phi}}}{\partial i^r_{j\psi}} = \begin{cases} 0 & \text{for } j \notin \Gamma \\ -x_j^{\phi\phi} & \text{for phase } \psi = \phi \text{ and branch } j \in \Gamma \\ -x_j^{\phi\psi} & \text{for phase } \psi \neq \phi \text{ and branch } j \in \Gamma \end{cases} \tag{A.33}$$

$$\frac{\partial h_{v^x_{i\phi}}}{\partial i^x_{j\psi}} = \begin{cases} 0 & \text{for } j \notin \Gamma \\ -r_j^{\phi\phi} & \text{for phase } \psi = \phi \text{ and branch } j \in \Gamma \\ -r_j^{\phi\psi} & \text{for phase } \psi \neq \phi \text{ and branch } j \in \Gamma \end{cases} \tag{A.34}$$

  where $r_j^{\phi\phi}$ and $x_j^{\phi\phi}$ are the real and the imaginary parts of the self-impedance of branch j, and $r_j^{\phi\psi}$ and $x_j^{\phi\psi}$ are the real and the imaginary parts of the mutual impedance in branch j between phases ϕ and ψ.

It is important to highlight that traditional and PMU measurements can also exist simultaneously. In this case, the presence of PMUs implies the use of the extended state vector with the real and imaginary slack bus voltage. Thus, even for the conventional measurements, it is necessary to compute the Jacobian terms corresponding to the derivatives with respect to real and imaginary slack bus voltage. As seen in Appendix A.2, power and current measurements do not depend on the voltage state, therefore, their derivatives with respect to the new state variables are null. The only modification is thus for the voltage magnitude measurements, which have the following derivative terms with respect to the slack bus voltage state (for measurement on the phase ϕ of the generic node i):

$$\frac{\partial h_{V_{i\phi}}}{\partial v^r_{s\psi}} = \begin{cases} \cos(\delta_{i\phi}) & \text{if phase } \phi = \psi \\ 0 & \text{if phase } \phi \neq \psi \end{cases} \tag{A.35}$$

$$\frac{\partial h_{V_{i\phi}}}{\partial v^x_{s\psi}} = \begin{cases} \sin(\delta_{i\phi}) & \text{if phase } \phi = \psi \\ 0 & \text{if phase } \phi \neq \psi \end{cases} \tag{A.36}$$

Bibliography

[1] F. C. Schweppe and J. Wildes, "Power system static-state estimation, part I: Exact model," *Power Apparatus and Systems, IEEE Transactions on*, vol. PAS-89, no. 1, pp. 120–125, Jan. 1970.

[2] F. C. Schweppe and D. B. Rom, "Power system static-state estimation, part II: Approximate model," *Power Apparatus and Systems, IEEE Transactions on*, vol. PAS-89, no. 1, pp. 125–130, Jan. 1970.

[3] F. C. Schweppe, "Power system static-state estimation, part III: Implementation," *Power Apparatus and Systems, IEEE Transactions on*, vol. PAS-89, no. 1, pp. 130–135, Jan. 1970.

[4] A. Abur and A. Gomez-Exposito, *Power System State Estimation. Theory and Implementation.* Marcel Dekker, New York, 2004.

[5] A. Monticelli, "Electric power system state estimation," *Proceedings of the IEEE*, vol. 88, no. 2, pp. 262–282, Feb. 2000.

[6] G. T. Heydt, "The next generation of power distribution systems," *Smart Grid, IEEE Transactions on*, vol. 1, no. 3, pp. 225–235, Dec. 2010.

[7] J. Mutale, "Benefits of active management of distribution networks with distributed generation," in *Power Systems Conference and Exposition, 2006. PSCE '06. 2006 IEEE PES*, Oct. 2006, pp. 601–606.

[8] L. Pieltain Fernandez, T. G. S. Roman, R. Cossent, C. M. Domingo, and P. Frias, "Assessment of the impact of plug-in electric vehicles on distribution networks," *Power Systems, IEEE Transactions on*, vol. 26, no. 1, pp. 206–213, Feb. 2011.

[9] K. Clement-Nyns, E. Haesen, and J. Driesen, "The impact of charging plug-in hybrid electric vehicles on a residential distribution grid," *Power Systems, IEEE Transactions on*, vol. 25, no. 1, pp. 371–380, Feb. 2010.

[10] S. Mocci, N. Natale, S. Ruggeri, and F. Pilo, "Multi-agent control system for increasing hosting capacity in active distribution networks with EV," in *Energy Conference (ENERGYCON), 2014 IEEE International*, May 2014, pp. 1409–1416.

[11] M. Farrokhifar, S. Grillo, and E. Tironi, "Loss minimization in medium voltage distribution grids by optimal management of energy storage devices," in *PowerTech (POWERTECH), 2013 IEEE Grenoble*, Jun. 2013, pp. 1–5.

[12] P. Palensky and D. Dietrich, "Demand side management: Demand response, intelligent energy systems, and smart loads," *Industrial Informatics, IEEE Transactions on*, vol. 7, no. 3, pp. 381–388, Aug. 2011.

[13] G. Celli, P. A. Pegoraro, F. Pilo, G. Pisano, and S. Sulis, "DMS cyber-physical simulation for assessing the impact of state estimation and communication media in smart grid operation," *Power Systems, IEEE Transactions on*, vol. 29, no. 5, pp. 2436–2446, Sep. 2014.

[14] D. Della Giustina, M. Pau, P. A. Pegoraro, F. Ponci, and S. Sulis, "Electrical distribution system state estimation: measurement issues and challenges," *Instrumentation Measurement Magazine, IEEE*, vol. 17, no. 6, pp. 36–42, Dec. 2014.

[15] W. H. Kersting, *Distribution System Modeling and Analysis*. Boca Raton, Florida, 2001.

[16] W. H. Kersting and R. K. Green, "The application of Carson's equation to the steady-state analysis of distribution feeders," in *Power Systems Conference and Exposition (PSCE), 2011 IEEE/PES*, Mar. 2011, pp. 1–6.

[17] E. Manitsas, R. Singh, B. C. Pal, and G. Strbac, "Distribution system state estimation using an artificial neural network approach for pseudo measurement modeling," *Power Systems, IEEE Transactions on*, vol. 27, no. 4, pp. 1888–1896, Nov. 2012.

[18] R. Singh, B. C. Pal, and R. A. Jabr, "Distribution system state estimation through gaussian mixture model of the load as pseudo-measurement," *Generation, Transmission Distribution, IET*, vol. 4, no. 1, pp. 50–59, Jan. 2010.

[19] T. Schlosser, A. Angioni, F. Ponci, and A. Monti, "Impact of pseudo-measurements from new load profiles on state estimation in distribution grids," in *Instrumentation and Measurement Technology Conference (I2MTC) Proceedings, 2014 IEEE International*, May 2014, pp. 625–630.

[20] M. R. Irving, R. C. Owen, and M. J. H. Sterling, "Power-system state estimation using linear programming," *Electrical Engineers, Proceedings of the Institution of*, vol. 125, no. 9, pp. 879–885, Sep. 1978.

[21] A. Garcia, A. Monticelli, and P. Abreu, "Fast decoupled state estimation and bad data processing," *Power Apparatus and Systems, IEEE Transactions on*, vol. PAS-98, no. 5, pp. 1645–1652, Sep. 1979.

[22] M. K. Celik and A. Abur, "A robust WLAV state estimator using transformations," *Power Systems, IEEE Transactions on*, vol. 7, no. 1, pp. 106–113, Feb. 1992.

[23] A. Abur and M. K. Celik, "Least absolute value state estimation with equality and inequality constraints," *Power Systems, IEEE Transactions on*, vol. 8, no. 2, pp. 680–686, May 1993.

[24] H. Singh and F. L. Alvarado, "Weighted least absolute value state estimation using interior point methods," *Power Systems, IEEE Transactions on*, vol. 9, no. 3, pp. 1478–1484, Aug. 1994.

[25] R. Baldick, K. A. Clements, Z. Pinjo-Dzigal, and P. W. Davis, "Implementing nonquadratic objective functions for state estimation and bad data rejection," *Power Systems, IEEE Transactions on*, vol. 12, no. 1, pp. 376–382, Feb. 1997.

[26] R. Singh, B. C. Pal, and R. A. Jabr, "Choice of estimator for distribution system state estimation," *Generation, Transmission Distribution, IET*, vol. 3, no. 7, pp. 666–678, Jul. 2009.

[27] I. Roytelman and S. M. Shahidehpour, "State estimation for electric power distribution systems in quasi real-time conditions," *Power Delivery, IEEE Transactions on*, vol. 8, no. 4, pp. 2009–2015, Oct. 1993.

[28] M. E. Baran and A. W. Kelley, "State estimation for real-time monitoring of distribution systems," *Power Systems, IEEE Transactions on*, vol. 9, no. 3, pp. 1601–1609, Aug. 1994.

[29] K. Li, "State estimation for power distribution system and measurement impacts," *Power Systems, IEEE Transactions on*, vol. 11, no. 2, pp. 911–916, May 1996.

[30] W. M. Lin and J. H. Teng, "Distribution fast decoupled state estimation by measurement pairing," *Generation, Transmission and Distribution, IEE Proceedings-*, vol. 143, no. 1, pp. 43–48, Jan. 1996.

[31] M. E. Baran and A. W. Kelley, "A branch-current-based state estimation method for distribution systems," *Power Systems, IEEE Transactions on*, vol. 10, no. 1, pp. 483–491, Feb. 1995.

[32] W. M. Lin, J. H. Teng, and S. J. Chen, "A highly efficient algorithm in treating current measurements for the branch-current-based distribution state estimation," *Power Delivery, IEEE Transactions on*, vol. 16, no. 3, pp. 433–439, Jul. 2001.

[33] M. E. Baran, J. Jung, and T. E. McDermott, "Including voltage measurements in branch current state estimation for distribution systems," in *Power Energy Society General Meeting, 2009. PES '09. IEEE*, Jul. 2009, pp. 1–5.

[34] J. H. Teng, "Using voltage measurements to improve the results of branch-current-based state estimators for distribution systems," *Generation, Transmission and Distribution, IEE Proceedings-*, vol. 149, no. 6, pp. 667–672, Nov. 2002.

[35] M. Pau, P. A. Pegoraro, and S. Sulis, "Branch current state estimator for distribution system based on synchronized measurements," in *Applied Measurements for Power Systems (AMPS), 2012 IEEE International Workshop on*, Sep. 2012, pp. 1–6.

[36] M. Pau, P. A. Pegoraro, and S. Sulis, "Efficient branch-current-based distribution system state estimation including synchronized measurements," *Instrumentation and Measurement, IEEE Transactions on*, vol. 62, no. 9, pp. 2419–2429, Sep. 2013.

[37] A. R. Ahmadi and T. C. Green, "Optimal power flow for autonomous regional active network management system," in *Power Energy Society General Meeting, 2009. PES '09. IEEE*, Jul. 2009, pp. 1–7.

[38] A. G. Phadke and J. S. Thorp, *Synchronized Phasor Measurements and Their Applications.* Springer Sciences, New York, 2008.

[39] J. A. de la Serna, "Dynamic phasor estimates for power system oscillations," *Instrumentation and Measurement, IEEE Transactions on*, vol. 56, no. 5, pp. 1648–1657, Oct. 2007.

[40] P. Castello, C. Muscas, and P. A. Pegoraro, "Performance comparison of algorithms for synchrophasors measurements under dynamic conditions," in *Applied Measurements for Power Systems (AMPS), 2011 IEEE International Workshop on*, Sep. 2011, pp. 25–30.

[41] G. Barchi, D. Macii, and D. Petri, "Synchrophasor estimators accuracy: A comparative analysis," *Instrumentation and Measurement, IEEE Transactions on*, vol. 62, no. 5, pp. 963–973, May 2013.

[42] P. Castello, J. Liu, C. Muscas, P. A. Pegoraro, F. Ponci, and A. Monti, "A fast and accurate PMU algorithm for P+M class measurement of synchrophasor and frequency," *Instrumentation and Measurement, IEEE Transactions on*, vol. 63, no. 12, pp. 2837–2845, Dec. 2014.

[43] S. Chakrabarti, E. Kyriakides, T. Bi, D. Cai, and V. Terzija, "Measurements get together," *Power and Energy Magazine, IEEE*, vol. 7, no. 1, pp. 41–49, Jan. 2009.

[44] J. De La Ree, V. Centeno, J. S. Thorp, and A. G. Phadke, "Synchronized phasor measurement applications in power systems," *Smart Grid, IEEE Transactions on*, vol. 1, no. 1, pp. 20–27, Jun. 2010.

[45] D. Novosel, K. Vu, V. Centeno, S. Skok, and M. Begovic, "Benefits of synchronized-measurement technology for power-grid applications," in *System Sciences, 2007. HICSS 2007. 40th Annual Hawaii International Conference on*, Jan. 2007, pp. 118–118.

[46] A. G. Phadke, J. S. Thorp, and K. J. Karimi, "State estimation with phasor measurements," *Power Engineering Review, IEEE*, vol. PER-6, no. 2, pp. 48–48, Feb. 1986.

[47] M. Zhou, V. A. Centeno, J. S. Thorp, and A. G. Phadke, "An alternative for including phasor measurements in state estimators," *Power Systems, IEEE Transactions on*, vol. 21, no. 4, pp. 1930–1937, Nov. 2006.

[48] G. Valverde, S. Chakrabarti, E. Kyriakides, and V. Terzija, "A constrained formulation for hybrid state estimation," *Power Systems, IEEE Transactions on*, vol. 26, no. 3, pp. 1102–1109, Aug. 2011.

[49] S. Chakrabarti, E. Kyriakides, G. Ledwich, and A. Ghosh, "Inclusion of PMU current phasor measurements in a power system state estimator," *Generation, Transmission Distribution, IET*, vol. 4, no. 10, pp. 1104–1115, Oct. 2010.

[50] J. Liu, J. Tang, F. Ponci, A. Monti, C. Muscas, and P. A. Pegoraro, "Trade-offs in PMU deployment for state estimation in active distribution grids," *Smart Grid, IEEE Transactions on*, vol. 3, no. 2, pp. 915–924, Jun. 2012.

[51] *IEEE Standard for Synchrophasor Measurements for Power Systems*, IEEE Std C37.118.1-2011 (Revision of IEEE Std C37.118-2005), Dec. 2011.

[52] J. Zhu and A. Abur, "Effect of phasor measurements on the choice of reference bus for state estimation," in *Power Engineering Society General Meeting, 2007. IEEE*, Jun. 2007, pp. 1–5.

[53] Model 1133A phasor measurement data sheet. [Online]. Available: http://www.arbiter.com/files/product-attachments/1133a.pdf

[54] W. M. Lin and J. H. Teng, "State estimation for distribution systems with zero-injection constraints," *Power Systems, IEEE Transactions on*, vol. 11, no. 1, pp. 518–524, Feb. 1996.

[55] A. Gjelsvik, S. Aam, and L. Holten, "Hachtel's augmented matrix method - a rapid method improving numerical stability in power system static state estimation," *Power Apparatus and Systems, IEEE Transactions on*, vol. PAS-104, no. 11, pp. 2987–2993, Nov. 1985.

[56] Y. Guo, W. Wu, B. Zhang, and H. Sun, "An efficient state estimation algorithm considering zero injection constraints," *Power Systems, IEEE Transactions on*, vol. 28, no. 3, pp. 2651–2659, Aug. 2013.

[57] C. Muscas, M. Pau, P. A. Pegoraro, and S. Sulis, "An efficient method to include equality constraints in branch current distribution system state estimation," *EURASIP Journal on Advances in Signal Processing*, accepted for publication.

[58] (2012) IEEE test feeder specifications. [Online]. Available: http://ewh.ieee.org/soc/pes/dsacom/testfeeders/

[59] C. N. Lu, J. H. Teng, and W. H. E. Liu, "Distribution system state estimation," *Power Systems, IEEE Transactions on*, vol. 10, no. 1, pp. 229–240, Feb. 1995.

[60] H. Wang and N. N. Schulz, "A revised branch current-based distribution system state estimation algorithm and meter placement impact," *Power Systems, IEEE Transactions on*, vol. 19, no. 1, pp. 207–213, Feb. 2004.

[61] M. Pau, P. A. Pegoraro, and S. Sulis, "WLS distribution system state estimator based on voltages or branch-currents: Accuracy and performance comparison," in *Instrumentation and Measurement Technology Conference (I2MTC), 2013 IEEE International*, May 2013, pp. 493–498.

[62] L. M. P. dos Santos, "Aperfeicoamento de um algoritmo de estimacao de estados para rede de distribuicao considerando grande penetracao de producao dispersa," Master's thesis, Faculdade de Engenharia da Universidade do Porto, Porto, Jun. 2008.

[63] G. D'Antona and M. Davoudi, "Effects of parameter and measurement uncertainties on the power system WLS state estimation," in *Instrumentation and Measurement Technology Conference (I2MTC), 2012 IEEE International*, May 2012, pp. 1015–1020.

[64] G. D'Antona and M. Davoudi, "Effect of phasor measurement unit on power state estimation considering parameters uncertainty," in *Applied Measurements for Power Systems (AMPS), 2012 IEEE International Workshop on*, Sep. 2012, pp. 1–5.

[65] P. A. Pegoraro and S. Sulis, "On the uncertainty evaluation in distribution system state estimation," in *Smart Measurements for Future Grids (SMFG), 2011 IEEE International Conference on*, Nov 2011, pp. 59–63.

[66] M. Asprou, E. Kyriakides, and M. Albu, "The effect of parameter and measurement uncertainties on hybrid state estimation," in *Power and Energy Society General Meeting, 2012 IEEE*, July 2012, pp. 1–8.

[67] M. Albu, E. Kyriakides, A. M. Dumitrescu, and I. M. Florea, "Analysis of distribution grids: State estimation using model uncertainties," in *Applied Measurements for Power Systems (AMPS), 2011 IEEE International Workshop on*, Sep. 2011, pp. 68–73.

[68] A. Shafiu, N. Jenkins, and G. Strbac, "Measurement location for state estimation of distribution networks with generation," *Generation, Transmission and Distribution, IEE Proceedings-*, vol. 152, no. 2, pp. 240–246, Mar. 2005.

[69] N. Nusrat, M. Irving, and G. Taylor, "Novel meter placement algorithm for enhanced accuracy of distribution system state estimation," in *Power and Energy Society General Meeting, 2012 IEEE*, Jul. 2012, pp. 1–8.

[70] R. Singh, B. C. Pal, and R. B. Vinter, "Measurement placement in distribution system state estimation," *Power Systems, IEEE Transactions on*, vol. 24, no. 2, pp. 668–675, May 2009.

[71] R. Singh, B. C. Pal, R. A. Jabr, and R. B. Vinter, "Meter placement for distribution system state estimation: An ordinal optimization approach," in *Power and Energy Society General Meeting, 2012 IEEE*, Jul. 2012, pp. 1–1.

[72] Y. Xiang, P. F. Ribeiro, and J. F. G. Cobben, "Optimization of state-estimator-based operation framework including measurement placement for medium voltage distribution grid," *Smart Grid, IEEE Transactions on*, vol. 5, no. 6, pp. 2929–2937, Nov. 2014.

[73] C. Muscas, F. Pilo, G. Pisano, and S. Sulis, "Optimal allocation of multichannel measurement devices for distribution state estimation," *Instrumentation and Measurement, IEEE Transactions on*, vol. 58, no. 6, pp. 1929–1937, Jun. 2009.

[74] P. A. Pegoraro and S. Sulis, "Robustness-oriented meter placement for distribution system state estimation in presence of network parameter uncertainty," *Instrumentation and Measurement, IEEE Transactions on*, vol. 62, no. 5, pp. 954–962, May 2013.

[75] P. A. Pegoraro, J. Tang, J. Liu, F. Ponci, A. Monti, and C. Muscas, "PMU and smart metering deployment for state estimation in active distribution grids," in *Energy Conference and Exhibition (ENERGYCON), 2012 IEEE International*, Sep. 2012, pp. 873–878.

[76] D. Echternacht, C. Linnemann, and A. Moser, "Optimized positioning of measurements in distribution grids," in *Innovative Smart Grid Technologies (ISGT Europe), 2012 3rd IEEE PES International Conference and Exhibition on*, Oct. 2012, pp. 1–7.

[77] P. Janssen, T. Sezi, and J. C. Maun, "Meter placement impact on distribution system state estimation," in *Electricity Distribution (CIRED 2013), 22nd International Conference and Exhibition on*, Jun. 2013, pp. 1–4.

[78] C. Muscas, S. Sulis, A. Angioni, F. Ponci, and A. Monti, "Impact of different uncertainty sources on a three-phase state estimator for distribution networks," *Instrumentation and Measurement, IEEE Transactions on*, vol. 63, no. 9, pp. 2200–2209, Sep. 2014.

[79] M. Pau, P. A. Pegoraro, S. Sulis, and C. Muscas, "Uncertainty sources affecting voltage profile in distribution system state estimation," in *Instrumentation and Measurement Technology Conference (I2MTC), 2015 IEEE International*, accepted for publication.

[80] K. S. Miller, "On the inverse of the sum of matrices," *Mathematics Magazine*, vol. 54, no. 2, pp. 67–72, Mar. 1981.

[81] C. D. Meyer, "Generalized inverse of block triangular matrices," *Journal on Applied Mathematics*, vol. 19, no. 4, pp. 741–750, Dec. 1970.

[82] C. Muscas, M. Pau, P. A. Pegoraro, and S. Sulis, "Smart electric energy measurements in power distribution grids," *Instrumentation Measurement Magazine, IEEE*, vol. 18, no. 1, pp. 17–21, Feb. 2015.

[83] A. Abur and A. Gomez-Exposito, "Detecting multiple solutions in state estimation in the presence of current magnitude measurements," *Power Systems, IEEE Transactions on*, vol. 12, no. 1, pp. 370–375, Feb. 1997.

[84] M. Asprou, E. Kyriakides, and M. Albu, "The effect of instrument transformer accuracy class on the WLS state estimator accuracy," in *Power and Energy Society General Meeting (PES), 2013 IEEE*, Jul. 2013, pp. 1–5.

[85] M. Asprou, E. Kyriakides, and M. Albu, "The effect of variable weights in a WLS state estimator considering instrument transformer uncertainties," *Instrumentation and Measurement, IEEE Transactions on*, vol. 63, no. 6, pp. 1484–1495, Jun. 2014.

[86] A. K. Ghosh, D. L. Lubkeman, M. J. Downey, and R. H. Jones, "Distribution circuit state estimation using a probabilistic approach," *Power Systems, IEEE Transactions on*, vol. 12, no. 1, pp. 45–51, Feb. 1997.

[87] J. M. Morales, L. Baringo, A. J. Conejo, and R. Minguez, "Probabilistic power flow with correlated wind sources," *Generation, Transmission Distribution, IET*, vol. 4, no. 5, pp. 641–651, May 2010.

[88] G. Valverde, A. T. Saric, and V. Terzija, "Stochastic monitoring of distribution networks including correlated input variables," *Power Systems, IEEE Transactions on*, vol. 28, no. 1, pp. 246–255, Feb. 2013.

[89] E. Caro, A. J. Conejo, and R. Minguez, "Power system state estimation considering measurement dependencies," *Power Systems, IEEE Transactions on*, vol. 24, no. 4, pp. 1875–1885, Nov. 2009.

[90] E. Caro and G. Valverde, "Impact of transformer correlations in state estimation using the unscented transformation," *Power Systems, IEEE Transactions on*, vol. 29, no. 1, pp. 368–376, Jan. 2014.

[91] Y. Chakhchoukh, V. Vittal, and G. T. Heydt, "PMU based state estimation by integrating correlation," *Power Systems, IEEE Transactions on*, vol. 29, no. 2, pp. 617–626, Mar. 2014.

[92] C. Muscas, M. Pau, P. A. Pegoraro, and S. Sulis, "Effects of measurements and pseudomeasurements correlation in distribution system state estimation," *Instrumentation and Measurement, IEEE Transactions on*, vol. 63, no. 12, pp. 2813–2823, Dec. 2014.

[93] "Evaluation of data - Guide to the expression of uncertainty in measurement," *JCGM 100:2008*, Sep. 2008.

[94] P. Castello, M. Lixia, C. Muscas, and P. A. Pegoraro, "Impact of the model on the accuracy of synchrophasor measurement," *Instrumentation and Measurement, IEEE Transactions on*, vol. 61, no. 8, pp. 2179–2188, Aug. 2012.

[95] *Instrument transformers - Part 1: Current transformers*, Int. Std. IEC 60044-1, 2003.

[96] *Instrument transformers - Part 2: Inductive voltage transformers*, Int. Std. IEC 60044-2, 2003.

[97] M. Pau, P. A. Pegoraro, and S. Sulis, "Effects of PMU measurements correlation on state estimation results," in *Energy Conference (ENERGYCON), 2014 IEEE International*, May 2014, pp. 420–425.

[98] C. Muscas, M. Pau, P. A. Pegoraro, and S. Sulis, "Impact of input data correlation on distribution system state estimation," in *Applied Measurements for Power Systems (AMPS), 2013 IEEE International Workshop on*, Sep. 2013, pp. 114–119.

[99] A. Gomez-Exposito, A. de la Villa Jaen, C. Gomez-Quiles, P. Rosseaux, and T. Van Cutsem, "A taxonomy of multi-area state estimation methods," *Electric Power Systems Research*, vol. 81, no. 4, pp. 1060–1069, Apr. 2011.

[100] T. Van Cutsem, J. L. Horward, and M. Ribbens-Pavella, "A two-level static state estimator for electric power systems," *Power Apparatus and Systems, IEEE Transactions on*, vol. PAS-100, no. 8, pp. 3722–3732, Aug. 1981.

[101] A. J. Conejo, S. de la Torre, and M. Canas, "An optimization approach to multiarea state estimation," *Power Systems, IEEE Transactions on*, vol. 22, no. 1, pp. 213–221, Feb. 2007.

[102] S. Iwamoto, M. Kusano, and V. H. Quintana, "Hierarchical state estimation using a fast rectangular-coordinate method," *Power Systems, IEEE Transactions on*, vol. 4, no. 3, pp. 870–880, Aug. 1989.

[103] G. N. Korres, "A distributed multiarea state estimation," *Power Systems, IEEE Transactions on*, vol. 26, no. 1, pp. 73–84, Feb. 2011.

[104] D. M. Falcao, F. F. Wu, and L. Murphy, "Parallel and distributed state estimation," *Power Systems, IEEE Transactions on*, vol. 10, no. 2, pp. 724–730, May 1995.

[105] R. Ebrahimian and R. Baldick, "State estimation distributed processing," *Power Systems, IEEE Transactions on*, vol. 15, no. 4, pp. 1240–1246, Nov. 2000.

[106] M. Y. Patel and A. A. Girgis, "Two-level state estimation for multi-area power system," in *Power Engineering Society General Meeting, 2007. IEEE*, Jun. 2007, pp. 1–6.

[107] M. Zhao and A. Abur, "Multi area state estimation using synchronized phasor measurements," *Power Systems, IEEE Transactions on*, vol. 20, no. 2, pp. 611–617, May 2005.

[108] L. De Alvaro Garcia and S. Grenard, "Scalable distribution state estimation approach for distribution management systems," in *Innovative Smart Grid Technologies (ISGT Europe), 2011 2nd IEEE PES International Conference and Exhibition on*, Dec. 2011, pp. 1–6.

[109] N. Nusrat, M. Irving, and G. Taylor, "Development of distributed state estimation methods to enable smart distribution management systems," in *Industrial Electronics (ISIE), 2011 IEEE International Symposium on*, Jun. 2011, pp. 1691–1696.

[110] C. Muscas, M. Pau, P. A. Pegoraro, S. Sulis, F. Ponci, and A. Monti, "Two-step procedures for wide-area distribution system state estimation," in *Instrumentation and Measurement Technology Conference (I2MTC) Proceedings, 2014 IEEE International*, May 2014, pp. 1517–1522.

[111] C. Muscas, M. Pau, P. A. Pegoraro, S. Sulis, F. Ponci, and A. Monti, "Multi-area distribution system state estimation," *Instrumentation and Measurement, IEEE Transactions on*, vol. PP, no. 99, pp. 1–1, 2015.

Publications as author or co-author

International Journals

1. **M. Pau**, P. A. Pegoraro, and S. Sulis, "Efficient branch-current-based distribution system state estimation including synchronized measurements", *Instrumentation and Measurement, IEEE Transaction on*, vol. 62, no. 9, pp. 2419-2429, Sep. 2013.

2. C. Muscas, **M. Pau**, P. A. Pegoraro, and S. Sulis, "Effects of measurements and pseudomeasurements correlation in distribution system state estimation", *Instrumentation and Measurement, IEEE Transaction on*, vol. 63, no.12, pp. 2813-2823, Dec. 2014.

3. D. Della Giustina, **M. Pau**, P. A. Pegoraro, F. Ponci, and S. Sulis, "Electrical distribution system state estimation: measurements issues and challenges", *Instrumentation Measurement Magazine, IEEE*, vol. 17, no. 6, pp. 36-42, Dec. 2014.

4. C. Muscas, **M. Pau**, P. A. Pegoraro, S. Sulis, F. Ponci, and A. Monti, "Multi-area distribution system state estimation", *Instrumentation and Measurement, IEEE Transaction on*, vol. PP, no.99, pp. 1-1, 2015.

5. C. Muscas, **M. Pau**, P. A. Pegoraro, and S. Sulis, "Smart electric energy measurements in power distribution grids", *Instrumentation Measurement Magazine, IEEE*, vol. 18, no. 1, pp. 17-21, Feb. 2015.

6. C. Muscas, **M. Pau**, P. A. Pegoraro, and S. Sulis, "An efficient method to include equality constraints in branch current distribution system state estimation", *EURASIP Journal on Advances in Signal Processing*, accepted for publication.

International Conference Proceedings

1. **M. Pau**, P. A. Pegoraro, and S. Sulis, "Branch current state estimator for distribution system based in synchronized measurements", in *Applied Measurements for Power Systems (AMPS), 2012 IEEE International Workshop on*, Sep. 2012, pp. 1-6.

2. **M. Pau**, P. A. Pegoraro, and S. Sulis, "WLS distribution system state estimator based on voltages or branch currents: Accuracy and performance comparison", in *Instrumentation and Measurement Technology Conference (I2MTC), 2013 IEEE International*, May 2013, pp. 493-498.

3. C. Muscas, **M. Pau**, P. A. Pegoraro, and S. Sulis, "Impact of input data correlation on distribution system state estimation", in *Applied Measurements for Power Systems (AMPS), 2013 IEEE International Workshop on*, Sep. 2013, pp. 114-119.

4. **M. Pau**, P. A. Pegoraro, and S. Sulis, "Effects of PMU measurements correlation on state estimation results", in *Energy Conference (ENERGYCON), 2014 IEEE International*, May 2014, pp. 420-425.

5. C. Muscas, **M. Pau**, P. A. Pegoraro, S. Sulis, F. Ponci, and A. Monti, "Two-step procedures for wide-area distribution system state estimation", in *Instrumentation and Measurement Technology Conference (I2MTC), 2014 IEEE International*, May 2014, pp. 1517-1522.

6. **M. Pau**, P. A. Pegoraro, S. Sulis, and C. Muscas, "Uncertainty sources affecting voltage profile in distribution system state estimation", in *Instrumentation and Measurement Technology Conference (I2MTC), 2015 IEEE International*, accepted for publication.

Acronyms

BC-DSSE Branch Current Distribution System State Estimation

CT Current Transformer

DER Distributed Energy Resource

DG Distributed Generation

DMS Distribution Management System

DSO Distribution System Operator

DSSE Distribution System State Estimation

EMS Energy Management System

EV Electric Vehicle

GPS Global Positioning System

HV/MV High Voltage to Medium VOltage

ISE Integrated State Estimation

LM Lagrange Multipliers

LSE Local State Estimation

LV Low Voltage

MA-DSSE Multi Area Distribution System State Estimation

MASE Multi Area State Estimation

MV Medium Voltage

NV-DSSE Node Voltage Distribution System State Estimation

PMU Phasor Measurement Unit

RMSE Root Mean Square Error

SCADA Supervisory Control And Data Acquisition

SE State Estimation

SG Smart Grid

SVR State Vector Reduction

TVE Total Vector Error

UTC Coordinated Universal Time

VM Virtual Measurements

VT Voltage Transformer

WLS Weighted Least Squares

List of Figures

List of Tables

Acknowledgements

Questa tesi conclude tre anni di lavoro durante i quali ho avuto la fortuna ed il piacere di collaborare con diverse persone che hanno contribuito in maniera significativa alla mia crescita professionale.

Il primo ringraziamento va doverosamente a Carlo per avermi guidato nel mondo della ricerca e per il costante supporto sia professionale che umano.

Un sentito ringraziamento a Sara che con i suoi preziosi consigli mi ha aiutato a crescere e stimolato a dare sempre il massimo.

Un ringraziamento particolare ai miei compagni di laboratorio: a Paolo per i tanti insegnamenti e l'attenta supervisione della mia attività di ricerca e a Paolo per gli scambi di idee, le chiacchierate e i molti momenti divertenti condivisi durante questo percorso.

Ringrazio inoltre la Professoressa Ponci, Professor Monti, e tutti i colleghi di Aachen per i sette mesi proficui e al tempo stesso divertenti trascorsi in Germania.

Al di fuori del contesto lavorativo, un ringraziamento speciale va ai miei genitori, ad Alessandro, a Stefania e a tutti gli amici che mi sono stati a fianco durante questi tre anni.

Infine, il ringraziamento più grande va ad Antonella, per avermi sopportato ed essermi sempre stata vicino sia nei momenti felici che in quelli più difficili.

Marco Pau